PONTIFICIA UNIVERSIDAD CATOLICA DE CHILE

ESCUELA DE INGENIERIA

EQUILIBRIUM PARTITION OF VEGETABLE EXTRACTS BETWEEN PRETREATED VEGETABLE SUBSTRATES AND PURE OR OIL-MODIFIED SUPERCRITICAL CO_2

FREDDY A. URREGO

Thesis submitted to the Office of Research and Graduate Studies in partial fulfillment of the requirements for the Degree of Doctor in Engineering Sciences

Advisor:

Dr. JOSÉ M. DEL VALLE

Santiago de Chile, (September, 2015)

PONTIFICIA UNIVERSIDAD CATOLICA DE CHILE

ESCUELA DE INGENIERIA

EQUILIBRIUM PARTITION OF VEGETABLE EXTRACTS BETWEEN PRETREATED VEGETABLE SUBSTRATES AND PURE OR OIL-MODIFIED SUPERCRITICAL CO_2

FREDDY A. URREGO

Members of the Committee:

Dr. JOSÉ M. DEL VALLE

Dr. CÉSAR SAEZ

Dr. JUAN C. DE LA FUENTE

Dr. PAZ ROBERTS

Dr. MARÍA JOSÉ COCERO

Dr. CRISTIAN VIAL

Thesis submitted to the Office of Research and Graduate Studies in partial fulfillment of the requirements for the Degree of Doctor in Engineering Sciences

Santiago de Chile, (September, 2015)

Dedicated to all those who drove me, accompanied and supported during this process, especially to my parents Efrén A. Urrego and Luz A. Camelo, my wife Julia A. Arango, and finally to my little angel, my daughter, Emma S. Urrego.

AKNOWLEDGEMENTS

My gratitude is first for my parents, Efrén and Luz, who have always been my greatest support, and for my wife, Julia, who shared the good and bad things of this road with me, with infinite love and understanding.

I would like to thank my advisor Dr. José M. del Valle. Your firm grasp made me know my limits and extend them in many ways, and I grew because of it. I hope, that in some way, this experience brought you something that you find valuable. I would also like to thank Dr. Feral Temelli (University of Alberta, Canadá), Dr. María J. Cocero (Universidad de Valladolid, España), and Dr. Helena Sovová (Academy of Sciences of the Czech Republic, Czech Republic), who made decisive and invaluable suggestions to my work during their visits to our laboratory.

To all the High Pressure Processes Research Group (Universidad de Valladolid, España) members, thanks for the time we shared, but most of all, thanks for the efforts to help me achieve the goals of my internship, in such an event that I arrived just after the fire in the building. I hope that everything went back to normal fast enough.

A special thanks to my partners in science from the Laboratorio de Extracción de Materiales Biológicos (LEMaB): Karina Araus, Raúl Aravena, Lorena Mödinger, Yazmin Donaire, Fabián Reyes, Arturo Bejarano, Eduardo Richter, Sofía Andrighetti, Caroline Sielfeld, Soledad Murias, and Andrea Reveco. Last, but most important, I would like to thanks Gonzalo Nuñez, because of his friendship and help.

Finally, I would like to thanks funding by: "*Comisión de Investigación Científica y Tecnológica* CONICYT", specifically the program "*Becas de doctorado en Chile para extranjeros sin permanencia definitiva*"; "*Fondo Nacional de Desarrollo Científico y Tecnologico* FONDECYT", specifically projects 108-0211, 108-0469, and 111-1008; "*Fondo de Fomento al Desarrollo Científico y Tecnológico* FONDEF", specifically the project D09I1207. And finally, funding by the "*Dirección de Postgrados de la Escuela de Ingeniería* DIPEI" from the Pontificia Universidad Católica de Chile is greatly acknowledged.

CONTENTS

DEDICATORY ii
AKNOWLEDGEMENTS iii
LIST OF FIGURES viii
LIST OF TABLES xvii
RESUMEN xviii
ABSTRACT xx
LIST OF PAPERS 1
1. INTRODUCTION 2
1.1. Hypothesis 3
1.2. Objectives 3
2. FREE SOLUTE CONTENT AND SOLUTE-MATRIX INTERACTIONS AFFECT APPARENT SOLUBILITY AND APPARENT SOLUTE CONTENT IN SUPERCRITICAL CO_2 EXTRACTIONS. A HYPOTHESIS PAPER 5
2.1. Introduction 5
2.2. Motivation 7
2.3. Approach 13
2.4. Results 16
2.4.1. The initial solute content in the substrate affects its apparent solubility 17
2.4.2. Solute partition between the substrate and supercritical CO_2 affects extraction yield 24
2.4.3. Discriminating solute partition and mass transfer effects is difficult from integral extraction curves 30
2.4.4. Best-fit parameters from a mathematical model are adequate only when the model fits reality 34
2.4.5. Inadequate mathematical models and best-fit parameters fail simulating process scale-up 40
2.5. Discussion and practical implications of results 42

2.6. Concluding remarks 48
3. EQUILIBRIUM PARTITION OF RAPESEED OIL BETWEEN SUPERCRITICAL CO_2 AND PREPRESSED RAPESEED 50
3.1. Introduction 50
3.2. Materials and methods 53
3.2.1. Substrate 53
3.2.2. Experimental device 54
3.2.3. Experimental procedure 55
3.2.4. Experimental plan 58
3.3. Results 58
3.4. Discussion 71
4. EQUILIBRIUM PARTITION OF RED PEPPER EXTRACT BETWEEN PURE OR VEGETABLE-OIL MODIFIED CO_2 AND PELLETIZED AND MILLED RED PEPPER 75
4.1. Introduction 75
4.2. Materials and methods 78
4.2.1. Materials 78
4.2.2. Experimental methodology 78
4.2.3. Experimental plan 79
4.2.4. Mathematical modelling 79
4.3. Results and discussion 80
4.3.1. Effect of the pressure on the sorption equilibrium of red pepper oleoresin 82
4.3.2. Effect of the temperature on the sorption equilibrium of red pepper oleoresin at isodensity condition of SC CO_2 82
4.3.3. Modelling the oleoresin isotherm/isobar curves 83
4.3.4. Effect of the addition of vegetable oil on the sorption equilibrium of red pepper oleoresin 86
4.3.5. Equilibrium partition of carotenoids 86

4.3.6. Inclusion of the isotherm/isobar model into the BIC extraction model 89
4.4. Conclusions 93
5. DYNAMIC MEASUREMENT OF THE EQUILIBRIUM PARTITION OF TOMATO EXTRACT BETWEEN SUPERCRITICAL CO_2 AND PRETREATED TOMATO 94
5.1. Introduction 94
5.2. Chromatographic methodologies to measure isotherm/isobar curves 96
5.3. Materials and methods 98
5.3.1. Tomato, tomato products, and analysis 98
5.3.2. Experimental device 99
5.3.3. Measurement of sorption isotherm/isobar curves using a static procedure 102
5.3.4. Measurement of sorption isotherm/isobar curves using a dynamic procedures 103
5.3.5. Mathematical model 104
5.4. Results and discussion 106
5.5. Conclusions 120
6. CONCLUSIONS AND FUTURE PERSPECTIVES 121
NOMENCLATURE 124
REFERENCES 129
A P P E N D I X E S 141
APPENDIX A: DETAILS OF MATHEMATICAL MODELS APPLIED IN SECTION (2). 142
A1. Initial condition 142
A2. Boundary condition 144
A3. Model 1 145
A4. Model 2 145
A5. Model 3 145
A6. Yield 147

APPENDIX B: STANDARDIZATION OF THE METHODOLOGY 148
B1. Implications of the close and open sampling modes.....148
B2. Effect of weight ratio on the gravimetric determination of oil 151
B2. Uncertainty analysis 152

LIST OF FIGURES

Figure 2-1. Main zones of a typical integral extraction curve. Zone I solubility dominated where Cfo is the "apparent" solubility, Zone II transition between solubility and mass transfer dominions, Zone III mass transfer dominated where segmented lines Cso represents the "apparent" initial solute content. 7

Figure 2-2. Equilibrium partition of oil between supercritical CO_2 an pre-pressed oilseed when there is no interaction between the solutes and the solid matrix in (A) a case where CO_2 cannot dissolve all oil so that there is excess oil deposited in pores and the CO_2 phase is saturated with oil, and (B) a case where CO_2 can dissolve all oil. 18

Figure 2-3. (A) Effect of initial oil content in pre-pressed oilseed on integral extraction curves with supercritical CO_2 at 353 K and 90 MPa. The initial solute content is expressed as a percentage of the amount required to saturate the CO_2 during the static extraction period (60% indicates that the oilseed contains 60% of the oil required to saturate CO_2). (B) Effect of dynamic extraction time on residual oil concentration profiles oil in pre-pressed oilseed along the extraction vessel for the 60% curve in Fig. (2-3A). Times are expressed as a fraction of the residence time of supercritical CO_2 in the extraction vessel (0.6 t_{res} corresponds to 60% of U/L). 19

Figure 2-4. Modified integral extraction curve of cumulative essential oil yield *versus* specific solvent consumption in a volume-by-weight basis for the extraction of ginger using high-pressure (near- and super-critical) CO_2 at (□) 293 K and 15 MPa, (○) 303 K and 15 MPa, (◇) 313 K and 15 MPa, (▽) 313 K and 20 MPa, and (△) 313 K and 25 MPa. Adapted data from Martinez et al. (2003). 21

Figure 2-5. Relationship between actual (C_{fo}) and expected (C_f*) apparent solubilities of essential oils from herbs and spices extracted using high-pressure (near- and super-critical) CO_2, where values of C_f* were estimated using Eq. (2.11) by assuming there were no interactions between extracts and the solid matrices. Literature data corresponds to the extraction of (○) nutmeg seed particles ($0.300 \leq d_p \leq 1.45$ mm) at 296 K and 9 MPa (Spricigo et al., 2001), (△) nutmeg seed particles ($0.556 \leq d_p \leq 2.12$ mm) at 313-323 K and 10-20 MPa (Machmudah et al., 2006), (□) 383-μm

caraway seed particles at 313 K and 9 or 10 MPa (Sovová et al., 1994), (◇) 720-μm rosemary bract particles at 308 or 313 K and 10 or 12.5 MPa (Coelho et al., 1997), (▽) 375-μm *Lippia sidoides* leaf particles at 282-298 K and ca. 7 MPa (Sousa et al., 2002), (⊠) 520-μm *Croton zehnteri* leaf particles at 288 K and 6.7 MPa (Sousa et al., 2005), and (⊕) 860-μm milled clove bud particles at 298 K and 10 MPa using extraction vessels of two sizes (Martínez et al., 2007).....23

Figure 2-6. (A) Effect of sorption parameters on integral extraction curves of oil in pre-pressed oilseed using supercritical CO_2 at 353 K and 90 MPa, when sorption follows pseudo-Sip's model. (B) Corresponding sorption isotherm/isobar for the partition of oil between pre-treated oilseed and supercritical CO_2 at 353 K and 90 MPa (insert provides a detailed view of the initial slopes of the sorption isotherms/isobars).....25

Figure 2-7. (A) Effect of sorption parameters on integral extraction curves of oil in pre-pressed oilseed using supercritical CO_2 at 353 K and 90 MPa, when sorption follows BET's model. (B) Corresponding sorption isotherm/isobar for the partition of oil between pre-treated oilseed and supercritical CO_2 at 353 K and 90 MPa. 29

Figure 2-8. (A) Effect of inner mass transfer on integral extraction curves of oil in pre-pressed oilseed using supercritical CO_2 at 353 K and 90 MPa. The ratio between the internal and external resistance to mass transfer, which is characterized by Biot's number was modified by changing particle diameter: 0.25 mm for Bi = 16; 0.40 mm for Bi = 24; 0.55 mm for Bi = 31; and, 0.70 mm for Bi = 37. (B) Effect of dynamic extraction time on residual concentration profiles of oil in pre-pressed oilseed along the extraction vessel for the Bi = 16 curve if Fig. (2-3A). Times are expressed as a fraction of the residence time (t_{res}) of SC-CO_2 in the extraction vessel.....31

Figure 2-9. Comparison between the curve for K = 17 in Fig. (2-6A) (equilibrium partition defined by BET's sorption model and no resistance to mass transfer) and Bi = 16 in Fig. (2-8A) (equilibrium partition defined by a linear sorption model, Eq. (2.9b), and resistance to mass transfer): (A) Integral extraction curves. (B) Residual concentration profiles of oil in pre-pressed oilseed along the extraction vessel for the time note (symbol) in Fig. (2-9A). 33

Figure 2-10. (A) Comparison between assumed (symbols) and best-fitted integral extraction of oil in pre-pressed oilseed using supercritical CO_2 at 353 K and 90 MPa. Synthetic data and best-curves were obtained using Model 3 for pseudo-Sips's sorption (continuous lines in B) and linear sorption (segmented line in B). (B) Comparison between assumed (continuous line) and best-fitted (segmented line) partition coefficient of oil between supercritical CO_2 at 353 K and 90 MPa and pre-pressed oilseed.....35

Figure 2-11. (A) Comparison between assumed (symbols) and best-fitted integral extraction of oil in pre-pressed oilseed using supercritical CO_2 at 353 K and 90 MPa. Synthetic data and best-curves were obtained using Model 3 for BET's sorption (continuous lines in B) and linear sorption (segmented line in B). (B) Comparison between assumed (continuous line) and best-fitted (segmented line) partition coefficient of oil between supercritical CO_2 at 353 K and 90 MPa and pre-pressed oilseed.....37

Figure 2-12. (A) Comparison between assumed (symbols) and best-fitted integral extraction of oil in pre-pressed oilseed using supercritical CO_2 at 353 K and 90 MPa. Synthetic data (symbols) was obtained using Model 3 for sorption according to Eq. (2.21) (continuous lines in B). Best-fitted line was obtained using a simplified version of Sovová (2005) model for PCPR-type sorption (segmented line in B). (B) Comparison between assumed (continuous line) and best-fitted (segmented line) sorption isotherms/isobars for the partition of oil between pre-treated oilseed and supercritical CO_2 at 353 K and 90 MPa. 39

Figure 2-13. Effect of a change of scale on simulated integral extraction curves of supercritical extractions (1-m^3 extractor using 2-mm particles *versus* 100-cm^3 extraction vessel using 0.55-mm particles) using CO_2 at 353 K and 90 MPa simulated using Model 3. Continuous lines represent simulation using assumed parameter values whereas segmented lines represent simulation using best-fitted parameters for **(A)** pseudo-Sip's applied sorption (same conditions as in Fig.2-10) and **(B)** BET's sorption (same conditions as in Fig 2-11). 41

Figure 2-14. Sorption isotherms/isobars for canola seed oil at 313 K and (△) 30 MPa or (○) 35 MPa. Symbols are experimental data taken from (Bulley et al., 1984) and trend lines were obtained using Eq. (2.21) and C_{sat} values estimated using the equation of del Valle et al. (2012). 44
Figure 2-15. Comparison of sorption isotherm/isobar models presented in this manuscript. 44
Figure 3-1. Schematic diagram of the high-pressure equilibration unit. The loading sub-system includes a liquid CO_2 cylinder, on-line filter (olF), ooling bath (CB), syringe pump (SP), and heating coil (HC). The equilibration sub-system consist of a gear pump (GP), equilibrium cell (EC), injection valve (IV), and UV/Vis detector held in thermostated air bath together with HC. The sampling subsystem consists of a micrometric valve (mv), a two-inlet sampling valve (TiSV), a sampling tube (ST) located in a dewar with a cooling mixture, and volumetric gas meter (GM). Valves a and b are on-off (quarter-turn-type) valves. 55
Figure 3-2. Graphical representation of loading, equilibration, and sampling operations. (A) In the loading step the system is pressurized with the syringe pump (not included) operating at constant flow, valve a (cf. Fig. 3-1) is opened, and valves b and mv are closed. (B) In the equilibration step the gear pump recirculates CO_2, valves a and mv are closed, valve b is opened, and valve IV is switched to the inject position to obtain a UV/Vis reading of the supercritical CO_2 phase in the detector. (C) In the sampling step the syringe pump (not included) is operated at constant pressure, valves a and mv are opened, and valve b is closed. Opened valves are marked white whereas closed valves are marked black. 56
Figure 3-3. Effects of sampling in a closed loop mode in the pressure and apparent concentration of oil in CO_2 for the three different equilibrium concentrations noted. Assumed initial conditions were 50 °C and 28 MPa. 60
Figure 3-4. Effects of sampling in a closed loop mode in the pressure and apparent concentration of oil in CO2 for the three different equilibrium concentrations noted. Dashed lines indicate perfect mixing, continuous lines indicate dispersed plug flow

for “ground” pellets, and dotted lines indicated dispersed plug flow for “square” pellets. Assumed initial conditions were 50 °C and 28 MPa. 61
Figure 3-5. Uncertainty analysis of the measurands (C_f, C_s) for “ground” pellets isotherm/isobar curve at 50 °C and 28 MPa. Parallel horizontal bars signal uncertainties in oil concentration in the SC CO_2 phase, whereas parallel vertical bars signal uncertainties in oil concentration in the oilseed phase. The dotted line represents the isotherm/isobar estimated neglecting sorption effects in the oilseed, whereas the continuous line represents the trend line for the experimental data. 63
Figure 3-6. Effect of the replication and substrate pre-treatment on isotherm/isobar curves at 50 ºC and 28 MPa, where (△ ,▽) represent duplicates using “square” pellets and (○) data obtained using “ground” pellets. Lines represent predictions using pseudo-Sips‟ model using complete models to study the effect of replication and substrate pretreatment. 66
Figure 3-7. Effect of pressure on isotherm/isobar curves measured at 40 °C. (◊) 22 MPa, (□) 25 MPa, and (○) 28 MPa. 66
Figure 3-8. Effect of temperature on isotherm/isobar curves measured at the same SC CO_2 density (857.1 kg/m^3). (◊) 40 °C-22 MPa, (□) 45 °C-25 MPa, and (○) 50 °C-28 MPa. 68
Figure 3-9. Arrehnius-type plot of oil concentration in CO_2 (C_f) *versus* reciprocal of absolute temperature (T^{-1}) as a function of the residual oil content in the substrate (C_s). 68
Figure 3-10. Dependence of the total heat of desorption from the substrate and solvation in CO_2 (ΔH) of the oil as a function of the residual oil contecnt in the substrate (C_s). 70
Figure 4-1. Integral extraction curves of oleoresin from red pepper at 40 (■) and 60 ºC (♦) - 28 MPa. Experimental data provided by Uquiche et al. (in preparation). 77
Figure 4-2. Exhaustive isotherm/isobar curve of red pepper oleoresin at 67ºC -28 MPa. 81
Figure 4-3. Effect of the pressure on the equilibrium partition of red pepper oleoresin. Measurements at 60ºC and 22 (■), 25 (●), and 28 (♦) MPa. 82

Figure 4-4. Effect of the temperate on the equilibrium partition of red pepper oleoresin at isodensity condition of SC CO_2. Measurements at SC CO2 density of 785 kg m^{-3}, 54ºC-22MPa (▲), 60ºC-25 MPa (●), and 67ºC-28 mPa (◊).....83
Figure 4-5. Effect of the addition of vegetable oil on the equilibrium partition of red pepper oleoresin at 60ºC-25 MPa. Isotherm/isobar curve without modified SC CO_2 (●), with modified SC CO_2 (+), and a simulated isotherm/isobar curve of vegetable oil (-) for the same operating conditions as reference.....87
Figure 4-6. Equilibrium concentration of carotenoid for isotherms/isobars measured with pure (●) and modified (○) SC CO_2 at 60 °C and 25 MPa. (A) carotenoids concentration in the extract, (B) carotenoid concentration in SC CO_2. 88
Figure 4-7. Simulated integral extraction curves of oleoresin from red pepper at 40 (■) and 60 ºC (♦) - 28 MPa. 92
Figure 5-1. Experimental device constituted of (1) CO_2 cylinder, (2) cooling bath, (3) syringe pump, (4) positive-displacement (HPLC-type) pump, (5, 6) 6-m heating coils, (7) recirculation (gear-type), (8) 40-cm^3 equilibrium cell, (9, 10) 12-cm^3 sorption columns, (11) automatized injection valve, (12) four-port, two-way manual valve, (13) two-port, two-way manual valve, (14) UV/Vis detector equipped with high-pressure cell, (15) back-pressure regulator, (16) two-inlet sampling valve, (17) micrometric valve, (18) 50-cm^3 sampling tube with dewar flask, and (19) drum-type volumetric gas meter. 100
Figure 5-2. Configuration of switching valves (11, 12, and 13 in Fig. 5-1), for different tasks when applying dynamic procedures to study sorption isotherm/isobars. Column 2 (10 in Fig. 5-1) was packed with glass beads when calibrating the UV/Vis detector, which applied two configurations: (A) to equilibrate the dynamic system to operation conditions; and, (B) to inject pulses of supercritical CO_2 saturated with tomato extract. Column 1 (9 in Fig. 5-1) was packed with glass beads and column 2 with fully extracted tomato when studying breakthrough curves of solutions of tomato extract in supercritical CO_2, which applied three configurations: (C) to equilibrate the dynamic system to operation conditions; (D) to inject and homogenize pulses of

supercritical CO_2 saturated with tomato extract; and, (E) to apply a negative perturbation (pulse of pure supercritical CO_2). Valve configurations in (A) and (E) are identical 101
Figure 5-3. Equilibrium partition of tomato extract between supercritical CO_2 and dried, pelletized, milled, and size-classified tomato measured using the static procedure at 40 °C and 29 MPa. Open circles represent experimental data points, and the line model predictions using best-fitted parameters of Freundlich's equation, Eq. (5.4). 106
Figure 5-4. Carotenoid concentrations in (A) tomato extract, and (B) supercritical CO_2, of the extracts sampled while measuring the sorption isotherm/isobar curve using the static procedure (Fig. 5-3). 107
Figure 5-5. (A) Response signal for different switching times of tomato extract diluted in supercritical CO_2 in a column packed with glass beads. (B) Pulses (1.5 s) of supercritical CO2 saturated with tomato extract (50-μL portions) injected into the packed column for different switching times (4, 9, and 21-s). (C) Actual traces (full lines) and moving averages (segmented lines) for times equal to the switching times in (B) for the boxes noted in (A). 109
Figure 5-6. Correlation between average absorbance at 486 nm (wavelength of maximal absorbance of tomato extract in CO_2) and average carotenoid concentration in supercritical CO_2. 111
Figure 5-7. (A) Dimensionless concentration responses to injection of different concentrations of tomato in supercritical CO_2 to a column packed with glass beads. (B) Curves from (A) following adjustment of time so as to make coincide the dimensionless concentrations for the half-height (0.5) value. 112
Figure 5-8. Summary of results for the frontal analysis, perturbation analysis, and desorption analysis for the partition of carotenes in tomato extract between supercritical CO_2 and fully extracted tomato at 40 ºC and 29 MPa. (A) Experimental response for the adsorption breakthrough curves as a function of the carotene concentrations in supercritical CO_2 (0.9–4.6 mg kg^{-1} carotene/CO_2), where arrows signal times when negative perturbation were induced. (B) Experimental response for

the desorption breakthrough curves using pure supercritical CO_2 following equilibration of fully extracted tomato with CO_2 containing these same carotene concentrations.....113

Figure 5-9. Details of the two perturbation peaks for the breakthrough curve for 4.1 mg kg^{-1} carotene/CO_2 in Figure 5-2 (close symbols) lined to the initiation of the perturbation, together with best-fits to the normal distribution function (lines); each end of arrow marks the onset of the negative peak, corresponding to the best-fit average (time for the minimal) minus twice the standard deviations. 114

Figure 5-10. Difference in the breakthrough curves between a column packed with glass beads (Fig. 5-5A) and a similar column packed with fully-extracted tomato (Fig. 5-8A), represented the carotenoids adsorbed by the solid substrate at 40 ºC and 29 MPa as a function of the carotenoid concentration in the supercritical CO_2 fed to the columns. The area under each curve represents the total amount of tomato carotenoids adsorbed by the fully-extracted tomato. 115

Figure 5-11. Best-fitting of the transport-dispersive model to breakthrough curves for carotene partition between supercritical CO_2 and fully extracted tomato at 40 ºC and 29 MPa. **(A)** Application of the inversion method to the desorption curve following equilibration of a column packed with fully-extracted tomato with a supercritical CO_2 solution containing 4.6 mg kg^{-1} carotene/CO_2; open circles represent experimental data points, and the line represents model predictions using best-fitted parameters of Freunlich's equation, Eq. (5.4). **(B)** Slope of the sorption isotherm/isobar *versus* carotene concentration in supercritical CO_2; open circles represent experimental data points from perturbation analysis (Fig. 5-9); whereas the line represented model predictions using Freundlich's equation with best-fit parameters from (A). 118

Figure 5-12. Sorption isotherm/isobars for tomato carotene partition between supercritical CO_2 and dried, pelletized, milled, and size-classified tomato. **(A)** Tomato desorption using the static method; closed circles outside highlighted area represent experimental data points. **(B)** Zoom of highlighted area in (A) showing results

obtained applying dynamic methods to fully-extracted tomato. Symbols represent experimental data points using frontal analysis for the sorption (closed circles) and desorption (open symbols) steps. Line represent predicts using best-fitted parameters obtained using inverse analysis (Fig. 5-11).....119
Figure A-1. Identification of elements defining mass transfer in packed bed extraction vessel in which porous spherical particles are extracted by a supercritical CO_2 up-flowing stream.....143
Figure A-2. Schematic representation of the algorithm used to solve differential mass balance equations for the supercritical CO_2 extraction of solid substrate particles in a packed bed extraction vessel, including actualization of concentration values in the solid and fluid phase as a function of axial position in the vessel and time.....146
Figure B-1. Uncertainty of oil weight measurements as a function of the ratio between the weight of the sample holder and the oil. 152

LIST OF TABLES

Table 2-1. Comparison of apparent (C_{fo}) and thermodynamic (C_{sat}) solubilites in supercritical CO_2 of different compounds in vegetable substrates. (Continued) 10

Table 2-2. Comparison of thermodynamic solubilities of orange essential oil components (limonene, linalool) in supercritical CO_2 in binary, ternary, and complex systems, and apparent solubility in orange peel.....12

Table 2-3. Comparison between adopted (non-linear sorption isotherm/isobar) and best-fit values (assuming linear partition of oil between SC CO_2 and pre-pressed oilseed) of model parameters. 36

Table 2-4. Isotherm/isobar sorption models presented in this manuscript. 46

Table 4-1. Experimental conditions, physical properties of SC CO_2, and model parameters. 91

Table B-1. Definition and values of parameters applied while modelling the sampling step with an open loop mode with a kinetic extraction model. Operation conditions of 50 °C and 28 MPa were assumed.....151

Table B-2. Variance of selected variables affecting calculations using Eqs. (B.7) and (B.8).....155

PONTIFICIA UNIVERSIDAD CATOLICA DE CHILE

ESCUELA DE INGENIERIA

EQUILIBRIO DE PARTICIÓN DE EXTRACTOS VEGETALES ENTRE SUSTRATOS VEGETALES PRETRATADOS Y CO_2 SUPERCRÍTICO PURO O MODIFICADO CON ACEITE

Tesis enviada a la Dirección de Investigación y Postgrado en cumplimiento parcial de los requisitos para el grado de Doctor en Ciencias de la Ingeniería.

FREDDY ANEIDHER URREGO CAMELO

RESUMEN

En la modelación de la extracción de sustratos vegetales con CO_2 supercrítico (CO_2 SC), es común considerar a las variables del equilibrio de partición (función que relaciona la concentración máxima que podría alcanzar un soluto en la fase fluida, C_f, con base en la concentración residual del soluto en la fase sólida, C_s, $C_f = f(C_s)$) como parámetros de ajuste, algunas veces desconociendo si los resultados obtenidos reflejan la realidad física. El objetivo de esta tesis fue estudiar (experimentalmente), el equilibrio de partición de extractos vegetales entre CO_2 SC y sustratos vegetales, modelar los resultados, y evaluar su inclusión en modelos de extracción. Para esto, se desarrolló, estandarizó, y validó una metodología que intercala etapas de equilibramiento (y muestreo), con etapas de extracción (para agotar el sustrato), midiendo el equilibrio de partición de aceite de raps entre CO_2 SC y raps preprensado, a 40-60ºC y 22-28 MPa. Luego, se aplicó en la medición del equilibrio de partición de oleorresina de pimentón (y carotenoides), entre CO_2 SC puro o modificado

con aceite vegetal, y pimentón peletizado-molido-tamizado, a 54-67ºC y 22-28 MPa. Por último, se diseñó y evaluó una metodología basada en principios cromatográficos, para medir el equilibrio de partición de oleorresina de tomate (y carotenoides) disuelta en CO_2 SC, en tomate peletizado-molido-tamizado que fue totalmente extraído. En las isotermas/isobaras de aceite de raps se observó un valor máximo de concentración en CO_2 SC que correspondió al valor de saturación, mientras que en las isotermas/isobaras de oleorresinas, la interacción soluto-sustrato impidió la saturación. En todos los casos, sin embargo, se observó un efecto positivo de la presión y la temperatura sobre la partición de los solutos hacia la fase de CO_2. Se propuso y aplicó una nueva ecuación matemática que modela los resultados obtenidos, y se observó un buen ajuste al aplicarla en modelos de extracción. Adicionalmente, se observó que la partición de carotenoides hacia la fase CO_2 SC se ve favorecida por la presencia ya sea de compuestos lipídicos propios de las oleorresinas, tanto como de un aceite vegetal añadido.

Miembros de la Comisión de Tesis Doctoral

Dr. José M. del Valle

Dr. César Saez

Dr. Juan C. de la Fuente

Dr. Paz Roberts

Dr. María J. Cocero

Dr. Cristian Vial

Santiago, Enero, 2015

PONTIFICIA UNIVERSIDAD CATOLICA DE CHILE

ESCUELA DE INGENIERIA

EQUILIBRIUM PARTITION OF VETABLE EXTRACTS BETWEEN PRETREATED VEGETABLE SUBSTRATES AND PURE OR OIL-MODIFIED SUPERCRITICAL CO_2

Thesis submitted to the Office of Research and Graduate Studies in partial fulfillment of the requirements for the Degree of Doctor in Engineering Sciences by

FREDDY A. URREGO

ABSTRACT

It the modelling of the extraction of vegetable substrates with supercritical CO_2 (SC CO_2), it is common to use the variables of the equilibrium partition (a function relating the maximal concentration of a solute in the fluid phase, Cf, with the residual concentration of the solute in the solid substrate, Cs, $C_f = f(C_s)$) as best-fitting parameters, sometimes ignoring if results are a real picture of the physical reality. The objective of this thesis was to experimentally measure the equilibrium partition of vegetable extracts between SC CO_2 and vegetable substrates, to model the results, and to evaluate the effect of introducing these results in the modelling of supercritical extraction processes. An experimental methodology that intersperses equilibrium (and sampling), and extraction steps (to accelerate the depletion of the substrate) was developed, standardized, and validated, by measuring the partition of rapeseed oil between SC CO_2 and prepressed rapeseed at 40-60ºC, and 22-28 MPa. The methodology was then applied to measure the partition of red pepper oleoresin (and carotenoids), between pure or vegetable-oil-modified SC CO_2, and

peletized-milled-sieved red pepper, at 54-67 ºC and 22-28 MPa. Finally, a methodology based on chromatographic principles was designed and evaluated to measure the partition of tomato oleoresin (and carotenoids) dissolved in SC CO_2 in peletized-milled-sieved tomato that was extracted to exhaustion. The rapeseed oil isotherm/isobar curves show a horizontal asymptote related to the saturation concentration of oil in SC CO_2 at the operation conditions, whereas in the oleoresin isotherm/isobar curves the solute-substrate interactions impeded the saturation. However, and in all cases, the increase of pressure and temperature had a positive effect on the partition of the solutes to the SC CO_2. A new equation was proposed to model the results, showing a good fit after applying it to supercritical extraction models. Additionally, it was observed that the partition of carotenoids to the SC CO_2 phase was enhanced by the presence of either the lipid components of the substrate or added vegetable oil.

Members of the Doctoral Thesis Committee:

Dr. José M. del Valle

Dr. César Saez

Dr. Juan C. de la Fuente

Dr. Paz Roberts

Dr. María J. Cocero

Dr. Cristian Vial

Santiago, January, 2015

LIST OF PAPERS

This thesis is based on the next scientific articles:

1. del Valle, J. M., & Urrego, F. A. (2012). Free solute content and solute-matrix interactions affect apparent solubility and apparent solute content in supercritical CO_2 extractions. A hypothesis paper. *The Journal of Supercritical Fluids* (66), 157-175.

2. Urrego, F. A., Nuñez, G. A., Donaire, Y. D., & del Valle, J. M. Equilibrium partition of rapeseed oil between supercritical CO_2 and prepressed rapeseed. *The Journal of Supercritical Fluids*. *The Journal of Supercritical Fluids* (102), 80-91.

3. Urrego, F. A., del Valle, J. M. & de la Fuente, J. C. Equilibrium partition of rapeseed oil between supercritical CO_2 and prepressed rapeseed. (in progress).

4. Urrego, F. A., del Valle, J. M., Cocero, M. J., & de la Fuente, J. C. Dynamic measurement of the equilibrium partition of tomato extract between supercritical CO_2 and pretreated tomato. *The Journal of Chromatography A.* (in progress).

1. INTRODUCTION

In extraction processes is always expected to find the conditions that improve the yield and reduce the processing time. In the case of the extraction of vegetable substrates with supercritical CO_2 (SC CO_2) this is influenced by the solubility of the solute (or mixture of solutes) in SC CO_2, and the interactions between the solute and the solid matrix (del Valle & de la Fuente, 2006; del Valle, Germain, Uquiche, Zetzl, & Brunner, 2006). On one hand, the solubility in SC CO_2 is a property that has been widely studied, and in literature is possible to find data compilations both for pure solutes, i.e., the solubility of carotenoids in SC CO_2 (Shi, Mittal, Kim, & Xue, 2007), as well as for complex systems, i.e., an equation to predict the solubility of vegetable oils based on experimental data compilation (del Valle, de la Fuente, & Uquiche, 2012). The addition of substances (co-solvents) that enhance the solubility of a solute in SC CO_2 has also been studied, i.e., the application of vegetable oils to enhance the solubility of carotenoids (Q. X. Ma, Xu, Gao, Wang, & Zhao, 2008; Sun & Temelli, 2006; Vasapollo, Longo, Rescio, & Ciurlia, 2004). On the other hand, the experimental research on the solute-matrix interactions, in the SC CO_2 extraction of vegetable systems, had less attention, and it was mainly used as a best-fit parameter in the modelling of supercritical fluid extraction (SCFE) processes.

In the SCFE of vegetable substrates, the solute-matrix interactions are quantified by measuring the equilibrium partition, which is a correlation (named sorption isotherm/isobar) between the concentration of a solute in the SC CO_2 (fluid, C_f) phase, and the concentration of the solute in the substrate (solid, C_s) phase, ($C_f = f(C_s)$), when phases are in contact enough time allowing the solute to migrate to the SC CO_2 until the two phases are in equilibrium. Therefore, this equilibrium represent a limitation to the mass transfer that should be included and properly measured in the modelling of the SCFE process.

This thesis consist of four articles that study the equilibrium partition of vegetable extracts between pretreated substrates and pure or oil-modified SC CO_2, so as to include it in the modeling of SCFE processes. Briefly, the first article (section 2) presents an introduction that highlights the importance, and presents a justification to experimentally

measure the equilibrium partition; the second article (section 3) presents the development, standardization, and validation of an experimental methodology (based on static methods) to measure sorption isotherm/isobar curves, applied to the partition of rapeseed oil between prepressed rapeseed and SC CO_2; the third article (section 4) presents the application of the aforementioned methodology to the partition of red pepper oleoresin (and carotenoids) between peletized-milled-sieved red pepper and pure or oil-modified SC CO_2; finally, the forth article (section 5) presents the application of a different methodology, based on chromatographic (dynamic) principles, to measure the partition of tomato oleoresin (and carotenoids) between peletized-milled-sieved and completely extracted tomato, and SC CO_2 loaded with tomato oleoresin.

1.1. Hypothesis

In the extraction of a vegetable substrate with pure or oil-modified SC CO_2, a vegetable and solid matrix interacts with their solutes through sorption phenomena, and its measurement, modelling, and inclusion in extraction models, improves the simulation of experimental extraction data.

1.2. Objectives

The main objective of this thesis is to study the equilibrium partition of vegetable extracts between pre-treated substrates and pure or modified SC CO_2, and its application on SCFE models.

The specific objectives of this thesis are:

1. to study the state of the art of the research on equilibrium partition of vegetable extracts between pre-treated substrates and pure or oil-modified SC CO_2, by identifying its relevance.
2. to develop a (static) methodology to measure the equilibrium partition, applied to a rapeseed oil – prepressed rapeseed – SC CO_2 system.
3. to measure and model the equilibrium partition of the red pepper (carotenoids) – peletized-milled-sieved red pepper – pure of oil-modified SC CO_2 system, and to apply it in the simulation of experimental extraction data.

4. to develop a (dynamic) methodology to measure and model the equilibrium partition of the tomato oleoresin (carotenoids) – peletized-milled-sieved (and completely extracted) tomato – SC CO_2 system, and to compare the differences between the methodologies.

2. FREE SOLUTE CONTENT AND SOLUTE-MATRIX INTERACTIONS AFFECT APPARENT SOLUBILITY AND APPARENT SOLUTE CONTENT IN SUPERCRITICAL CO_2 EXTRACTIONS. A HYPOTHESIS PAPER

Abstract

This manuscript stresses the need of experimental measurements and mathematical models of sorption isotherms/isobars to properly account for mass transfer in the SuperCritical (SC) Fluid Extraction (SCFE) processes. A reliable sorption isotherm/isobar model is a requirement, on one hand, for the determination of relevant inner mass transfer coefficients in SC CO_2 extractions of vegetable substrates and other biological materials at the laboratory scale, and on the other hand, for a simulation tool successfully applicable to describe industrial SCFE process, which should be based both on a reliable mathematical descriptions of SC CO_2 extraction processes. Having a reliable simulation model and model parameters would allow limiting expensive experimental pilot-scale work to validation purposes. Based on simulations of oil extraction from pre-pressed oilseeds using SC CO2 at 353 K and 90 MPa, this manuscript shows that the initial oil content in the pre-treated seed affects the apparent solubility of the oil, that the partition of the oil between the seed and CO2 affects oil yield, that it is difficult to discriminate oil partition from inner mass transfer effects, that the best-fit parameters from a mathematical model are adequate only when the model accounts for the true physical picture of the extraction process, and that failure of the mathematical model to account the true physical picture of the extraction process impedes reliable simulations, scale-up, and economical evaluation of industrial SCFE process. Being sorption phenomena of such paramount importance to build a reliable mathematical model for simulation of SCFE processes, this manuscript proposes a mathematical model that fits experimental sorption isotherm/isobars for oil from seeds.

2.1. Introduction

SuperCritical (SC) Fluids (SCFs) are conveniently applied in environment-friendly extraction processes because of their liquid-like solvent properties and gas-like transport

properties, that allow efficient and fast extraction processes, and complete elimination of solvent traces (SCFs are gases under normal conditions) from extracts and treated substrates. Among potential candidates, inexpensive carbon dioxide (CO_2), offers safe and selective SCF Extraction (SCFE) processes at near-environmental temperatures, which justifies commercial applications of SC CO_2 extraction over the last three decades, particularly for high-value compounds in vegetable substrates (Brunner, 1994).

Modelling and simulation are important for process design purposes, particularly of SCFE processes. Commercial SCFE plants for vegetable substrates can be designed estimating relevant equilibrium and rate parameters from integral extraction curves obtained in the laboratory (Núñez, Gelmi, & del Valle, 2011). An integral extraction curve is a plot of cumulative yield (e.g., grams of extract per kilogram of substrate) versus specific solvent consumption (e.g., kilograms of CO_2 per kilogram of substrate) that, according to Brunner (Brunner, 1994), "is of relative simple form… (so that) it is not possible to calculate many parameters with significance from such a curve" (p. 181).

Typical integral extraction curves have three zones (Sovová, 1994) (Fig. 2-1). In Zone I the curve has a constant slope having as units, e.g. grams of solute per kilogram of CO_2, which represents a so-called "apparent" solubility of the extract (a multicomponent mixture of solutes in the substrate that can be extracted simultaneously) in SC CO_2 (C_{fo}). When there is free solute on the surface of the substrate particles, this migrates to the interparticle SC CO_2 phase in an amount that is restricted only by the solubility of the solute in SC CO_2 under process conditions. The slope of the integral extraction curve decreases continuously in Zone II because there is no enough free solute on the surface of the particle, there are constraints to mass transfer within the substrate and a stationary film of CO_2 next to the particle, and/or there are equilibrium constraints to the liberation of solute from the substrate to the intra-particle SC CO_2 phase. Finally, in Zone III the integral extraction curve approaches a horizontal asymptote that represents the total amount of solute in the substrate that SC CO_2 can remove under process conditions.

Integral extraction curves can be used for scaling-up purposes and determining the cost of the SCFE process. Indeed, Rosa and Meireles (2005) claim that "the minimum estimated cost (can be) obtained in extraction times close to the end of the constant extrac-

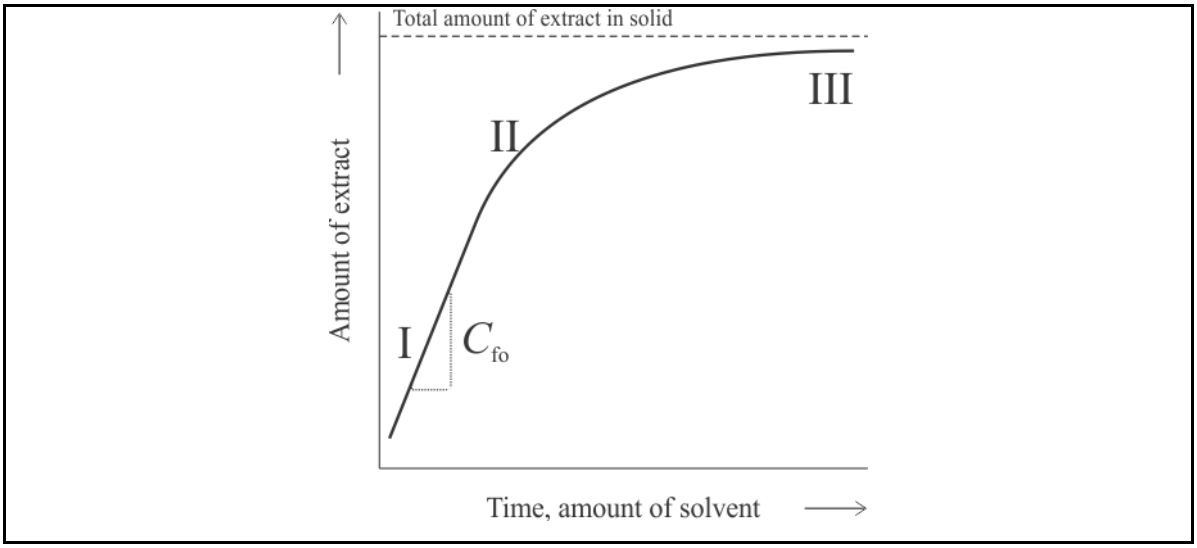

Figure 2-1. Main zones of a typical integral extraction curve. Zone I solubility dominated where Cfo is the "apparent" solubility, Zone II transition between solubility and mass transfer dominions, Zone III mass transfer dominated where segmented lines Cso represents the "apparent" initial solute content.

tion rate region and thus, in order to have low (cost of manufacturing) the constant extraction rate region should have short time and high yields" (p. 238). This is not entirely true because, as authors' will show in this manuscript, integral extraction curves may be scale-specific under selected conditions.

The objective of this manuscript is to show the effect of the residual solute content in a vegetable substrate on the apparent solubility and yield of a SC CO_2 extraction process, as well as the implications of solute partition between the substrate and SC CO_2 on kinetics and scale-up of SCFE processes. This is done using mathematical simulations and re-analysing data in literature.

2.2. Motivation

According to Brennecke and Eckert (1989) "any really widespread applications of SCFE in the future are highly dependent on the ability of engineers to model and predict phase equilibria in the complex systems represented" (p. 1409). This is partially true when applying SCFE to vegetable substrates and other biological substrates because under

certain conditions the optimal extraction process does not depend on "thermodynamic" solubility as exemplified next.

The apparent solubility is a fraction of the thermodynamic solubility in the SCFE of many solutes contained in vegetable substrates. Data compilation in Table (2-1) explores the relationship between apparent (C_{fo}) and thermodynamic (C_{sat}) solubilities by reporting values of the ratio C_{fo} / C_{sat} for several solutes in vegetable substrates. By analogy with the definition of C_{fo} in Fig. (2-1), the apparent solubility of a specific solute is the product of C_{fo} for the whole extract, times the concentration of the solute in the extract. Apparent solubilities were taken from graphics (de Azevedo et al., 2008; Gomez-Prieto, Caja, & Santa-Maria, 2002; Gopalán, Goto, Kodama, & Hirose, 2000; Topal, Sasaki, Goto, & Hayakawa, 2006), tables (Puah, 2005; Puah, Choo, Ma, & Chuah, 2007; Saldaña, Sun, Guigard, & Temelli, 2006; Saldaña, Temelli, Guigard, Tomberli, & Gray, 2010; Shi et al., 2009; Silva, Gamarra, Oliveira, & Cabral, 2008), or the text (del Valle, Rogalinski, Zetzl, & Brunner, 2005; Saldaña, Mohamed, Baer, & Mazzafera, 1999), or estimated from an integral extraction curve (del Valle, Jimenez, & de la Fuente, 2003). Required values of C_{sat} at corresponding process conditions (temperature and pressure) were taken directly from tables with experimental data (Silva et al., 2008) or estimated with the equation of Mendez-Santiago and Teja (1999) (MS-T) using best-fitting parameters for experimental solubility as a function of CO_2 density, and the absolute temperature and pressure of the system. Best-fitting parameters were taken from Araus, Canales, de la Fuente, and del Valle (2011) for β-carotene, and from de la Fuente, Oyarzun, Quezada, and del Valle (2006) for lycopene, capsaicin (de la Fuente, Valderrama, Bottini, & del Valle, 2005), and boldine (de la Fuente, Quezada, & del Valle, 2005). On the other hand, authors of this manuscript fitted MS-T's equation to experimental data for caffeine (Saldaña et al., 1999), theobromine (Saldaña et al., 1999), thyophilline (Saldaña et al., 1999), turmerone (Kao, Chen, & Chang, 2007), and α-tocopherol (Johannsen & Brunner, 1997). Values of C_{fo} are below corresponding values of C_{sat} in most cases (Table 2-1). Single exceptions are bixin in annatto seeds (Silva et al., 2008), and an experimental point for β-carotene in carrot (323K and 12 MPa) in the study of Saldaña et al. (2006) that is not included in Table (2-1) (C_{fo} / C_{sat} = 1.6). The decrease in apparent as compared to thermodynamic solubility ranges

from 1.1 times for the extraction of β-carotene in carrot using SC CO_2 at 323 K and 15 MPa (Saldaña et al., 2006) to 1.1 million times for the extraction of boldine in boldo leaves using SC CO_2 at 323 K and 60 MPa (del Valle et al., 2005). Typical extracts are complex mixtures of several interacting solutes, and solute-solute interactions affect the behaviour of the solubility of a constituent in the mixture as compared with the solubility of the pure counterpart (Brennecke & Eckert, 1989). For example, Silva et al. (2008) explained the increase in the solubility in SC CO_2 of bixin in annatto seed extract as compared with the solubility of 93% pure bixin in SC CO_2 as due to the co-solvency effect of the oil in the seeds (Araus et al., 2011). Table (2-1) shows that anti-solvency effects are more common than co-solvency effects in SC CO_2 extraction of vegetable substrates.

The difference between apparent and thermodynamic solubilities can be explained by the interactions between solutes in complex extract mixtures as well as their interaction with the substrate. An attempt to isolating the effects of solute-solute and solute-matrix interactions is possible by comparing thermodynamic solubilities in model binary systems, model ternary systems, and extracts in phase equilibrium experiments, and apparent solubilities in SCFE experiments. Differences in solubility for increasingly complex systems can be illustrated for essential oils from orange peel (Table 2-2). Selected temperature and pressure conditions are typical of equilibrium (333 K, 10 MPa) and extraction (323 K, 15 MPa) experiments, and missing entries in Table (2-2) show the need of additional data for this type of analysis. The critical pressure of limonene and linalool are above 10 MPa but below 15 MPa at 323 and 333 K (Iwai, Hosotani, Morotomi, Koga, & Arai, 1994; Iwai, Morotomi, Sakamoto, Koga, & Arai, 1996). Data for binary CO_2 + limonene (Iwai et al., 1996) and CO_2 + linalool (Iwai et al., 1994) systems, and ternary CO_2 + limonene + linalool system (Morotomi, Iwai, Yamaguchi, & Arai, 1999) was estimated from experimental measurements done by the Iwai-Morotomi-Arai team.

Thus data trends should not be affected by differences in precision and accuracy between experimental measurements. Based on binary solubilities in SC CO_2, the ternary solubility is affected by limonene-linalool interactions in that the solubility of a mixture of 98.5% (w/w) limonene and 1.5% (w/w) linalool should have been closer to that of limonene (weighed average of 31.06 g/kg). The essential oil of oranges is a mixture of pre-

Table 2-1. Comparison of apparent (C_{fo}) and thermodynamic (C_{sat}) solubilites in supercritical CO_2 of different compounds in vegetable substrates. (Continued)

Solute	Substrate	Temperature (K)	Pressure (MPa)	Data points	"Apparent" solubility (C_{fo}, mg/kg)	C_{fo}/C_{sat}	Ref.
Turmerone	Turmeric	313, 323, 333	20, 30, 40	5	1900 - 13000	0.032 – 0.18	(Gopalán et al., 2000)
Bixin	Annatto seeds	313	10 - 35	6	2.7 – 46	1.8 – 12	(Silva et al., 2008)
β-Carotene	Tomato skin	313, 323, 333	9.0 – 26	14	0.034 – 0.39	0.041 – 0.49	(Gomez-Prieto et al., 2002)
β-Carotene	Tomato skin and pulp	313	40	1	7.56	1.75	(Saldaña et al., 2010)
β-Carotene	Crude palm oil	313, 333, 353	14, 22, 30	4	0.13 – 1.6	0.054 – 0.46	(Puah, 2005)
β-Carotene	Carrot	313, 323	12, 15, 20	5	0.29 – 2.92	0.32 – 0.92	(Saldaña et al., 2006)
Lycopene	Tomato skin	313, 323, 333	9.6 - 26.3	10	0.018 – 1.4	0.0041 – 0.022	(Gomez-Prieto et al., 2002)
Lycopene	Tomato skin	343, 353, 363	20, 30, 40, 50	12	1.8 – 57	0.016 – 0.079	(Topal et al., 2006)
Lycopene	Tomato skin and pulp	313	40	1	0.49	0.0088	(Saldaña et al., 2010)

Table 2-1. Comparison of apparent (C_{fo}) and thermodynamic (C_{sat}) solubilites in supercritical CO_2 of different compounds in vegetable substrates.

Solute	Substrate	Temperature (K)	Pressure (MPa)	Data points	"Apparent" solubility (C_{fo}, mg/kg)	C_{fo}/C_{sat}	Ref.
Lycopene	Tomato skin and seeds	323, 333, 343, 353	20, 25, 30, 35, 40	20	7.9 – 23	0.038 – 0.19	(Shi et al., 2009)
α-Tocopherol	Crude palm oil	313, 333, 353	14, 22, 30	8	0.13 – 1.8	$(1.7 – 7.0)x10^{-5}$	(Puah et al., 2007)
Caffeine	Green coffee oil	323, 333, 343	15.2, 24.8, 28.3, 35.2	12	15 – 78	0.0091 – 0.041	(de Azevedo et al., 2008)
Caffeine	Mate tea	343	25.5	1	94	0.026	(Saldaña et al., 1999)
Theobromine	Mate tea	343	25.5	1	4.4	0.66	(Saldaña et al., 1999)
Theophylline	Mate tea	343	25.5	1	0.13	0.0088	(Saldaña et al., 1999)
Boldine	Boldo Leaves	323	60	1	0.0042	$9.2x10^{-7}$	(del Valle et al., 2005)
Capsaicine	Jalapeño peppers	318	36	1	~ 0.12	$\sim 5.2x10^{-5}$	(del Valle et al., 2003)

Table 2-2. Comparison of thermodynamic solubilities of orange essential oil components (limonene, linalool) in supercritical CO_2 in binary, ternary, and complex systems, and apparent solubility in orange peel.

System	Solubility (g/kg)		Reference
	333 K / 10 MPa	323 K / 15 MPa	
SC-CO_2 + limonene	31.15	C.M.*	(Iwai et al., 1996)
SC-CO_2 + linalool	11.65	C.M.	(Iwai et al., 1994)
SC-CO_2 + 98.5% limonene + 1.5% linalool	19.73	-	(Morotomi et al., 1999)
SC-CO_2 + orange essential oil	19.03	C.M.	(Budich & Brunner, 1999)
SC-CO_2 + orange essential oil + orange peel	-	86.75	(Mira, Blasco, Subirats, & Berna, 1996)

* Completely miscible.

dominantly monoterpenes (MTs) hydrocarbons (many, but mostly limonene) and a remainder of oxygenated monoterpenes (OMTs) responsible for its characteristic odour (many, with linalool representing slightly less than half) (del Valle, de la Fuente, Uquiche, Zetzl, & Brunner, 2011). Data of Budich and Brunner (1999) suggests that minor MTs and OMTs do not interact with the main MT and main OMT because of small differences between the solubility of (limonene + linalool) and orange essential oil. Being the critical pressure of the complex CO_2 + orange essential oil system below 13 MPa (Budich & Brunner, 1999), orange essential oil is completely miscible in SC CO_2 at 323 K and 15 MPa. However, the apparent solubility of orange essential oils in their extraction from peels reported by Mira et al. (1996), although large, is finite under those conditions, suggesting a contribution of additional factors to apparent solubility. This manuscript will show that these differences may be due not only to solute-matrix interactions but also to the residual amount of extract in the vegetable substrate.

2.3. Approach

In order to simulate the SCFE process of a substrate, exemplified by a pre-pressed oilseed in this manuscript, authors implemented several mass transfer models based on mass balance equations for thin, differential sections of a packed bed (Appendix A). Authors selected pre-pressed oilseed extraction as a model system because literature contains enough information (predictive tools) to treat this problem in absence of experimental data. The extract (a vegetable oil) can be treated as a single compound, because in most cases vegetable oils are mostly mixtures of triacylglycerol of linear fatty acids having 18 carbon atoms and, for example, the solubility in CO_2 does not depend on the degree of unsaturation or position in the molecule of the fatty acids (del Valle & de la Fuente, 2006). Furthermore, there are correlations for the solubility (del Valle et al., 2012) and diffusivity (Funazukuri, Kong, & Kagei, 2008) of vegetable oils in CO_2 as a function of system conditions based on ample experimental data from several sources. Finally, there are correlations among dimensionless numbers for mass transfer parameters in packed beds operating with SCFs (del Valle & de la Fuente, 2006; del Valle et al., 2011; Puiggené, Larrayoz, & Recasens, 1997) that can be used to estimate values of model parameters.

The microstructure of pre-pressed oilseeds corresponds to a network of interconnected pores that contains all oil originally entrapped in cells because the tissue is completely obliterated by strong shear efforts applied during pre-pressing. The effective diffusivity of oil in this pre-pressed oilseed depends on a microstructural factor (F, Eq. 2.1) (Wakao & Smith, 1962) exhibiting little variation for different oilseeds (del Valle et al., 2006) that depends on their inner porosity. Particle porosity (ε_p), in turn, can be estimated as a function of the residual oil content [$(C_s)_i$] and true density (ρ_s) of the oilseed following pressing, and the density of the oil (ρ_{oil}) using Eq. (2.2), which assumes that the oil fills completely the interconnected pore network resulting from oilseed de-oiling, as it can be observed under the microscope (del Valle et al., 2006).

$$F = \frac{1}{\left(\varepsilon_p\right)^2} \tag{2.1}$$

$$\varepsilon_p = \frac{\rho_s \left(C_s\right)_i}{1000\ \rho_{oil} + \rho_s \left(C_s\right)_i} \tag{2.2}$$

The assumptions of the adopted "predictive" model are typical in SCFE literature: 1) porous spherical particles; 2) constant interstitial velocity of the SC CO_2 in the extraction vessel (packed bed); 3) absence of axial dispersion of solute in SC CO_2 in the packed bed; 4) negligible pressure losses and temperature gradients within the bed; and, 5) constant physical properties of SC CO_2 and the substrate. To accomplish the objectives of the manuscript, authors applied three versions of this predictive model with different assumptions about solute binding and mass transfer constraints. As the initial condition in all cases, authors assumed an equilibrium condition of the oil between the pre-pressed oilseed and SC CO_2 during stabilisation of the temperature and pressure within the extraction vessel (the static extraction period). As the boundary condition, authors assumed that the SC CO_2 stream entering the extraction vessel (during the dynamic extraction period) did not contain oil. The specific assumptions of the three models are as follows (the interested reader can refer to Appendix A for further details):

Model 1 neglects mass transfer resistances and oil binding, so that an instantaneous equilibrium condition establishes where the concentration of the oil in the SC CO_2 within the pores of a particle (intra-particle volume) equals its concentration in the SC CO_2 in the void space between the particle and its neighbours in the packed bed (inter-particle volume). The upper limit of oil concentration in SC CO_2 is its solubility under extraction conditions; excess oil remains condensed within particle pores. This case represents the case of a solute that does not interact with an "inert" matrix, and represents the simplest possible equilibrium partition condition. The resulting linear partition coefficient depends on the ratio between intra- and inter-particle volumes in the packed bed.

Model 2 also neglects mass transfer resistances, but assumes that oil partitions between the pre-pressed oilseed and SC CO_2 according to a sorption isotherm/isobar model (Eq. 2.3). This case represents an interacting solid matrix that affects solute transfer to SC CO_2 depending on its concentration in the substrate. Oil interacts with the pre-pressed oilseed in a way that its liberation is progressively more difficult because of a strengthening of solute-matrix interactions. Model 1 is a special case of Model 2 for a two-

step sorption isotherm/isobar model. The mathematical treatment is different though, as it can be surmised in Appendix (A).

$$C_f^* = f\left(C_s\right) \tag{2.3}$$

Model 3 also assumes equilibrium partition according to a sorption isotherm/isobar, but it includes resistances to mass transfer from pre-pressed oilseed to SC CO_2 phase, both within the particles and in a stationary SCF film surrounding them. The resistance to mass transfer in the SC CO_2 film (or external resistance) depends on a film coefficient (k_f), whereas the resistance in the particle (or internal resistance) depends on the effective diffusivity of the oil (D_e) in pre-pressed oilseed. A further assumption was that flux might be estimated using a Linear Driving Force (LDF) approximation (Eq. 2.4) with a global mass transfer (k_p) and specific surface area (a_s) given for spherical particles by Eq. (2.5) and Eq. (2.6), respectively:

$$J = k_p\left(C_f^* - C_f\right) \tag{2.4}$$

$$k_p = \frac{5\,k_f}{5 + Bi}, \text{ and} \tag{2.5}$$

$$a_s = \frac{6\,\left(1-\varepsilon\right)}{d_p} \tag{2.6}$$

In Eq. (2.5), *Bi* (dimensionless Biot number) describes the ratio between the internal resistance to mass transfer in the substrate and the external resistance to mass transfer in SC CO_2 surrounding the particle, that is defined by Eq. (2.7):

$$Bi = \frac{k_f d_p}{2\,D_e} \tag{2.7}$$

For simulations, authors considered the SC CO_2 extraction of pre-pressed oilseeds at 353 K and 90 MPa. Authors assumed that physical properties of mixtures of SC CO_2 and dissolved oil are not affected by the oil (low solubility assumption), so that they can be estimated using NIST Database (Lemmon, Huber, & McLinden, 2007) for pure CO_2 as a function of extraction temperature and pressure. Estimated values of density (ρ) and

viscosity (μ) at extraction conditions are ρ = 1000 kg/m^3 and μ = 1.20 × 10^{-4} Pa s. The binary diffusion coefficient of the oil (component 2) in CO_2 (component 1) (D_{12} = 2.76 × 10^{-9} m^2/s) was estimated using the correlation of Funazukuri, Toriumi, Yui, Kong, and Kagei (2009). Authors assumed a typical value of residual oil concentration in a pre-pressed oilseed [$(C_s)_i$ = 176.5 g/kg substrate], and used data of del Valle et al. (2006) for pre-pressed rapeseed (ρ_{oil} = 914 kg/m^3, ρ_s = 1366 kg/m^3) to estimate the porosity (ε_p = 0.21, Eq. 2.2) and microstructural factor (F = 25, Eq. 2.1) of the particle. The effective diffusivity of oil in the pre-pressed oilseed (D_e = 2.76 × 10^{-9} m^2/s) was estimated as the fraction of D_{12} and F (del Valle et al., 2006; Funazukuri et al., 2008). The film coefficient (k_f) was estimated using the physical properties (ρ, μ, D_{12}) and superficial velocity (U) of the CO_2 stream, and the particle diameter (d_p) as independent variables using the dimensionless correlation of Puiggené et al. (1997) for forced convection. The solubility of the oil in SC CO_2 (C_{sat} = 97 g oil/kg CO_2) was estimated as a function of extraction temperature and CO_2 density using the correlation of del Valle et al. (2012). The superficial velocity of the CO_2 stream was estimated as a function of the mass flow rate (Q), CO_2 density under process conditions, and cross-sectional area of the extraction vessel. For the packed bed, the inter-particle porosity of a packed bed of regularly spherical particles (ε = 0.36) was adopted (Carman, 1937).

2.4. Results

As a way to fulfil the objectives of the manuscript, mathematical simulations in next sections show that 1) the initial oil content in the pre-pressed oilseed may affect its apparent solubility, 2) oil partition between the pre-pressed oilseed and CO_2 may affect extraction yield, 3) discriminating solute partition effects and mass transfer effects is difficult from integral extraction curves, 4) best-fit parameters from a mathematical model appear adequate only when the model fits reality (assumed and true physical pictures coincide), and 5) best-fitting parameters of inadequate mathematical models applied to laboratory-scale experiments fail simulating large-scale operations.

2.4.1. The initial solute content in the substrate affects its apparent solubility

The effect of initial solute content in a substrate on the apparent solubility in SC CO_2 was analyzed for the SCFE of oil from pre-pressed oilseed particles in a laboratory scale, 3.2 cm-diameter, 12.8 cm-height extractor (length-to-diameter or aspect ratio L/d_E = 4, empty volume V = 100 cm^3). The extraction vessel was fed with 48 g CO_2/min, which resulted in a superficial velocity U = 1 mm/s. If there are no interactions between the oil and the pre-pressed oilseed the equilibrium partition of the oil between the substrate and SC CO_2 depends on the total amount of solute as compared to the fraction SC CO_2 can dissolve. Fig. (2-2A) shows a condition where there is excess oil that remains condensed within a pre-pressed oilseed particle while the SC CO_2 phase (in the intra- and inter-particle space) is saturated with oil, whereas Fig. (2-2B) shows a condition where there is a deficit of oil and the SC CO_2 phase has less oil than a saturated mixture of the two. In the limit between the two conditions, there is no condensed oil within the pre-pressed seed, and the concentration of oil in SC CO_2 corresponds to the solubility of the oil (Eq. 2.8):

$$\left[\varepsilon+\left(1-\varepsilon\right)\varepsilon_p\right]\rho\, C_{sat}=\left(1-\varepsilon\right)\left(1-\varepsilon_p\right)\rho_s C_t \tag{2.8}$$

where C_t is a transition concentration. According to Eq. (2.8), the isotherm/isobar model for a case when there are no solute-matrix interactions is as follows (Eq. 2.9):

$$C_f^* = C_{sat}, \text{ if } C_s \geq \frac{C_{sat}}{K}, \text{ and} \tag{2.9a}$$

$$C_f^* = K\, C_s, \text{ otherwise,} \tag{2.9b}$$

where the linear partition coefficient is given by Eq. (2.10):

$$K=\frac{\left(1-\varepsilon\right)\left(1-\varepsilon_p\right)}{\varepsilon+\left(1-\varepsilon\right)\,\varepsilon_p}\frac{\rho_s}{\rho} \tag{2.10}$$

Fig. (2-3) summarizes the results of the simulations carried out using Model 1 using different initial oil contents in the pre-pressed oilseed. Some curves in Fig. (2-3A) have same initial slopes but reach horizontal asymptotes that depend on the initial oil content in the particles. However, curves in those cases where the initial oil content is not enough to

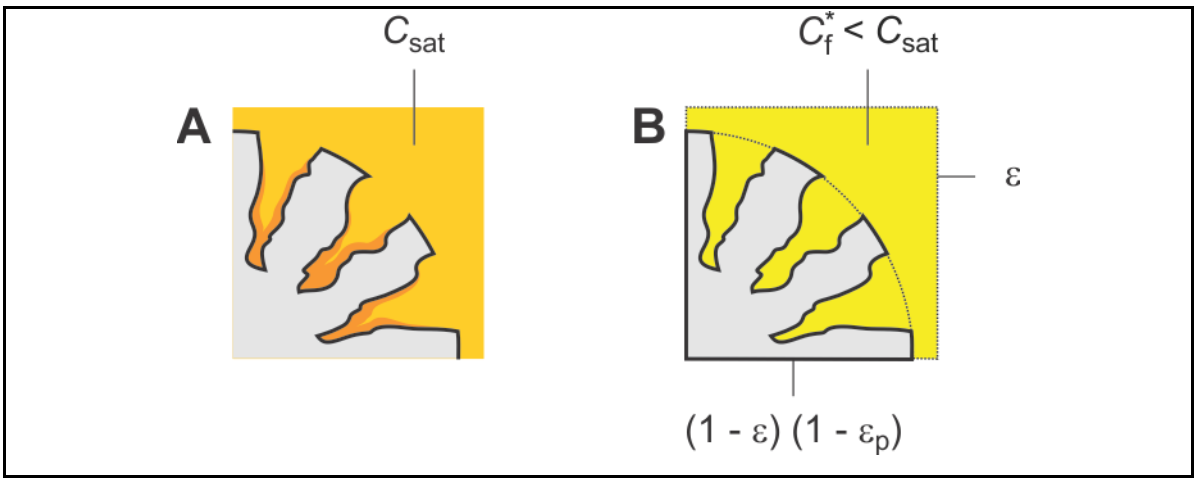

Figure 2-2. Equilibrium partition of oil between supercritical CO_2 an pre-pressed oilseed when there is no interaction between the solutes and the solid matrix in (A) a case where CO_2 cannot dissolve all oil so that there is excess oil deposited in pores and the CO_2 phase is saturated with oil, and (B) a case where CO_2 can dissolve all oil.

saturate the SC CO_2 phase ($C_s < C_{sat}/K$) have different initial slopes (different apparent solubilities) and reach their corresponding horizontal asymptotes for a specific CO_2 consumption that is related to the residence time of SC CO_2 in the extraction vessel.

Fig. (2-3B) shows residual oil concentrations in pre-pressed oilseed particles placed along the packed bed for selected times in the case $C_{so} = 0.8\ C_t$ (pre-pressed oilseeds contain 80% of the oil required to saturate SC CO_2 during the static extraction period). Selected times correspond to 20, 60, and 100% of the residence time of SC CO_2 in the extraction vessel. In this case (when there are no resistances to mass transfer in the SC CO_2 and solid phases) a wave develops in the extraction vessel with a step transition from no residual oil in the pre-pressed oilseed to the initial (equilibration) oil content. In the upstream side of this transition, the oil in the intra-particle space is quickly washed out by the flowing SC CO_2 stream, whereas in the downstream side there is no transfer of oil from the pre-pressed oilseed particles to a SC CO_2 stream having the same oil content as the SC CO_2 stationed in the intra-particle space. Reverchon and Marrone (1997) observed a step transition similar to the one in Fig. (2-3B) when using an equilibrium model with constant equilibrium partition.

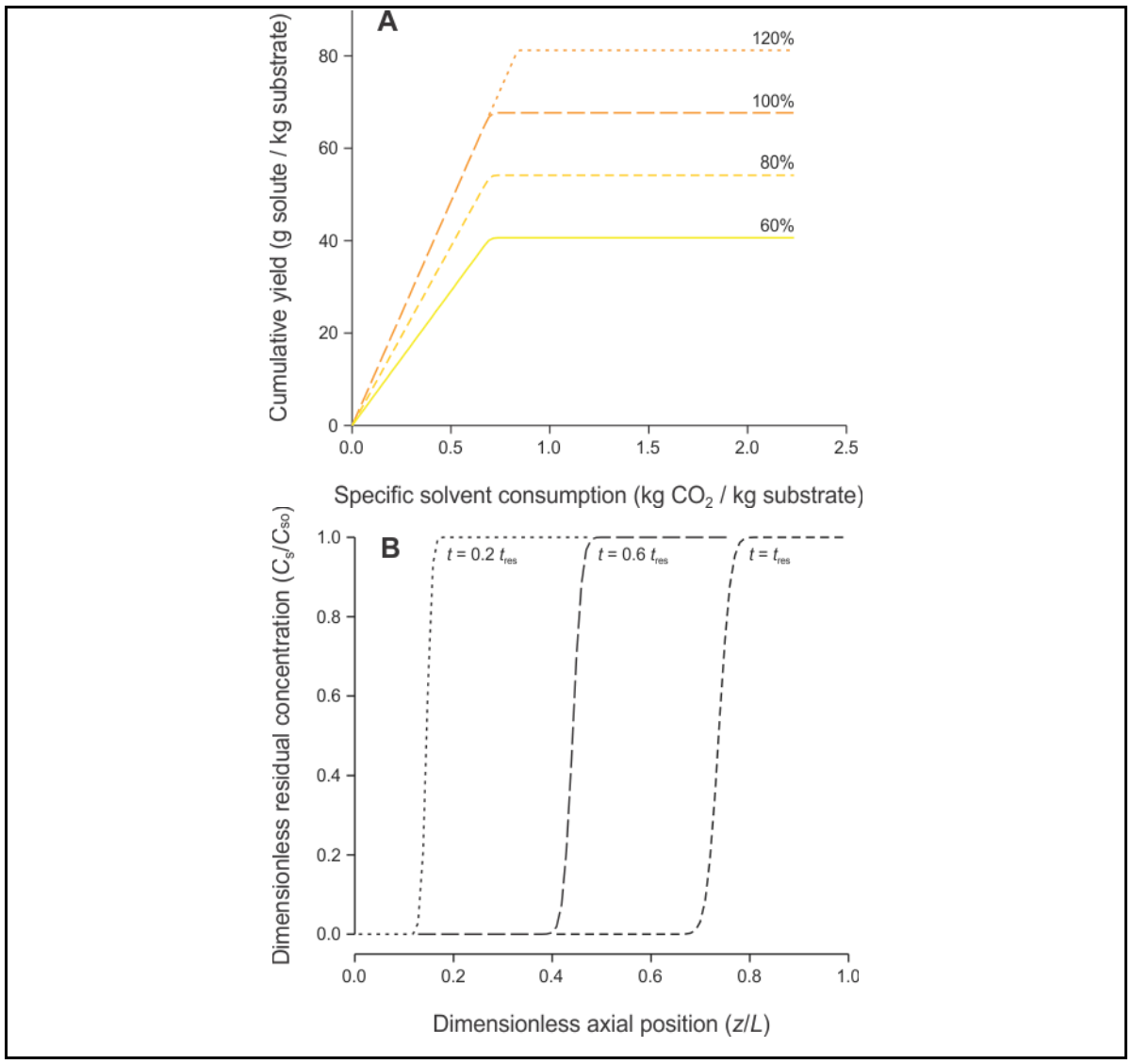

Figure 2-3. (A) Effect of initial oil content in pre-pressed oilseed on integral extraction curves with supercritical CO_2 at 353 K and 90 MPa. The initial solute content is expressed as a percentage of the amount required to saturate the CO_2 during the static extraction period (60% indicates that the oilseed contains 60% of the oil required to saturate CO_2). (B) Effect of dynamic extraction time on residual oil concentration profiles oil in pre-pressed oilseed along the extraction vessel for the 60% curve in Fig. (2-3A). Times are expressed as a fraction of the residence time of supercritical CO_2 in the extraction vessel (0.6 t_{res} corresponds to 60% of U/L).

Based on these results as the reference extraction condition for comparison in sections 2.4.2 and 2.4.3, authors selected an equilibrium condition of the system at the end of the static extraction period given by $C_{fo} = 0.375 \times C_{sat}$ (g oil/kg CO_2) and C_{so} = 25.4 g oil/kg oilseed, or approximately the condition noted 80% in Fig. (2-3). [Note: C_{so} differs from the initial oil content in pre-pressed oilseed, $(C_s)_i$ = 44.4 g/kg, because part of the oil dissolves in SC SCO_2 so that it reaches a concentration corresponding to 37.5% of the solubility of the oil in CO_2 under process conditions.]

For a vegetable substrate containing a limited amount of high-solubility extract (*e.g.*, essential oils in herbs and spices) that does not interact with the solid matrix, the apparent solubility in weigh-to-volume units is, based on Eq. (2.8), given by Eq. (2.11):

$$C_f^* \rho = \frac{(1-\varepsilon)(1-\varepsilon_p)}{\varepsilon + (1-\varepsilon)\ \varepsilon_p} C_{so} \rho_s \qquad (2.11)$$

Given that the right-hand side of Eq. (2.11), or the modified apparent solubility (unlike the apparent solubility in a weight-by-weight basis defined in Fig. 2-1), is a constant that depends only on properties of the vegetable substrate (ρ_s, ε_p, C_{so}) and packed bed (ε), plotting cumulative yield *versus* specific CO_2 consumption in a volume-by-weigh basis (modified integral extraction curve) would result in curves having same modified apparent solubility values in cases of substrates with limited solute content and no solute-matrix interactions. This is exemplified in Fig. (2-4), which shows integral extraction curves for the SC CO_2 extraction of ginger oleoresin at 293 - 313 K and 15 - 25 MPa (Martinez, Monteiro, Rosa, Marques, & Meireles, 2003). Fig. (2-4) suggests that the oleoresin content in ginger does not depend on system temperature for extractions at 15 MPa nor on extraction temperature for extractions at ≥20 MPa, and that all extract components are fully miscible in SC CO_2 and do not interact with the vegetable substrate. Indeed there is proportionality between $C_{fo}\rho$ (the slope of the modified integral extraction curves) and C_s (the horizontal asymptote of the modified integral extraction curve) (cf. Eq. 2.11).

An expected solubility (C_f^*, Eq. 2.9b) can be estimated and compared with the true apparent solubility (C_{fo}) with coincidence between the two giving support to the hypothesis of no-interaction between the solutes in the extract and the solid matrix. However, it is dif-

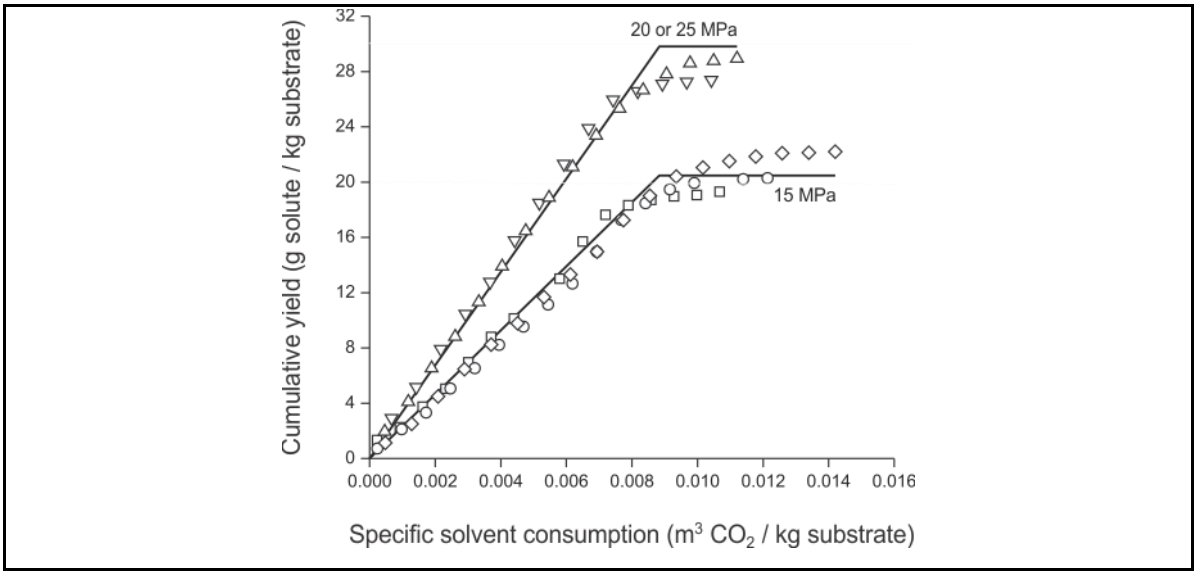

Figure 2-4. Modified integral extraction curve of cumulative essential oil yield *versus* specific solvent consumption in a volume-by-weight basis for the extraction of ginger using high-pressure (near- and super-critical) CO_2 at (□) 293 K and 15 MPa, (○) 303 K and 15 MPa, (◇) 313 K and 15 MPa, (▽) 313 K and 20 MPa, and (△) 313 K and 25 MPa. Adapted data from Martinez et al. (2003).

ficult to estimate C_f^* using Eq. (2.9b) and Eq. (2.10) because few experimental studies report values of ρ_s, ε_p, and ε, such as the one of Spricigo, Bolzan, Machado, Carlson, and Petrus (2001). Other studies report values from which ρ_s, ε_p, and ε can be estimated. For example, when the true density of the vegetable substrate and total porosity (ε_t, Eq. 2.12) of the bed are reported (Machmudah, Sulaswatty, Sasaki, Goto, & Hirose, 2006; Sovová, Komers, Kucera, & Jez, 1994) the intra-particle porosity can be estimated using Eq. (2.13):

$$\varepsilon_t = \varepsilon + (1-\varepsilon)\ \varepsilon_p, \text{ and} \tag{2.12}$$

$$\varepsilon_p = \frac{\varepsilon_t - \varepsilon}{1-\varepsilon} \tag{2.13}$$

In absence of inter-particle porosities, authors of this manuscript estimated them as a function of the sphericity (Ψ) of the particles using values plotted by Brown et al. (1950). Ψ , the ratio of the surface of a sphere having the same volume of the particle, to the actual

surface of the particle, can be estimated using Eq. (2.14), where α is an aspect or height-to-diameter (Eq. 2.15) ratio that depends on the thickness (δ) of disk-shaped, milled leaf particles.

$$\Psi = \frac{(1.5\,\alpha)^{2/3}}{\alpha + 0.5}, \text{ and} \tag{2.14}$$

$$\alpha = \frac{\delta}{d_p} \tag{2.15}$$

We applied Eq. (2.15) assuming δ = 300 μm in those cases where coarsely milled leaf particles are extracted (Coelho et al., 1997; Machmudah et al., 2006). In the cases (Martínez, Rosa, & Meireless, 2007; Sousa et al., 2002; Sousa et al., 2005; Sovová et al., 1994), where fine fractions are separated by sieving (sieve openings smaller than 300 μm) we assumed α = 1. When the bulk (ρ_b) and true densities of the substrate are reported (Martínez et al., 2007; Sousa et al., 2002; Sousa et al., 2005), total porosity can be estimated using Eq. 2.16, and then the previous procedure used to estimate ε_p:

$$\varepsilon_t = 1 - \frac{\rho_b}{\rho_s} \tag{2.16}$$

Finally, in the case where ρ_b and ε are reported (Coelho et al., 1997), ρ_s can be estimated using Eq. (2.17), then ε_t can be estimated as a function of ρ_b and ρ_s using Eq. (2.16), and finally ε_p can be estimated as a function of ε_t and ε using Eq. (2.13):

$$\rho_s = \frac{\rho_b}{1 - \varepsilon} \tag{2.17}$$

Fig. (2-5) shows that expected solubilities are within a band of the actual apparent solubilities with discrepancies within a factor of 4. Despite this relatively large discrepancies, considering the limitations of the experimental data and of our simplifying assumptions, it is reasonable to claim that extracts of herbs and spices containing a limited amount (from *ca.* 0.7% w/w for rosemary to 15% w/w for clove) of high-solubility essential oil (monoterpenes are fully miscible in SC CO_2 above ca. 10 MPa) are completely

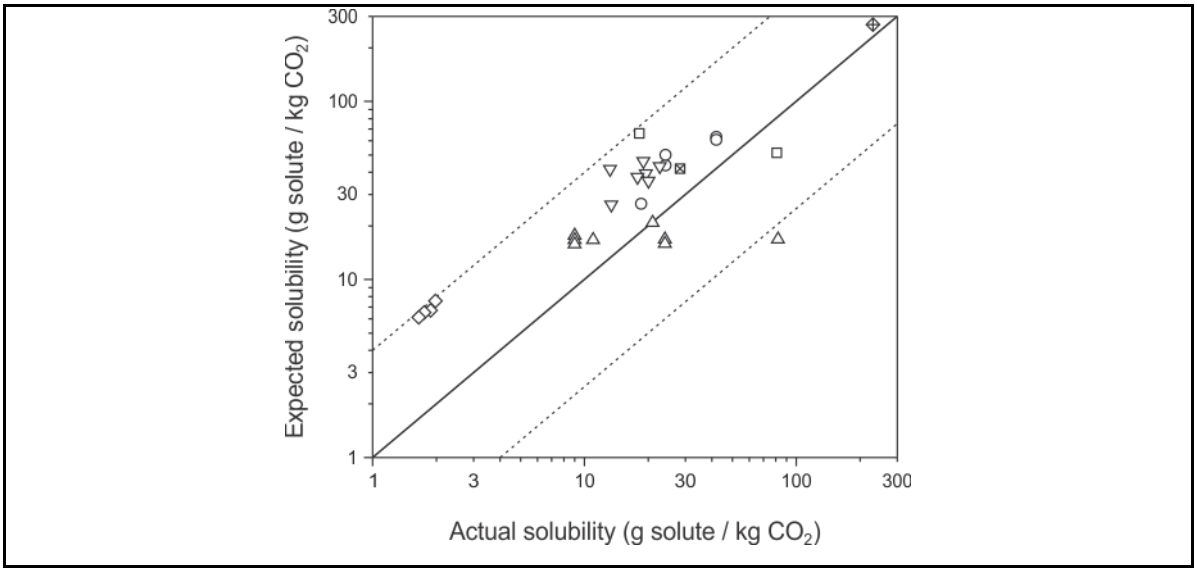

Figure 2-5. Relationship between actual (C_{fo}) and expected (C_f*) apparent solubilities of essential oils from herbs and spices extracted using high-pressure (near- and super-critical) CO_2, where values of C_f* were estimated using Eq. (2.11) by assuming there were no interactions between extracts and the solid matrices. Literature data corresponds to the extraction of (○) nutmeg seed particles ($0.300 \leq d_p \leq 1.45$ mm) at 296 K and 9 MPa (Spricigo et al., 2001), (△) nutmeg seed particles ($0.556 \leq d_p \leq 2.12$ mm) at 313-323 K and 10-20 MPa (Machmudah et al., 2006), (□) 383-μm caraway seed particles at 313 K and 9 or 10 MPa (Sovová et al., 1994), (◇) 720-μm rosemary bract particles at 308 or 313 K and 10 or 12.5 MPa (Coelho et al., 1997), (▽) 375-μm *Lippia sidoides* leaf particles at 282-298 K and ca. 7 MPa (Sousa et al., 2002), (⊠) 520-μm *Croton zehnteri* leaf particles at 288 K and 6.7 MPa (Sousa et al., 2005), and (⊕) 860-μm milled clove bud particles at 298 K and 10 MPa using extraction vessels of two sizes (Martínez et al., 2007).

dissolved in SC CO_2 under process conditions, and do not interact with the vegetable substrate to a large extent. Discrepancies between estimated and actual values of the apparent solubility, that are related to distances of experimental points to the continuous diagonal line in Fig. (2-5), can be also due to eventual interaction between the essential oils and the cellular matrix of the herb or spice.

2.4.2. Solute partition between the substrate and supercritical CO_2 affects extraction yield

Pre-treated vegetables are complex matrices that may interact with extract components so as to establish thermodynamic constraints to their release to the SC CO_2 phase. Consequently, several authors included solute-matrix interactions, in the form of sorption isotherm/isobar models (Eq. 3) in modelling SC CO_2 extractions of vegetable substrates.

Typically the applied mass transfer models are adaptations of others describing adsorptive separations. Daghero, Ruetsch, Zacchi, and Mattea (2004) and Salimi, Fatemi, Nei, and Safaralie (2008) used Langmuir's isotherm to describe the SC CO_2 extraction of clove buds and valerian roots, respectively. Langmuir (1916) assumed a monolayer coverage of the solid matrix (the adsorbent) with solute, which imposes a constraint to the maximal amount of solute in the substrate (C_m) depending on its specific surface, and Daghero et al. (2004) arbitrarily assumed that all essential oils in clove where contained in such a monolayer. Both Daghero et al. (2004) and Salimi et al. (2008) placed an upper limit, corresponding to the saturation of SC CO_2 with extract under process conditions, to the validity of Langmuir's sorption model. To account for S-shaped sorption isotherm/isobar for low solute contents Salimi et al. (2008) applied the Langmuir-Freundlich's or so-called Sips' (Sips, 1948) modification of Langmuir's sorption isotherm/isobar to correlate experimental data on SC CO_2 extraction of valerian roots. This manuscript uses a pseudo-Sips' sorption model (Eq. 2.18) by interchanging solute concentrations in the fluid (C_f^*) and solid (C_s) phases to account for a solubility-limited upper concentration of solute in the SC CO_2 phase and unlimited concentration of solute in the solid phase (determined by substrate composition):

$$\frac{C_f^*}{C_{sat}} = \frac{(C_s)^n}{A + (C_s)^n} \tag{2.18}$$

Fig. (2-6) shows the effect of pseudo-Sips'-type sorption on integral extraction curves of oil from pre-pressed oilseed. Four sorption isotherms/isobars were selected with the first one starting in the same point and with the same slope as the linear isotherm/isobar

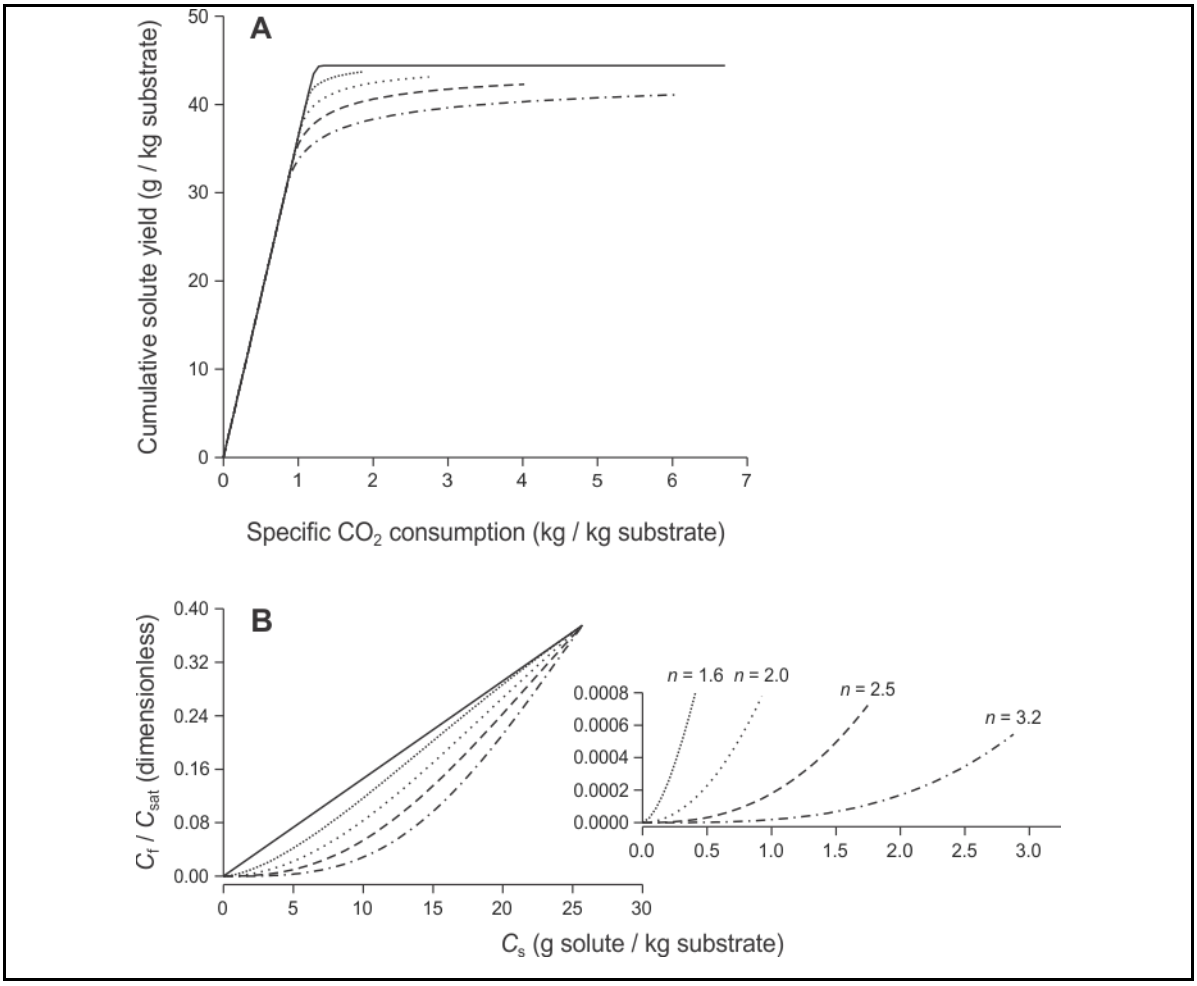

Figure 2-6. (A) Effect of sorption parameters on integral extraction curves of oil in pre-pressed oilseed using supercritical CO_2 at 353 K and 90 MPa, when sorption follows pseudo-Sip's model. (B) Corresponding sorption isotherm/isobar for the partition of oil between pre-treated oilseed and supercritical CO_2 at 353 K and 90 MPa (insert provides a detailed view of the initial slopes of the sorption isotherms/isobars).

of the reference curve. Values of parameters in Eq. (2.18) were A = 300 and n = 1.6 under these conditions. Values of n for the three additional isotherms were arbitrarily set to 2.0, 2.5, and 3.2, and values of A were calculated so that all included the common point C_{so} = 25.4 g solute/kg substrate and C_{fo} = 36.4 g oil/kg CO_2 (C_{fo}/C_{sat} = 0.375) (Fig. 2-6B). Integral extraction curves for the four pseudo-Sips' sorption isotherms/isobars differ in horizontal asymptotes that move down as the value of n increases (Fig. 2-6A). This is due to the shape of pseudo-Sips' isotherms/isobars for low oil contents that are characterized

by a null initial slope ($dC_f^*/dC_s = 0$ for $C_s \rightarrow 0$); for a *n*-dependent solute content there is virtually no oil being transferred to CO_2. The apparent oil content is defined by the equilibrium concentrations corresponding to $C_f \sim 0.07$ g oil/kg CO_2 in Fig. 6B (*cf.* insert) that cannot be practically extracted by SC CO_2 under process conditions, and consequently defines the apparent oil content in the pre-pressed oilseed or horizontal asymptote of integral extraction curves simulated using Model 2 (Fig. 2-6A). The integral extraction curve reaches only 99.0% of the true oil content for $n = 1.6$, and this value decreases to 97.8% for $n = 2.0$, 96.0% for $n = 2.5$, and 93.4% for $n = 3.2$. In conclusion, pseudo-Sips' sorption model can be used in cases where there is a fraction of strongly bound solutes that are not practically released from a solid matrix in the final stages of a SCFE process.

There are some manuscripts in literature aimed at isolating the influence of the substrate on the extraction process for analytical purposes. Björklund, Jaremo, Mathiasson, Jonsson, and Karlsson (1998), for instance, studied the interaction of dihydropyridine with "allegedly inert materials," and found differences in total yield using SC CO_2 at 313 K and 13.4 MPa [slightly less for glass than Stainless Steal (SS) beads, and 68.5 and 12.1% of the yield for SS beads for sea sand and filter paper, respectively], which in the case of filter paper they attributed to hydrogen bonding of dihydropyridine to hydroxyl groups in cellulose. In the case of SC CO_2 extraction of vegetable substrates there have been some unsuccessful attempts in literature to identify solute-matrix interactions affecting yield. Subra, Castellani, Jestin, and Aoufi (1998) compared the extraction of β-carotene impregnated in synthetic (glass and silica) particles and in lyophilized carrot particles of different sizes at 330 K and 17.6 or 25 MPa, but no claims about irreversible sorption can be made because yields were not reported as percentages of total β-carotene in glass and silica. Because β-carotene adsorbs in silica gel from *n*-hexane solution (Ahmad, Chan, Abd Shukor, & Mashitah, 2009), partial extraction of β-carotene in 105-μm silica particles would be expected, unlike in the case of β-carotene in 300-μm glass beads. Ambrogi, Cardarelli, and Eggers (2002) compared the SC CO_2 extraction (333 K and 30 MPa) of a vegetable-oil emulsion of β-carotene impregnated in glass beads, paprika oleoresin impregnated in glass beads, and paprika powder particles but did not report carotenoid yields as percentages of the total in the first two cases. However, because reported yields

were 100% in the case of paprika oleoresin in the power (200-μm particles), irreversible binding can be discarded in this case (Ambrogi et al., 2002).

Other manuscripts in literature on SC CO_2 extraction of vegetable substrates showed differences in yield depending on substrate pre-treatment but experimental results did not show convincingly that these differences were due to solute-matrix interactions. An alternative explanation for these differences in apparent solute content was solute confinement in impervious pockets. This is reasonable to expect in biological materials containing cells that, in the case of microbial and vegetable substrates, are surrounded by cells walls. This claim is supported by the common experimental observation that it is nearly impossible to extract oil from un-cracked colza seeds, peanut halves, and coriander halves (Catchpole, Grey, & Smallfield, 1997; Goodrun, Kilgo, & Santerre, 1996; Stahl, Schutz, & Mangold, 1980). Because milling breaks and releases solutes from surface cells, moderate milling (to large sizes, corresponding to several layers of cells in parenchymatous tissue) should leave intact cells in inner tissue portions so that a particle-size-dependent yield would be observed if the cells walls are impervious to SC CO_2. Subra et al. (1998), for instance, found differences in the apparent carotenoid content of freeze-dried carrot particles milled to different mean diameters (from ≤ 250 μm to 1 mm), with higher values being associated to smaller particles, as expected. This was not the case, however, in a study of Marrone, Poletto, Reverchon, and Stassi (1998) using milled almond seeds that released the same amount of oil independently of particle size. Femenia, Garcia-Marin, Simal, Rossello, and Blasco (2001) critically assessed the hypothesis that cell walls are impervious to SC CO_2 by measuring compositional changes in cell walls of almond seeds as a function of extraction time at 50 °C and 33 MPa. After removing 33% of oil only pectic and hemicellulosic components were modified, but after removing 67% of the oil cellulose suffered chemical changes as well. Light microphotographs showed that these chemical changes increased the porosity of cell walls, thus allowing the extraction of fatty acids. Alternatives to milling exist that do not rely solely on particle size reduction to rupture cell walls and thus result in a particle-size-independent SC CO_2 extraction yield. As examples, pre-pressing, flaking, and pelletizing rupture cell walls throughout the tissue by relying on strong shear stresses (del Valle et al., 2006). Cells can explode as a result of

a violent pressure release with the end result of an increase in the porosity and a release of irreversibly confined solute from different vegetable substrates, including whole soybeans (Rochova, Sovova, Sobolik, & Allaf, 2008).

Another popular sorption model is the BET (Brunauer-Emmett-Teller) equation (Eq. 2.19) that corrects Langmuir's model by considering sorption of solute in several layers with interactions weakening as the distance to the surface increases (Brunauer, Emmett, & Teller, 1938):

$$\frac{C_s}{C_m} = \frac{K C_f^* / C_{sat}}{\left[1 - C_f^* / C_{sat}\right]\left[1 + (K-1) C_f^* / C_{sat}\right]} \tag{2.19}$$

Goto, Roy, Kodama, and Hirose (1998) and Ruetsch, Daghero, and Mattea (2003) used BET's equation to model solute-matrix interactions during SC-CO_2 extraction of peppermint leaves and clove buds, respectively. A strength of the BET model (Eq. 2.19) as compared to the pseudo-Sips' model (Eq. 2.18) is that it places an upper limit to the maximal concentration of the solute in the SCF phase that depends on its solubility (*i.e.*, it does not require an arbitrary exchange of C_f^* by C_s). A limitation, on the other hand, is that is an implicit equation for the dependent variable (C_f^*).

Fig. (2-7) shows the effect of BET-type sorption on integral extraction curves of oil from pre-pressed oilseed. The same as in the previous case for pseudo-Sips'-type sorption, four isotherms were selected with the first one starting in the same point and with the same slope as the linear isotherm of the reference curve. Values of parameters in Eq. (2.19) were C_m = 21.2 and K = 5 under these conditions. Values of K for the three additional isotherms were arbitrarily set to 9, 17, and 33, and values of C_m were calculated so that all included the common point C_{so} = 25.4 g oil/kg substrate and C_{fo} = 36.4 g oil/kg CO_2 (Fig. 2-7B). Extraction rate decreased as a result of progressively stronger oil binding associated with an increase in the value of K. However, unlike in the case of pseudo-Sips'-type sorption, where there was a sorption-dependent apparent oil content in the pre-pressed oilseed (Fig. 2-6A), in this case extraction yields reached a common horizontal asymptote for C_s = 44.4 g oil/kg substrate (Fig. 2-7A). This binding-independent apparent oil content is due to the fact that the BET isotherm has a positive (no-null) slope throughout, including for very low

oil contents in the substrate (Fig. 2-7B), which results in non-negligible extraction rates up to removing all oil from the pre-pressed oilseed.

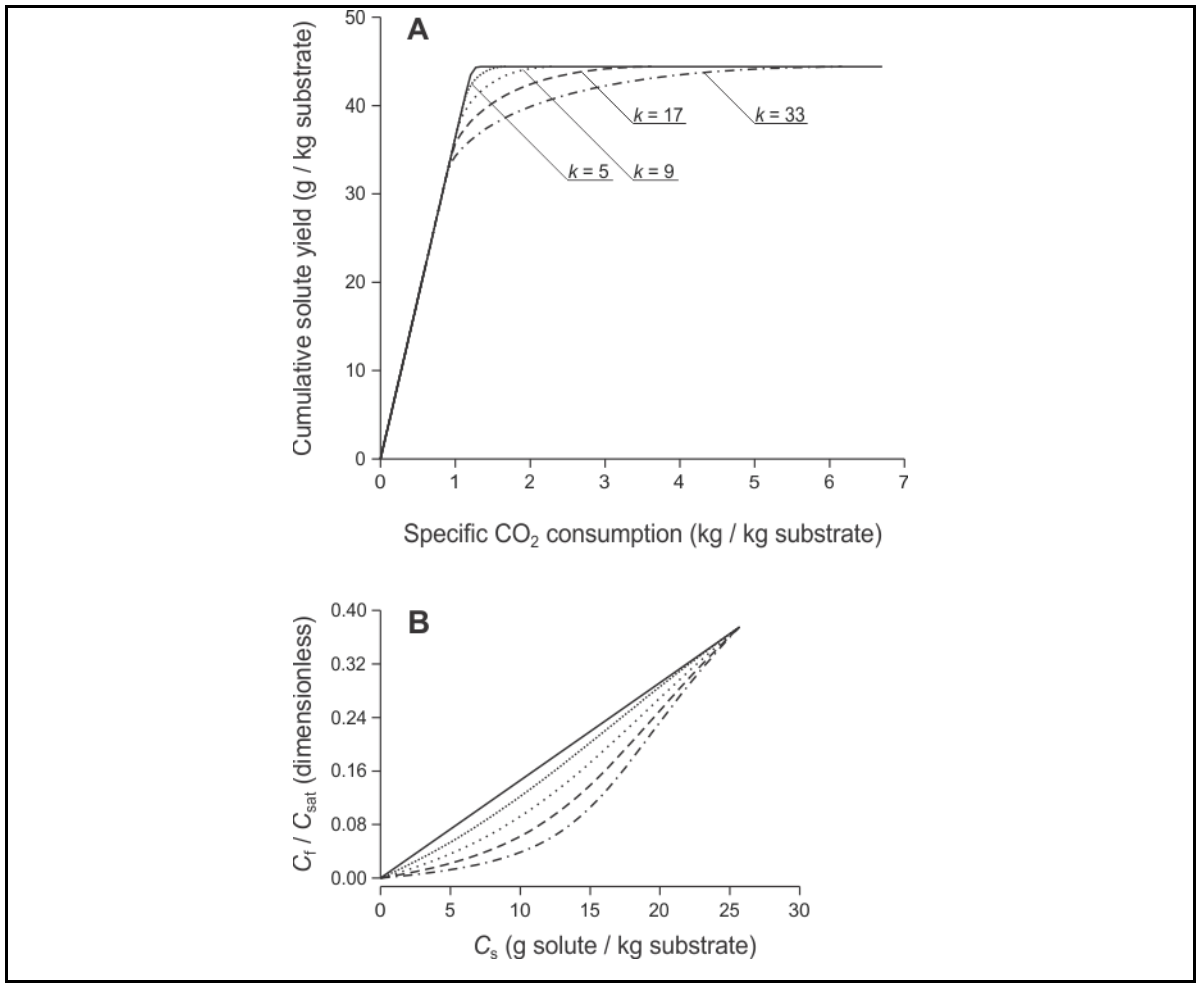

Figure 2-7. (A) Effect of sorption parameters on integral extraction curves of oil in pre-pressed oilseed using supercritical CO_2 at 353 K and 90 MPa, when sorption follows BET's model. (B) Corresponding sorption isotherm/isobar for the partition of oil between pre-treated oilseed and supercritical CO_2 at 353 K and 90 MPa.

2.4.3. Discriminating solute partition and mass transfer effects is difficult from integral extraction curves

In this case, unlike those in which mass transfer is defined by equilibrium partition of the solute between the substrate and SC CO_2, solute diffusion in the solid matrix limits mass transfer, and additional parameters such particle size affect solute flux from the solid to SC CO_2 phase.

Fig. (2-8) shows integral extraction curves simulated with Model 3 using a constant partition coefficient (K = 1.43 kg substrate/kg CO_2) together with the–reference curve in sections 2.4.1 and 2.4.2. The same as in section 2.4.2, initial conditions were set to C_{so} = 25.4 g oil/kg substrate and C_{fo} = 36.4 g oil/kg CO_2. Using a linear partition relationship allowed us isolating the effect of mass transfer resistances on the integral extraction curve. For comparison purposes, authors arbitrarily changed particle diameter (d_p = 0.70, 0.55, 0.40, or 0.25 mm) to change values of *Bi*. Increases in *Bi* markedly decreased extraction rates in the transition zone (II, Fig. 2-1) of integral extraction curves (Fig. 2-8A) as observed by others before (Björklund et al., 1998; del Valle, Napolitano, & Fuentes, 2000).

There is ample literature on kinetic effects on SC CO_2 extraction rates of several process variables including some associated with the solvent and affecting external resistance to mass transfer, such as superficial SC CO_2 velocity, others associated with the substrate and affecting internal resistance to mass transfer, such as substrate pre-treatment and particle size, and others associated with the transport properties in the two phases and affecting both resistances, such as extraction temperature and pressure. For brevity authors will refer only to some of the studies discussed in connection with sorption effects in section 2.4.2. Björklund et al. (1998) isolated the effect of the inner mass transfer resistance by loading lubricating oil into a hole drilled along the axis of an aluminium rod placed upright in a 7-cm^3 extraction vessel, and extracting the oil with 0.5-4.0 cm^3/min of SC CO_2 at 313 K at 28.1 MPa ($0.062 \leq U \leq 0.65$ mm/s, estimated assuming a typical aspect ratio of the extraction vessel between 4 and 6). Björklund et al. (1998) concluded that the extraction of the oil in this model system was a diffusion-controlled process because extraction rate depended on extraction time (and not on specific CO_2 consumption; extraction rate was the largest when extraction-vessel volumes swept during the 2-h

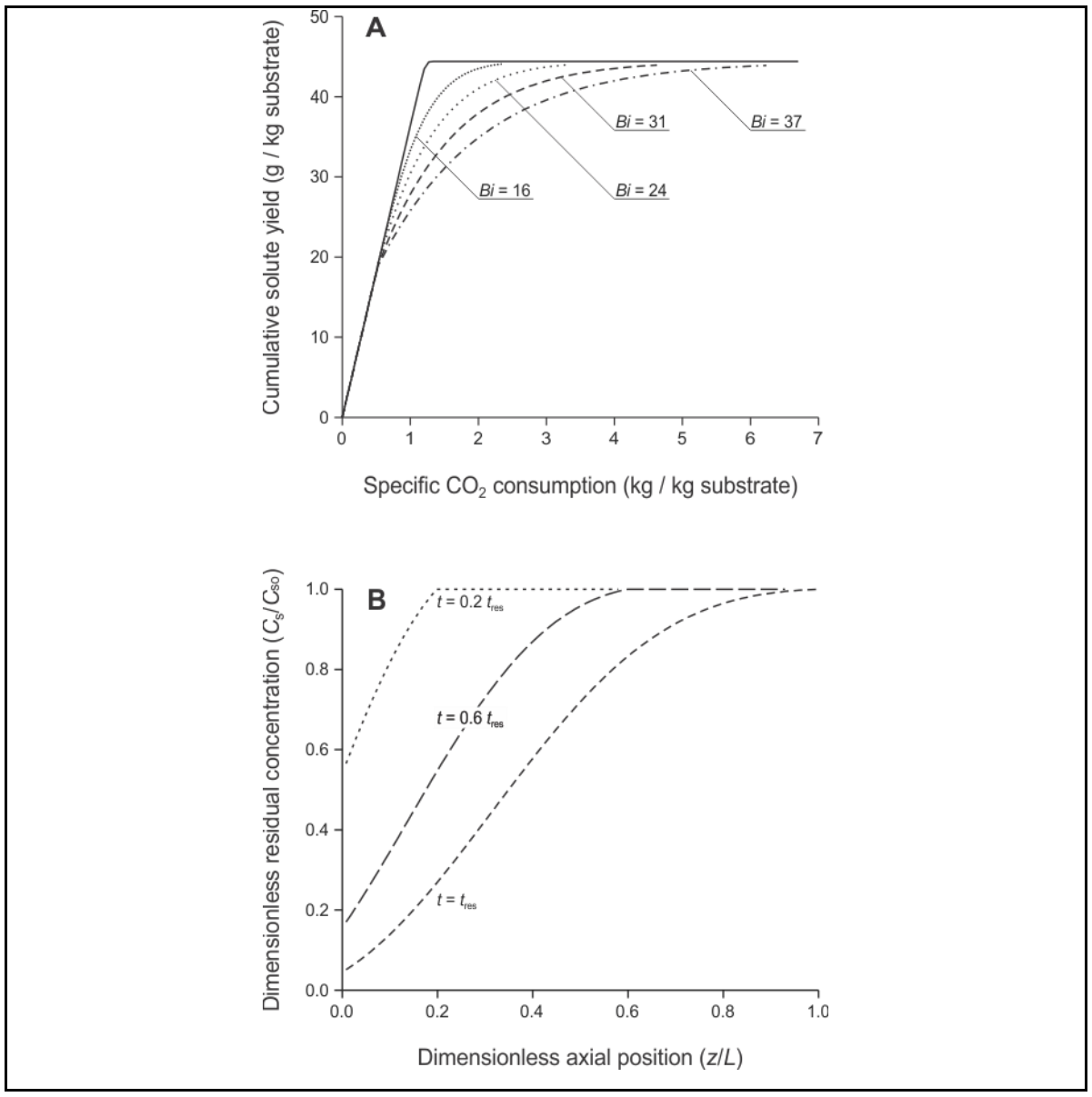

Figure 2-8. (A) Effect of inner mass transfer on integral extraction curves of oil in pre-pressed oilseed using supercritical CO_2 at 353 K and 90 MPa. The ratio between the internal and external resistance to mass transfer, which is characterized by Biot's number was modified by changing particle diameter: 0.25 mm for *Bi* = 16; 0.40 mm for *Bi* = 24; 0.55 mm for *Bi* = 31; and, 0.70 mm for *Bi* = 37. (B) Effect of dynamic extraction time on residual concentration profiles of oil in pre-pressed oilseed along the extraction vessel for the *Bi* = 16 curve if Fig. (2-3A). Times are expressed as a fraction of the residence time (t_{res}) of SC-CO_2 in the extraction vessel.

extraction were the lowest). Ambrogi et al. (2002) found that SC CO_2 extracted paprika oleoresin faster from impregnated glass beads than paprika powder (the initial, solubility-controlled extraction period was shorter) and claimed differences were due to additional resistances mass transfer within the powder.

Fig. (2-9) re-plots integral extraction curves simulated using Model 2 for BET's equation (curve for K = 17 in Fig. 2-7A) and using Model 3 for constant partition coefficient (curve for Bi = 16 in Fig. 2-8A) and shows that the two are qualitatively similar (with differences not larger than typically observed as a result of random errors in SCFE experiments). This highlights difficulties in ascertaining if an integral extraction curve is consistent with restrictions to mass transfer in the substrate imposed by equilibrium constraints (Model 2), kinetic constraints (Model 3), or a combination of the two. Additional constraints may negatively affect SC CO_2 extraction rates, as observed in the case of β-carotene-impregnated glass beads by Subra et al. (1998). These authors reported a departure from a reference curve for $Bi \rightarrow 0$ (what is expected in a case where only equilibrium partition and external mass transfer resistance affect extraction rate) similar to the ones observed in Fig. (2-8A) for larger values of Bi, which they explained by a decrease in specific surface area for mass transfer associated with shrinkage of the area on glass beads covered with β-carotene. (Subra et al. (1998) made observations under a microscope to support this claim.)

According with Fig. (2-9A), it would be difficult to discriminate between equilibrium partition and mass transfer effects to explain integral extraction curves obtained experimentally without additional evidence supporting either one. Fig. (2-9B), however, shows large quantitative differences between residual concentration profiles predicted by Model 2 (using BET's isotherm) and Model 3 (using a LDF hypothesis) even at a time in zone II where there is coincidence in the yield (noted by circle in Fig. 2-9A).

Consequently, although most SCFE models predict similar smooth integral extraction curves (Brunner, 1994), residual concentration profiles may show differences, and experimental determination of these residual concentration profiles, although difficult (Brunner, 1994; Lee, Bulley, Fattori, & Meisen, 1980; Stahl et al., 1980), may help ascertaining the factor (equilibrium partition or mass transfer) contributing the most to

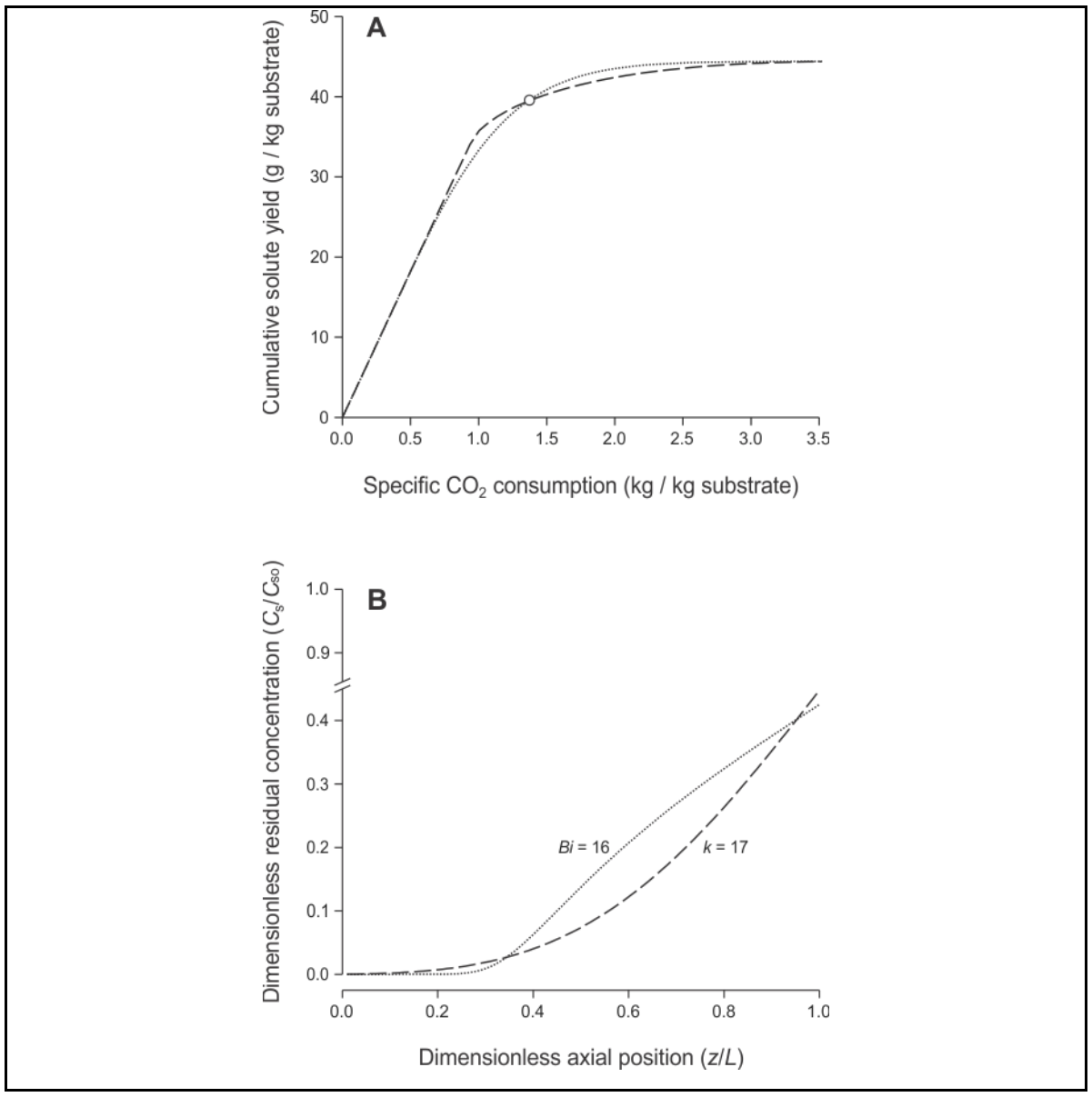

Figure 2-9. Comparison between the curve for K = 17 in Fig. (2-6A) (equilibrium partition defined by BET's sorption model and no resistance to mass transfer) and Bi = 16 in Fig. (2-8A) (equilibrium partition defined by a linear sorption model, Eq. (2.9b), and resistance to mass transfer): (A) Integral extraction curves. (B) Residual concentration profiles of oil in pre-pressed oilseed along the extraction vessel for the time note (symbol) in Fig. (2-9A).

reductions in extraction rate during SC CO_2 extraction of vegetable substrates (del Valle et al., 2000). It is worth mentioning here that sorption effects analysed in section 2.4.2

resulted in residual concentration profiles between those in Fig. (2-2B) and Fig. (2-8B) (unreported results).

2.4.4. Best-fit parameters from a mathematical model are adequate only when the model fits reality

To explore the effect of the mathematical model on best-fit parameters authors fitted synthetic data. Synthetic data was generated using Model 3 for 0.55-mm particles containing 44.4 g oil/kg substrate. Fig. (2-10) shows data generated using pseudo-Sips' sorption model for n = 2.5 and A = 5410, as well as a best fitting curve obtained using Model 3 but with a constant partition coefficient. Values of apparent solubility of the oil (C_{fo}) and apparent oil content of the pre-pressed oilseed (C_s) were estimated from inspection of synthetic data as the initial slope and horizontal asymptote in the integral extraction curve. C_{so} was then estimated by subtracting from C_s the amount of oil transferred to SC CO_2 during the static extraction period. Finally, K was estimated as the ratio C_{fo} / C_{so}. Model 3 was then used having Bi as the single adjustable parameter, and D_e was subsequently estimated from the best-fit value of Bi using Eq. (2.4). Fig. (2-10A) superimposes the synthetic data to the best-fitting curve, and shows excellent agreement between the two, with discrepancies no larger than those commonly associated with random errors in SCFE experiments. However, Table (2-3) shows differences between best-fitted and true values of model parameters. Furthermore, Fig. (2-10B) shows large discrepancies between assumed and true values of the oil partition coefficient.

Fig. (2-11) shows excellent agreement between synthetic data generated using Model 3 with BET's sorption model (K = 17 and C_m = 17.42) and the best-fitting curve obtained using Model 3 with constant partition coefficient. As in the previous case, C_{fo}, C_s, and K were estimated by inspection of synthetic data in the integral extraction curve, and D_e was best-fitted to the synthetic data using Model 3. As before, Table 2-3 shows differences between best-fitted and true values of model parameters, and Fig. (2-11B) shows large discrepancies between assumed and true values of the oil partition coefficient.

Best-fitting values of C_{fo}, C_s, and D_e assuming constant partition coefficient are smaller than values used in simulations of Model 3 with pseudo-Sips' or BET's sorption

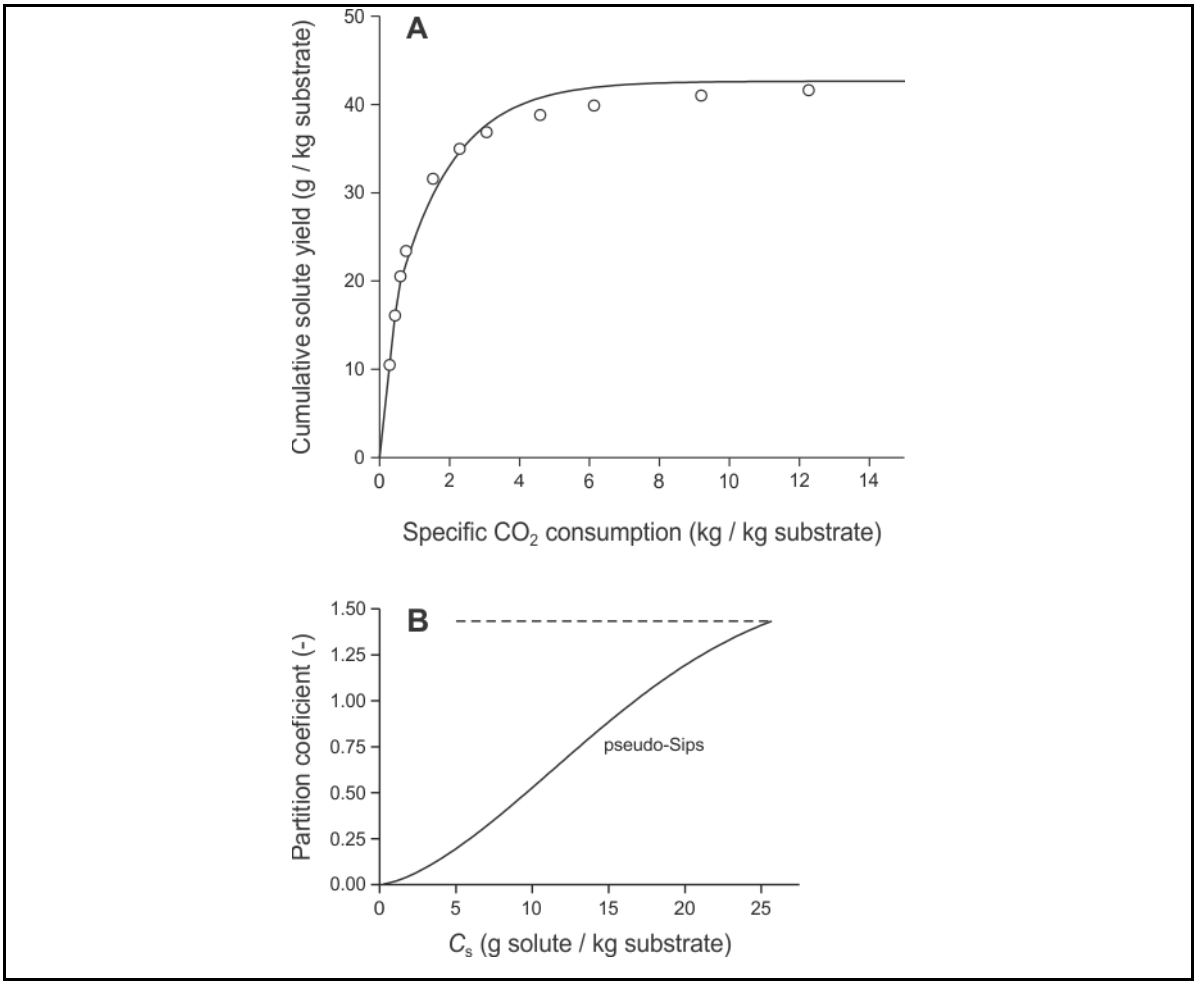

Figure 2-10. (A) Comparison between assumed (symbols) and best-fitted integral extraction of oil in pre-pressed oilseed using supercritical CO_2 at 353 K and 90 MPa. Synthetic data and best-curves were obtained using Model 3 for pseudo-Sips's sorption (continuous lines in B) and linear sorption (segmented line in B). (B) Comparison between assumed (continuous line) and best-fitted (segmented line) partition coefficient of oil between supercritical CO_2 at 353 K and 90 MPa and pre-pressed oilseed.

(Table 2-3). The apparent solubility of the oil is lower than its corresponding thermodynamic solubility because there is no enough oil in the pre-pressed oilseed to saturate CO_2 under process conditions, as explained in section 2.4.1. The apparent oil content in pre-pressed oilseed estimated by inspection of Fig. (2-10A) was smaller than the true oil content because of the unfavourable oil partition towards the SC CO_2 phase for low oil contents seen in Fig. (2-10B) and explained in section 2.4.2. This was not the case for

Table 2-3. Comparison between adopted (non-linear sorption isotherm/isobar) and best-fit values (assuming linear partition of oil between SC CO_2 and pre-pressed oilseed) of model parameters.

Parameter	True value	Pseudo-Sips' isotherm/isobar	BET's isotherm/isobar
C_{sat} *versus* C_{fo} (g solute/kg CO_2)	97.0	36.4	36.4
$(C_s)_i$ (g solute/kg pre-pressed oil seed)	44.4	42.6	44.4
D_e (m^2/s x 10^{-11})	11.0	5.28	3.10

the oil content in the other case because when oil partitions according to BET's sorption model, it transfers to the SC CO_2 phase even when little oil remains in the pre-pressed seed (Fig. 2-11B). Partition of oil to the SC CO_2 phase is overestimated when assuming a constant partition coefficient (Figs. 2-10B and 2-11B), and this is compensated by overestimation of the inner resistance to mass transfer in the vegetable substrate as indicated by lower best- fitted than true values of D_e (3.6-fold lower in the case of the pseudo-Sips' sorption model, and 2.1-fold lower in the case of BET's sorption model).

Sorption models simpler than pseudo-Sips' or BET's have been proposed to model SC CO_2 extraction of vegetable substrates, and it is important to analyse if the conclusions above are also applicable in these cases. In some cases there is a lot of solute in the substrate that can saturate the SC CO_2 phase, at least initially. In some others, at least at the end, there is a little amount of solute tightly bound to the substrate that distributes between the SCF and solid phases according to a constant partition coefficient. Perrut, Clavier, Poletto, and Reverchon (1997) proposed a sorption model (named PCPR in this manuscript) englobing these extremes, with a sharp transition between the two for an intermediate solute content in the substrate (Eq. 2.20).

$$C_f^* = C_{sat}, \text{ if } C_s > C_t, \tag{2.20a}$$

$$C_f^* = KC_s, \text{ otherwise.} \tag{2.20b}$$

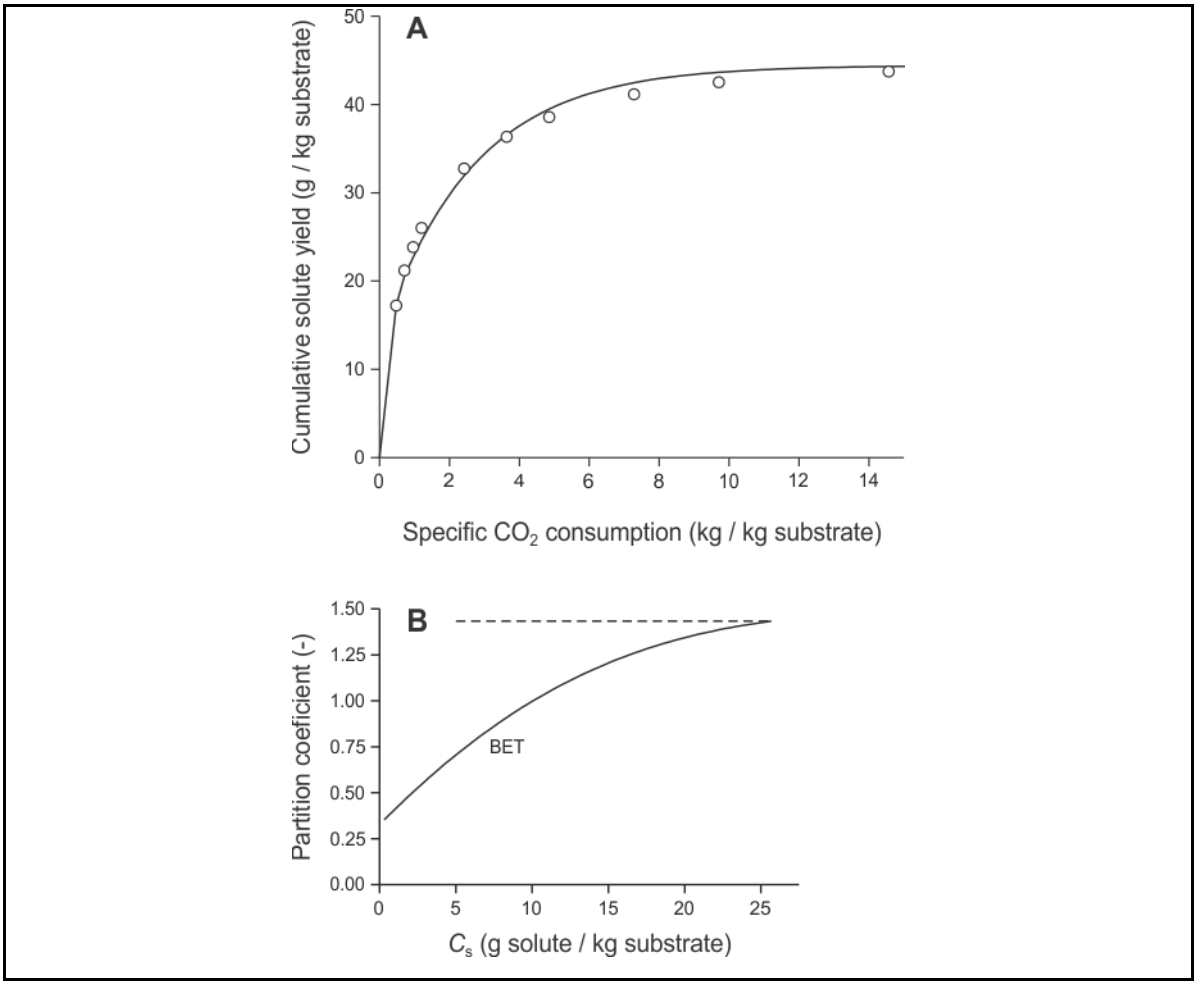

Figure 2-11. (A) Comparison between assumed (symbols) and best-fitted integral extraction of oil in pre-pressed oilseed using supercritical CO_2 at 353 K and 90 MPa. Synthetic data and best-curves were obtained using Model 3 for BET's sorption (continuous lines in B) and linear sorption (segmented line in B). (B) Comparison between assumed (continuous line) and best-fitted (segmented line) partition coefficient of oil between supercritical CO_2 at 353 K and 90 MPa and pre-pressed oilseed.

Sovová (2005) adapted her broken-and-intact-cells' (BIC) mass transfer model to the PCPR's sorption model. BIC's model hypothesizes that pre-treated vegetable tissues such as those subjected to mild milling contain broken surface cells and intact inner cells. The model considers a solute flux from intact to broken cells defined by an inner mass transfer coefficient and gradients in solute concentration, and a flux from broken cells to SC CO_2 defined by a film coefficient and an effective gradient in solute concentration

dependent on solute equilibrium partition. When equilibrium partition is given by PCPR's sorption model, simulated integral extraction curves have an initial stage defined by the solubility of the solute in SC CO_2 under process conditions, a second stage defined by the constant partition coefficient, and a third stage defined by inner mass transfer within intact tissue.

To generate relevant synthetic data for a case where PCPR-type sorption occurs, authors proposed a continuous, smooth function without the sharp transition at an intermediate solute content (Eq. 2.21) that could be applied in conjunction with Model 3.

$$\frac{C_{\mathrm{f}}^{*}}{C_{\mathrm{sat}}} = \alpha\, C_{\mathrm{sat}} + \frac{\left(C_{\mathrm{s}}\right)^{n}}{A+\left(C_{\mathrm{s}}\right)^{n}}\left(1-\alpha\, C_{\mathrm{sat}}\right) \tag{2.21}$$

Synthetic data was generated for particles of 0.55-mm diameter containing 44.4 g oil/kg substrate using Model 3 and Eq. (2.18) with n = 50, A = $5\text{x}10^{62}$, and α = 0.015 that is presented in Fig. (2-12A). Fig. (2-12B) includes the sorption model together with PCPR's approximation that was adopted to help fitting the synthetic data to Sovova's BIC model. Sovová (2005) proposed an analytical solution to a simplified version of her model that neglects the external resistance to mass transfer, and authors used this analytical solution to best-fit a grinding efficiency (that states the percentage of broken cells in the tissue) and an inner mass transfer coefficient ($k_s a_s$, that depends on D_e and d_p). Best fit values were 87% of broken cells (no broken cells but all solute deposited in an interconnected pore network in reality), for the grinding efficiency and D_e = $5.91\text{x}10^{-8}$ m^2/s (as compared to D_e = $1.10\text{x}10^{-10}$ m^2/s in reality) estimated from a best-fit value. Furthermore, computation of dimensionless Biot number using Eq. (2.7) based on the actual value of the film coefficient (k_f = $1.23\text{x}10^{-5}$ m/s) resulted in a value of Bi = 31 (suggesting indeed external resistance to mass transfer, cf. Fig. 2-8), that is far from infinity (no external resistance to mass transfer) as assumed in the simplified version of the model of Sovová (2005).

In conclusion, if assumptions of the mathematical model for SC CO_2 extraction do not fit reality, then the best-fit values of model parameters do not coincide with true values. Errors occur when assumptions about sorption equilibrium are wrong as illustrated for pseudo-Sips' or BET's *versus* linear isotherm/isobar models, or when assumptions about

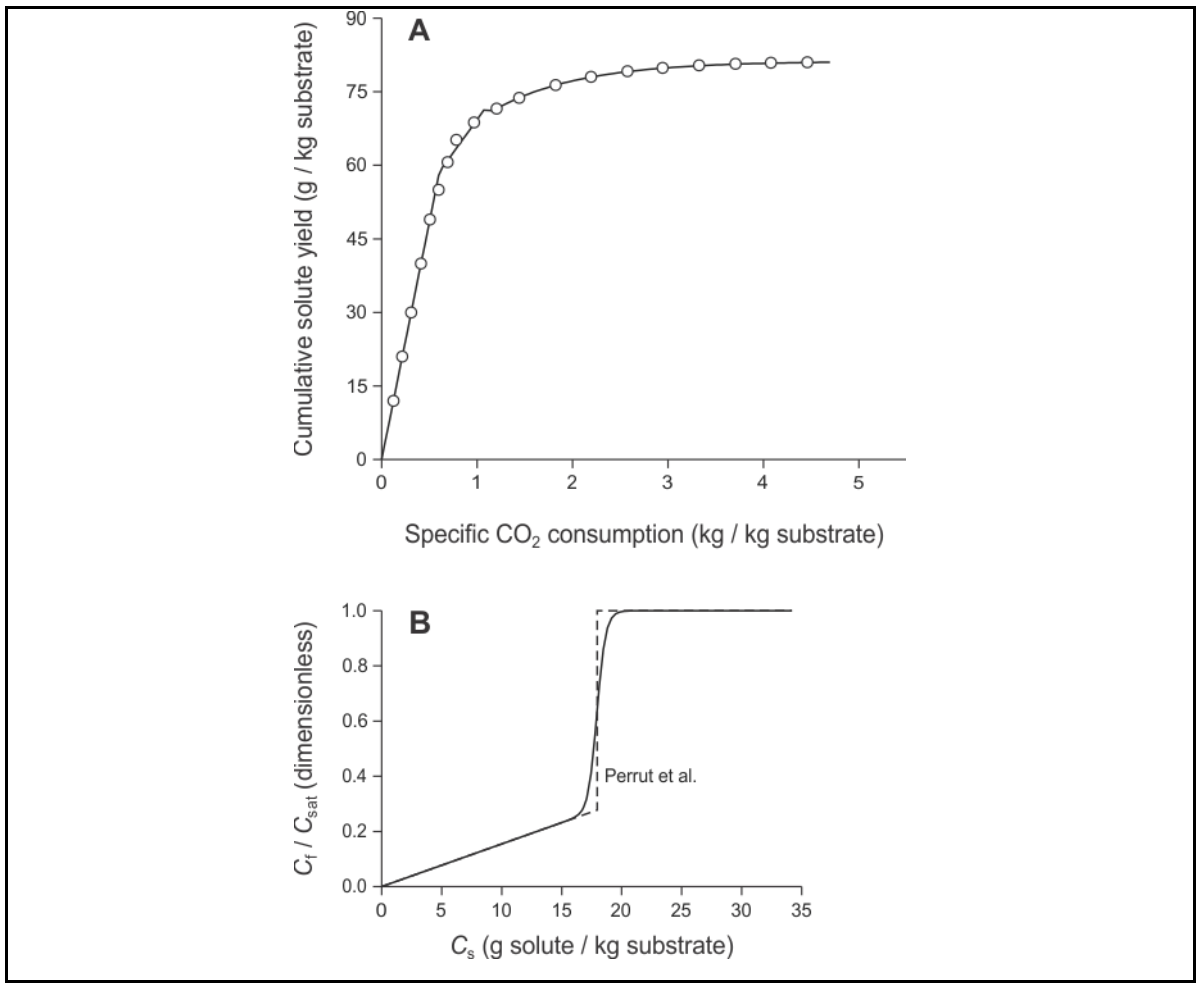

Figure 2-12. (A) Comparison between assumed (symbols) and best-fitted integral extraction of oil in pre-pressed oilseed using supercritical CO_2 at 353 K and 90 MPa. Synthetic data (symbols) was obtained using Model 3 for sorption according to Eq. (2.21) (continuous lines in B). Best-fitted line was obtained using a simplified version of Sovová (2005) model for PCPR-type sorption (segmented line in B). (B) Comparison between assumed (continuous line) and best-fitted (segmented line) sorption isotherms/isobars for the partition of oil between pre-treated oilseed and supercritical CO_2 at 353 K and 90 MPa.

the mass transfer mechanism are wrong as illustrated for LDF's *versus* BIC's models. Discrepancies between values of equilibrium and mass transfer parameters of different models, even when applied to same experimental data, is not an uncommon occurrence in literature on SCFE, as illustrated by del Valle et al. (2011) for the extraction of essential

oils from herbs and spices.

2.4.5. Inadequate mathematical models and best-fit parameters fail simulating process scale-up

The effect of change of scale was analysed for the SCFE of oil from 2-mm pre-pressed oilseed particles in a 1-m^3 industrial-size extraction vessel having the same length-to-diameter ratio (L/d_E = 4) as the laboratory vessel (d_E = 0.70 m and L = 2.8 m). Because the superficial velocity was also kept constant during the change of scale (U = 1 mm/s), the extraction vessel was fed with 48 kg CO_2/min. Integral extraction curves were simulated using true [with pseudo-Sips'-type, Fig. 2-10B, and BET's-type (Fig. 2-11B) partition] and best-fit (with assumedly constant oil partition) mass transfer parameters reported in Table 2-3.

Integral extraction curves show slower initial extraction rates and higher yields when using best-fitting than true parameters both in the case of pseudo-Sips' (Fig. 2-13A) and BET's (Fig. 2-13 B) sorption. Overestimation of oil partition to the SC CO_2 phase weighs more than underestimation of inner mass transfer in the final stages of the integral extraction curve, and this explains that curves using best-fit effective diffusivity values reach the horizontal asymptote earlier. This should be an unexpected result considering that the underestimation of D_e was compounded by the increase in particle diameter (from 0.55 mm in the laboratory to 2 mm in the industrial plant) thus resulting in overestimation of the internal resistance to mass transfer in simulations carried out assuming constant partition of the oil.

A change in the integral extraction curve as a result of a change of scale is especially worrisome considering scale-up proposals such as the one of Rosa and Meireles (2005), who assume these integral extraction curves remain unchanged and suggest using those obtained in optimization studies carried out in the laboratory to estimate production costs at the industrial level. Integral extraction curves do not change only due to an increase in size of the extraction vessel, but they are also amenable to other modifications associated to changes of scale that are not considered in this manuscript. The recycled CO_2 feed to an industrial extractor may contain residual solute that is not precipitated out in the

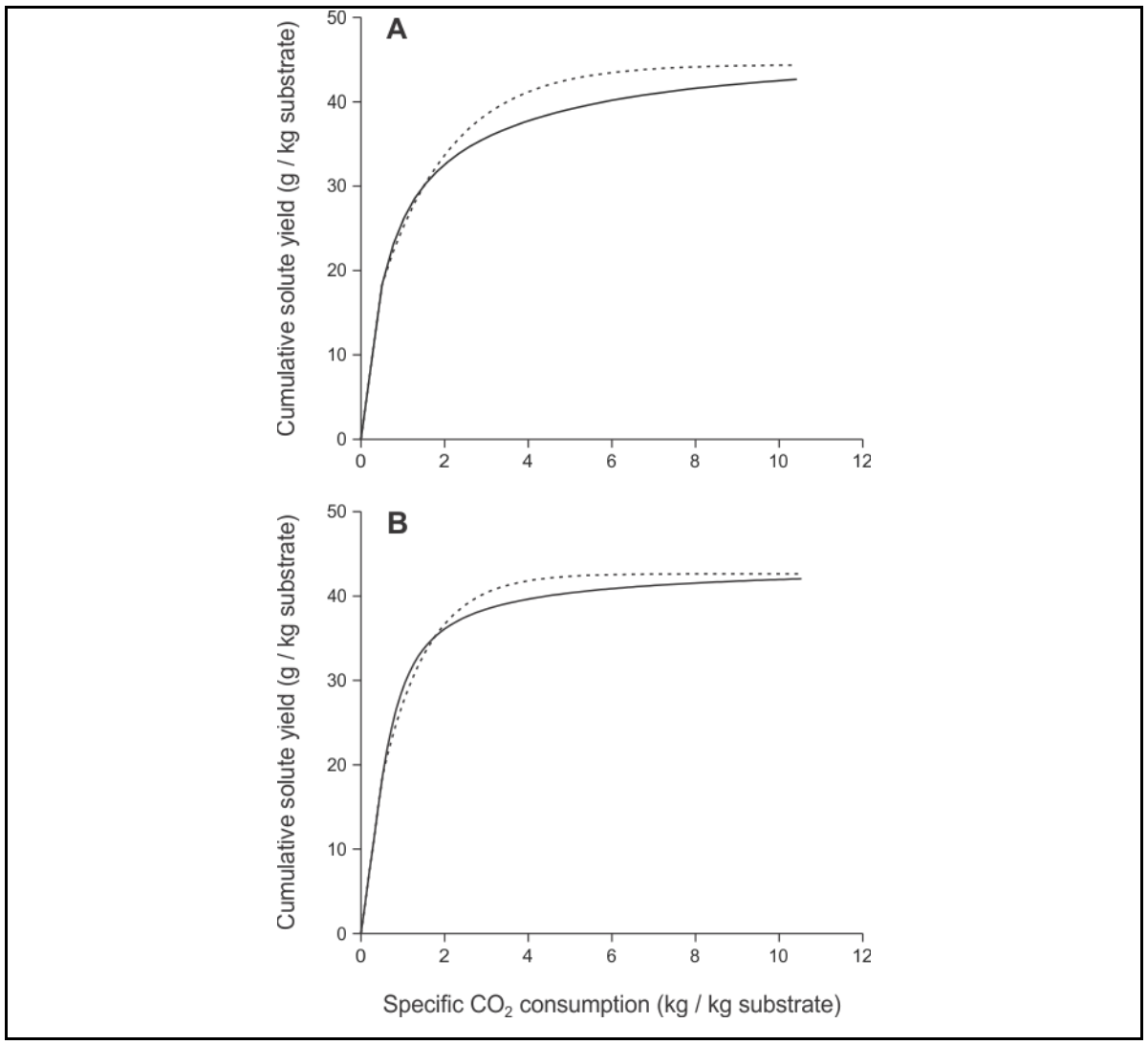

Figure 2-13. Effect of a change of scale on simulated integral extraction curves of supercritical extractions (1-m^3 extractor using 2-mm particles *versus* 100-cm^3 extraction vessel using 0.55-mm particles) using CO_2 at 353 K and 90 MPa simulated using Model 3. Continuous lines represent simulation using assumed parameter values whereas segmented lines represent simulation using best-fitted parameters for **(A)** pseudo-Sip's applied sorption (same conditions as in Fig.2-10) and **(B)** BET's sorption (same conditions as in Fig 2-11).

separator(s) in the plant, and remain in the solvent cycle (del Valle et al., 2004).

Furthermore, in plants having three or more extraction vessels, the concentration of solute in the feed of a particular extraction vessel changes with time because it carries

solute extracted in other vessel(s) located before in the solvent cycle, and this concentration also suffers step changes when the vessel in question is moved backwards in the solvent cycle (when the vessel with "fully" extracted substrate is taken out of the solvent cycle) (Núñez et al., 2011). Obviously, the integral extraction curve would move down if the border (entrance) condition accounts for the solute fed with SC CO_2 to the extraction vessel.

2.5. Discussion and practical implications of results

Arguments developed in section 2.4 strongly suggest the need to measure experimentally sorption isotherms/isobars describing solute partition between a substrate and CO_2 to better model SC CO_2 integral extraction curves. This way, fitting experimental integral extraction curves to mathematical models can be limited to inner mass transfer parameters. There is the risk of misrepresenting the SC CO_2 extraction process if additional phase equilibrium parameters in the mass transfer model are best-fitted to integral extraction curves, especially when little is known about the partition of the solute between the substrate and SC CO_2.

To make an independent determination of a sorption isotherm/isobar, it is necessary to measure the concentration of solute in an equilibrated SC CO_2 phase, as a function of the residual solute concentration in the substrate. This manuscript describes a method to estimate the apparent solubility following a static extraction period that gives the concentration of the solute in a SC CO_2 phase equilibrated with a substrate with known solute content (the initial solute content minus that one transferred to the SC CO_2 phase during static extraction, *cf.* section 2.4.1). Experiments can be repeated with partially extracted substrates, as done by Bulley, Fattori, Meisen, and Moyls (1984) with crushed, hexane-treated canola seeds (Fig. 2-14), so as to determine additional points along the sorption isotherm/isobar. A better alternative is to combine extraction (to remove part of the solute in the substrate), and attainment of true equilibrium by recirculating the SC CO_2 phase, as done to determine phenanthrene partition between spiked soil samples and pure or methanol-modified CO_2 (Young & Weber, 1997). To the best of the author's knowledge, this recirculation method has been applied to vegetable substrates to assess

only the partition of oil between and oilseed and SC CO_2 (King, Bott, Barr, Mahmud, & Sanders, 1987). The two aforementioned static methods are time consuming and dynamic methods such as those used to determine sorption isotherms/isobars in chromatographic separations using model SC-CO_2 + chemical + adsorbent systems (Brunner & Johannsen, 2006) can be alternatively applied if the adsorbent is replaced by a fully extracted vegetable substrate, and the chemical (solute or solute mixture) replaced by a SC CO_2 extract of the same vegetable substrate.

Besides experimental measurements of sorption isotherms/isobars, there is a need of sorption models to represent the data thus facilitating modelling and simulation (Table 2-4). Many dynamic methods fit breakthrough curves to simple sorption models (*e.g.*, Freundlich (1906)), and results can be improved if the sorption model fits physical reality. In this sense the static methods described above can provide useful information about the shape of the sorption isotherm/isobar (Fig. 2-15). Table 2-4 summarizes sorption models presented in this manuscript, including the number of parameters, the apparent extract partition [a cord between the origin of the graph (Fig. 2-15) and any point along the sorption isotherm/isobar, *cf.* Fig. 2-9B and Fig. 2-10B], and the lowest value of the apparent extract partition (initial slope of the sorption isotherm/isobar in the origin of the graph). In this manuscript, a form of the linear model assumes no-interaction between extract and vegetable substrate (Eq. 2.9), and in this case the value of K (Eq. 2.10) depends mainly on the split between inter- and intra-particle volumes in the packed bed. This no-interaction hypothesis is possibly unrealistic for typical extracts and vegetable substrates. Pseudo-Sips' and BET's models fit typical S-shaped sorption isotherms/isobars (Fig. 2-14). Integral extraction curves simulated using pseudo-Sips' model (Eq. 2.18) reach horizontal asymptotes limited by null initial slopes, which imposes a restriction to the maximal yield of the SCFE process (Fig. 2-6). BET's model (Eq. 2.19) has a positive initial slope that allows full extraction of the vegetable substrate (Fig. 2-7) but imposes restrictions to the maximal concentration of extract in SC CO_2 below the saturation concentration (Fig. 2-15) unlike experimentally observed in vegetable substrates such as oilseeds containing a large amount of extract (oil) (Fig. 2-14). PCPR's model (Eq. 2.20) allows SC CO_2 getting saturated with extract as well as full extraction of the vegetable

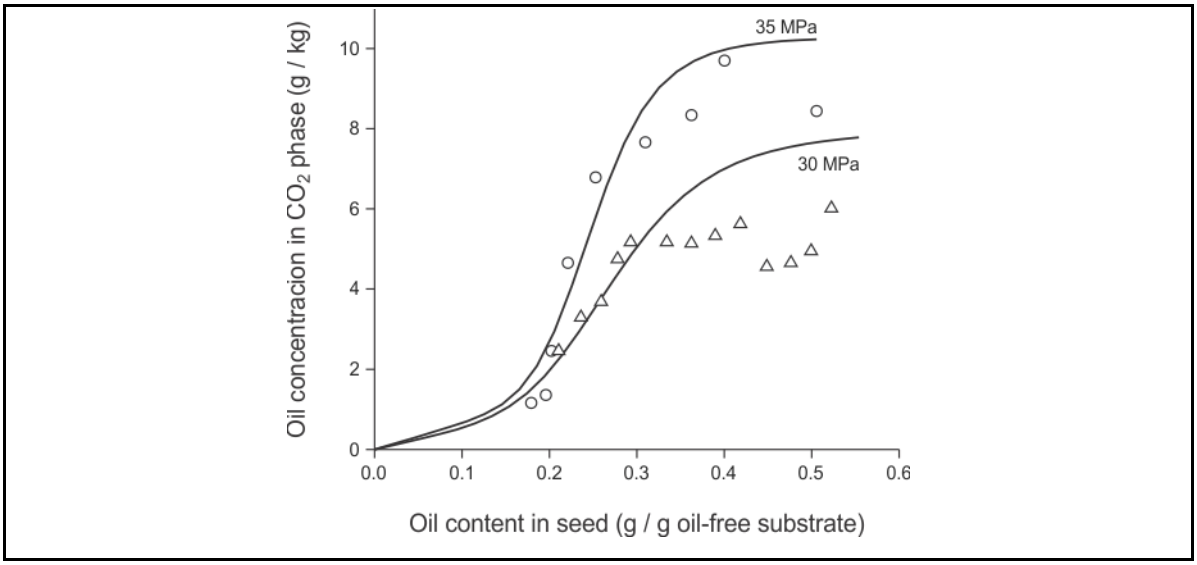

Figure 2-14. Sorption isotherms/isobars for canola seed oil at 313 K and (△) 30 MPa or (○) 35 MPa. Symbols are experimental data taken from (Bulley et al., 1984) and trend lines were obtained using Eq. (2.21) and C_{sat} values estimated using the equation of del Valle et al. (2012).

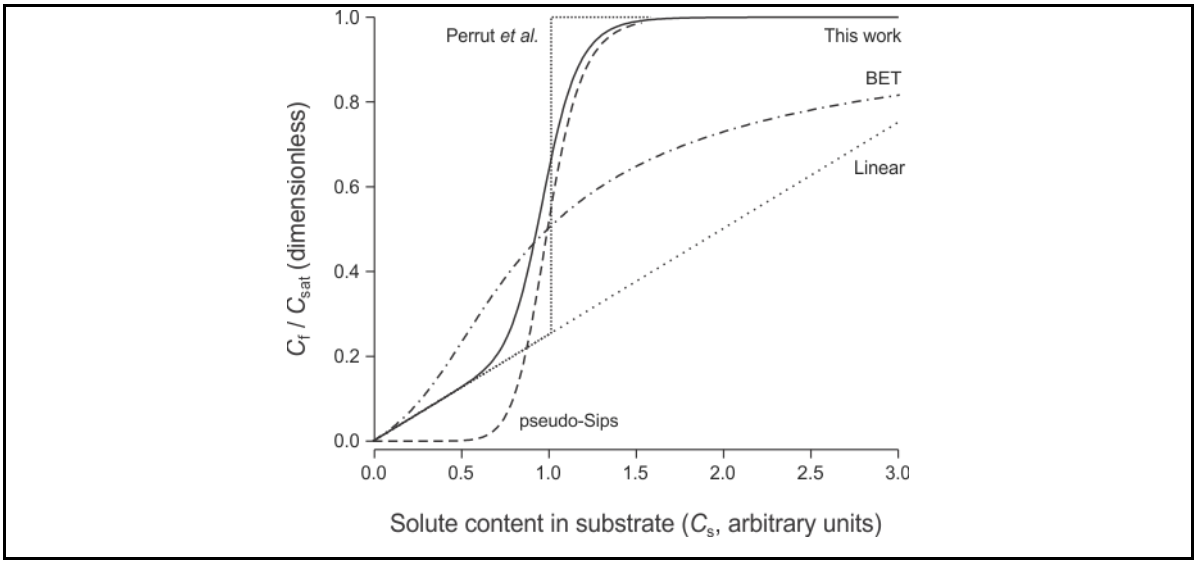

Figure 2-15. Comparison of sorption isotherm/isobar models presented in this manuscript.

substrate and thus addresses the limitations of both pseudo-Sips' and BET's models, but does not necessarily fit the shape of the sorption isotherm/isobar experimentally observed (Fig. 2-14). In that sense, the model proposed in this manuscript (Eq. 2.21) fits physical reality (Fig. 2-14) at the expense of a large number of parameters (Table 2-4).

Model parameters informed in section 2.3 represent extreme (high temperature and pressure) conditions for the SC CO_2 extraction of vegetable substrates in general and oilseeds in particular. This system and process conditions fulfilled the needs in section 2.4.1 for simulations using Model 1. Allowing complete dissolution of the extract in SC CO_2 during static extraction requires a substrate containing a small amount of high-solubility extract. Pre-pressed oilseeds do not comply with these requirements under typical extraction conditions (*e.g.* 313 K and 30 MPa (del Valle et al., 2012)). This is not the case at 353 K and 90 MPa for a pre-pressed oilseed containing *ca*. 15% (w/w) oil in a void space accounting for 20% of the total volume of the substrate, for which a typical microestructural value (F = 25) for pre-pressed and flaked oilseeds (del Valle et al., 2006) is estimated. Use of available information on solubility of vegetable oils in SC CO_2 as a function of system conditions (del Valle et al., 2012) and on the relationship between the effective diffusivity of the oil and microstructure of pre-pressed oilseeds (del Valle et al., 2006) allowed analysis at these selected, extreme conditions.

There are other vegetable substrates such as herbs that contain a small amount of high-solubility extract such as essential oils. However, the solubility of essential oils is not a simple function of system conditions but depends strongly in their specific chemical make-up (del Valle et al., 2011). Furthermore, advantage is taken of inner barriers to mass transfer in the intact tissue to effect a selective extraction of the desirable components. Indeed, herbs are typically subjected to mild pre-treatments that are not aimed at fully disrupting cells, so that their inner microstructure does not correspond to a network of interconnected pores (del Valle et al., 2011), as required by authors' simple mass transfer model.

Despite of its simplicity, Model 3 can describe mass transfer in SC CO_2 extraction processes adequately for the purposes of this manuscript. del Valle and Uquiche (2003) showed that different hypotheses about inner mass transfer mechanisms such as diffusion

Table 2-4. Isotherm/isobar sorption models presented in this manuscript.

Sorption model	Equation	Parameters*	Initial slope	Partition coefficient**
Linear (no interaction)	9	None	K (Eq. 2.10)	K, for $C_s < C_t$
Pseudo-Sips	18	A, n	∞, for $n < 1$ $1/A$, for $n = 1$ (pseudo-Langmuir) 0, for $n > 1$	$\frac{(C_s)^{n-1}}{A+(C_s)^n}$
BET	19	K, C_m	$\frac{1}{K\ C_m}$	$\frac{\left[1-C_f^*/C_{sat}\right]\left[1+(K-1)C_f^*/C_{sat}\right]}{K\ C_m}$ (implicit solution)
PCPR	20	K, C_t	K	K, for $C_s < C_t$
This manuscript	21	A, n, α	α	$\alpha\ + \frac{(C_s)^{n-1}}{A+(C_s)^n}(1-\alpha\ C_s)$

* In all cases C_{sat} is not listed as an additional parameter.

** Chord between the origin and any point along the sorption isotherm/isobar.

(homogenous vegetable substrates), desorption-dissolution-diffusion (porous vegetable substrates), and their LDF approximations can describe SC CO_2 extraction processes equally effectively, and established the relationship between D_e values of the different models. Model assumptions about particle shape and microstructure, flow conditions, and physical properties appear reasonable.

1) Model 3 can be applied even in the case of non-spherical particles. Dimensionless solutions for the extraction of various bodies of regular geometry in a perfectly agitated medium virtually superimpose when using a characteristic dimension of the body three times the ratio between its total volume and external surface ($d_p/2$, in the case of a sphere) (Y. H. Ma & Evans, 1968). In the case of a cylindrical body, which is a typical shape for pre-pressed oilseeds particles, the characteristic dimension equals the cylinder radius if aspect (height-to-diameter) ratio equals one. del Valle et al. (2006) assumed also that their pre-pressed oilseed particles behaved as if they were spherically shaped.
2) The assumption of constant interstitial velocity of the SC CO_2 within the extraction vessel is reasonable when the ratio between its inner diameter and the diameter of substrate particles is sufficiently large (d_E/d_p = 13 in the worst case for simulated laboratory extraction using 0.70-mm particles) (Delgado, 2006). However, caking of small, moistened particles may cause undesirable channelling of CO_2 in the packed bed (del Valle, Mena, & Budinich, 2008; Eggers, Ambrogi, & Schnitzler, 2000).
3) del Valle and de la Fuente (2006) showed that it is possible to neglect axial dispersion phenomena to describe SCFE of oil from seeds in a typical industrial extractor operating with SC CO_2 at 313 K and 30 MPa without crippling the fitting capabilities of a mathematical model such as the one used in this manuscript. Re-doing calculations, least favorable (lower) values of dimensionless group $L\ U\ D_L^{-1}\ \varepsilon^{-1}$ (or Pe/ε) were 228 at the laboratory scale (0.7-mm particles extracted in a 100-cm^3 vessel) and 234 at the industrial scale (2-mm particles extracted in a 1-m^3 vessel) using SC CO_2 at 353 K and 90 MPa flowing at a superficial velocity of 1 mm/s, where D_L is the axial dispersion coefficient, which was estimated using the dimensionless correlation of del Valle et al. (2011) for packed beds operating with SCFs. The least favorable

values of Pe/ε are above the limit of 100 for which axial dispersion phenomena can be disregarded according to Goto, Roy, and Hirose (1996).

4) The assumptions of negligible pressure losses and temperature gradients within the bed are valid for small (short) extractors, highly permeable substrate (with no caking tendencies), and vessel wall temperatures similar to the one of the flowing SC CO_2.
5) The assumption of constant physical properties is valid if, under process conditions, the extract has low solubility in SC CO_2 that does not affect the density or viscosity of the SC CO_2 even when saturated with extract, and if during extraction the vegetable substrate does not swell nor shrink as result of extract removal and SC CO_2 infiltration. The assumption of no effect of dissolved solute on physical properties of the SC CO_2 phase as compared to those of pure CO_2 is possibly questionable when 97 grams of oil are dissolved in per kilogram of CO_2, to the best of the author's knowledge there is no data available to make corrections to ρ, μ, and D_{12} under those conditions.

2.6. Concluding remarks

Researchers interested in applying SCFE to vegetable and other biological substrates should be careful not to rely to an excessive extent on chemical analysis of substrates to anticipate extraction yields, phase equilibrium studies to predict initial (solubility-controlled) extraction rates, and laboratory studies to optimize the process. If researchers attempt reducing some of the expense associated with validation studies at the pilot plant o larger scale, they should devote efforts in the laboratory to validate assumptions about solute-matrix interactions and inner mass transfer mechanisms so as to develop a reliable model of the extraction process that can be used in process optimization *via* mathematical simulations. The following three hypotheses can be inferred from this manuscript that may contribute to planning research aimed at the design and economical evaluation of SCFE processes.

1) The amount of extract in a vegetable substrate affects the "apparent" solubility to the point that this might be smaller than the "thermodynamic" solubility under equivalent SCFE process conditions;
2) The maximal yield of a SCFE process does not depend solely on the amount of extract

partially or fully soluble in CO_2 under process conditions but also on solute-matrix binding.

3) Best-fitting parameters to experimental integral extraction curves results in unreliable estimates if mathematical models of SCFE fail in describing true sorption equilibrium or inner mass transfer mechanisms in the vegetable substrate.

This manuscript provides partial support to these hypotheses. Data is taken from literature on SCFE of essential oils from herbs and spices to show that the apparent solubility of high-solubility compounds in vegetable substrates having little of them is below their true solubility under process conditions (Hypothesis 1). There is evidence of "irreversible" binding negatively affecting recovery when using SCFs in analytical applications (Hypothesis 2), but to the best of the authors' knowledge, little evidence of irreversible binding in SCFE of vegetable and other biological substrates. The maximal yield from a biological tissue may be influenced by physical entrapment of solutes in the cellular structure, and there is no irrefutable experimental support to the claim that the yield is also negatively affected by solute-matrix interactions. Mathematical simulations in this manuscript present ample evidence, on one hand, that sorption equilibrium affects extraction rate and yield, and on the other hand, that scaled-up integral extraction curves are unreliable when the true sorption equilibrium and mass transfer effects are compensated by alternative sorption equilibrium or mass transfer effects in parallel simulations fitting the target integral extraction curve without fitting the physical picture of the SCFE process (Hypothesis 3). The claim that, depending on its content in a vegetable substrate, solute partition towards the SCF phase is determined either by its solubility in SC CO_2 under process conditions or by a constant partition coefficient is questionable based on sorption equilibrium measurements using oilseeds. Being sorption phenomena of such paramount importance to build a reliable mathematical model of the SCFE process for simulation purposes, this manuscript proposes a sorption model that fits experimental sorption isotherms/isobars for oil from seeds. Furthermore, this manuscript proposes a sorption model (a special case of the aforementioned one) that may account for "irreversible" sorption in case this type is later identified in the SCFE of vegetable and other biological substrates.

3. EQUILIBRIUM PARTITION OF RAPESEED OIL BETWEEN SUPERCRITICAL CO_2 AND PREPRESSED RAPESEED

Abstract

The equilibrium partition of a vegetable extract between SC CO_2 (fluid phase) and the vegetable substrate (solid phase) is a fundamental parameter in mathematical models of supercritical fluid extraction processes. However, because the function relating extract concentration in the fluid (C_f) and solid (C_s) phases is commonly best-fit to extraction curves, inaccuracies of results estimated using mathematical simulation might be due to wrong parameter values that misrepresent physical reality. We experimentally measured and modelled sorption isotherm/isobar curves of rapeseed oil between SC CO_2 and prepressed rapeseed using a methodology that intersperses extraction (to reduce oil content) and equilibration (by recirculation of the SC CO_2 phase) steps, with oil being sampled in each step. In this method oil concentration in SC CO_2 is measured directly whereas that in prepressed rapeseed is estimated using mass balances. Oil desorption was a two-stage process; when rapeseed contains more than ~70-80 g kg^{-1} oil/substrate the SC CO_2 phase gets saturated with oil ($C_f = C_{sat}$), whereas when it contains less oil this is bound to the solid matrix in such a way that C_f dips below C_{sat}. Increasing pressure from 22 to 28 MPa at constant temperature (40 ºC) increases C_f, partly due to an increase in the solvent power of SC CO_2 with an increase in density. If SC CO_2 density is kept constant (857.1 kg/m^3) by simultaneously increasing temperature from 40 to 50 ºC, the effect of the increase in pressure is less pronounced. Grinding rapeseed pellets fastened equilibration without major effect on oil partition. The heat of desorption of the oil is ~100 kJ/mol which suggests it is bound to the prepressed seed by van der Waals interaction forces. However experimental values in this region are uncertain due to propagation of uncertainties to estimate C_s.

3.1. Introduction

SuperCritical (SC) Fluids (SCFs), namely fluids at state conditions above the

corresponding critical temperature (T_c) and critical pressure (P_c), have been successfully applied to extract high-value-added compounds for the food, cosmetic, and pharmaceutical industries. Carbon dioxide (CO_2) is the most suitable fluid for applications in these industries (Brunner, 1994). SC CO_2 is not only highly selective for the extraction of high-value compounds, but it is also noncorrosive (unlike water), non-flammable (unlike hydrocarbons), and inexpensive. Furthermore, because SCF extractions are carried out usually at a near-critical temperature, the convenient critical properties of CO_2 (T_c = 31.2 °C, P_c = 7.38 MPa) allow recovering labile compounds without thermal damage.

Reliable mathematical descriptions of the SCF Extraction of vegetable substrates depend critically on the determination of equilibrium and mass transfer parameters, including those characterizing solute partition between SC CO_2 and the pretreated substrate. Mass transfer parameters include an axial dispersion coefficient (D_L) describing solute migration in the SCF phase moving along the packed bed, a film mass transfer coefficient (k_f) describing transport of the solute from solid particles to the SCF phase through a thin layer of SCF stationed next to the particles, and an internal mass transfer coefficient (e.g., effective diffusivity, D_e) describing the transport of solute within solid particles under the influence of solute gradients imposed by the removal of solute at the surface of the particles (del Valle, 2015; del Valle & de la Fuente, 2006). Equilibrium parameters correspond to those of a sorption isotherm/isobar equation relating solute concentration in the SC CO_2 phase (C_f) with solute concentration in the solid (pretreated vegetable substrate) phase (C_s) (del Valle & Urrego, 2012). Parameters D_L and k_f can be estimated using dimensionless correlations for packed beds operating with SCFs (del Valle, 2015; del Valle & de la Fuente, 2006). On the other hand, D_e and the parameter(s) of a simple sorption isotherm/isobar equation (e.g., a constant partition coefficient K) are usually estimated by best-fitting integral extraction curves (plots of cumulative yield, e.g., grams of solute per kilogram of substrate, *versus* specific solvent consumption, e.g., kilograms of CO_2 per kilogram of substrate) obtained in laboratory or pilot-plant units. However, best-fit parameters of mathematical models that do not fit reality may fail in simulating extractions at larger scales, including industrial extractions (del Valle & Urrego, 2012).

There is a need to experimentally measure equilibrium parameters to limit best-fitting of integral extraction curves to estimate a single parameter (D_e) representing inner mass transfer within the pretreated substrate (del Valle & Urrego, 2012). However, to the best of the authors‟ knowledge there are experimental reports in literature only for the partition of oil between partially-extracted canola seeds (Bulley et al., 1984) or neat rapeseeds (King et al., 1987) and SC CO_2, and of phenanthrene between spiked soil samples and pure or methanol-modified SC CO_2 (Young & Weber, 1997). In their experiments, Bulley et al. (1984) reduced the initial oil content of canola samples to various extents by partial extraction with hexane, and estimated corresponding equilibrium concentrations in CO_2 from the initial slope of integral extraction curves. These results may have been negatively impacted by residual traces of hexane (potential co-solvent/modifier) in the oil, and difficulties in attainment of equilibrium in a single pass of SC CO_2 through the extraction vessel. These difficulties can be circumvented by partially removing solute using SC CO_2, and by recirculating the SCF phase through the extraction vessel, as done by others (King et al., 1987; Young & Weber, 1997). For their measurements, Young and Weber (1997) built an experimental device in which it was possible to combine equilibration (by recirculation of the SCF phase) and extraction (to reduce the phenantrene content in the soil sample) steps. To an extent, a similar methodology was adopted by King et al. (1987), who modified existing facilities at the University of Birmingham to that end. Data of King et al. (1987) agree with that of Bulley et al. (1984) for high residual oil contents in the oilseeds (del Valle & de la Fuente, 2006), but for low residual oil contents the two data sets do not agree and the data of King et al. (1987) is not as expected (the saturation concentration of oil in SC CO_2 stays in an intermediate plateau instead of dropping to very low values). There were no further reports on the use of the experimental setup at the University of Birmingham to measure equilibrium partition involving SC CO_2 and solid substrates.

The objectives of this work were (1) to develop a methodology to measure sorption isotherm/isobar curves of extracts between vegetable substrates and SC CO_2, by measuring the system oil – prepressed rapeseed – SC CO_2, and (2) to model the results.

3.2. Materials and methods

3.2.1. Substrate

Commercial prepressed rapeseeds (Oleotop, Temuco, Chile) used in this study were cylindrical pellets 5 mm thick and ~15 mm long, containing 17.3% w/w oil and 7.49% w/w water. Rapeseed pellets were either cut with a knife into segments ~5 mm long ("square" pellets), or ground in a mill Condux-werk (Hanau, Germany) with 1.25 mm openings (ground pellets). A fraction of particles (-24/+42 mesh, $354 \leq d_p \leq 707$ μm diameter) was separated using a test sieve-shaker for further analysis. Samples of "square" and "ground" pellets were packaged in polyethylene bags and stored in a refrigerator (5 °C) up to analysis.

The true density of prepressed and milled rapeseed samples (ρ_s = 1.367 g/cm^3) was measured in a gas pycnometer Quantachrome Ultrapyc 1200e (Boynton Beach, FL) using 99.9%-pure nitrogen from Aga S.A. (Santiago, Chile). This information, combined with the bulk density of the material (ρ_b), and an estimate of the interparticle void fraction (ε) of the packed bed, allowed an estimate of the intraparticle void fraction (ε_p) of the substrate using Eq. (3.1):

$$\varepsilon_p = 1 - \frac{\rho_b / \rho_s}{1 - \varepsilon}, \qquad (3.1)$$

where ρ_b was estimated as 0.569 g/cm^3 considering that 24 grams could be loaded in the 42- cm^3 equilibrium cell of our experimental device (cf. Section 3.2.2), and ε was estimated as 0.390 using the equation proposed by Benyahia and O'Neill (2005) for D/d_p = 32 and ϕ = 0.85 (assumed sphericity of "ground" pellets). The resulting value of ε_p was 0.318. Corresponding values for "square" pellets were d_p = 5.724 mm (diameter of a sphere having the same surface as our cylindrical pellets), ε = 0.505 (using the equation of Benyahia and O'Neill (2005) for packed bed of solid cylinders when D/d_p = 3.00), and ε_p = 0.161.

3.2.2. Experimental device

The experimental device, consisting of loading, equilibration, and sampling sub-systems, was designed and built by Eurotechnica (Bargteheide, Germany) on request, Fig. (3-1). The loading sub-system includes a cooling bath PolyScience (Niles, IL), a syringe pump Teledyne Isco 260D (Lincoln, NE), and a 3-m (1/8" high-pressure tubing) heating coil. The equilibration sub-system consists of a loop containing a 42-cm^3 equilibrium cell (D = 1.72 cm diameter, L = 18.3 cm height), a high-pressure gear pump Micropump GAH-T23 (Vancouver, WA) powered by a motor Siemens Micromaster 411 (Congleton, UK), and a UV/Vis detector Agilent G1314A (Santa Clara, CA). The heating coil, equilibrium cell, and micropump (excluding its motor) are placed within a thermostated air bath equipped with a controller Hillesheim HT42-10P (Waghäusel, Germany), and a hot-air blower Leister Hotwind S (Sarnen, Switzerland). The sampling sub-system contains a micrometric valve, a 50-cm^3 sampling tube placed in a dewar flask with a cooling mixture (ice + water), where solute precipitates, and a drum-type volumetric gas meter Ritter TG-05/5 (Bochum, Germany). Components are connected using 1/16" high-pressure tubing. The operation limits of the system are 100 °C and 30 MPa.

The total volume of the system (V_{loop}) was estimated by pressurizing the empty cell to 28 MPa with SC CO_2 using the syringe pump and thermally stabilizing the air bath to 40 ºC (ρ =0.8985 g/cm^3 estimated using NIST database (Lemmon et al., 2007)), 50 ºC (ρ = 0.8571 g/cm^3), or 60 ºC (ρ = 0.8140 g/cm^3) and then in using the volumetric gas meter to measure the volume of expanded CO_2 (V_{CO_2}, NL) when fully depressurizing the system:

$$V_{loop} = \frac{V_{CO_2}\rho'}{\rho}, \tag{3.2}$$

where ρ' is the density of CO_2 at environmental conditions (1.8532 g/NL at 18 ºC and 1 atm). The estimated value was V_{loop} = 65.5 ± 3.4 cm^3, which suggest that the sum of dead volumes of all components of the loop but the equilibrium cell was about 23 to 24 cm^3.

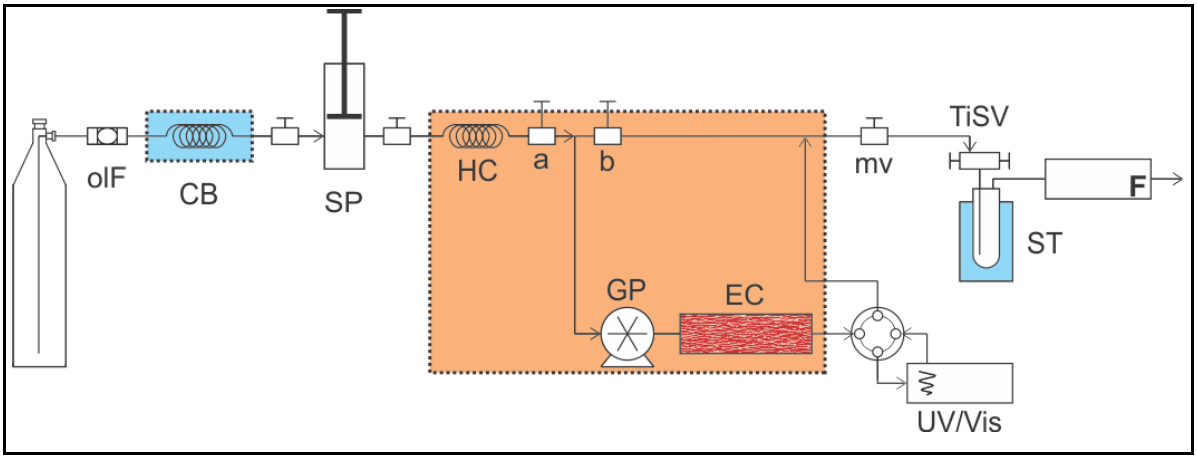

Figure 3-1. Schematic diagram of the high-pressure equilibration unit. The loading sub-system includes a liquid CO_2 cylinder, on-line filter (olF), ooling bath (CB), syringe pump (SP), and heating coil (HC). The equilibration sub-system consist of a gear pump (GP), equilibrium cell (EC), injection valve (IV), and UV/Vis detector held in thermostated air bath together with HC. The sampling subsystem consists of a micrometric valve (mv), a two-inlet sampling valve (TiSV), a sampling tube (ST) located in a dewar with a cooling mixture, and volumetric gas meter (GM). Valves a and b are on-off (quarter-turn-type) valves.

3.2.3. Experimental procedure

After loading sample to the equilibrium cell, the system is conditioned by heating the air bath to the desired temperature and then pressurizing the equilibration sub-system to the desired pressure by feeding CO_2 with the syringe pump operating in a pressure-controlled mode, Fig. (3-2A). Equilibration is done by recirculating SC CO_2 through the equilibrium cell with the gear pump while monitoring extract concentration in the SC CO_2 using the UV/Vis detector, Fig. (3-2B). During equilibration, the gear pump operates at 15 Hz (~24 cm^3/min). When the absorbance registered in the UV/Vis detector does not change during 1 h, the assumption is made that an equilibrium condition has been reached, and the pump is stopped to initiate sampling. Sampling is done in an open loop mode operating the syringe pump in a pressure-controlled mode, Fig. (3-2C). The two-inlet sampling valve is opened carefully to adjust a sampling rate (0.5 NL/min) that is limited by the maximum

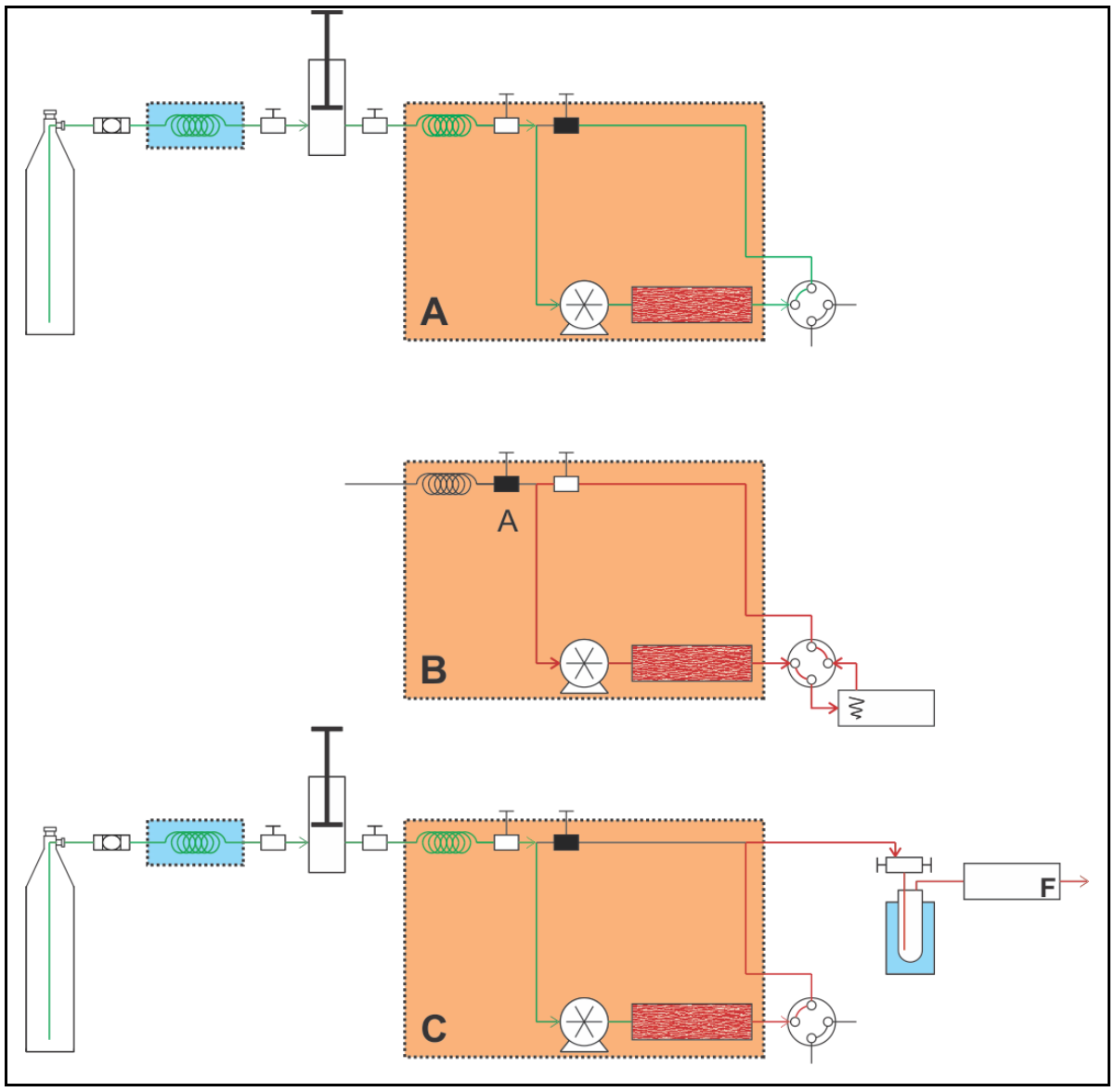

Figure 3-2. Graphical representation of loading, equilibration, and sampling operations. (A) In the loading step the system is pressurized with the syringe pump (not included) operating at constant flow, valve a (cf. Fig. 3-1) is opened, and valves b and mv are closed. (B) In the equilibration step the gear pump recirculates CO_2, valves a and mv are closed, valve b is opened, and valve IV is switched to the inject position to obtain a UV/Vis reading of the supercritical CO_2 phase in the detector. (C) In the sampling step the syringe pump (not included) is operated at constant pressure, valves a and mv are opened, and valve b is closed. Opened valves are marked white whereas closed valves are marked black.

rate detectable by the gas meter (1 NL/min). Extract is collected in pre-weighed glass vials (4-cm^3 capacity) inserted into the sampling tube; precipitated extract in the sampling line is recovered in 14-cm^3 vials, by adding 10 cm^3 of HPLC-grade hexane from J.T. Baker (Phillipsburg, NJ) through the second inlet of the sampling valve in 1 cm^3 portions. After measuring and computing the concentration of oil in the saturated SC CO_2 phase, the system re-equilibrates, and these steps are repeated until depletion of the substrate. However, to deplete rapeseed oil faster, between equilibrium measurements, extraction is carried out at equilibration temperature and pressure conditions, Fig. (3-2C). As the amount of oil removed from the sample in this stage is larger than in the sampling stage, precipitated extract into the sampling line is recovered by adding 20 cm^3 of hexane through the second inlet of the sampling valve in 1 cm^3 portions and transferred to 22-cm^3 vials. Hexane is evaporated at 55 °C in a hot air oven for >12 h. Following cooling in a desiccator with silica gel at room temperature (>2 h), the recovered extract is assessed gravimetrically by difference with cleaned and dried vials.

The concentration of oil in the SC CO_2 phase (C_f) was estimated gravimetrically. For that, the oil dissolved in the SC CO_2 or extract was recovered in glass vials and weighed (S) in an analytical balance Runsun FA2104N (Hebei, China). The mass of CO_2 was calculated as the product of the evaporated CO_2 measured by the gas meter (V_{CO_2}) and the CO_2 density at environmental conditions (ρ') calculated using NIST database (Lemmon et al., 2007). The concentration of oil in the fluid phase (g kg^{-1} oil/CO_2) was calculated using Eq. (3.3):

$$C_{f(i)} = \frac{S_{(i)}}{V_{CO_2}\rho'} \tag{3.3}$$

The concentration of oil in the solid phase (C_s), on the other hand, was estimated using mass balances. It was estimated as the ratio of the oil still remaining in the solid substrate, and the oil-free substrate (M_o), Eq. (3.4):

$$C_{s(i)} = \frac{S_o - \sum_{j=1}^{i-1} S_{(j)} - \left(C_{f(i)} V_{loop}\rho\right)}{M_o}, \tag{3.4}$$

where the oil still remaining in the solid substrate was estimated by discounting from the initial oil content (S_o) all oil sampled up to that stage, as well as the oil dissolved in the SC CO_2 remaining in the loop (density of SC CO_2 calculated with NIST database (Lemmon et al., 2007) at operation conditions, ρ).

The initial oil content in the oil-free substrate (S_o), in turn, was calculated at the end of each experiment (n stages) as the sum of all sampled oil and the oil remaining in the extracted substrate ($C_{s(n)}$), that was determined by Soxhlet extraction using hexane, Eq. (3.5):

$$S_o = \sum_{i=1}^{n} S_{(i)} + \left(C_{s(n)} M_o \right) \tag{3.5}$$

3.2.4. Experimental plan

Approximately 24 g of pre-pressed rapeseeds (weighed accurately) were used in each experiment, and equilibrated/extracted with 99.9%-pure CO_2 from Aga S.A. (Santiago, Chile). Seven-to-sixteen experimental points were measured for each sorption isotherm/isobar curve. Following equilibration (periods >8 h), ~4 NL of CO_2 at gas meter temperature and pressure conditions (~9.0 g CO_2) were sampled for each sorption isotherm/isobar equilibrium point, whereas ~30-to-80 NL were sampled in extractions carried out in between equilibrium points (the amount increased during measurements to account for the reduction in the solubility of oil in SC CO_2 as its concentration in the substrate decreases). [The minimal amount of sampled SC CO_2 phase is limited by the gravimetric method to quantify oil, whereas the maximal amount is limited by the need to maintain the equilibrium conditions of the system.] Measurements were carried out at 40, 45 or 50 °C, and 22, 25 or 28 MPa. The precision of the method was evaluated using "square" pellets by duplicating isotherm/isobar curve measurements at 50 °C and 28 MPa. The pre-treatment effect was evaluated by measuring an additional sorption isotherm/isobar curve at 50 °C and 28 MPa using "ground" pellets.

3.3. Results

In phase equilibrium measurements with fluid mixtures at high pressure, it is

important to minimize disturbances in the equilibrium during system sampling, as well to minimize losses of the solute on samples lines (precipitation) or with the expanded fluid (carryover) (Peper & Dohrn, 2012). In this work, authors analysed (1) changes in apparent oil concentration in SC CO_2 brought about by dilution when sampling in an open loop mode, (2) changes in apparent oil concentration in SC CO_2 brought about by pressure drop when sampling in a closed loop mode, (3) precipitation of solute in the sampling line, and (4) uncertainty resulting from weight differences between sample and sample holder. Sampling in an open loop mode dilutes the oil with the CO_2 used to keep the system pressure constant. On the other hand, sampling in a closed loop mode results in a pressure drop that in turn reduces the solubility in SC CO_2 of the oil, which may precipitate out in the equilibrium sub-system. Oil precipitation may also occur in sampling lines due to the pressure drop across valve D. Besides disturbances in equilibrium conditions brought about by sampling in closed or open loop modes, solubility measurements using a gravimetric method may be negatively impacted upon by difficulties in measuring minute amounts of recovered oil.

Sampling in a closed loop mode may underestimate oil concentration in SC CO_2 equilibrated with pre-treated oilseeds, Fig. (3-3). If there is no carryover of precipitated oil with CO_2, then the concentration of oil in sampled CO_2 may be limited by its decreasing solubility in pure SC CO_2 at the prevailing pressure and temperature in the equilibration sub-system, and not by the equilibrium partition that is being measured. Fig. (3-3) shows changes in pressure and apparent oil concentration as a function of sampled CO_2 (<36 g) and initial oil concentration in SC CO_2 at 50 ºC and 28 MPa equilibrated with the pre-treated oilseed. Fig. (3-3) was built by assuming that depressurization occurs isothermally, that the density of the loaded CO_2 phase is not affected by dissolved oil and can be estimated as a function of instantaneous system pressure using NIST database (Lemmon et al., 2007), that oil and CO_2 in the loop are perfectly mixed, and that the instantaneous solubility of the oil in SC CO_2 can be estimated as a function of the instantaneous density of CO_2 and system temperature (50 ºC) using the equation of del Valle et al. (2012) (Appendix B-1). Fig. (3-3) shows that the drop in solubility during sampling in the closed loop mode leads to 39, 57, and 79% of the initial concentrations (evaluated as the sum of

sampled oil divided by the sum of sampled CO_2) when nine grams are sampled from loops initially equilibrated at 6.78 g kg^{-1} oil/CO_2 (100% of saturation concentration (del Valle et al., 2012)), 4.07 g kg^{-1} oil/CO_2 (60% of saturation concentration), and 2.03 g kg^{-1} oil/CO_2 (30% of saturation concentration), respectively.

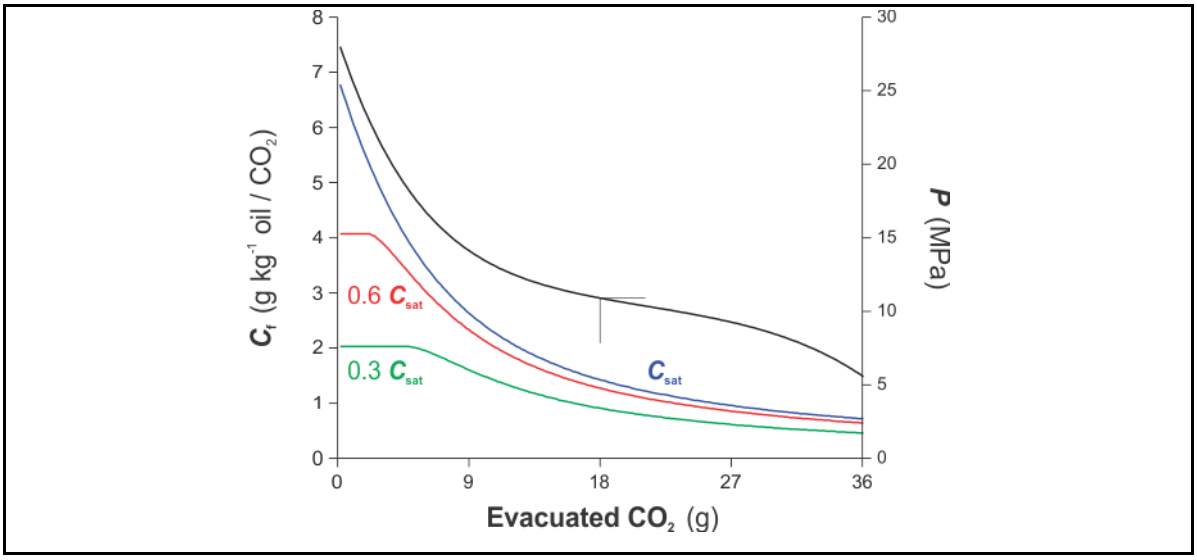

Figure 3-3. Effects of sampling in a closed loop mode in the pressure and apparent concentration of oil in CO_2 for the three different equilibrium concentrations noted. Assumed initial conditions were 50 °C and 28 MPa.

Sampling in an open loop mode causes smaller discrepancies between true and measured (apparent) oil concentration in SC CO_2 than sampling in a closed loop. Authors assumed that either there was perfect mixing of the SCF fluid phase in the equilibration sub-system or that oil transferred from the solid to the SCF phase in the equilibrium cell as in a conventional extraction process during sampling in the open loop mode. If the solid matrix in the equilibrium cell does not interact with the SC CO_2 phase in equilibration sub-system, and if this phase is perfectly mixed, the net effect of adding fresh CO_2 to the loop to keep the pressure constant is to continuously dilute the oil remaining in the SC CO_2 phase (Appendix B-2). Fig. (3-4) shows changes in apparent oil concentration as a function of sampled CO_2 (<36 g) and initial oil concentration in SC CO_2 at 50 ºC and 28 MPa equilibrated with the pre-treated oilseed under same conditions analysed in Fig. (3-3).

Under the assumption of perfect mixing, when nine grams are sampled from loops initially equilibrated to 30, 60 and 100% of the saturation concentration the open loop mode leads to 90% (1.83, 3.67, and 6.11 g kg^{-1} oil/CO_2 respectively) of the actual concentrations, Fig. (3-4). This assumption is questionable because mass transfer from, and equilibrium partition with the solid substrate in the equilibrium cell are neglected that may add oil to the SC CO_2 in the loop during sampling.

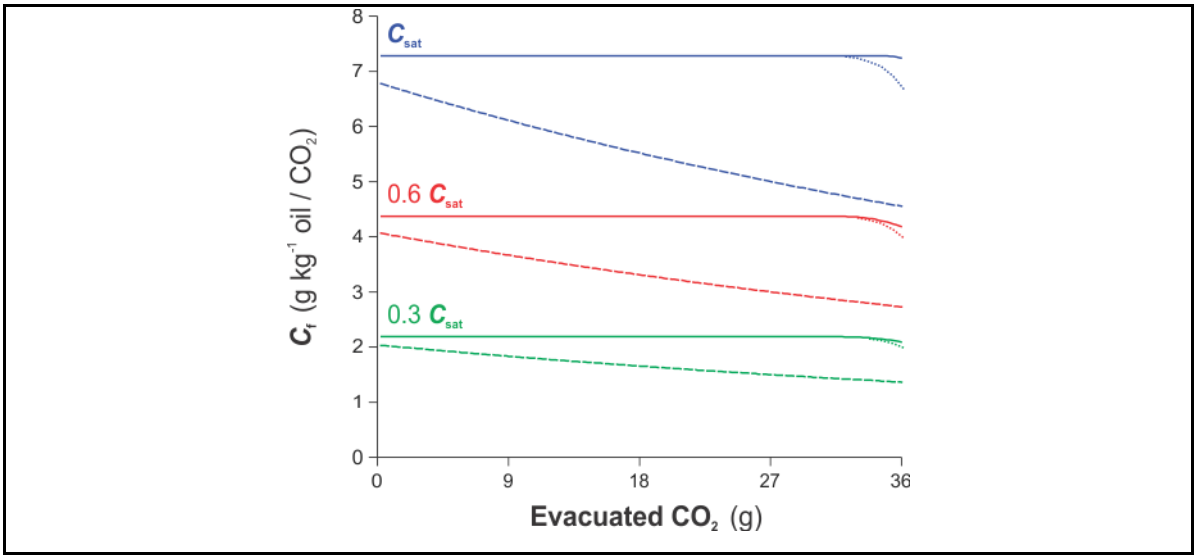

Figure 3-4. Effects of sampling in a closed loop mode in the pressure and apparent concentration of oil in CO_2 for the three different equilibrium concentrations noted. Dashed lines indicate perfect mixing, continuous lines indicate dispersed plug flow for "ground" pellets, and dotted lines indicated dispersed plug flow for "square" pellets. Assumed initial conditions were 50 °C and 28 MPa.

If the solid matrix in the equilibrium cell does interact with the fresh SC CO_2 added to the equilibration sub-system, the amount of additional oil released can be estimated by using mathematical simulation (Appendix B-1). Authors modelled the equilibrium cell as a packed bed extractor discretized in time and space, coupling equilibrium partition of the oil, mass transfer by diffusion in the interconnected pore network of the prepressed seed, and mass transfer by convection in a film of stagnant SC CO_2 next to "square" or "ground" pellets using a Linear Driving Force (LDF) approximation with a global mass transfer

coefficient, and accounting for the axial dispersion of the oil along the extractor. Authors considered that the cell was fed with pure SC CO_2, and assumed that the concentration of oil in the sampled SC CO_2 equalled that in SC CO_2 phase leaving the cell. Under the assumption that the substrate interacts with fresh SC CO_2, the equilibrium concentrations of oil virtually do not change as a result of sampling of nine grams of CO_2 (Fig. 3-4).

Sampling lines should be washed out with an organic solvent after completing sampling or extraction steps in order to recover the precipitated solute. In the sampling sub-system, pressure drops to the atmospheric level causes precipitation of part of the oil on the inner walls of the sampling lines between valve D and the sampling tube. Unreported preliminary experimental runs showed that >90% of the solute remains in the sampling lines. By weighing the oil recovered using 1 cm^3 portions of hexane authors observed no further oil recovery after washing the sampling lines with 8 and 16 cm^3 for equilibrium and extraction steps, respectively.

To minimize weighing uncertainties, the weight ratio between sampled oil, on one hand, and sampling tube and tube holder, on the other, should be as large as possible, Appendix (B-2). Because authors found a linear relationship between the uncertainty in the weight of oil and the ratio of its weight and that of its container and container holder, 4-cm^3 vials were placed within the test tube and used to recover and quantify the oil. Under those conditions, average uncertainties (0.1%) were considerable smaller than when using the original 50-cm^3 test tube (average uncertainties of 61%).

The measurement methodology applied in this work is less uncertain about oil concentrations in the SC CO_2 than oil concentrations in the prepressed rapeseed along the isotherm/isobar curve, Fig. (3-5). Authors applied an uncertainty analysis, Appendix (B-3), to the isotherm/isobar curve measured at 50 °C and 28 MPa with “ground” pellets. The uncertainty of oil concentration in SC CO_2 was 1.3% of the calculated values, which ranged between 0.002 and 0.104 g kg^{-1} oil/CO_2 (for the lowest and highest calculated values, respectively). On the other hand, the uncertainty of oil concentration in the substrate (noted with horizontal bars in Fig. (3-5)) was constant at 0.0118 kg kg^{-1} oil/substrate, between 7.0 and 55% (for the lowest and highest calculated values, respectively). Coverage intervals for 95% of the data obtained with a Monte Carlo

simulation described in Appendix (B-3) fitted exactly within the calculated standard uncertainties (unreported result).

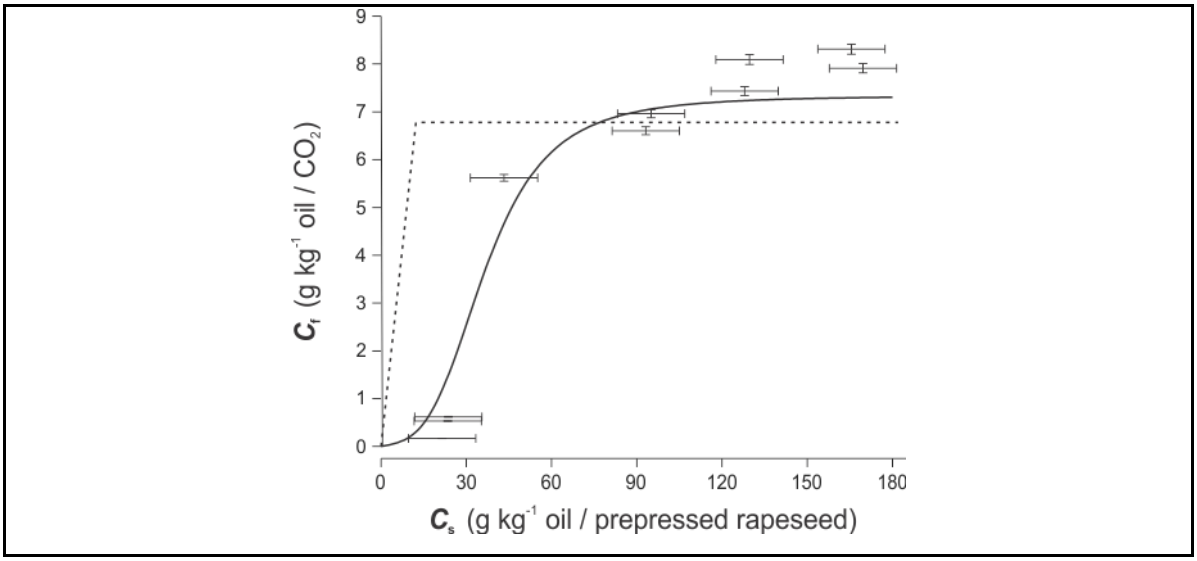

Figure 3-5. Uncertainty analysis of the measurands (C_f, C_s) for "ground" pellets isotherm/isobar curve at 50 °C and 28 MPa. Parallel horizontal bars signal uncertainties in oil concentration in the SC CO_2 phase, whereas parallel vertical bars signal uncertainties in oil concentration in the oilseed phase. The dotted line represents the isotherm/isobar estimated neglecting sorption effects in the oilseed, whereas the continuous line represents the trend line for the experimental data.

Isotherm/isobar curves measured in this work are not adequately represented with isotherm/isobar equations neglecting sorption effects between the oil and the prepressed rapeseed. If rapeseed oil completely dissolves in SC CO_2 up to an amount corresponding to the saturation concentration of the oil in the SC CO_2 and then partitions between the inter- and intra-particle spaces, equilibrium partition is described by a straight line by the origin, Eq. (3.6a), whose slope is given by Eq. (3.7) (del Valle & Urrego, 2012) and presented in Fig. (3-5). Being the solvent power of SC CO_2 limited, under selected conditions not all oil in a sample can be dissolved so that some excess rapeseed oil remains precipitated within inner substrate pores, and this described by the horizontal portion of the linear isotherm, Eq. (3.6b).

$$C_f = K\ C_{sat},\ \text{if } C_s \le \frac{C_{sat}}{K},\ \text{and} \tag{3.6a}$$

$$C_f = C_{sat},\ \text{otherwise} \tag{3.6b}$$

$$\text{where } K = \frac{(1-\varepsilon')(1-\varepsilon_p)}{\varepsilon' + (1-\varepsilon')\varepsilon_p}\frac{\rho_s}{\rho}. \tag{3.7}$$

The value of ε' in Eq. (7) considers the extra volume for SC CO_2 in the recirculation loop of the equilibrium (volume of tubing and fittings and dead volume of components) and can be computed using Eq. (8):

$$\varepsilon' = 1-(1-\varepsilon)\frac{V_{cell}}{V_{loop}} = 0.607 \tag{3.8}$$

Replacing ε' from Eq. (3.8) and the values of other parameters in Eq. (3.7), the value of K in Eq. (3.6a) was 0.584 kg kg^{-1} substrate/CO_2. Fig. (3-5) also includes Eq. (3.9), that was proposed by del Valle and Urrego (2012) to model isotherm/isobar curves of vegetable extracts between the vegetable substrate and SC CO_2, which presents a sigmoidal shape, where C_{sat}, α, A and n are fitting parameters (details on the values and significance parameters discussed later).

$$C_f = C_{sat}\left[\alpha\ C_s + (1-\alpha\ C_s)\frac{C_s^n}{A+C_s^n}\right] \tag{3.9}$$

Authors asked questions about the reproducibility of the experiments, and about the effect of rapeseed pretreatment on the equilibrium partition of the oil between SC CO_2 and prepressed seeds, which were answered using F tests. F tests measure if improvement in data fitting resulting from segregation of data sets warrants separation of the data sets, or if the data sets can be pooled together with no loss of statistical significance. For comparisons the pseudo-Sip's equation [α = 0 in Eq. (3.9)] was adopted using a single value of C_{sat} for all data sets. Statigraph F was computed using Eq. (3.10) (del Valle, Aguilera, Hohlberg, Richardson, & Stanley, 1993), where *SSE*s correspond to Sums of Squared Errors (or sums of squared discrepancies between experimental and fitted data

points), *df*s correspond to degrees of freedom (or differences between numbers of data points and best-fitting model parameters), subindex 'c' represents the so-called 'complete' model (with best-fitting parameters *A* and *n* segregated by data set), and subindex 'r' represents the so-called 'reduced' model (with single best-fitting parameters *A* and *n* for all data sets). Thus, ($SSE_c - SSE_r$) in the numerator represents the increase in the discrepancies when using single best-fitting values of *A* and *n* for all data sets, and ($df_c - df_r$) is the additional number of best-fitting parameters required to segregate data sets. *F* follows a Fisher-Snedecor distribution with ($df_r - df_c$) degrees of freedom in the numerator and df_c degrees of freedom in the denominator (del Valle et al., 1993).

$$F = \frac{\left(SSE_r - SSE_c\right)/\left(df_r - df_c\right)}{SSE_c/df_c} \tag{3.10}$$

Fig. (3-6) summarizes the reproducibility of experiments at 50 ºC and 28 MPa using "square" pellets with best-fitting lines of the complete model showing some discrepancies between replicates (≤0.66 g kg^{-1} oil/CO_2) within the interval from 10 to 140 g kg^{-1} oil/rapeseed. The value of *F* computed using Eq. (3.10), 0.98, was greater than 0.72 ($f_{0.50}$,2,19) indicating that there is a significant ($p > 0.50$) difference between replicates at a large (50%) probability level.

Fig. (3-6) summarizes also the effect of supplementary milling on the partition of oil between SC CO_2 and prepressed rapeseed at 50 ºC and 28 MPa. In this case (not all best-fitting lines shown) the complete model showed less discrepancies between pretreatments (≤0.38 g kg^{-1} oil/CO_2) within a wider interval from 8 to 180 g kg^{-1} oil/rapeseed. The value of *F* computed using Eq. (3.10) when pooling together the two replicates using "square" pellets, 0.87, is greater than 0.71 ($f_{0.50}$,2,29) indicating that there is also a significant ($p > 0.50$) difference between pretreatments at the 50% probability level. Statistical significance notwithstanding, all predictions were within the band that can be surmised in Fig. (3-6) that is comparatively narrow as compared to the data scattering intrinsic to the method (Fig. 3-5).

Under isothermal conditions (40 ºC), an increase in pressure from 22 to 28 MPa has a large effect on equilibrium partition of oil between SC CO_2 and milled rapeseeds, Fig. (3-7), particularly for residual oil concentrations in the substrate above ~40 g kg^{-1} oil rapese-

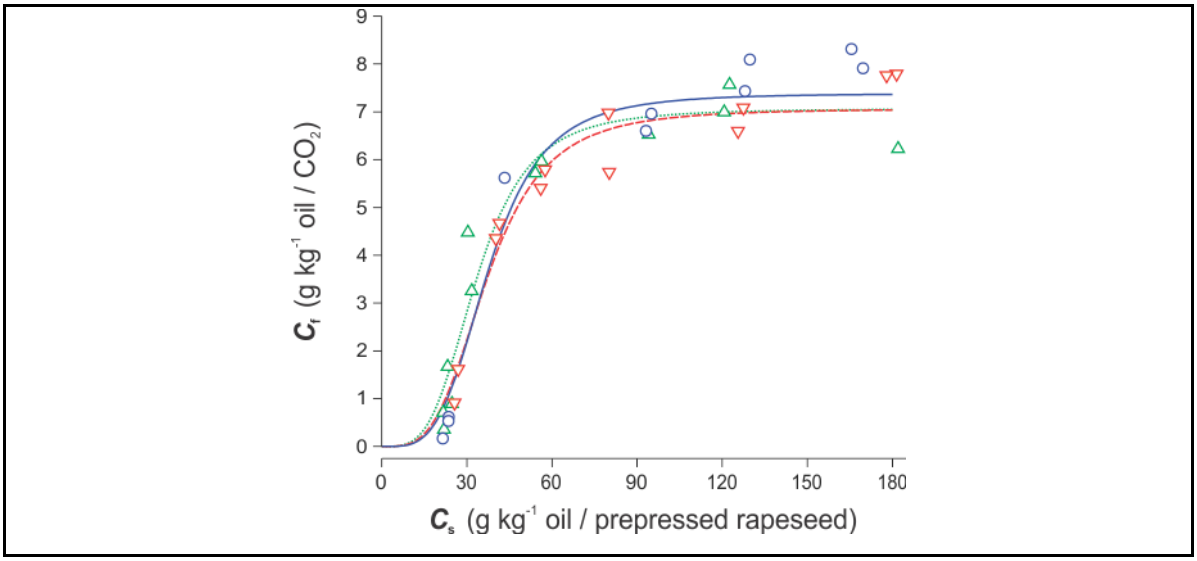

Figure 3-6. Effect of the replication and substrate pre-treatment on isotherm/isobar curves at 50 ºC and 28 MPa, where (△ ,▽) represent duplicates using "square" pellets and (○) data obtained using "ground" pellets. Lines represent predictions using pseudo-Sips‟ model using complete models to study the effect of replication and substrate pretreatment.

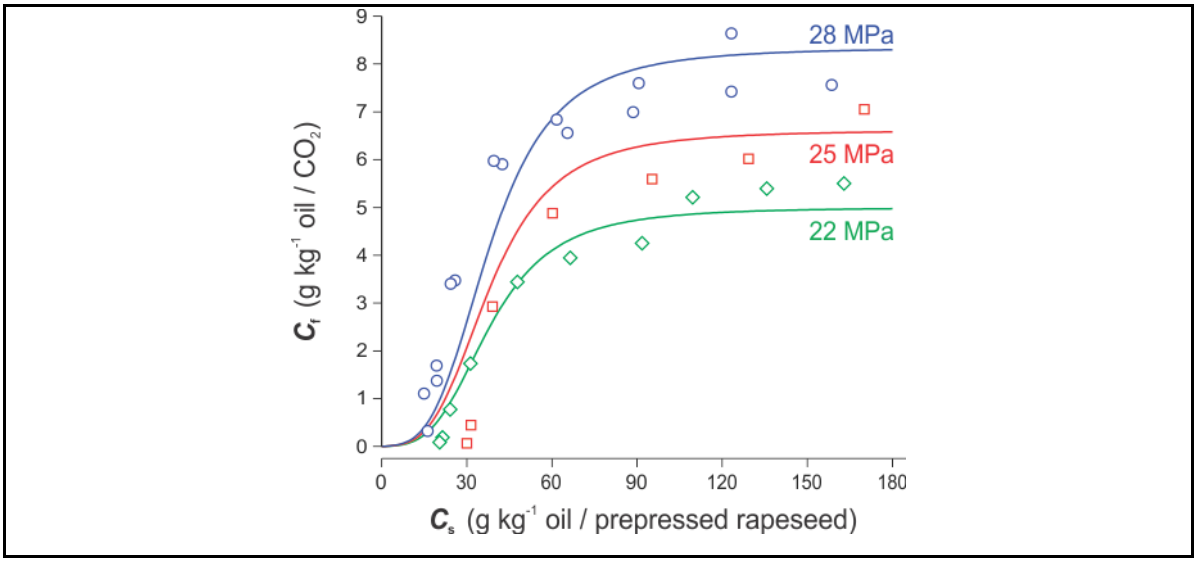

Figure 3-7. Effect of pressure on isotherm/isobar curves measured at 40 °C. (◊) 22 MPa, (□) 25 MPa, and (○) 28 MPa.

ed. Authors believe this is due in part to the increase in the solvation power of CO_2 associated with the increase in density brought about by the increase in pressure (from 857.1 kg/m^3 at 22 MPa to 898.5 kg/m^3 at 28 MPa). Indeed, using the equation of del Valle et al. (2012) authors estimated that the solubility of vegetable oil in SC CO_2 at 40 ºC may increase from 4.44 g kg^{-1} oil/CO_2 at 22 MPa to 7.15 g kg^{-1} oil/CO_2 at 28 MPa. On the other hand, differences in oil partition as a function of pressure virtually disappear when the residual concentration of oil in the substrate diminishes below ~20 g kg^{-1} oil/rapeseed. However, as previously presented, there is a lot of uncertainty in experimental values in this region.

In the case of isotherm/isobar curves measured at the same SC CO_2 density (857.1 kg/m^3), Fig. (3-8), pressure values were the same as those in Fig. (3-7) (22, 25 and 28 MPa), but in this case temperature values were 40, 45, and 50 °C, respectively. Main differences occur also in the zone of the horizontal asymptotes (residual oil concentrations in the substrate above ~90 g kg^{-1} oil/rapeseed) but were smaller than those observed in Fig. (3-7). In this case the effect of the increase in the solvation power was brought about by the temperature instead of the SC CO_2 density, and using the equation of del Valle et al. (2012) authors estimated that the solubility of vegetable oil may increase from 4.44 g kg^{-1} oil/CO_2 at 40 °C and 22 MPa to 6.78 g kg^{-1} oil/CO_2 at 50 °C and 28 MPa.

Data in Fig. (3-8) containing sorption isotherms at the same SC CO_2 density allows estimating the total heat of sorption ΔH (energy required to desorb the oil from the rapeseed and solvate it in SC CO_2) using an Arrhenius-type relationship, Eq. (3.11), between the equilibrium concentration of oil in SC CO_2 (C_f) as a function of absolute temperature (T):

$$C_f = C_f^\circ \exp\left[-\frac{\Delta H}{R}\left(\frac{1}{T}-\frac{1}{T^\circ}\right)\right], \qquad (3.11)$$

where C_f° is the equilibrium concentration of oil in SC CO_2 at an absolute temperature T°, and R (0.008314 kJ mol^{-1} K^{-1}) is the gas constant. This is exemplified in Fig. (3-9), where the slope of lines of log (C_f) *versus* T^{-1} represents -0.434 $\Delta H(C_f)/R$. The negative value of the slopes qualifies oil desorption using SC CO_2 as an endothermic process.

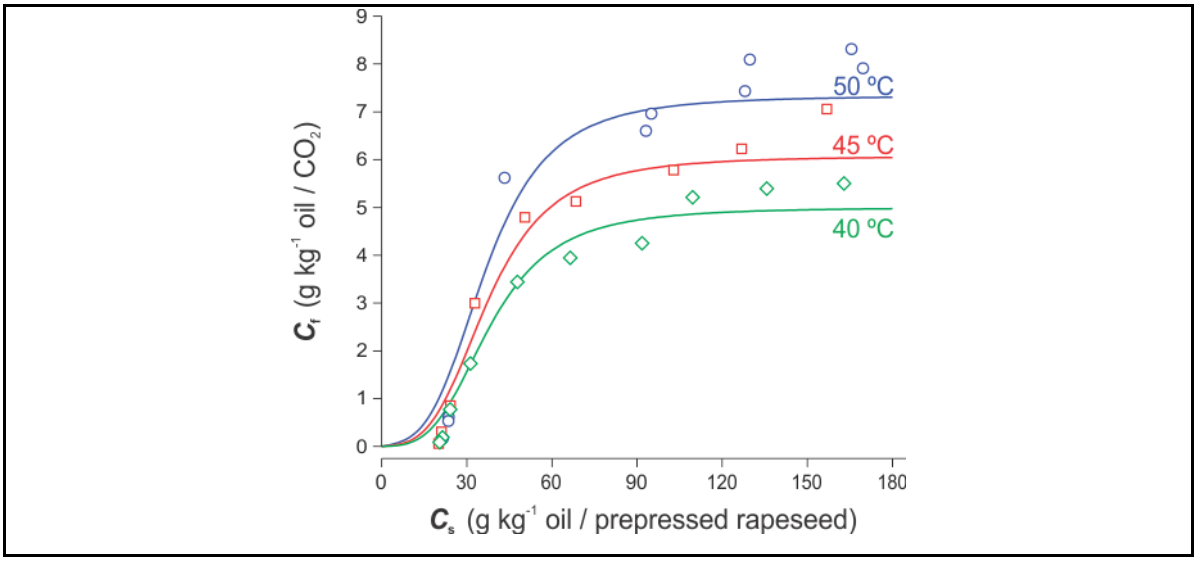

Figure 3-8. Effect of temperature on isotherm/isobar curves measured at the same SC CO_2 density (857.1 kg/m^3). (◊) 40 °C-22 MPa, (□) 45 °C-25 MPa, and (○) 50 °C-28 MPa.

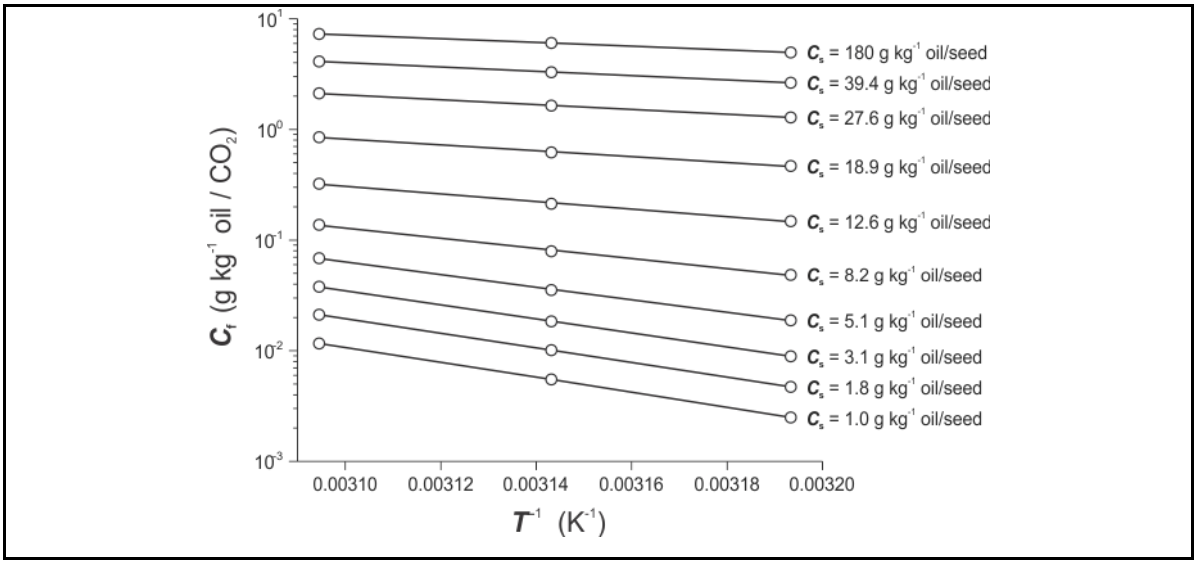

Figure 3-9. Arrehnius-type plot of oil concentration in CO_2 (C_f) *versus* reciprocal of absolute temperature (T^{-1}) as a function of the residual oil content in the substrate (C_s).

The values of ΔH estimated from Fig. (3-9) for different residual concentrations of oil in prepressed rapeseed increase as the oil content decreases, as expected, Fig. (3-10). It varies from 32 kJ/mol from the horizontal asymptote zone, (heat of solvation), up to 128 kJ/mol when there is virtually no residual oil in the substrate (heat of desorption plus solvation). Physisorption is due to van der Waals' weak (~10-100meV) interaction forces between solute atoms and binding sites on the solid adsorbent associated with permanent, induced, or transient electrical dipoles. This translates roughly to activation energies of about 1-10 kJ/mol but does not account for the increase in activation energy associated with the increase in the number of atoms that participate in binging per molecule as the molecular weight increases. For example, in the case of the binding of alkanes on an Au(111) surface, the activation energy for desorption increases from 40.5 kJ/mol for pentane to 80.1 kJ/mol for decane (Wetterer, Lavrich, Cummings, Bernasek, & Scoles, 1998) (or about 4-8 kJ/mol per CH_2 group (Salem, 1962)). In contrast, chemisorption is due to stronger (~100-1000 kJ/mol). The activation energies for chemisorption depen less on chain length than those for physisorption as shown by Lavrich, Wetterer, Bernasek, and Scoles (1998) for the desorption of alkanethiols and dialkyl sulphides from an AU(111) surface. Based on these antecedents we believe that physisorption is responsible for the activation energy of ca. 96 kJ/mol noted in Fig. (3-10) for desorption of very large oil molecules (three hydrocarbon chains of 18 carbon groups (del Valle & de la Fuente, 2006)) from prepressed rapedeeds. However, as previously discussed, oil partition values for residual oil contents in prepressed rapeseed below ~20 g kg_{-1} oil/CO_2 are highly speculative and therefore the differences between the total heats of desorption at that level and the heat of solvation are questionable.

Trend lines in Figures (3-7) and (3-8) were obtained using Equation (3.9). All experimental results were fitted to the model simultaneously under the assumption that sorption was not affected by milling of prepressed rapeseeds, and that parameter C_{sat} depended on the absolute temperature of the system (T, K) and the density of SC-CO_2 at system conditions (ρ, kg/m^3) as predicted by Chrastil's model (1982), Eq. (3.12a), α depended on T as predicted by Arrhenius' model, Eq. (3.12b), A depended on T as predicted by an empirical model, Eq. (3.12c), and n was independent on system conditions:

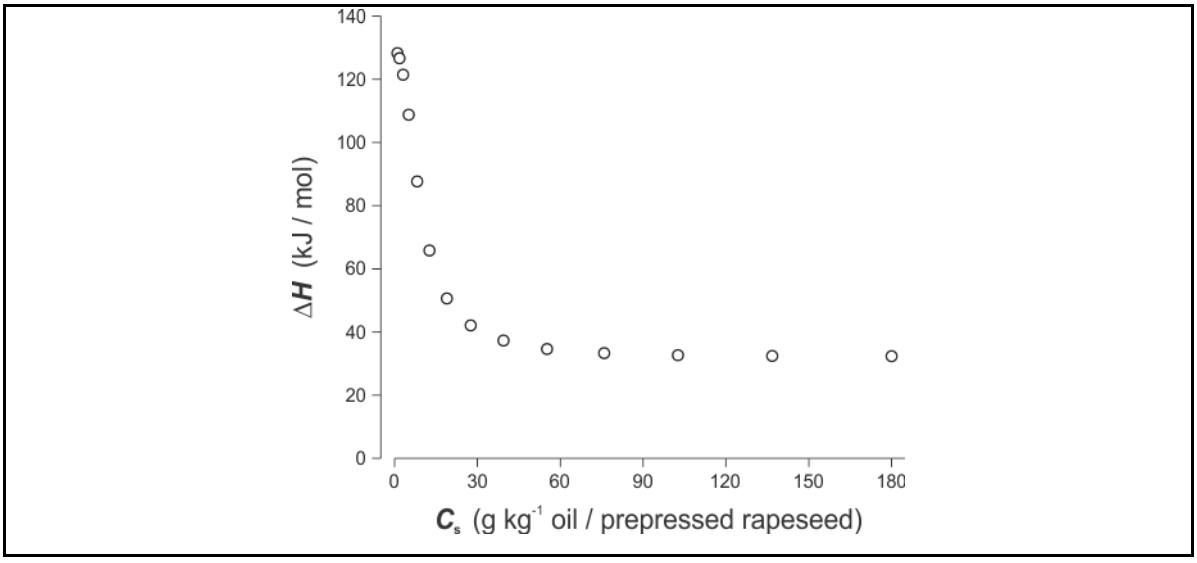

Figure 3-10. Dependence of the total heat of desorption from the substrate and solvation in CO_2 (ΔH) of the oil as a function of the residual oil contecnt in the substrate (C_s).

$$C_{sat} = C_{sat}^{\circ}\left(\frac{\rho}{857.1}\right)^{k-1}\exp\left[-\frac{\Delta H_{solv}}{0.008314}\left(\frac{1}{T}-\frac{1}{313.3}\right)\right], \tag{3.12a}$$

$$\alpha = \alpha^{\circ}\exp\left[-\frac{\Delta H_{sorp}}{0.008314}\left(\frac{1}{T}-\frac{1}{313.3}\right)\right], \text{ and} \tag{3.12b}$$

$$A = \frac{b\,A^{\circ}}{b+\left(T-313.2\right)}, \tag{3.12c}$$

where C_{sat}° is the solubility of rapeseed oil at a reference condition of 40 ºC (313.2 K) and 22 MPa for which the density of SC CO_2 is 857.1 kg/m^3, k is an association number representing the number of SC CO_2 molecules that form a complex with a single molecule of rapeseed oil (Chrastil, 1982), ΔH_{solv} is the heat required to synthesize the solvato complex that includes the heat of vaporization and dissolution in SC CO_2 of the oil (Chrastil, 1982), α^{o} is the equilibrium partition of the oil between SC CO_2 and prepressed rapeseed at 40 ºC, ΔH_{sorp} is the heat of sorption of the oil in prepressed rapeseed (Nollet,

Roels, Lutgen, Van der Meeren, & Verstraete, 2003), A^o is the value of parameter A at 40 ºC, and b is an empirical parameter. The best-fitting model parameters were estimated using standard Solver's function of Microsoft Excel 2010® by minimizing the sum of discrepancies, which calculated as the square of differences between the experimental values C_f and those estimated using Eq. (3.9) using definitions in Eqs. (3.12a-c). Best-fitting values of model parameters were as follows: C°_{sat} = 5.00 g kg^{-1} oil/CO_2, k = 11.8, ΔH_{solv} = 32.2 kJ/mol, α^o = 0.5 kg k-1 substrate/oil, ΔH_{sorp} = 96.7 kJ/mol, n = 3.34, A^o = 1.895×10^{-5}, and b = 177.5 K.

3.4. Discussion

Sorption isotherms/isobars in Fig. (3-6) and Fig. (3-7) and data fitting suggest that oil desorption is a two-stage process that conforms the "realistic shape" suggested by Perrut et al. (1997). There is a region for high residual oil contents in the prepressed substrate (>60-90 g kg^{-1} oil/substrate) where there is enough free oil on the surface of the pellets to allow the SC CO_2 phase to get saturated with oil. Based on 238 data points from fifteen experimental studies of eleven vegetable substrates, del Valle et al. (2012) proposed a general equation to estimate C_{sat} of seed oils as a function of the absolute temperature of system and the density of SC CO_2 to within ±40% experimental values. This applied to values of C_{sat} estimated in this work using Eq. (3.12a) and best-fitting values of C°_{sat}, k, and ΔH_{solv} that were within 8-17% of the values predicted using the equation of del Valle et al. (2012). The best-fitted association number for isotherm/isobar curves measured in this work (k = 11.8) lies within the limits observed by del Valle et al. (2012) (8.45-11.4, with an average value of 10.6), whereas the heat of solvation (ΔH_{solv} = 32.2 kJ/mol) was smaller than observed in that work (75.6-94.7 kJ/mol, with an average value of 83.7 kJ/mol). These diffrences may be explained by the much larger temperature interval studied by del Valle et al. (2012) (80ºC, from 20 to 100ºC) than used in this work (10ºC) that allowed them a more precise estimate of solvation heat. Because C_{sat} might be estimated using a literature relationship, if available, or using thermodynamic data for the binary SC CO_2 – vegetable extract system, the number of best-fitting parameters in the sorption model proposed by del

Valle and Urrego (2012), Eq. (3.9), might be reduced to α, *A*, and *n*.

For residual oil contents in the prepressed substrate below 60-90 g kg^{-1} oil/substrate, sorption effects define the equilibrium concentration of oil in the SC CO_2 phase that cannot get saturated with oil. Because of this sorption effects, this equilibrium concentration is below the one attainable if all oil were dissolved in SC CO_2 and partitioned between the inter and intraparticle void fraction as noted by the straight line containing the origin of Fig. (3-5). The linear isotherm/isobar curve in Fig. (3-5) shows that when there is >12 g kg^{-1} oil/substrate in the equilibrium cell, remaining oil is still enough to saturate the SC CO_2 in the loop, but data shows this is not possible when there is <77 g kg^{-1} oil/substrate where the ideal isotherm/isobar curve with no interaction between the oil and substrate, and experimental curve intercept. Perrut et al. (1997) proposed a linear partition of the oil between the SC CO_2 and solid substrate in this region, but this is not supported by the data, partially due to large experimental uncertainties.

During equilibrium, solute flux from the solid to the fluid phase reach a maximum only limited by sorption or solubility effects, so it might be assumed that substrate size and shape does not affect the sorption isotherm/isobar curve, as noted when analysing the effect of sample pre-treatment. However, it is apparent in Fig. (3-5) that decreasing particle size is helpful in decreasing data dispersion and speeding up the process by improving mass transfer.

The precision and accuracy of the method is questionable for low residual oil contents in the vegetable substrate as suggested by poor reproducibility and the analysis of inherited errors. Therefore, results for parameter α, and consequently results for the heat of sorption in Fig. (3-10) are highly speculative. To the best of the authors' knowledge this might be overcome by modifying the method to include analytical measurements of the sampled vegetable extracts. Furthermore, when using a gravimetric method, the limit of detection of dissolved solutes in SC CO_2 depends on the limits of the balance used. This limit may be reduced by making a calibration curve of a solute of interest from the vegetable extract to allow its quantification with the UV/Vis detector, but in this case the solutes should be diluted so that their concentration is within the range chosen for the calibration curve.

Each point in each isotherm/isobar curve demands an eight-hour equilibration period (one experimentation day) plus one day for extractions between each pair of equilibration points. Thus measuring each isotherm/isobar took three weeks in average. Furthermore, no mistake was allowed in this period because of the need to close the mass balance for the oil for the overall experiment, as required to estimate the equilibrium concentrations in solid substrate. There are alternative dynamic (chromatographic) procedures to determine the sorption isotherm/isobar curve using less time than this static procedure, which can be used to limit experimental work. These methods use a packed bed with an extract-free solid matrix (previously extracted to exhaustion) as the adsorbent column, inject pulses or bands of modified SC CO_2 with controlled and increasing concentrations of extract, and continuously register the concentration of extract in the stream leaving the column. In frontal analysis the shape and retention time of the front of the breakthrough curve (extract concentration in the SC CO_2 stream leaving the adsorbent column *versus* time) signal the chord (compressed fronts) or local slope (dispersed fronts) of the sorption isotherm/isobar curve for the interval between the initial and final equilibrium concentration of extract in the solid matrix (Seidel-Morgenstern, 2004). Alternatively, a mass balance estimates the total amount of extract adsorbed by the solid matrix based on the integration of the breakthrough curve (Brunner & Johannsen, 2006). In perturbation analysis the retention time of a small pulse over a band gives the local slope of the sorption isotherm/isobar curve for the equilibrium concentration of extract in the solid matrix corresponding to the concentration of extract in SC CO_2 in the band (Brunner & Johannsen, 2006; Seidel-Morgenstern, 2004). Both frontal and perturbation analysis may consume large amounts of CO_2, extract, and time, but give discrete and precise points of the sorption isotherm/isobar curve. In addition, the dispersed rear part of the chromatogram when switching the feed to pure SC CO_2 gives continuous information about the (de)sorption isotherm/isobar curve, because each point relates the concentration of extract in SC CO_2 given by the chromatogram with the “equilibrium” concentration of solute in the solid matrix at the end of the adsorption column. The dispersed rear part of the chromatogram can be used as input for a continuous (de)sorption isotherm/isobar curve model that can be fitted using inverse analysis (Brunner & Johannsen, 2006; Seidel-

Morgenstern, 2004). Because inverse analysis of chromatograms corresponding to injection of bands without enough solute to fully saturate the column may also give best-fitting parameters of mathematical models of sorption isotherm/isobar curves in limited ranges below saturation of the solid matrix, this method may require less CO_2, extract, and time than frontal or perturbation analysis, but has limitations for inefficient columns (with few theoretical plates) when mass transfer limitations affect extract desorption, and when little is known about the shape of the (de)sorption isotherm/isobar curve. Authors believe it is possible limiting experimental effort without reducing precision in estimation of desorption isotherm/isobar curve to a great extent by combining dynamic methods with our static method. The later provides a mathematical model that fits the shape of the isotherm/isobar curve, and validate results using dynamic methods.

4. EQUILIBRIUM PARTITION OF RED PEPPER EXTRACT BETWEEN PURE OR VEGETABLE-OIL MODIFIED CO_2 AND PELLETIZED AND MILLED RED PEPPER

Abstract

The importance of measuring the equilibrium partition of a solute between a vegetable substrate and SC CO_2 becomes more significant when a co-solvent (a compound that aids and enhance the extraction) is added, because its influence remains unidentified. We applied a previously validated and standardized experimental methodology, to measure the equilibrium partition of red pepper oleoresin (and carotenoids) between pelletized-milled red pepper and pure or vegetable-oil modified SC CO_2, at 54-67 °C and 22-28 MPa. Oleoresin partition for non-modified SC CO_2 showed no saturation of the SC CO_2 phase and was modelled with a pseudo-Sip's equation, whereas extract (a mixture of oleoresin and vegetable oil) partition for modified SC CO_2, showed higher oleoresin concentrations in SC CO_2 with a trend to reach the value of the saturation concentration, and was modelled with the del Valle-Urrego equation. For measurements with the non-modified red pepper, the partition of the carotenoids to the SC CO_2 phase decreased together with the oleoresin contents in SC CO_2, and for the measurement with the modified red pepper, two diminishing trends were observed, one less pronounced when extract concentration in the solid is between 20-40 g kg^{-1} extract/solid, and one more pronounced below 20 g kg^{-1} extract/solid. The sorption isotherm/isobar model was included in the Broken and Intact Cells (BIC) extraction model, and two extraction conditions were simulated, one at an operational condition studied in this work (60ºC-28 MPa), and one where the isotherm/isobar model was extrapolated (40ºC-28 MPa). A good fit was obtained when all but one (S_o, the initial amount of extractable solute) of the parameters of the model were calculated with correlations available in literature.

4.1. Introduction

The food industry is interested in isolating carotenoids from biological substrates

because of their tinctorial and nutraceutical (antioxidant) properties. Although supercritical CO_2 (SC CO_2) has arisen as a suitable solvent in food extraction applications, carotenoids have low solubilities in SC CO_2 (Sovova, Stateva, & Galushko, 2001). To circumvent this problem, vegetable oils have been used as modifiers for the SC CO_2 extraction of carotenoids from tomato (Vasapollo et al., 2004), carrot (Sun & Temelli, 2006), and marigold (Q. X. Ma et al., 2008), but their effect in the equilibrium partition has not been identified.

The effect of vegetable oils on the solubility in SC CO_2 of carotenoids was already investigated by Araus et al. (2011), whom measured the solubility of β-carotene (chemical standard) in pure and modified (ethanol, and high-oleic-oil or triolein) SC CO_2 at 40-60 ºC and 17-34 MPa. Araus et al. (2011) fount that the solubility of β-carotene in triolein-modified SC CO_2 increased by factor of up to 4 compared with the solubility of β-carotene in pure CO_2 at the same operating conditions, which might respond to an increase in the polarizability of SC CO_2, growing markedly when the system pressure becomes higher as SC CO_2 dissolves more triolein. Araus, del Valle, Robert, and de la Fuente (2012) measured the solubility of capsanthin (isolated from red pepper *Capsicum annuum* L.) in pure and modified (triolein) SC CO_2 at 40-60ºC and 19-34 MPa. Araus et al. (2012) found that the solubility of capsanthin in triolein-modified SC CO_2 increased by factor of up to 3 compared with the solubility of capsanthin in pure CO_2 at the same operating conditions. However, in the extraction of vegetable substrates, the solutes may interact with the solid matrix, affecting the solvation power of the CO_2, and/or the partition of the solute between the fluid (SC CO_2) and solid (substrate) phases.

Uquiche, Araus, and del Valle (in preparation) evaluated the use of pelletization (as pretreatment) of red pepper (*Capsicum annuum* L) to enhance the extraction of oleoresin (and carotenoids) with pure or triolein-modified SC CO_2. Uquiche et al. (in preparation) extracted pelletized red pepper at 40-60ºC and 28-50 MPa, and found that the extraction rate and yield, of oleoresin, total carotenoids, and capsanthin, increased with the temperature, pressure, and the addition of sunflower oil. Uquiche et al. (in preparation) modeled the integral extraction curves of total carotenoids, and capsanthin, using the Desorption-Dissolution-Diffusion (DDD) model. Although the integral extraction curves

of oleoresin were not reported, two integral extraction curves one at 60ºC – 28 MPa (condition studied in this work), and one at 40ºC-28 MPa (outside the conditions studied in this work to evaluate extrapolation capabilities), were facilitated by the authors for the extraction modelling purposes of this work (Fig. 4-1). Integral extraction curves of modified SC CO_2 were not provided because it was difficult to discriminate the oleoresin from the triolein extraction.

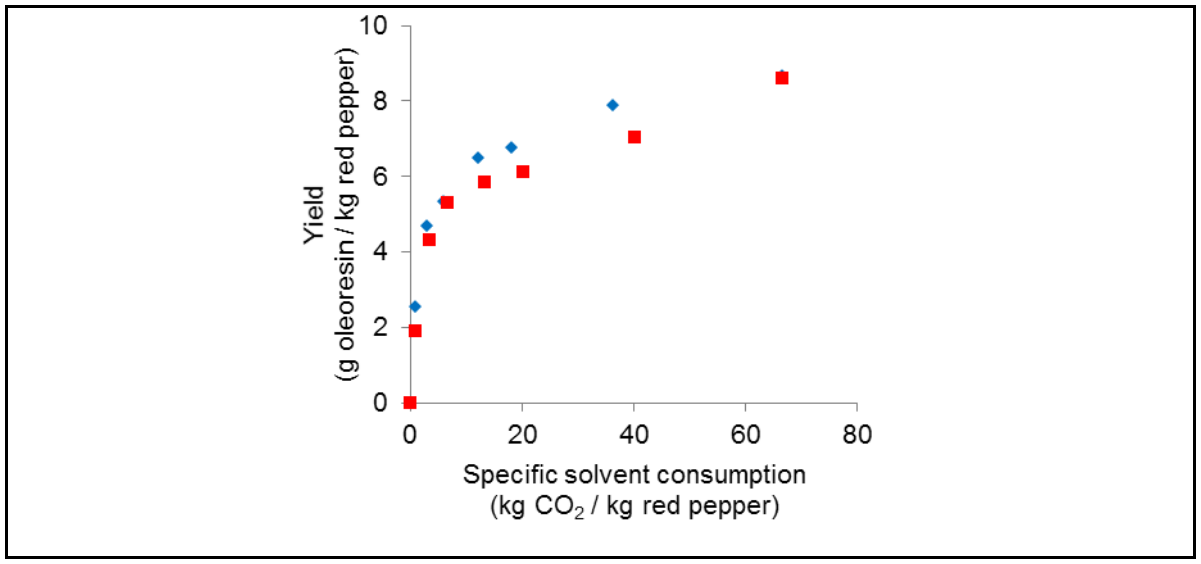

Figure 4-1. Integral extraction curves of oleoresin from red pepper at 40 (■) and 60 ºC (♦) - 28 MPa. Experimental data provided by Uquiche et al. (in preparation).

del Valle and Urrego (2012) claimed that the equilibrium partition of vegetable extracts should be experimentally determined instead of being calculated from best-fitting extraction experiments, so as to reduce the possibility that best-fit parameters do not respond to the physical reality. Urrego, Nuñez, Donaire, and del Valle (Submitted) developed, standardized, and validated an experimental methodology to measure the equilibrium partition of vegetable extracts between vegetable substrates and SC CO_2, by measuring the equilibrium partition of rapeseed oil between prepressed rapeseed and SC CO_2 at 40-60 ºC and 22-28 MPa, they found that the fluid concentration (C_f) is limited by the saturation concentration (C_{sat}), which in turn approximately equaled the solubility of vegetable oil in SC CO_2 under the same operating conditions. However, they also observed

that there was a residual oil concentration in the substrate (C_s) below which oil-substrate interactions impeded the saturation of the SC CO_2, even when there was enough oil to do it, concluding that besides the solubility and saturation concentration determinations, it is also important to experimentally measure the solute-substrate interactions.

The objective of this work was to measure and model oleoresin (carotenoids) partition between pelletized and milled red pepper (*Capsicum annuum* L.) and pure or vegetable-oil modified SC CO_2. The experimental methodology interspersed extraction (to reduce oleoresin content) and equilibration (by recirculation of the SC CO_2 phase) steps. Two experimental cumulative extraction curves were modelled including the equilibrium partition with simulated isotherm/isobar curves.

4.2. Materials and methods

4.2.1. Materials

Commercial flakes of red pepper (Invertec Foods, Santiago, Chile) used for this study contained ~2.4% w/w oleoresin (total extractable oleoresin by soxhlet extraction with hexane), and ~11% w/w (h.b.) moisture (dried in an oven at 105 °C). Flakes were extruded in a Haake Polydrive 120N device (Newington, NH) into cylindrical particles of 4-mm diameter and ~10-mm length, extruded particles were milled in a mortar with pestle, and milled particles were sieved so as to separate a fraction of 355-710-μm diameter. Samples were packed in kraft paper into polethylene bags and stored in a refrigerator (5 °C) up to analysis.

4.2.2. Experimental methodology

The experimental device was previously described by Urrego et al. (Submitted). Briefly, the equipment consists of loading, equilibration, and sampling sub-systems (Fig. 3-1). The experimental methodology intersperses extraction (to reduce oleoresin content) and equilibration (by recirculation of the SC CO_2) steps. Equilibration is monitored measuring SC CO_2 absorbance at 460 nm, and equilibrium concentrations are estimated based on mass balances.

4.2.3. Experimental plan

Twenty-seven grams of pre-treated red pepper were used in each experiment, and equilibrated/extracted with 99.8%-pure or vegetable-oil-modified SC CO_2 from Aga S.A. (Santiago, Chile). Five-to-eight measurements were carried out for each sorption isotherm/isobar measured with pure CO_2 at 54, 60, or 67 °C, and 22, 25 or 28 MPa, and eight points were taken for the sorption isotherm/isobar measured with vegetable-oil-modified CO_2 at 60 °C and 25 MPa. In this last experiment, 0.87 grams of high-oleic sunflower oil (Camilo Ferrón Chile S.A, Chile) were added to the pre-treated red pepper while loading it into the equilibrium cell. Added oil is the amount required to saturate (with triolein, based in the equation proposed by del Valle et al. (2012)) expanded SC CO_2 in the first half of the isotherm/isobar measured with pure CO_2, discounting the oleoresin extracted up to that point. Following equilibration (periods of >8.5 h), eight cubic decimetres of CO_2 at environmental temperature (13.6 – 15.8 g) were sampled for each sorption isotherm/isobar data point, whereas 16-to-150 NL (27.7 - 270 g) were sampled in extractions carried in between data points (the amount increased to account for the reduction in the "apparent" solubility of oleoresin in SC CO_2 as its concentration in red pepper decreases).

Total carotenoid content in oleoresin samples was determined using the spectrophotometric method ISO7541:1989(E). Extracts were dissolved in HPLC grade acetone (J.T. Baker, NJ) and absorbance measurements were performed at 460 nm in a Unicam UV/Vis spectrophotometer (ATI UNICAM, Cambridge, UK). Carotenoid concentration was estimated with the extinction coefficient ($E^{1\%}$ = 2250) in acetone of capsanthin, the most important carotenoid pigment in red pepper, and the results were expressed in mg kg^{-1} carotenoid/oleoresin and mg kg^{-1} carotenoid/CO_2.

4.2.4. Mathematical modelling

Authors of this work applied a modified version of the Broken and Intact Cells (BIC) model described by Sovová (2005), by including the experimentally obtained isotherm/isobar equation plus to the axial dispersion (D_L) terms to the mass transfer balance. The mass balance equations per unit volume of extraction bed for plug flow are

presented in Eqs. (4.1-4.3), for the solute in fluid phase (C_f), solid phase with broken cells (C_{sb}), and solid phase with intact cells (C_{si}), respectively.

$$\rho\varepsilon\left(\frac{\partial C_f}{\partial t}+U\frac{\partial C_f}{\partial h}-D_L\frac{\partial^2 C_f}{\partial h^2}\right)=j_f, \tag{4.1}$$

$$r\rho_s\left(1-\varepsilon\right)\frac{\partial C_{sb}}{\partial t}=j_s-j_f, \tag{4.2}$$

$$\left(1-r\right)\rho_s\left(1-\varepsilon\right)\frac{\partial C_{si}}{\partial t}=-j_s, \tag{4.3}$$

with initial and boundary conditions presented in Eqs. (4.4-4.7).

$$C_f\big|_{t=0}=C_{f0} \tag{4.4}$$

$$C_{sb}\big|_{t=0}=C_{sb0} \tag{4.5}$$

$$C_{si}\big|_{t=0}=C_{si0} \tag{4.6}$$

$$C_f\big|_{h=0}=-\frac{D_L\varepsilon}{U}\frac{\partial C_f}{\partial z}\bigg|_{h=0} \tag{4.7}$$

The experimental isotherm/isobar curves were best fitted to minimize the sum of quadratic residues between experimental and simulated values of C_f for the equation proposed del Valle and Urrego (2012), Eq. (2.21).

Experimental integral extraction curves of red pepper oleoresin were best-fitted together with the modified BIC model by minimizing the sum of quadratic residues between the modelled and experimental extraction yields. Mass balances were made to discretized sections of the extractor at discretized times, following the procedure described by del Valle and Urrego (2012).

4.3. Results and discussion

Fig. (4-2) shows the first measured isotherm/isobar curve. This curve was used to

define the extension of the equilibration and extraction steps that are needed to obtain enough points and a distinguishable trend in the experiments. This isotherm/isobar curve shows that below substrate concentrations (C_s) of ~6 grams of oleoresin per kilogram of substrate, and around 0.4 grams of oleoresin per kilogram of CO_2 (C_f), oleoresin concentrations in SC CO_2 remained apparently constant, even when larger amounts of CO_2 were sampled. In the work of Urrego et al. (Submitted) for the partition of rapeseed oil between prepressed rapeseed and SC CO_2 as the value of C_f diminishes the uncertainty inherent to the methodology increases, and care should be taken by interpreting the equilibrium partition behaviour at such low values. This, in combination with the fact that a residual oleoresin content in the substrate was not detected (with a Soxhlet extraction with hexane) at the end of the measurement, made that (for the rest of the measurements) the methodology were stopped after residual oleoresin contents falls below (C_s) ~ 6 g kg^{-1} oleoresin/red pepper, and that the oleoresin mass balance were based on the content determined by the Soxhlet extraction experiment (2.36%).

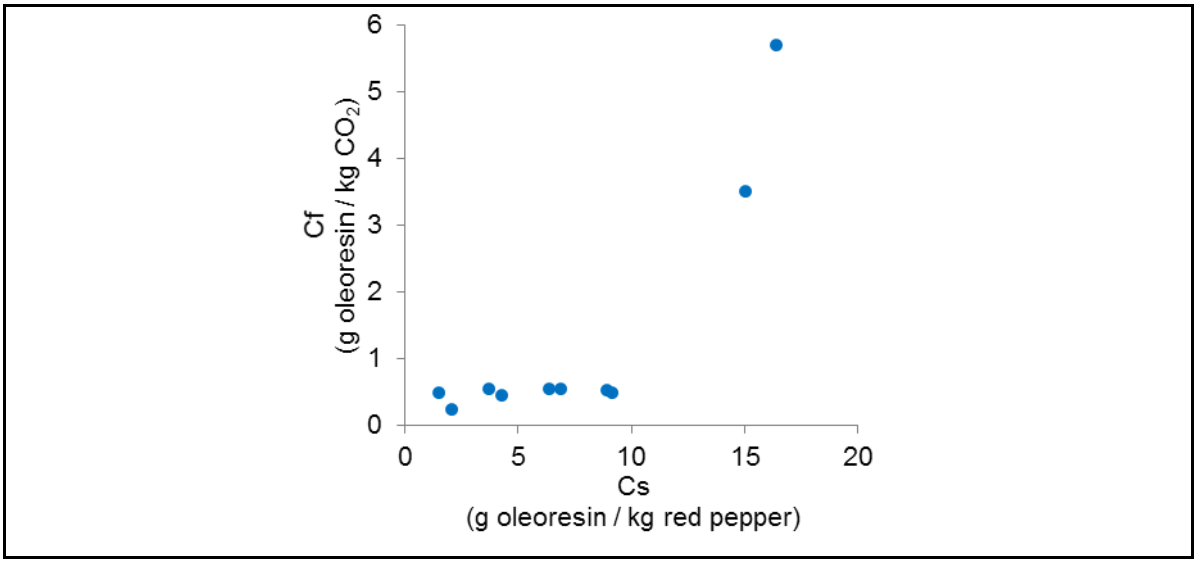

Figure 4-2. Exhaustive isotherm/isobar curve of red pepper oleoresin at 67ºC -28 MPa.

4.3.1. Effect of the pressure on the sorption equilibrium of red pepper oleoresin

Under isothermal conditions (60 ºC), an increase in pressure from 22 to 28 MPa has a large effect on equilibrium partition of oleoresin between SC CO_2 and pelletized-milled red pepper, Fig. (4-3), particularly for residual oleoresin concentrations in the red pepper above ~10 g kg^{-1} oleoresin/red pepper. Authors believe this is due to the increase in the solvation power of CO_2 associated with the increase in density brought about by the increase in pressure (from 752.3 kg/m^3 at 22 MPa to 814.0 kg/m^3 at 28 MPa). On the other hand, differences in oleoresin partition as a function of pressure virtually disappear when the residual concentration of oleoresin in the red pepper diminishes below ~10 g kg^{-1} oleoresin/red pepper. However, as previously presented in section (3.3), there is a lot of uncertainty in experimental values in this region.

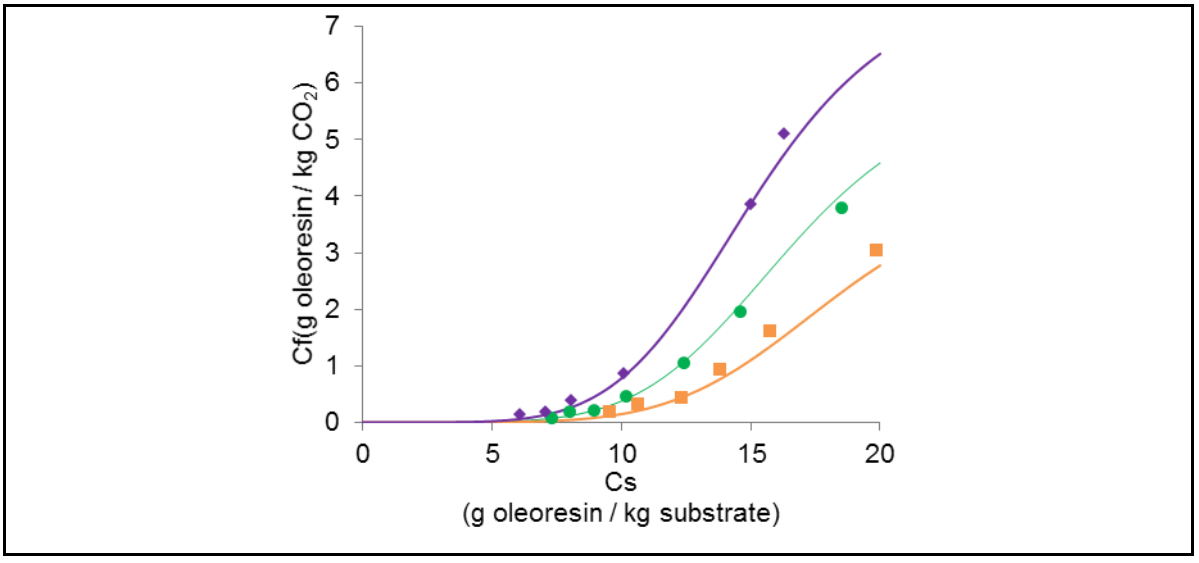

Figure 4-3. Effect of the pressure on the equilibrium partition of red pepper oleoresin. Measurements at 60ºC and 22 (■), 25 (●), and 28 (♦) MPa.

4.3.2. Effect of the temperature on the sorption equilibrium of red pepper oleoresin at isodensity condition of SC CO_2

In the case of isotherm/isobar curves measured at the same SC CO_2 density (~785

kg/m^3), Fig. (4-4), pressure values were the same as those in Fig. (4-4) (22, 25 and 28 MPa), but in this case temperature values were 54, 60, and 67 °C, respectively. Main differences occur also in the zone above oleoresin concentrations in the red pepper of ~10 g kg^{-1} oleoresin/red pepper, but were smaller than those observed in Fig. (4-3). In this case the effect of the increase in the solvation power was brought about by the temperature instead of the SC CO_2 density.

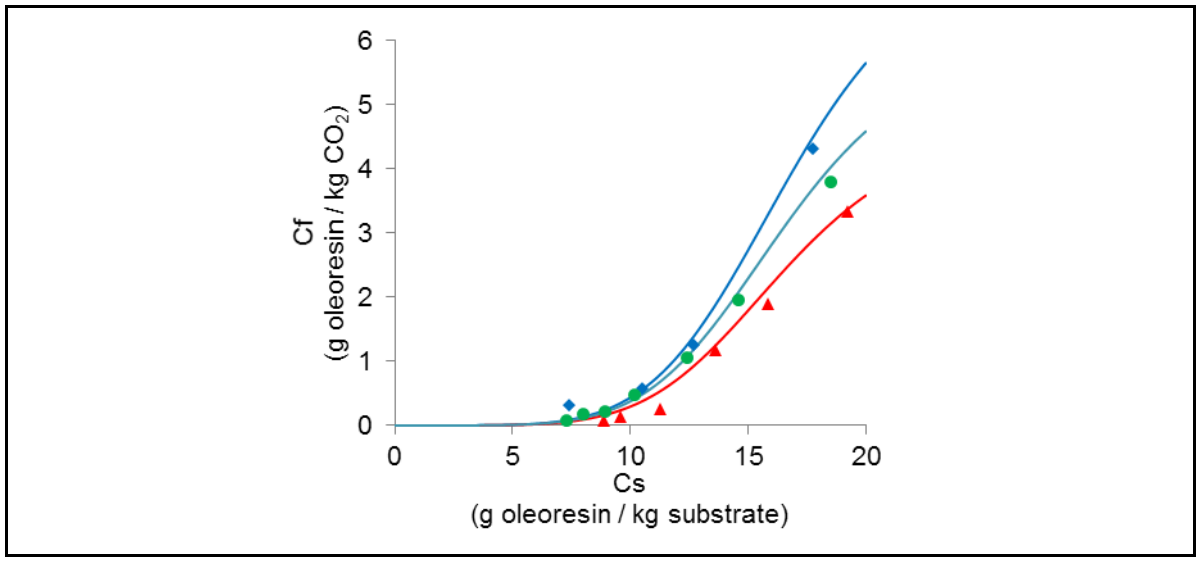

Figure 4-4. Effect of the temperate on the equilibrium partition of red pepper oleoresin at isodensity condition of SC CO_2. Measurements at SC CO2 density of 785 kg m^{-3}, 54ºC-22MPa (▲), 60ºC-25 MPa (●), and 67ºC-28 mPa (◊).

4.3.3. Modelling the oleoresin isotherm/isobar curves

In the best-fitting process of these curves, the parameter α from the isotherm/isobar model, Eq. (2.21), was found to have no representative effect on the fit, being this the case where the model turns into Eq. (2.18), named as pseudo-Sip's by del Valle and Urrego (2012). The isotherm/isobar curves, Figs. (4 – 1-4), show no saturation concentration C_{sat} (there is a lack of a horizontal asymptote), but the sum of quadratic residues between the experimental and best-fitted C_f was significantly smaller with Eq. (2.18) than with an equation without this parameter ($C_f = KC_s^n$ (Freundlich, 1906), unreported results). In

order to reduce the number of best-fitting parameters in Eq. (2.18), authors applied a correlation to calculate C_{sat}, that is based in the experimental saturation concentration of red pepper oleoresin in SC CO_2 (experiments without the solid substrate) measured by Fernandez-Ronco et al. (2010). These authors studied the SCFE of liquid oleoresins of two capsicum species at 40-60 °C and 14-30 MPa and evaluated three models to predict the oleoresin saturation concentration in SC CO_2 (reported as solubility (*S*) in their work), finding that it was better correlated with the Adachi and Lu model (1983), Eqs. (4.8a-b, C_1=-28.00, C_2=-4266, C_3=6.060, C_4=3.80x10^{-4}, C_5=1.42x10^{-14}). Saturation concentrations calculated for the operation conditions studied in this work are 160±15% the highest oleoresin concentrations in SC CO_2 for each isotherm/isobar curve, therefore, it may imply that sorption equilibrium (substrate-solute affinity and interactions) in conjunction with a low initial content impeded the saturation of SC CO_2 with oleoresin at the initial stage of the extraction of pre-treated red peppers. *A* was best-fitted as *A*'(=1/*A*, to avoid imprecisions due to small numbers while best-fitting) and correlated to the temperature, Eq. (4.9), T_{ref}=333K, and *n* was correlated to the SC CO_2 density and *A*', Eq. (4.10), A'_{ref}=4.511x10^9. The result of the best-fitting process is represented by lines in Fig. (4 - 3,4). The variation of *n* with the CO_2 density was not observed in the work of Urrego et al. (Submitted), and authors assume that this is related to more detailed information at low oleoresin concentrations in the red pepper of this work. The term *n* influences the residual oleoresin concentration in the red pepper at which there is an increase in the slope of the curve, around 10 g kg^{-1} oleoresin/red pepper in Figs. (4 – 2-4).

$$\ln C_{sat} = C_1 + \frac{C_2}{T} + K \ln \rho \tag{4.8a}$$

$$K = C_3 + C_4 \rho + C_5 \rho^2 \tag{4.8b}$$

$$A' = 4.510 \times 10^9 - 1.096 \times 10^6 * \left(T - T_{ref}\right) \tag{4.9}$$

$$n = 8.615 - 4.058 \times 10^{-3} * \rho_{CO_2} * \frac{A'}{A'_{ref}} \tag{4.10}$$

In Fig. (4-1), the highest oleoresin concentration in the saturated SC CO_2 phase of

the 54 °C – 22 MPa isotherm/isobar curve was lower than in the other two due to an extent to the decrease in solubility (Chrastil, 1982), and unfavourable solute partition to the solid phase in endothermic sorption processes as temperature decreases, related to a combined effect between unfavourable temperature and pressure conditions on the solubility of the oleoresin in the SC CO_2. The highest oleoresin concentration in SC CO_2 is directly related to the change in solubility associated with the change in SC CO_2 density (785 kg/m^3 at 67 ºC versus 814 kg/m^3 at 60 ºC).

Several authors claim that the solubility of a solute in SC CO_2 may be calculated from the initial slope of integral extraction plots of solute yield *versus* specific CO_2 consumption (with an initial slope with units of solubility, grams of solute per kilogram of CO_2), assuming a long period before extraction begins when temperature and pressure equilibrate to the desired conditions (static extraction period). del Valle and Urrego (2012) claimed that the amount of extract in a vegetable substrate may affect this "apparent" solubility (initial amount of solute and solute-matrix interactions are neglected) to the point that this is smaller than the "thermodynamic" solubility (solubility measured for a pseudo-binary system vegetable extract – SC CO_2) under equivalent SCFE process conditions. Ambrogi et al. (2002) extracted paprika at 60 °C and 30 MPa, and reported an "apparent" oleoresin solubility in SC CO_2 (density = 830 kg/m^3) of 7.5 g/kg, being this value higher than the observed in Fig. (4-2) at the same temperature but at a slightly higher pressure (30 MPa), which may be due either to the difference in SC CO_2 density that increases solubility (Chrastil, 1982), or the difference in oleoresin content between the substrates (2.36% in this work versus 17.1% in Ambrogi et al. (2002)) that favour solute transfer to the SC CO_2 phase.

Kwon et al. (2011) extracted red pepper at 30-60 °C and 10-35 MPa, and reported lower oleoresin solubilities in SC CO_2 (values between 0.18 and 1.18 g/kg). In order to compare our results, we modelled these solubilities with the Adachi and Lu model (C_1 = -3.158, C_2 = -2913, C_3 = 1.508, C_4 = 3.200x10^{-4}, and C_5 = 1.500x10^{-14}), then, we calculated the corresponding values for conditions studied in this work, and the values obtained are 28±3% the highest oleoresin concentrations in SC CO_2 for each isotherm/isobar curve, therefore, results obtained by Kwon et al. (2011) might be called apparent solubilities, in

order to differentiate them from the thermodynamic solubility.

4.3.4. Effect of the addition of vegetable oil on the sorption equilibrium of red pepper oleoresin

Fig. (4-5) shows isotherm/isobar curves at 60 °C and 25 MPa. Continuous lines represents the best-fitted data to the pseudo-Sip's model of the red pepper modified with vegetable oil, with parameters values of C_{sat} = 6.54 (g oleoresin kg^{-1} CO_2), n = 3.10 (-), and A = 1.10x10^{-5} (kg kg^{-1} oleoresin/red pepper). The oleoresin saturation concentration calculated with Eq. (4.8) (6.25 g kg^{-1} oleoresin/CO_2) is 4.50% below the best-fitted C_{sat}, authors attribute this to measurement uncertainties of the methodology (Urrego et al., Submitted). Dotted line (··) shows an oilseed isotherm/isobar curve simulated at the same operation conditions, based in the results obtained by Urrego et al. (Submitted) for rapeseed oil, with parameters values of C_{sat} = 4.05 (g kg^{-1} oil/CO_2), n = 3.55 (-), and A = 5.58x10^{-6} (-), this curve shows that this vegetable oil has more affinity with its substrate while partitioning with SC CO_2 at the same residual solute concentrations, and might suggest that by adding a vegetable oil to the red pepper previous to a extraction procedure, the partition of the oleoresin (or the mixture of the oleoresin and oil) to the SC CO_2 is disfavoured, and that the affinity of the mixture with a vegetable substrate stands between the individual affinities of each solute with its substrate, in this case with a little trend to be closer to that of the oleoresin.

4.3.5. Equilibrium partition of carotenoids

The analysis of sorption of carotenoids was approached qualitatively, in terms of their concentration in the sampled mixture of oleoresin and SC CO_2 *versus* the residual oleoresin concentration in the vegetable substrate. Authors did not considered the residual carotenoid concentration in the substrate, because there is uncertainty about the effect of carotenoid-degradation sources, in combination with the measurement uncertainty of the methodology itself. On one hand, each isotherm/isobar curve represents a period of three weeks of continuous equilibration and extraction steps, working all the time at the operation temperature, and adding CO_2 which is only 99.8% pure, therefore, the level of

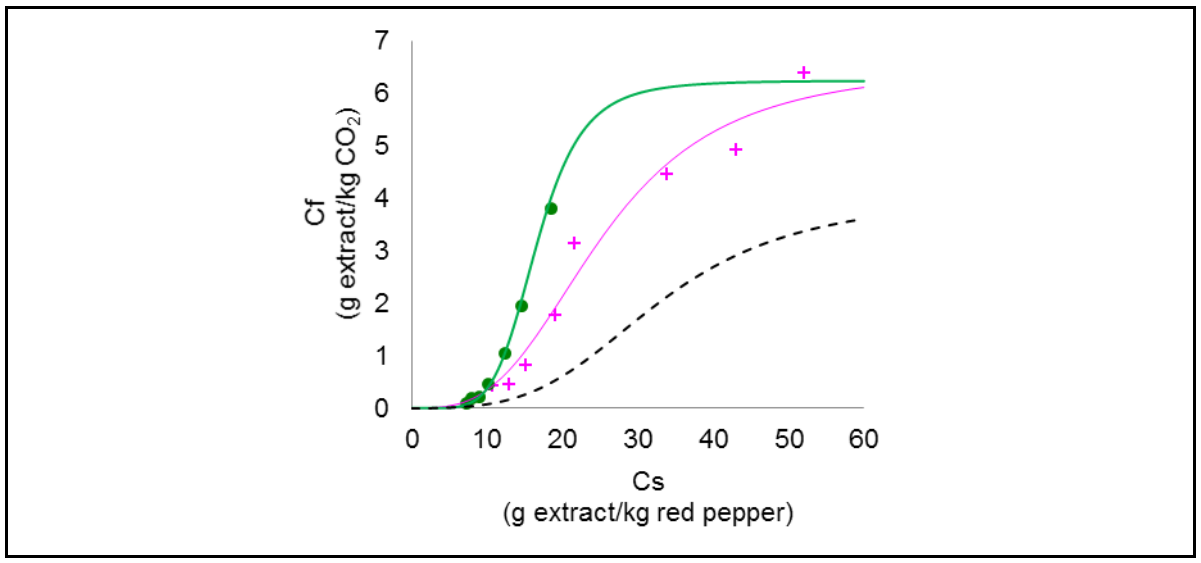

Figure 4-5. Effect of the addition of vegetable oil on the equilibrium partition of red pepper oleoresin at 60ºC-25 MPa. Isotherm/isobar curve without modified SC CO_2 (●), with modified SC CO_2 (+), and a simulated isotherm/isobar curve of vegetable oil (-) for the same operating conditions as reference.

degradation due to the time the carotenoids were exposed to temperature and oxygen was not accounted. In this matter Cocero, González, Pérez, and Alonso (2000) presented results that suggest that β-carotene was oxidized during a supercritical fluid extraction process, by comparing the extraction of β-carotene from alumina-impregnated balls with and without the addition of Butylated hydroxytoluene (BHT, a widely applied antioxidant), the concentration after 15 h of extraction fell from 250 ppm to ~140 and ~0 ppm, respectively. On the other hand, Urrego et al. (Submitted) calculated the uncertainty of the experimental methodology for oil from an oilseed and found that it increases as the concentration of the solute in SC CO_2 and the substrate diminishes, as well as it falls below the saturation concentration. Fig. (4-6) shows carotenoid concentration in the sampled extracts of isotherm measured at 60 ºC and 25 MPa, as well as the corresponding concentration in SC CO_2 (by mass balance calculation) when it was solubilized prior to the sampling step. This curve represents the trend of carotenoid composition in the oleoresin-SC CO_2 mixture after each equilibration step. Carotenoid concentrations in extracts (milligrams of total carotenoids per gram of oleoresin), Fig. (4-6A), followed an opposite trend to the oleoresin

concentrations in SC CO_2, that is, oleoresins were more carotenoid-concentrated as they were extracted from the vegetable matrix (extracted meaning continuous equilibration and sampling steps), this behaviour was observed, to some extent, in fractional extraction of paprika by Ambrogi et al. (2002), whom (in-line) measured the carotenoid concentration in SC CO_2 at the exit of the extraction vessel, with an online near infrared visible NIR-Vis detector, and calculated the corresponding (in-line) continuous oleoresin concentration.

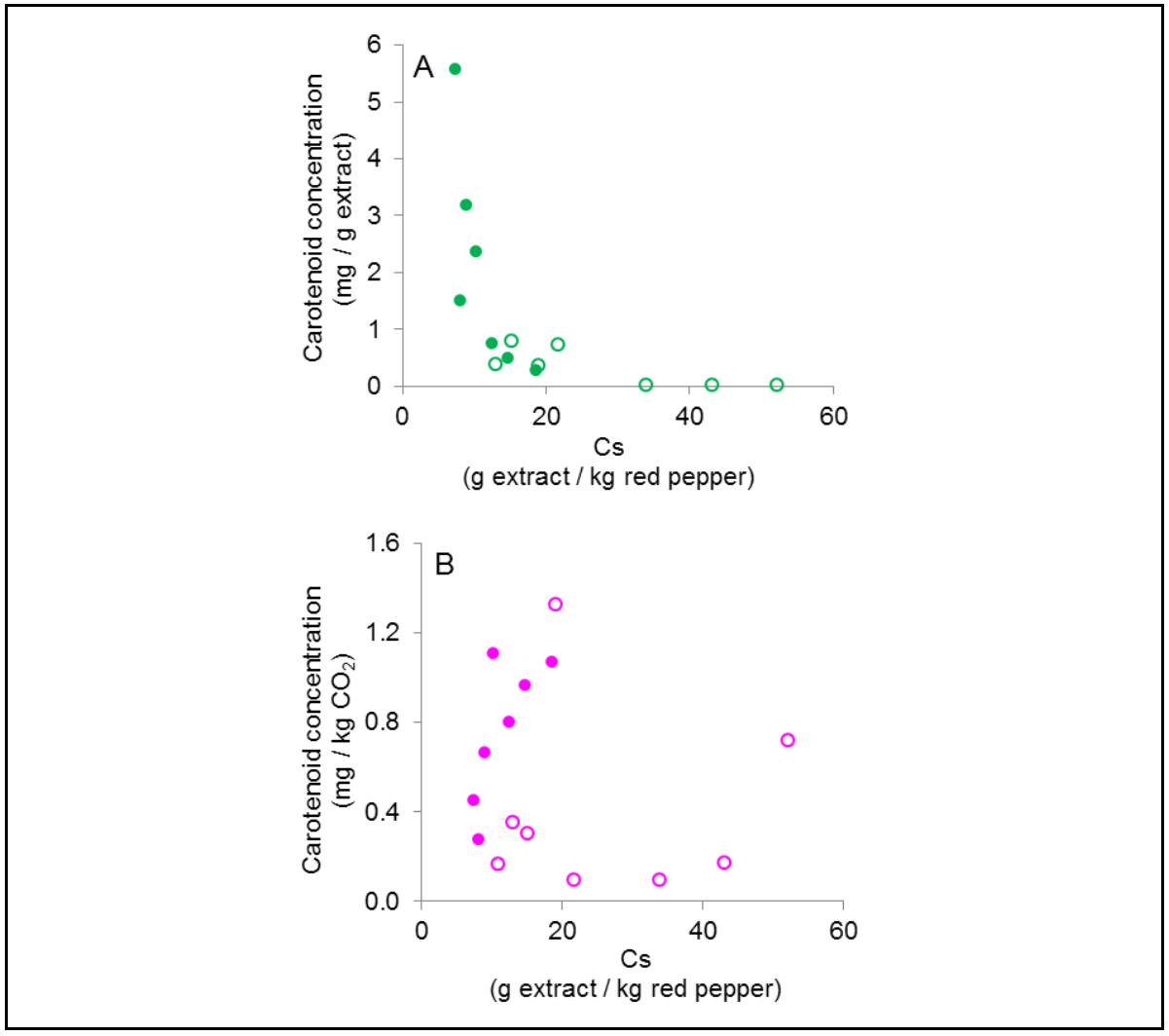

Figure 4-6. Equilibrium concentration of carotenoid for isotherms/isobars measured with pure (●) and modified (○) SC CO_2 at 60 °C and 25 MPa. (A) carotenoids concentration in the extract, (B) carotenoid concentration in SC CO_2.

The isotherm/isobar curve without vegetable oil in Fig. (4-6B), shows a decreasing trend of the carotenoid concentration in SC CO_2 (in the direction of red pepper extraction, C_s < 20 g kg^{-1} oleoresin/substrate), which means that extract concentration in SC CO_2, Fig. (4-2), and carotenoid concentration in SC CO_2, Fig. (4-3B), are correlated (higher amounts of extract in SC CO_2 yields higher amounts of carotenoid in SC CO_2), being this trend the idea behind the addition of vegetable oils as cosolvents (Sun & Temelli, 2006) in supercritical fluid extraction processes, however, isotherm/isobar curve measured with added-high-oleic oil shows two decreasing trends, one more pronounced below 20 g kg^{-1} oleoresin/substrate as in the isotherm/isobar measured with pure CO_2, and the other between 20 and 52 g kg^{-1} oleoresin/substrate, this behaviour might be also related to that observed by Ambrogi et al. (2002) where carotenoid concentration in SC CO_2 is low at the beginning of the extraction (while oleoresin amounts in SC CO_2 are higher in the zone of saturation), followed by a raise of the concentration when >80% of oleoresin had been extracted (around ~20 g kg^{-1} extract/substrate, Fig. (4-6B), and then carotenoid concentration decreases until substrate is finally exhausted.

4.3.6. Inclusion of the isotherm/isobar model into the BIC extraction model

Results provided by (Uquiche et al., in preparation) of the red pepper oleoresin extraction made at 60ºC and 28 MPa, Fig. (4-1), shows a maximal extraction yield of ~0.87%, which is around 3 times smaller than the total extracted amount with the sorption methodology at the same operation conditions. The effect of longer experimental times of the sorption methodology plus the continuous CO_2 recirculation might induce changes in in the substrate that are not triggered in a regular extraction procedure. A possible hypothesis to explain this behaviour is that the exhaustive sorption methodology allows mass transfer barriers to be broken, i.e, continuous drying of the substrate, exposing more area to the SC CO_2 solvation effect, or giving the process enough time to allow the migration of the solute either throughout intraparticle pores of a caked substrate, or from intact cells that remain intact after the substrate pretreatment, *inter alia*. However, evaluation of these hypothesis requires approaches not assessed in this work. Instead, and for modelling purposes, authors chose to apply a kinetic extraction model that has a

parameter that could explain what causes the difference of the extractable solute between the sorption and extraction methodologies. The grinding efficiency parameter (r) in the BIC model of Sovová (2005) is related to a ratio of broken to intact cells in the substrate (making allusion of a portion of the substrate that was not obliterated to the point of breaking all the cells walls), where the solute from broken cells is directly transferred to the interparticle SC CO_2, named a film mass transfer coefficient (k_f), and the solute from intact cells is transferred to the broken cells to a much lower rate, named a solid mass transfer coefficient (k_s). Thus, a smaller amount of extractable solute during the 3.6 h extraction experiment might be well represented by the combined effect of the parameters of this model. In unreported results, a desorption-dilution-diffusion (DDD) kinetic extraction model (Goto et al., 1998), which accounts for the solute-solid interaction (experimental sorption results were included), was not suitable to simulate well this behaviour.

del Valle and Urrego (2012) claimed that there is enough information in literature to allow the calculation of most of the parameters involved in mathematical kinetic models, so as to reduce the number of best-fitting parameters, as well as the uncertainty about combined effects from parameters representing different physical phenomena, i.e., best-fitting the effective diffusivity (D_e, the diffusion of the solute through the pores of the particle) and the partition equilibrium at the same time. In this work, authors assumed that physical properties of mixtures of SC CO_2 and dissolved oleoresin are not affected by the oleoresin (low solubility assumption), so that they can be estimated using NIST Database (Lemmon et al., 2007) for pure CO_2 as a function of extraction temperature and pressure. The superficial velocity of the CO_2 stream (U=1 mm/s) was estimated as a function of the mass flow rate (Q), CO_2 density under process conditions, and cross-sectional area of the extraction vessel. The particle porosity (ε_p=0.17), the dry-bone substrate density (ρ_s=1421 kg m^{-3}), and the tortuosity of the particles (τ=2.91), were obtained of Uquiche et al. (in preparation). The bed porosity (ε) was calculated with the dry-bone substrate density, the amount of substrate loaded in the extractor (M_o), the particle porosity, and the volume of the extractor (V=50 cm^3). The microstructural factor (F_m=17.12) was calculated as the ratio between τ and ε_p, the binary diffusion coefficient of the oleoresin (component 2) in CO_2

(component 1), D_{12}, was estimated using the correlation of Funazukuri et al. (2008), and the effective diffusivity (D_e) was calculated as the ratio between D_{12} and F_m (del Valle et al., 2006; Funazukuri et al., 2008). The film mass transfer coefficient (k_f) was estimated using the physical properties (ρ, μ, D_{12}) and superficial velocity, and the particle diameter (d_p) as independent variables using the dimensionless correlation of Puiggené et al. (1997) for forced convection. The internal or solid mass transfer coefficient (k_s) was estimated using D_e and the particle radius using the correlation proposed by Sovová (2012). The axial dispersion (D_L) was calculated using the correlation proposed by del Valle et al. (2011). The initial concentrations C_{fo} and C_{sbo} were calculated as the partition of the initial solute contained in the broken cells to the interparticle SC CO_2, following the relationship of the isotherm/isobar curve equation, Eq. (2.18), and therefore, C_{sio} remained with the initial oleoresin concentration in the red pepper (C_{so}). Values of the parameters are summarized in Table (4-1). To avoid forcing the total oleoresin mass balance to that obtained with the extraction methodology (a common assumption), it was assumed that the supercritical fluid extraction was partially finished (which is apparent in the extraction curves because there are no distinguishable horizontal asymptotes) and therefore the amount of extractable solute (S_o) was a best-fitting parameter.

Table 4-1. Experimental conditions, physical properties of SC CO_2, and model parameters.

Parameter	Unit	Value	Value
T	ºC	40	60
ρ	kg m^{-3}	898.53	813.98
μ	Pa s × 10^5	9.10	7.40
D_{12}	m^2 s^{-1} × 10^9	3.29	4.22
D_L	m^2 s^{-1} × 10^6	4.02	4.02
D_e	m^2 s^{-1} × 10^{10}	1.92	2.47
k_f	m s^{-1} × 10^5	1.00	1.25
k_s	m s^{-1} × 10^7	4.80	6.17
S_o/M_o	%	1.10	1.37

Lines in Fig (4-7) show the best-fit of the cumulative extraction curves of oleoresin from red peppers. Despite the differences between the amount of extractable solute from the sorption methodology (2.36%) and the calculated extractable solute for the extraction experiments (1.10 and 1.37% for 40, 60 ºC – 28 MPa, respectively), the model fits well the experimental data, with a little overestimation (7.40% in average for the last three points of the curve) of the curve measured at 60 ºC. Authors consider this a result that demonstrates the advantage of experimentally measure isotherm/isobar curves, because the applied model had only one best-fit parameter, related only to the impossibility to elucidate it with precision from the cumulative extraction plots. However, caution should be taken, and more data evidencing this phenomena should be evaluated, to assess the cases where the total amount of extractable solute under specific operational conditions is better determined by an exhaustive method such as the sorption methodology applied in this work, than by a typical SFE process, so as to eventually develop a predictive model based on parameters values that responds to the physical reality.

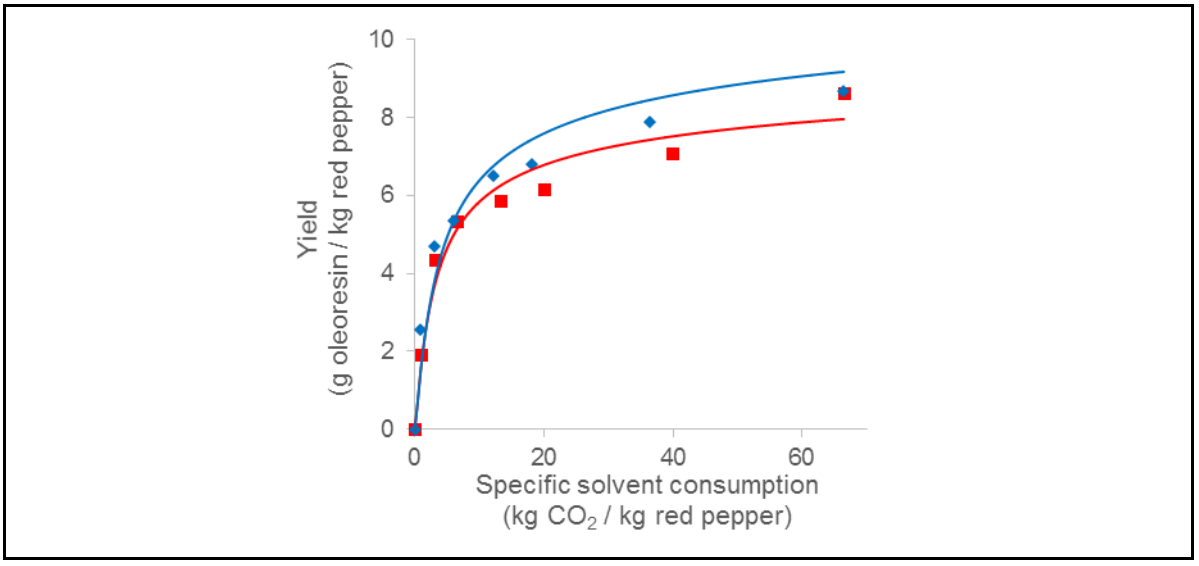

Figure 4-7. Simulated integral extraction curves of oleoresin from red pepper at 40 (■) and 60 ºC (♦) - 28 MPa.

4.4. Conclusions

With the experimental determination of the isotherm/isobar curves it was possible to identify the equilibrium partition of the major (lipid) as well as of the minor (carotenoids) compounds when these are extracted from red pepper with SC CO_2. A combination of a small initial amount of oleoresin, and a solute-substrate interaction in function of pressure, temperature and density of the SC CO_2, lead to a partition that was favoured to the substrate phase, to the point that saturation concentrations were not achieved at the beginning of the sorption experiments. The carotenoids showed a similar trend in the equilibration between the pretreated red pepper and SC CO_2, decreasing as the extract (mixture of oleoresin and carotenoids) in the substrate decreased, however, the concentration of carotenoids in the oleoresin increased as the extract in the substrate decreased, showing that the equilibrium was related to the physical properties of the CO_2 rather than to its affinity with the oleoresin. With the addition of a vegetable oil to the red pepper previous to a sorption experiment, it was possible to observe that the equilibrium partition of the extract (the mixture of oleoresin and vegetable oil) stands between the equilibrium partition of the two solutes, that the saturation concentration of the extract is close to the predicted for the oleoresin, and that carotenoids are equilibrated with the SC CO_2 in two trends, one decreasing trend for the portion of isotherm/isobar related to the amount of vegetable oil added to the red pepper (C_s > 20 g kg^{-1} extract/red pepper), and a second and more pronounced decreasing trend related to the initial oleoresin amount and similar to the measured with the non- high-oleic-oil-modified red pepper, which means that the effectiveness of vegetable oils as co-solvents besides its effect on the solubility might also be due to the increase of lipid compounds in the mixture helping to dissolve more carotenoids in the SC CO_2. Finally, with the inclusion of the isotherm/isobar model into a kinetic extraction model it was possible to represent experimental kinetic extraction data, by using only one best-fit parameter. However, more data need to be produced so as to elucidate factors influencing the difference of the extractable solute obtained with the extraction and sorption methodologies.

5. DYNAMIC MEASUREMENT OF THE EQUILIBRIUM PARTITION OF TOMATO EXTRACT BETWEEN SUPERCRITICAL CO_2 AND PRETREATED TOMATO

Abstract

A function (isotherm/isobar) relating the partition of a vegetable extract (solute) between supercritical (SC) carbon dioxide (CO_2) and a vegetable substrate commonly is a best-fit parameter in the modelling of supercritical fluid extraction processes, and inaccuracies of scale-up procedures might be related to adjusted parameters misrepresenting the physical reality. We developed a dynamic experimental methodology based in chromatographic principles to experimentally measure extract (lycopene) partition between pelletized and milled carotenoid-rich tomato and SC CO_2 and made measurements at 40 °C and 29 MPa. The methodology proposes the injection of tomato extract dissolved in SC CO_2 into a column packed with pretreated (pelletized, milled, size-classified, and fully-extracted) tomato. Constant and stable extract concentrations in SC CO_2 at the inlet of the tomato column were achieved by injecting pulses to a column packed with glass beads. Elution profiles were monitored measuring SC CO_2 absorbance at 486 nm. Five curves of dissolved extract injected to a completely SC CO_2-extracted tomato column were measured. Frontal analysis, perturbation, and inverse methods were applied to calculate isotherm/isobar parameters of the Freundlich equation. Results from this dynamic method were compared with results from a standardized and mainly static method and observed discrepancies were attributed to an irreversibility desorption process of lycopene when it was extracted from the vegetal substrate.

5.1. Introduction

Carotenoids function in foods as pigments, antioxidants, and essential nutrients. Because of these functional properties, the food industry is interested in isolating carotenoids from biological substrates to use them as ingredients in nutraceutical and functional foods. Tomatoes and tomato-derived products are important sources of

carotenoids, particularly lycopene, and their extraction with SC CO_2, represents an interesting alternative to their extraction with organic solvents (Zuknik, Norulaini, & Omar, 2012).

The viability of an industrial SC CO_2 extraction process depends critically on scale-up analysis of experimental data gathered at laboratory and pilot-plant scales. In our opinion, a reliable scale-up procedure should be based on robust mathematical models to simulate the industrial extraction process, to account for scale-specific issues that are less relevant in onepass laboratory units and pilot plants with CO_2 recycling capabilities, such as residual extract in the SC CO_2 stream entering the extraction vessel, a variable extract content in the SC CO_2 stream entering the vessel in industrial plants equipped with three or more (Núñez et al., 2011), and non-ideal flow conditions (e.g., channelling) resulting in radial gradients of residual extract concentration within large vessels (Brunner, 1994; del Valle, 2015). Mathematical simulation demands information about kinetic and equilibrium factors affecting mass transfer during SC CO_2 extraction of vegetable substrates (del Valle, 2015; del Valle & de la Fuente, 2006). In our opinion these factors should be experimentally measured instead of best-fitted to integral extraction curves measured in laboratory and pilot plant units.

Extraction rate depends on the partition of the extract between the substrate and SC CO_2 defined by a sorption isotherm/isobar equation relating solute concentrations in the fluid (C) and solid (q) phase, internal mass transfer defined by the effective diffusivity of the extract in the substrate (D_e), and external mass transfer defined by the axial dispersion (D_L) and film (k_f) coefficients (del Valle, 2015). In the case of sheared substrates devoid of inner mass transfer barriers, such as those obtained by pelletization (del Valle et al., 2006), del Valle and Urrego (del Valle & Urrego, 2012) proposed using dimensionless correlations for packed beds operating with SC Fluids (SCFs) to estimate D_L and k_f, and an independent measurement of the sorption isotherm/isobar to characterize the equilibrium, so as to limit the model to best-fit D_e.

Urrego et al. (Submitted) proposed and standardized a methodology to measure the sorption isotherm/isobar of vegetable extracts between SC CO_2 and a pretreated (pelletized and ground) substrate. This methodology interspersed extraction (to reduce the extract

content) and equilibration (by recirculation of the SC CO_2 phase) steps, with the vegetable extract being sampled in each step; the extract concentration in the SC CO_2 was obtained by direct measurement, whereas the extract concentration in the substrate was back-calculated using mass balances. This methodology, however, required long periods of time to obtain an isotherm/isobar curve (due to the lengthy equilibration steps) making it necessary to develop alternative methodologies.

The objective of this work was to measure tomato extract (lycopene) partition between pretreated (dried, pelletized, milled, and size-classified) tomato and pure SC CO_2, using a modified methodology derived from chromatographic principles and methods (tomato extract diluted in SC CO_2 injected into a column packed with fully-extracted tomato), and to compare results with the sorption isotherm/isobar measured using the aforementioned standardized static methodology.

5.2. Chromatographic methodologies to measure isotherm/isobar curves

Static methods to measure sorption isotherm/isobar curves have the advantage that no kinetic effects disturb the results. However, because static methods are time consuming, alternative dynamic methods are of practical interest. Dynamic methods proposed to determine sorption isotherm/isobar curves in fluid-solid systems include (1) breakthrough methods, (2) perturbation methods, and (3) peak-fitting (or inverse) methods.

In the analysis of breakthrough curves a solute-free substrate is contacted with a CO_2 phase containing a certain concentration of a solute, and contact between phases continues until the concentration of the solute at the column outlet is the same as at its inlet. The substrate is assumed to be equilibrated and the equilibrium loading can be determined using a mass balance. The method has some complications for mixtures because absorbance varies between mixture component and equilibrium might be reached at different concentration levels at the outlet (Brunner & Johannsen, 2006). According to Seidel-Morgenstern (2004), with the initial loadings (q^{Init}), the packed bed porosity (ε), the height of the column (L), and the superficial velocity of the solvent (U), the unknown loadings (q^{Feed}) in equilibrium with all feed concentrations (C^{Feed}), might be determined by making successive step changes at the column inlet, and calculating the retention times (t_R)

of shock fronts or the retention times of dispersed fronts, Eq. (5.1). In the case of dispersed fronts, it might be required to do a numerical integration of the individual breakthrough curves, but this is considered to be difficult and often inaccurate.

$$q^{\text{Feed}}\left(C^{\text{Feed}}\right) = q\left(C^{\text{Init}}\right) + \frac{\left(t_{\text{R}}^{*} - \frac{L}{U}\right)\left(C^{\text{Feed}} - C^{\text{Init}}\right)}{\left(\frac{1-\varepsilon}{\varepsilon}\right)\left(\frac{L}{U}\right)} \tag{5.1}$$

In the perturbation method, the substrate is brought to equilibrium as in the previous case, and from a small change of the concentration of the solute, the slope (dq/dC) of the sorption isotherm/isobar curve might be determined, Eq. (5.2) (Michel, Epping, & Jupke, 2005):

$$\left.\frac{dq}{dC}\right|_{C_{\text{i}}} = \frac{t_{\text{R,i}} - t_{\text{o}}}{t_{\text{o}}} \frac{\varepsilon_{\text{t}}}{1-\varepsilon_{\text{t}}}, \tag{5.2}$$

where t_{o} is the so-called dead time of the column (or the residence time of the solvent in the column), and ε_{t} is the total porosity of the packed bed column. By systematic collection of these derivatives, $q\left(\bar{C}\right)$ might be calculated by integration of an isotherm/isobar derived equation. Because this method requires injections small enough to maintain equilibrium in the column, the retention time of responses do not depend on the type of perturbation (positive when injecting higher concentrations, negative otherwise).

For the peak fitting method, or inverse method (Seidel-Morgenstern, 2004), an adequate mathematical model accounting an isotherm/isobar equation is used to minimize discrepancies between an experimental chromatogram and model predictions. An equilibrium dispersive model is commonly applied (Seidel-Morgenstern, 2004) following estimation of additional parameters such as D_{e}, D_{L}, and k_{f}, The disadvantage of this method is that errors associated to estimation of these additional parameters, assumption of wrong sorption isotherm/isobar model, and assumption of inadequate mass transfer model for the packed bed column translate into wrong estimates of sorption isotherm/isobar parameters (Michel et al., 2005).

5.3. Materials and methods

5.3.1. Tomato, tomato products, and analysis

Commercial tomato flakes were acquired from Invertec Foods (Santiago, Chile). Flakes were pelletized in a Pellet Pros PP85 device (Dubuque, IA) into cylindrical particles of 4-mm diameter and ~10-mm length that were milled in a Moulinex chopper (Barcelona, Spain), sieved to separate the -35 +42 mesh fraction (355–425 μm diameter), and further dried in an WTB Binder (Tutlingen, Germany) oven set at 60 °C overnight. Pretreated tomato contained ~1.8% w/w extract (total extractable oleoresin obtained using hexane in a Soxhlet apparatus), and ~12% w/w moisture (estimated by drying in the oven at 105 °C to constant final weight). The true density of sieved tomato samples was measured in a gas pycnometer Quantachrome Ultrapyc 1200e (Boynton Beach, FL) using 99.9%-pure nitrogen from Indura S.A. (Santiago, Chile). Samples were packed in kraft paper into polethylene bags and stored in a refrigerator (5 °C) up to analysis.

Pretreated tomato was extracted using the method of Germain, del Valle, and de la Fuente (2005) at 60 ºC and 50 MPa for 12 h. The experiment was carried out in a Thar Technologies' (Pittsburgh, PA) SFE-1L process development unit equipped with a computer-controlled system to adjust the extraction pressure and solvent flow rate, and complimented with a CO_2 recycling system from Eurotechnica (Bargteheide, Germany). Extraction experiments of *ca.* 400 g of pretreated tomato were done in a 500-cm^3 extraction vessel (model 500-mL-ph) using food-grade CO_2 from Aga S.A. (Santiago, Chile). The system was equipped with a P-200A-220V pump that was operated at 150 g/min (U = 1.10 mm/s) using a Micro Motion CMF010M324NU (Boulder, CO) mass flow sensor to maintain the desired CO_2 flow rate. The temperature inside the extraction vessel was controlled by passing through an external jacket hot water from a PolyScience 8205 (Niles, IL) thermostated bath set at 60 ºC. The extraction pressure (50 MPa) was maintained by a back-pressure regulator (BPR) BPR-A-200B1 placed at the outlet of the extractor, whose outlet line was connected to a 200-cm^3 cyclone separator (model CS-200-mL) where tomato extract was recovered. Tomato extract collected in this cyclone was transferred into a 10-cm^3 amber vial, extracted water was removed with a Pasteur Pipette

from the bottom of the vial, and remaining extract (~ 4 g) was dried with a nitrogen stream for ~10 min. The vial was closed with a nitrogen atmosphere and stored in a freezer (-20 °C) up to analysis.

Residual tomato powder was re-extracted (up to an additional 6 h) until residual extract was not gravimetrically detected. This fully-extracted tomato was packed in kraft paper into polyethylene bags and stored in a refrigerator (5 °C) up to analysis.

Total carotenoid content in tomato extracts was determined using the spectrophotometric method of Estrella et al. (2004). Extracts were dissolved in HPLC-grade hexane (J.T. Baker, Phillipsburg, NJ) and absorbance measurements were performed at 472 nm (wavelength of maximum absorbance for tomato extract in hexane) in a Shimadzu UVmini-1240 (Kyoto, Japan) UV/Vis spectrophotometer. Carotenoid concentration in the extracts was estimated using the extinction coefficient in hexane of lycopene ($E^{1\%}$ = 3450), the most important carotenoid pigment in tomato, and the results were expressed in mg g^{-1} carotenoid/extract.

5.3.2. Experimental device

The experimental device consists of two systems (Fig. 5-1). The upper part delimits equipment and accessories used to measure the isotherm/isobar with chromatographic methods and procedures (dynamic system), whereas the lower part (background gray area) delimits equipment and accessories described by Urrego et al. (Submitted) that were used for two different purposes: (1) to measure the sorption isotherm/isobar with the previously standardized static methodology (Urrego et al., Submitted); and, (2) to dilute tomato extract in SC CO_2 (to be injected to the dynamic system). The static system is constituted of a Teledyne Isco 260D (Lincoln, NE) syringe pump, a 6-m (1/8" high-pressure) heating coil, a Micropump GAH-T23 (Vancouver, WA) gear pump powered by a Siemens Micromaster 411 (Congleton, UK) engine, and a 42-cm^3 equilibrium cell (D = 1.72 cm inner diameter, L = 18.3 cm length) from Eurotechnica (Bargteheide, Germany). The dynamic system is constituted by a Jasco PU-2086 Plus (Tokyo, Japan) HPLC pump, a 3-m (1/16" high-pressure) heating coil, two 11.7-cm^3 sorption columns (D = 7.04 mm; L = 30.0 cm) with sintered metal filters at each end, and a Swagelok KHB-6000 (London, UK)

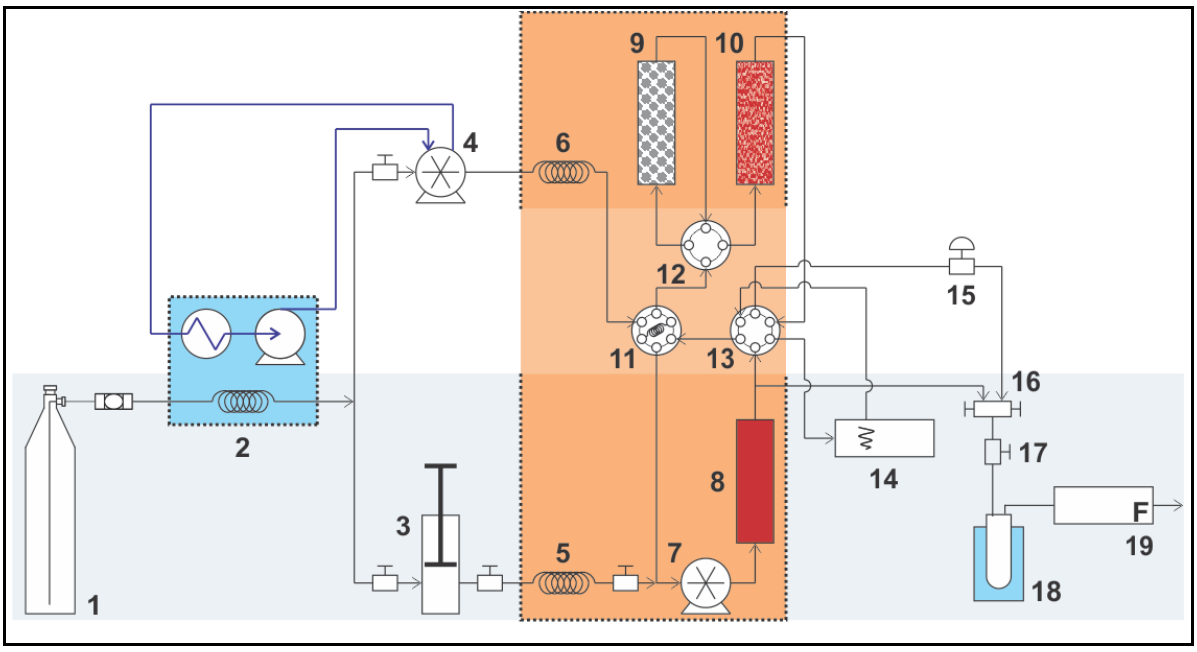

Figure 5-1. Experimental device constituted of (1) CO_2 cylinder, (2) cooling bath, (3) syringe pump, (4) positive-displacement (HPLC-type) pump, (5, 6) 6-m heating coils, (7) recirculation (gear-type), (8) 40-cm^3 equilibrium cell, (9, 10) 12-cm^3 sorption columns, (11) automatized injection valve, (12) four-port, two-way manual valve, (13) two-port, two-way manual valve, (14) UV/Vis detector equipped with high-pressure cell, (15) back-pressure regulator, (16) two-inlet sampling valve, (17) micrometric valve, (18) 50-cm^3 sampling tube with dewar flask, and (19) drum-type volumetric gas meter.

BPR. The two systems share a PolyScience (Niles, IL) cooling bath operated at -10 °C with a 3-m (1/16") cooling coil, a thermostated air bath equipped with a Leister Hotwind S (Sarnen, Switzerland) hot-air blower, and a Hillesheim HT42-10P (Waghäusel, Germany) controller, an Agilent G1314A (Santa Clara, CA) UV/Vis detector equipped with a high-pressure cell, and a sampling system consisting of a two-inlet sampling valve, a micrometric valve, a 50-cm^3 sampling tube placed in a dewar flask with a cooling mixture (ice + water), where tomato extract precipitates, and a Ritter TG-05/5 (Bochum, Germany) drum-type volumetric gas meter. The two systems are interfaced by a Jasco HV-2080-01 (Tokyo, Japan) injection valve powered by a Siemens LOGO 230RC (Munich, Germany) timing relay, and two Rheodyne 7000 (Rohnert Park, CA) manual switching valves

highlighted at the centre of the diagram with a light orange underlay whose operation is described in Fig. (5-2). The system had a Jasco LC-NET II/ADC (Tokyo, Japan) interface to digitalize the analog output signal of the UV/Vis detector as well as to allow the operation of the HPLC pump with the Jasco ChromPass Chromatography Data System ver. 1.7.403.1 (Tokyo, Japan) software.

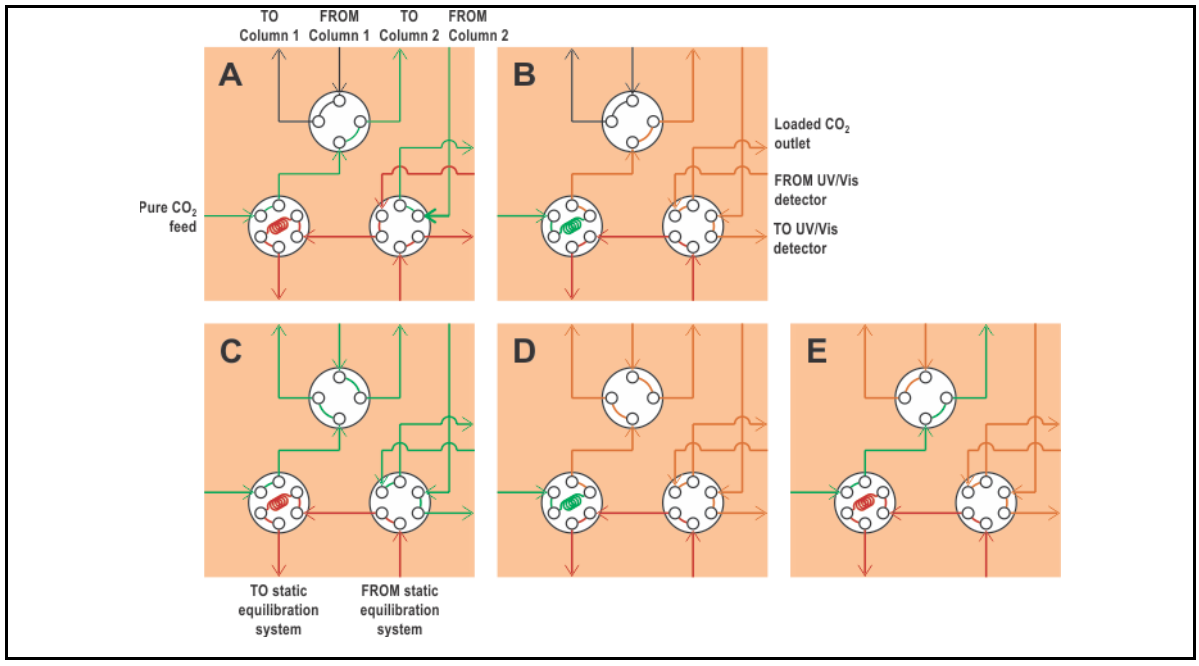

Figure 5-2. Configuration of switching valves (11, 12, and 13 in Fig. 5-1), for different tasks when applying dynamic procedures to study sorption isotherm/isobars. Column 2 (10 in Fig. 5-1) was packed with glass beads when calibrating the UV/Vis detector, which applied two configurations: (A) to equilibrate the dynamic system to operation conditions; and, (B) to inject pulses of supercritical CO_2 saturated with tomato extract. Column 1 (9 in Fig. 5-1) was packed with glass beads and column 2 with fully extracted tomato when studying breakthrough curves of solutions of tomato extract in supercritical CO_2, which applied three configurations: (C) to equilibrate the dynamic system to operation conditions; (D) to inject and homogenize pulses of supercritical CO_2 saturated with tomato extract; and, (E) to apply a negative perturbation (pulse of pure supercritical CO_2). Valve configurations in (A) and (E) are identical

5.3.3. Measurement of sorption isotherm/isobar curves using a static procedure

To measure isotherm/isobar curves using the static method of Urrego et al. (Submitted), pelletized, milled, and size-classified tomato was loaded in the equilibrium cell and connected to the system, the air bath was heated up to the desired temperature, and the system was pressurized to the desired pressure feeding food-grade CO_2 from Indura S.A. (Santiago, Chile) with the syringe pump. Equilibration was done recirculating SC CO_2 through the equilibrium cell with the gear pump operating at 30 Hz (~40 cm^3/min) while monitoring carotenoid concentration in the SC CO_2 stream with the UV/Vis detector set at 486 nm (wavelength of maximum absorbance for tomato extract in CO_2). Equilibration was stopped when the absorbance reading remained unchanged for 1 h, and then sampling was carried out operating the syringe pump in a pressure-controlled mode at the operating condition. Tomato extract was collected in the 50-cm^3 sampling tube whereas expanded CO_2 was measured in the gas meter. After sampling, 1-cm^3 portions of HPLC-grade hexane were added through the second inlet of the sampling valve (to collect any solute adhered to the inner walls of the lines) and transferred to an amber volumetric flask (10-cm^3) up to complete volume. From this, 0.25–1.50 cm^3 were separated for spectrophotometric analysis, whereas the remaining solution was transferred to a 10-cm^3 vial, dried in the oven at 60 °C, and weighed. After measuring and computing the concentration of extract in the saturated SC CO_2 phase, the system was re-equilibrated, and steps were repeated up to depleting of the substrate.

Thirty grams of pretreated tomato were used for the static isotherm/isobar curve, and six equilibrium measurements were carried out for the sorption isotherm/isobar measured at 40 °C and 29 MPa. Following each equilibration (periods of >12 h), 8 NL of CO_2 at environmental temperature (14.6–19.1 g) were sampled for each sorption isotherm/isobar data point, whereas 12-to-70 NL (21.9–126 g) were sampled in extractions carried in between data points (the amount increased to account for the reduction in the solubility of tomato extract in SC CO_2 as its concentration in tomato decreases) to accelerate substrate depletion (Urrego et al., Submitted).

5.3.4. Measurement of sorption isotherm/isobar curves using a dynamic procedures

These measurements consisted of several steps, including dissolution of tomato extract in SC CO_2, setting up the system, and actual measurements using dynamic procedures. To dissolve tomato extract in SC CO_2, the 4-g sample (amount below 40% of the cell volume) together with 3-mm glass beads were loaded in the equilibrium cell that was placed horizontally within the oven, the air bath was heated up to the desired temperature, and the system was pressurized with SC CO_2 using the syringe pump. As before, equilibration was done by recirculating SC CO_2 through the equilibrium cell with the gear pump operating at 30 Hz while monitoring carotenoid concentration in the SC CO_2 stream using the UV/Vis detector at 486 nm. Equilibration was assumed after absorbance remained unchanged for 1 h. The system then remained in standby to subsequently inject portions (defined by the volume of the loop) of SC CO_2 saturated with tomato extract to the dynamic system.

To obtain a stable extract concentration in SC CO_2 at the inlet of the column packed with fully-extracted tomato, which contains enough carotenoids to adsorb in the range 0–1 absorbance unit (AU), three loop sizes (5.0, 20 and 50 μL), switching times between 3 and 21 s (based on residence times of CO_2 that ensured the loop volume was washed out completely with the automatic injection in the on position or connecting the loop with the dynamic system), and two SC CO_2 flow rates (2.5 and 3.0 cm^3/min) were tested. In order to study and record the extract concentration at the outlet of the column packed with glass beads (first column) in normal operation, the system was modified to bypass the first column, and by packaging glass beads in the second column (Figs. 5-2A and 5-2B). After connecting the two columns to the system into the thermostated air bath, they were pressurized with SC CO_2 using the HPLC pump set at 3 cm^3/min. Pressure was controlled with a manual BPR, and the actual CO_2 flow was measured with the gas meter. Seven different concentrations with maximal absorbance in the range 0–1 AU were tested in this stage (calibration of UV/Vis detector) as described below.

To measure the sorption isotherm/isobar, the dynamic system was set with the first 11.7-cm^3 column carefully packed with glass beds (500-μm diameter), and second 11.7-

cm^3 column with fully-extracted tomato (chromatographic-like column packing). Once stabilized the temperature, pressure, and CO_2 flow conditions, the automatic switching valve and timing relay were switched on, and the UV/Vis detector and the chromatographic software were set to record the change in absorbance of the SC CO_2 stream exiting the column packed with fully-extracted tomato. With each pair of switches of the 2-way, automatic injection valve, SC CO_2 saturated with tomato extract was injected to the dynamic system and replaced by pure SC CO_2 that was fed to the static system. Thus, pulses (pure and saturated SC CO_2) are fed to the column of glass beads where they are homogenized so that a stable concentration of tomato extract in SC CO_2 was achieved at the inlet of the column with fully-extracted tomato (Figs. 5-2C and 5-2D). This way, the system allowed measuring the sorption isotherm/isobar curve using frontal analysis and the peak-fitting method. For the perturbation method, the manual switching valve (12 in Fig. 5-1) allows bypassing the first column (for a short period of time), therefore pumping pure SC CO_2 to the column packed with fully-extracted tomato causing a negative perturbation (Fig. 5-2E).

Six grams of fully-extracted tomato were used for the dynamic isotherm/isobar curve. From the analysis of a stable extract concentration in SC CO_2 six different switching times (keeping constant the loop volume and CO_2 flow) were selected.

5.3.5. Mathematical model

Several mathematical models are found in literature to simulate chromatographic separation processes (Michel et al., 2005). In this work, authors applied the transport-dispersive model, where external convection and inner mass transfer resistances are lumped into a single, effective film mass transfer coefficient (k_p), and sorption equilibrium is accounted for by using a linear driving force (LDF) approximation. This model assumes k_p as independent of the axial dispersion and thereby of the column packing quality. The transport-dispersive model consists of the differential balance equation in the mobile phase, Eq. (5.3a):

$$\frac{dC_f}{dt} + u\frac{dC_f}{dz} + \frac{1-\varepsilon}{\varepsilon}\left[\varepsilon_p \frac{\partial C_p}{\partial t} + \left(1-\varepsilon_p\right)\frac{\partial q}{\partial t}\right] = D_L \frac{\partial^2 C_f}{\partial z^2}, \qquad (5.3a)$$

as well as in the stationary phase of assumedly spherical particles, Eq. (3b):

$$\varepsilon_{\mathrm{p}} \frac{\partial C_{\mathrm{p}}}{\partial t} + \left(1-\varepsilon_{\mathrm{p}}\right) \frac{\partial q}{\partial t} = \frac{6\, k_{\mathrm{p}}}{d_{\mathrm{p}}} \left[\, f\left(q\right) - C_{\mathrm{p}} \,\right]. \tag{5.3b}$$

In this work, authors adapted Freundlich's equation (Freundlich, 1906), to mathematically describe equilibrium partition, in the case of the extraction of vegetable matrices, where extract concentration in the fluid is set as a function of its concentration in the solid, $f(q)$, Eq. (5.4):

$$C_{\mathrm{p}}^{*} = f\left(q\right) = k\; q^{n} \tag{5.4}$$

Solving these differential mass balance equations requires initial and boundary conditions. It was assumed that initially there was no extract in the interpaticle fluid, Eq. (5.5a), intraparticle fluid, Eq. (5.5b), or fully-extracted tomato, Eq. (5.5c). In addition, the closed boundary conditions proposed by Danckwerts (1953) for the entrance, Eq. (5.5d), and exit, Eq. (5.5e), of dispersive devices, were adopted:

$$C_{\mathrm{f}}\big|_{t=0,z} = 0, \tag{5.5a}$$

$$C_{\mathrm{p}}\big|_{t=0,z} = 0, \tag{5.5b}$$

$$q\big|_{t=0,z} = 0, \tag{5.5c}$$

$$C_{\mathrm{f}}\big|_{t,z=0} = C_{\mathrm{f}}^{\mathrm{Init}} - \frac{D_L \varepsilon}{U} \frac{\partial C_{\mathrm{f}}}{\partial z}\bigg|_{t,z=0}, \text{ and} \tag{5.5d}$$

$$\frac{\partial C_{\mathrm{f}}}{\partial z}\bigg|_{t,z=L} = 0. \tag{5.5e}$$

To solve Eqs. (5.3)-(5.5) using Matlab 2009b from Math Works (Natick, MA), authors discretized the space and time domains, and calculated the concentration in the fluid and solid phases as described by Urrego et al. (Submitted).

5.4. Results and discussion

Fig. (5-3) shows the sorption isotherm/isobar curve for tomato extract measured using the static methodology. The absence of an horizontal asymptote might be due to either insufficient initial extract content to saturate SC CO_2 at operation conditions, or its limitation by equilibrium partition between SC CO_2 and pretreated tomato (del Valle & Urrego, 2012). Evidently sorption effects of the tomato on the extract did not allow it to saturate SC CO_2 (which, as it will be informed later, should have reached 6.68 g kg^{-1} extract/CO_2 for tomato oleoresin at 40 ºC and 29 MPa). The shape of the isotherm/isobar was relatively well modelled using Freundlich's equation, Eq. (5.4), (k = 1.92×10^{-9}, n = 8.04).

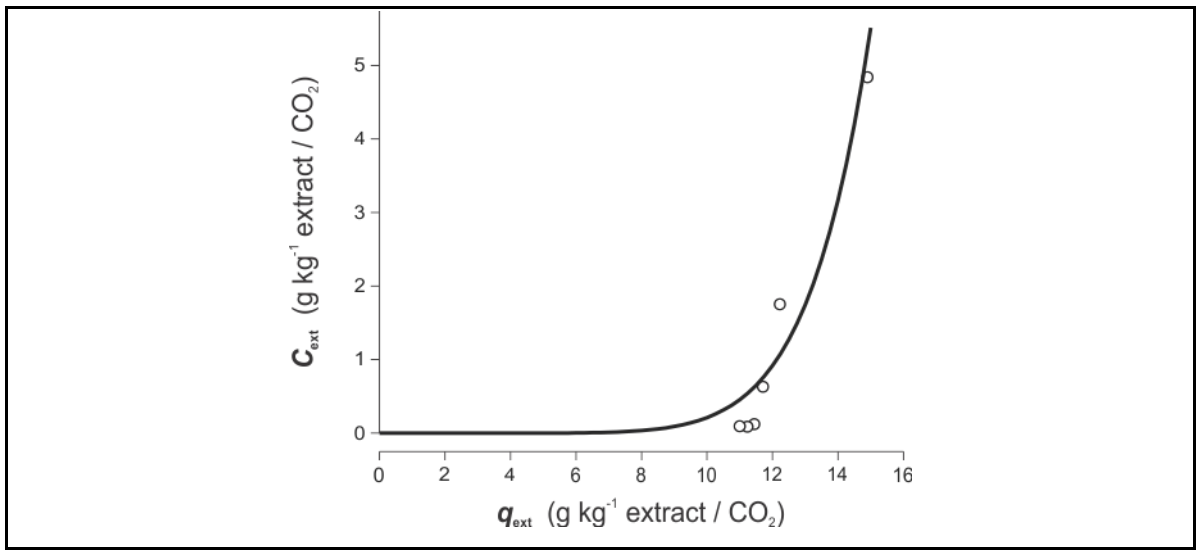

Figure 5-3. Equilibrium partition of tomato extract between supercritical CO_2 and dried, pelletized, milled, and size-classified tomato measured using the static procedure at 40 °C and 29 MPa. Open circles represent experimental data points, and the line model predictions using best-fitted parameters of Freundlich's equation, Eq. (5.4).

Fig. (5-4) shows carotenoid concentration in sampled extracts, as well as carotenoid concentrations in the corresponding sampled SC CO_2. Carotenoid concentrations in sampled extracts (Fig. 5-4A) were inversely proportional to extract concentration in SC CO_2. This was observed also in the fractional extraction of paprika containing 17.1% of fat

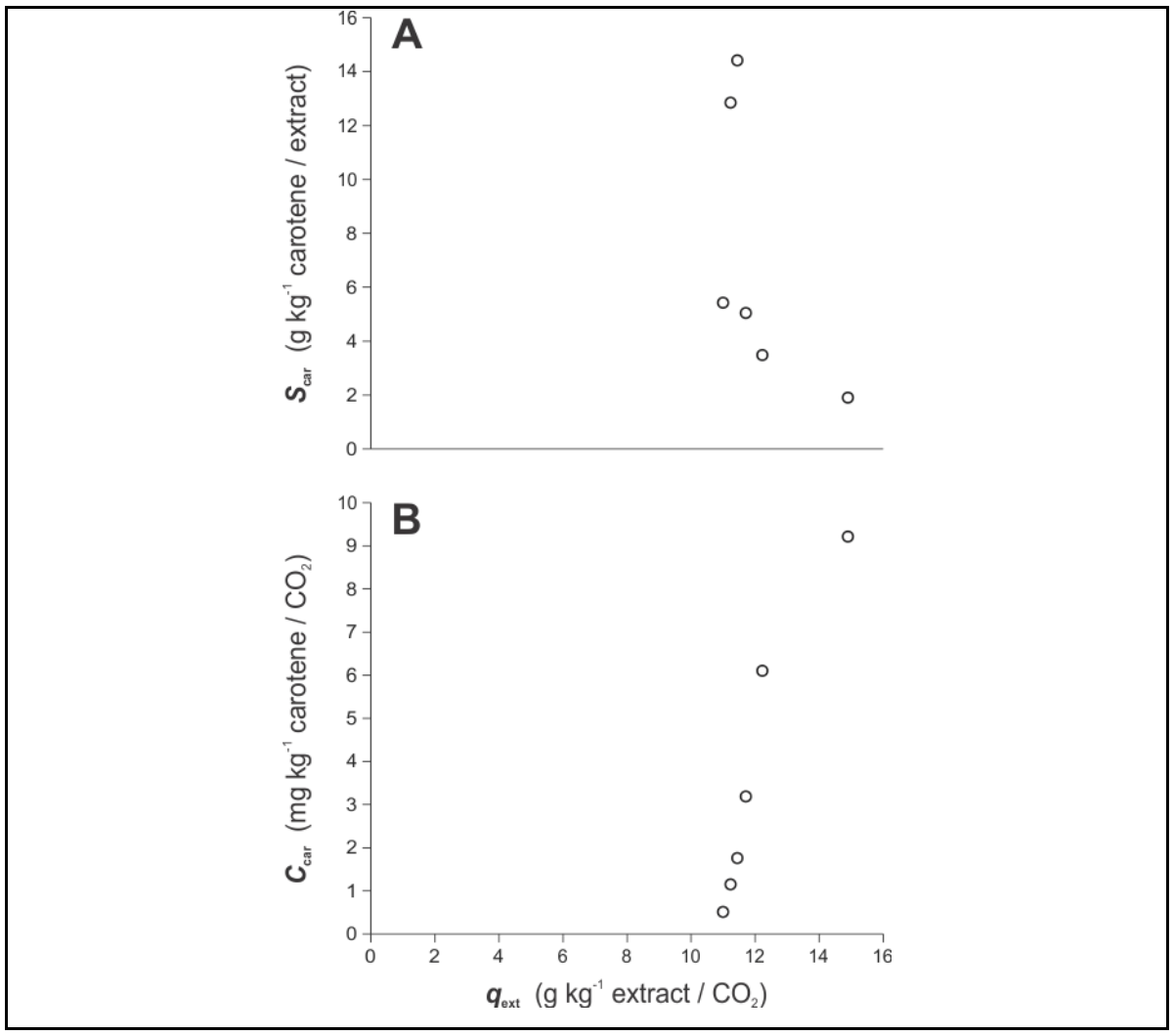

Figure 5-4. Carotenoid concentrations in (A) tomato extract, and (B) supercritical CO_2, of the extracts sampled while measuring the sorption isotherm/isobar curve using the static procedure (Fig. 5-3).

matter by Ambrogi et al. (2002), who measured carotenoid concentration at the exit of an extraction vessel with an online near-infrared/visible detector. Carotenoid concentration in SC CO_2 (Fig. 5-4B) shows a decreasing trend (in the direction of tomato extraction, $q <$ 0.03 g kg^{-1} carotene/ substrate), which means that extract concentration in SC CO_2 (Fig. 5-3) and carotenoid concentration in SC CO_2 (Fig. 5-4B) are correlated (higher amounts of extract in SC CO_2 yields higher amounts of carotenoid in SC CO_2). Thus, a co-solvency effect might be inferred of some higher-solubility component, possibly triglycerides, in

tomato extract. Reports in literature propose the application of vegetable oils as co-solvents for SCF extraction processes that change the solvent properties of SC CO_2 so as to improve the recovery of lower-solubility lipophilic compounds such as carotenoids (Sun & Temelli, 2006).

The injection procedure proposed in this work for the dynamic methods differs from those commonly applied in chromatographic procedures, where there is a constant solute concentration diluted in the solvent pumped into the column (Brunner & Johannsen, 2006). In this work, the injected "solute" is a vegetable extract whose carotenoid content is of interest. Initial and unreported results showed that the carotene concentration in extract-saturated SC CO_2 was above the UV/Vis measuring range (>3 AU), therefore extract dilution in SC CO_2 was required. Authors explored the use of pulses and a column packed with glass beads as an alternative to achieve stable, but lower carotenoid concentrations.

Fig. (5.5A) shows the response signal recorded at the outlet of the column packed with glass beads for switching times varying from 4 to 21 s. Fig. (5-5) suggests that the column packed with glass beads allowed stabilization of the extract concentration thanks to mixing and dispersion effects. Nevertheless, it must be noted that at the lowest switching time the horizontal asymptote shows a high dispersion, and switching values above 4 s should be preferred. At longer switching time values, noisy effects appear. The combinations of Injection Loop volume (V_{IL} = 50 μL), switching times ($4 \leq t_s \leq 21$ s), and CO_2 flow (Q_c = 3 cm^3/min) used in Fig. (5-5) were the only ones giving horizontal asymptotes in the full range of 0–1 AU, and were applied to measure the sorption isotherm/isobar curve dynamically. Results from other combinations are not reported. Differences in the width of the runs are only due to differences in the total time of injections and are not related to any adsorption or desorption effects, and this is represented by the compressed (shock) fronts and rear of the curves (Seidel-Morgenstern, 2004).

Fig. 5B also shows the actual steps of carotenoid concentration in SC CO_2 being injected into the glass beads column for three total switching times (4, 9 and 21 s, each including 1.5 s to elute loop contents) in a one-minute lapse, the carotenoid concentration represents the case when the HPLC pump operated at Q_c = 3.0 cm^3/min (2.3 g CO_2/min for

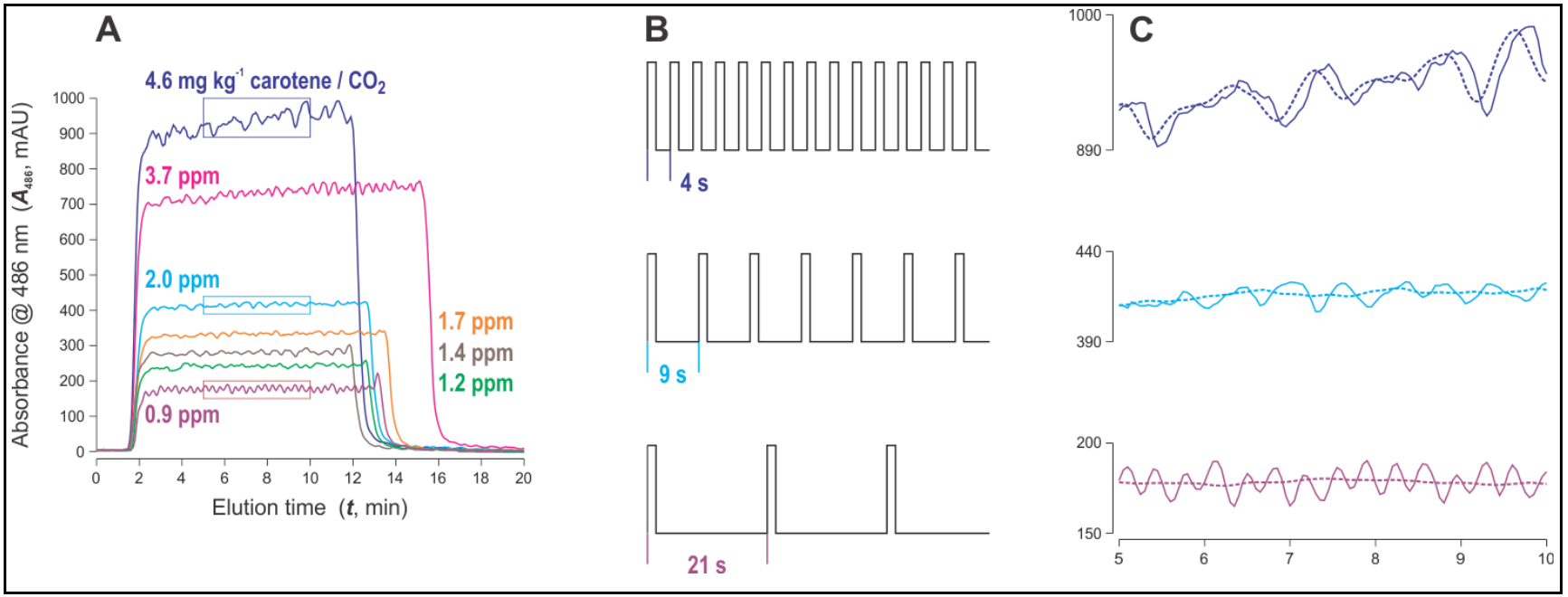

Figure 5-5. (A) Response signal for different switching times of tomato extract diluted in supercritical CO_2 in a column packed with glass beads. (B) Pulses (1.5 s) of supercritical CO2 saturated with tomato extract (50-µL portions) injected into the packed column for different switching times (4, 9, and 21-s). (C) Actual traces (full lines) and moving averages (segmented lines) for times equal to the switching times in (B) for the boxes noted in (A).

a solvent superficial velocity of U = 1.1 mm/s) and the automatic switching valve had a 50-μL loop containing C_{ext}^{Sat} = 6.68 g kg^{-1} extract/CO_2 containing 2.32 g kg-1 carotenoids/extract (concentrations were measured by sampling 7.29 g of SC CO_2 from the static system following equilibration) so that carotenoid concentration in SC CO2 was C_{car}^{Sat} = 15.5 mg/kg. In order to identify the effect of pulses on the response signal, authors calculated the moving averages (according to switching frequencies) for the horizontal asymptotes of the curves for 4, 9, and 21 s switching times (Fig. 5C). In the case of 9 and 21 seconds the smoothing effect is evident, but in the case of 4 seconds it is not. This might be related to the length of the column of glass beads, so that it allowed a better uniformity (due to mixing and diffusion effects) of the average concentration at the outlet of the column for switching times of ≥ 9 s.

Fig. (5-6) shows the correlation between the average absorbance (with error bars representing the standard deviation) observed in Fig. (5-5) and the average concentrations of carotenoids in SC CO_2. Under the assumption that the CO_2 + extract in the loop of the automatic switching valve is completely eluted by SC CO_2 fed by the HPLC pump (because 1.17 s are required by the pump to displace V_{IL} = 50 μL using Q_c = 3.0 cm^3/min, the timing relay was set to stay at this position for 1.50 s), and that the loop is completely refilled with extract-saturated SC CO_2 by the recirculating gear pump, average extract and carotene concentrations on each set of switching times were calculated as a function of total switching time (t_s, s) using Eq. (5.6):

$$C = \frac{3}{50}\frac{V_{IL}}{Q_c t_s} C_{sat} \qquad (5.6)$$

The line in Fig. (5-6) represents a linear regression of the data and the fit suggests that the assumptions of complete elution of the loop contents in 1.5 s, and constant carotenoid concentration in the extract during experiments were correct. The linear regression in Fig. (5-6) was applied to convert the recorded absorbance into carotenoids concentration for further analyses.

The assumption of negligible adsorption/desorption on glass beads was also evaluated by comparing curves from Fig. (5-5) under a same basis, by converting absorba-

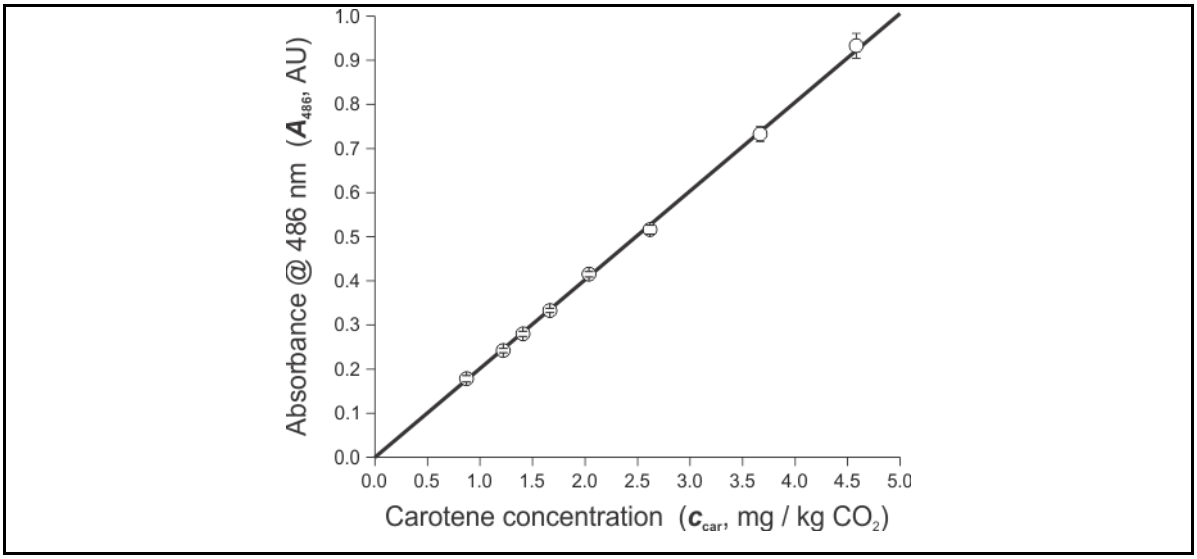

Figure 5-6. Correlation between average absorbance at 486 nm (wavelength of maximal absorbance of tomato extract in CO_2) and average carotenoid concentration in supercritical CO_2.

nce into carotenoid concentration in SC CO_2 and dividing it by the theoretical-average concentration (Fig. 5-7A). The shared shape of the breakthrough curves implies that glass beads do not adsorb carotenoids since different carotenoid concentrations in SC CO_2 reach the outlet of the column at almost the same time, so that any eventual difference gets confounded with the noise of the methodology. Fig. (5-7B) shows the curves when time was corrected so that all the dimensionless concentration at the value of 0.5 did coincide at the same time; a width of 6 seconds was observed and interpreted as random variations in the time response of the methodology.

Based in the correlation observed in Fig. (5-6), six average carotene concentrations in SC CO_2 (C = 0.90, 1.50, 2.80, 3.30, 4.10, and 4.60 mg kg^{-1} carotenoid/CO_2) were selected, and the required switching times to achieve those concentrations were calculated using Eq. (5.6) (t_s = 20.5, 12.0, 6.50, 5.50 4.50, and 4.00 s, respectively) to measure the isotherm/isobar with the pretreated and fully-extracted tomato. Fig. (5-8A) shows the experimental runs obtained with the dynamic methodology, with perturbations made once equilibration was assumed to be set and the elution profiles produced by turning off the injection valve and allowing pure CO_2 to desorb the carotenoids from the equilibrated

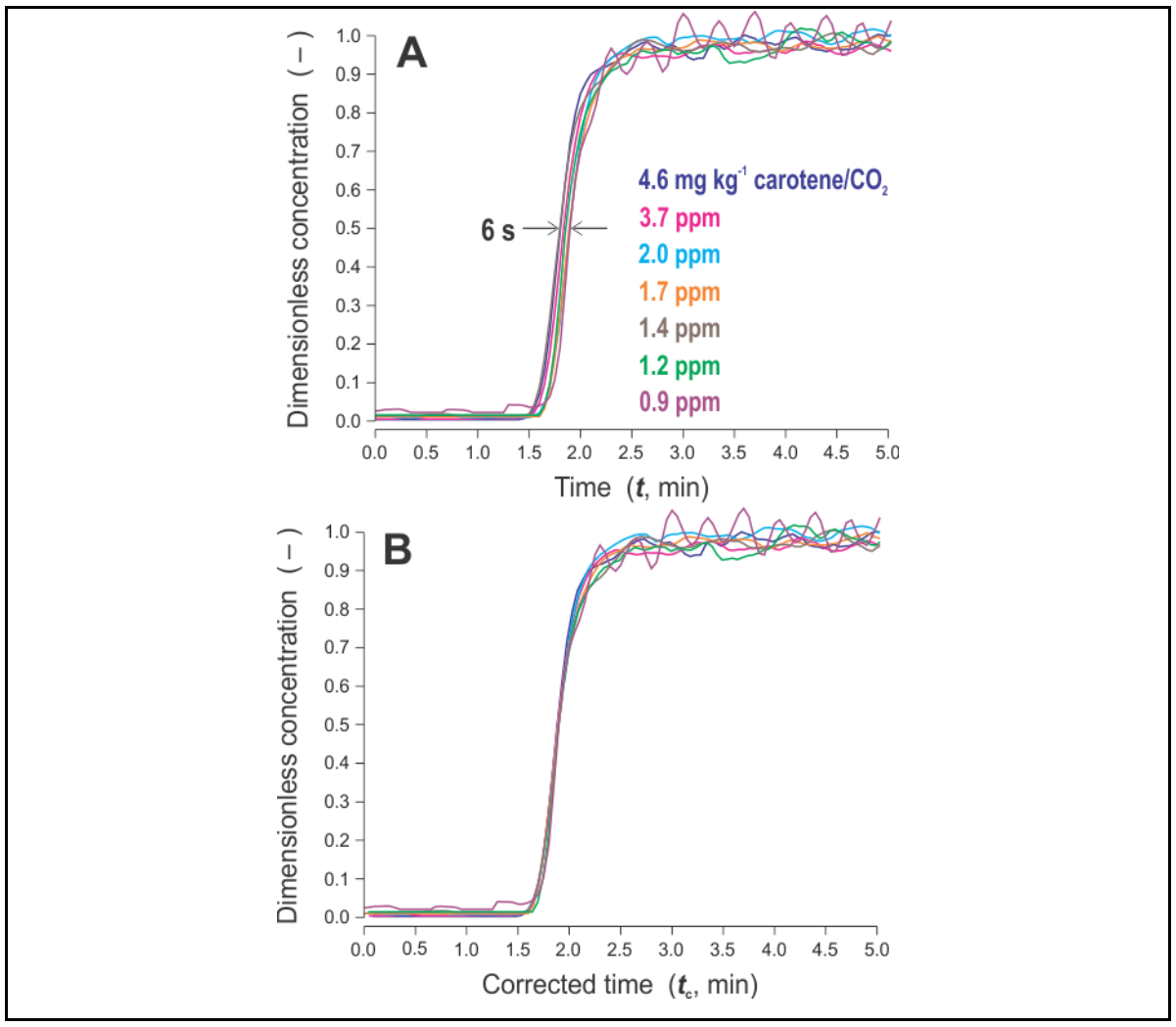

Figure 5-7. (A) Dimensionless concentration responses to injection of different concentrations of tomato in supercritical CO_2 to a column packed with glass beads. (B) Curves from (A) following adjustment of time so as to make coincide the dimensionless concentrations for the half-height (0.5) value.

column. Elution profiles in Fig. (5-8B) represent cases when an equilibrated pretreated tomato is desorbed with pure SC CO_2 (analysis of the desorption front, with time reset to zero at the moment when the switching valve was turned off).

Arrows in Fig. (5-8A) represent the time when perturbations were applied, and in order to better analyse them, authors fitted data with the normal distribution function (distr.norm.n) of Excel® 2010 from Microsoft (Redmond, WA) with the average, standard

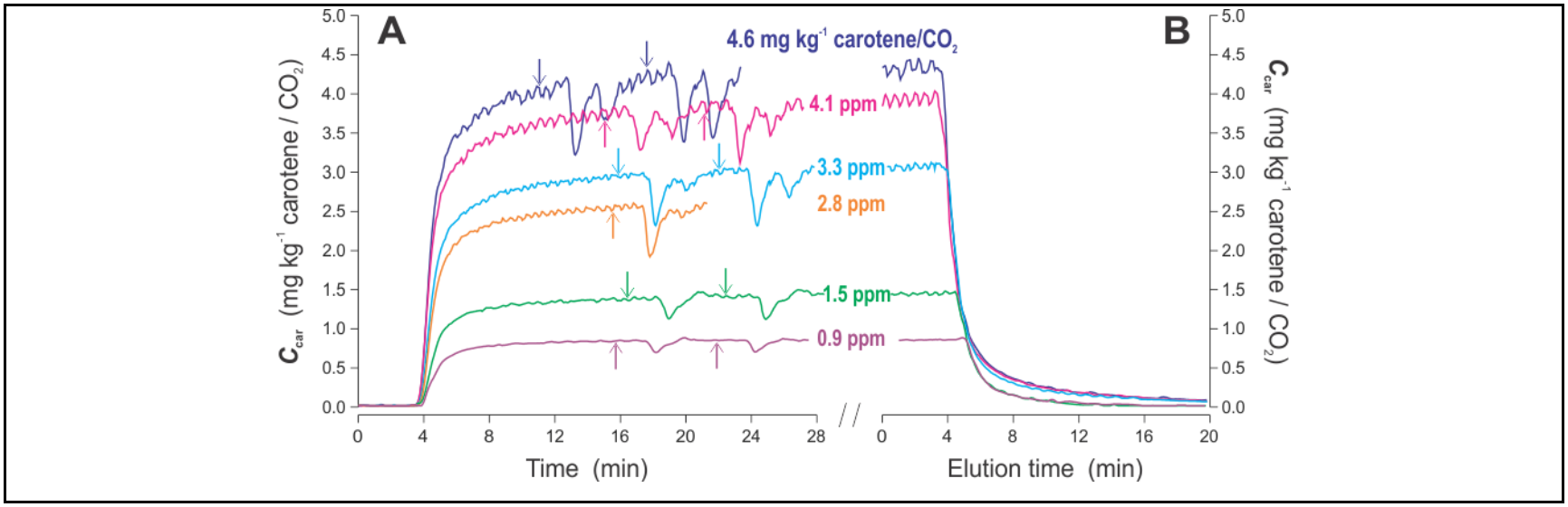

Figure 5-8. Summary of results for the frontal analysis, perturbation analysis, and desorption analysis for the partition of carotenes in tomato extract between supercritical CO_2 and fully extracted tomato at 40 ºC and 29 MPa. (A) Experimental response for the adsorption breakthrough curves as a function of the carotene concentrations in supercritical CO_2 (0.9–4.6 mg kg^{-1} carotene/CO_2), where arrows signal times when negative perturbation were induced. (B) Experimental response for the desorption breakthrough curves using pure supercritical CO_2 following equilibration of fully extracted tomato with CO_2 containing these same carotene concentrations.

deviation, and height of the peak as parameters. Fig. (5-9) shows response to two perturbations applied to the same sample, and from the superposition on an equal time scale authors concluded that peaks (and therefore the equilibrium conditions) are reproducible. Fig. (5-9) also shows arrows representing the time from the perturbation up to the beginning of the peaks, calculated as the fitted average values minus twice the fitted standard deviation (method applied in chromatography to identify the beginning of a peak). This time was then applied in Eq. (5.7) to calculate values of the slopes (dq/dC) at the specified concentrations in SC CO_2 (C) using Eq. (5.2). Due to the scarcity of data and the possible miscalculation of real parameter values, these are compared later with results obtained using the inverse method.

$$\frac{dq}{dC} = \frac{1}{k\,n}\left(\frac{C}{k}\right)^{\left(\frac{1}{n}-1\right)} \tag{5.7}$$

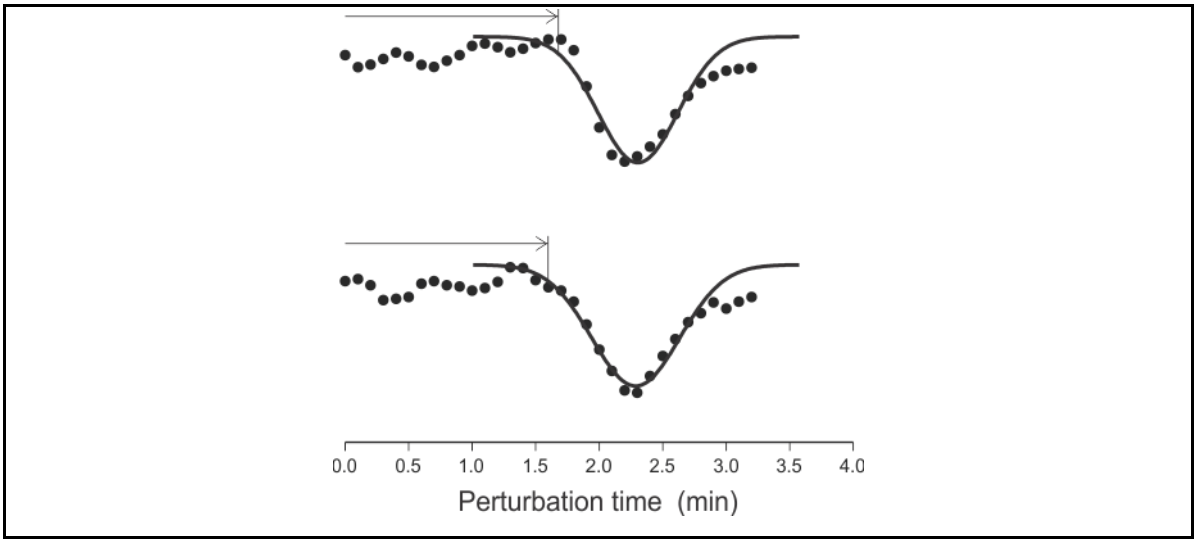

Figure 5-9. Details of the two perturbation peaks for the breakthrough curve for 4.1 mg kg^{-1} carotene/CO_2 in Figure 5-2 (close symbols) lined to the initiation of the perturbation, together with best-fits to the normal distribution function (lines); each end of arrow marks the onset of the negative peak, corresponding to the best-fit average (time for the minimal) minus twice the standard deviations.

The position and difference between frontal shocks observed in Fig. (5-8A) impeded applying the frontal analysis method described in Eq. (5.1), therefore, a numerical integration of individual breakthrough curves was applied. Authors compared data between the recorded carotenoid concentrations in SC CO_2 of the column packed with glass beads and the breakthrough curves, and the difference between responses was assumed to be the adsorbed carotene (Fig. 5-10). The difference between signals decreases with time as equilibrium between phases establishes, as expected. The cumulative sum of adsorbed carotene divided by the amount of substrate loaded in the column represents the equilibrium concentration in the substrate. A similar approach was applied to analyse frontal shocks of desorption curves.

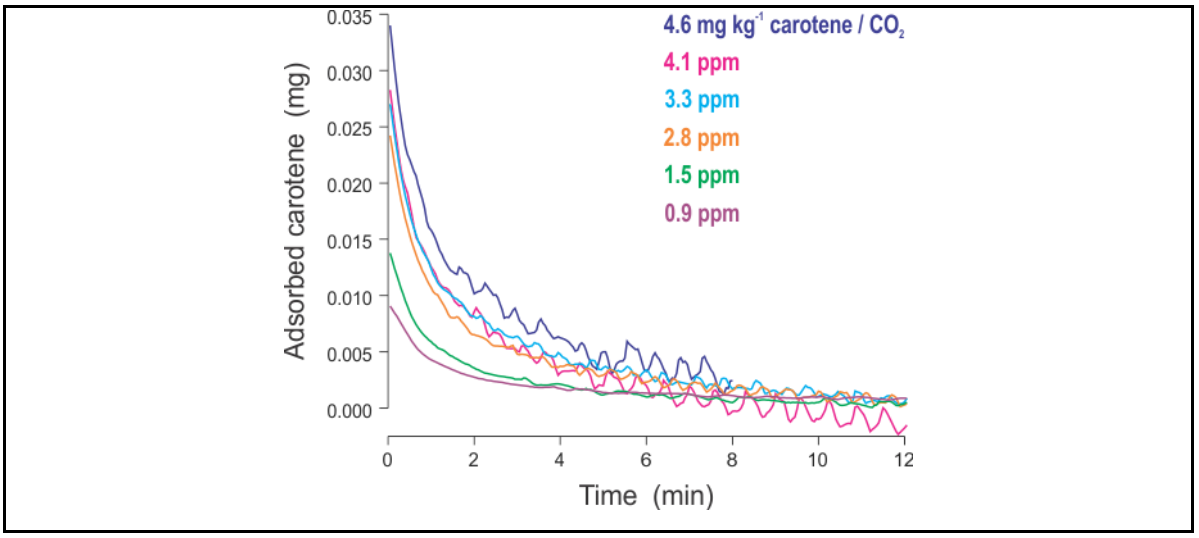

Figure 5-10. Difference in the breakthrough curves between a column packed with glass beads (Fig. 5-5A) and a similar column packed with fully-extracted tomato (Fig. 5-8A), represented the carotenoids adsorbed by the solid substrate at 40 ºC and 29 MPa as a function of the carotenoid concentration in the supercritical CO_2 fed to the columns. The area under each curve represents the total amount of tomato carotenoids adsorbed by the fully-extracted tomato.

To apply the inverse method, authors fitted the desorption profile of the highest curve in Fig. (5-8B), to a simulated desorption profile modelled with the transport-dispersive model, by minimizing the difference between the experimental and simulated

profiles. In order to estimate values of model parameters, authors applied the procedure outlined by del Valle (2015), as done by Urrego et al. (Submitted), so as to leave the sorption isotherm/isobar parameters ─*k* and *n* in Eq. (5.4) ─ as best-fitting parameters. The density, ρ (=904 kg/m^3), and viscosity, μ (9.29×10^{-5} Pa s), of SC CO_2 at operating conditions (40 °C and 29 MPa) were estimated using mini-REFPROP (Lemmon et al., 2007) software for pure CO_2. The binary diffusion coefficient of lycopene (component 2) in CO_2 (component 1), D_{12} (=3.88×10^{-9} m/s), was estimated as a function of the reduced temperature T_r (= T/T_c, T_c = 304.3 K), and reduced density, ρ_r (= ρ/ρ_c, ρ_c = 468 kg/m^3) of CO_2, and the molecular weight, MW_2 (= 536.9 g/mol) and critical volume, V_{c2} (=2024 cm^3/mol) of lycopene (representative compound in tomato extract) using the correlation of Catchpole and King (1994), where V_{c2} was estimated using Joback's modification of Lydersen's group contribution method (Poling, Prausnitz, & O'Connell, 2000). Authors estimated the amount of SC CO_2 in the column based on the total porosity, ε_t (= 0.620), that was estimated as a function of the mass, m_o (=6.00 g), and true density of dried, pelletized, milled, size-classified, and fully-extracted tomato, ρ_s (=1.43 g/cm^3), and the volume of the column, V_c (=11.7 cm^3) using Eq. (5.8):

$$\varepsilon_t = 1 - \frac{m_o}{\rho_s V_c} \tag{5.8}$$

Then, using the average diameter of the particle, d_p (=390 μm) and the column diameter, authors estimated the the interparticle porosity of packed, ε (=0.370) using the equation proposed by Ribeiro, Neto, and Pinho (2010) for packed beds of monosized spheres. The intraparticle porosity, ε_p (=0.400), and a microstructural factor, F (=6.16), were then calculated using Eqs. (5.9a) (Urrego et al., Submitted), and (5.9b) (del Valle et al., 2006; Wakao & Smith, 1962), respectively:

$$\varepsilon_p = \frac{\varepsilon_t - \varepsilon}{1 - \varepsilon}, \text{ and} \tag{5.9a}$$

$$F = \frac{1}{\left(\varepsilon_p\right)^2}. \tag{5.9b}$$

Finally, the effective diffusivity, D_e (=6.31×10^{-10} m^2/s), was calculated as the ratio of D_{12} and F. Following estimation of the bed height-to-particle diameter (L/d_p) ratio, and dimensionless Reynolds, *Re* (= $\rho\ U\ d_p\ \mu^{-1}$), and Schmidt, *Sc* (= $\mu\ \rho^{-1}\ D_{12}^{-1}$) numbers, the axial dispersion-to-binary diffusivity (D_L/D_{12}) ratio was estimated as a function of *Re*, *Sc*, and L/d_p, using the correlation of del Valle et al. (2011), and the dimensionless Sherwood number, *Sh* (= $kf\ d_p\ D_{12}^{-1}$) was estimated as a function of *Re* and *Sc* using the correlation of Puiggené et al. (1997). From estimated values of D_L/D_{12} and *Sh* it was possible to estimate D_L (= 3.48×10^{-6} m^2/s) and k_f (= 1.90×10^{-5} m/s) describing oil movement within and towards the CO_2 phase in the packed bed, respectively. Finally, the effective film mass transfer coefficient, k_p (= 8.74×10^{-6} m/s) was estimated using Eq. (5.10) for packed beds of spherical particles (del Valle & Urrego, 2012):

$$k_p = \frac{10\ k_f}{10 + \left(k_f d_p / D_e\right)} \tag{5.10}$$

Fig. (5-11A) shows the experimental and fitted desorption profiles obtained with the model, where isotherm/isobar parameters *k* (=13.7) and *n* (=1.56) were obtained. Fig. (5-11B) shows data calculated from the perturbation method and a line representing the derivative of the isotherm/isobar corresponding to Freundlich's model, Eq. (5.7), on top of experimental data obtained using perturbation data. Clearly the perturbation method appears to be much less sensitive than the inverse method (Fig. 5-11A) to best-fit sorption isotherm/isobar parameters.

Fig. (5-12A) shows isotherm/isobar curves calculated with the dynamic and the static methodologies, and the evident differences might be related to an irreversible desorption process of carotenoids once they were removed from the tomato matrix, so as to pass almost without interaction through a column packed with fully-extracted tomato. Nevertheless, data fitting to Freundlich's model implies concentration-dependent equilibrium partition that can be credited to sorption phenomena on the vegetable substrate. Fig. (5-12B) shows a magnification of the dynamic isotherm/isobar curves show-

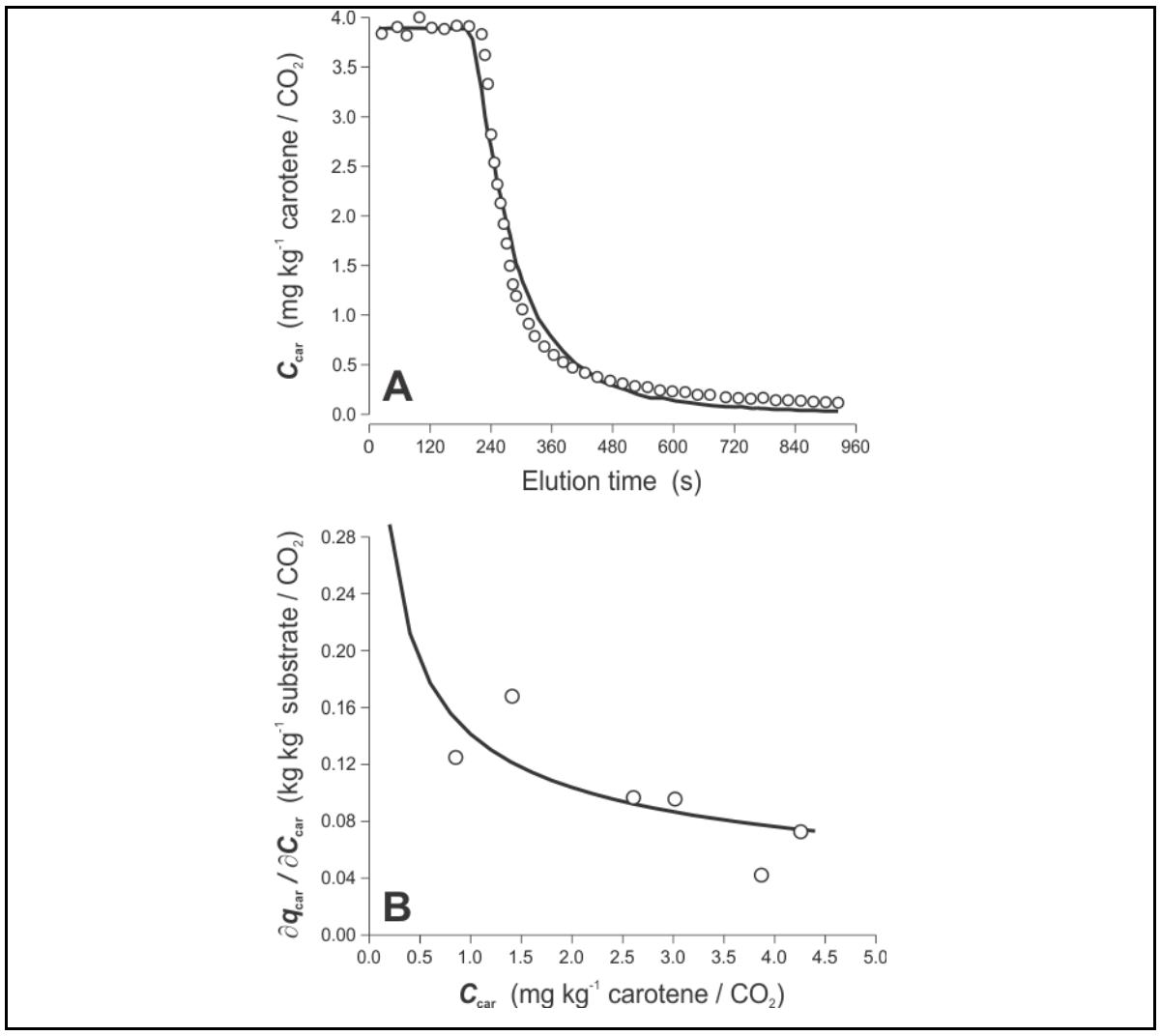

Figure 5-11. Best-fitting of the transport-dispersive model to breakthrough curves for carotene partition between supercritical CO_2 and fully extracted tomato at 40 ºC and 29 MPa. **(A)** Application of the inversion method to the desorption curve following equilibration of a column packed with fully-extracted tomato with a supercritical CO_2 solution containing 4.6 mg kg^{-1} carotene/CO_2; open circles represent experimental data points, and the line represents model predictions using best-fitted parameters of Freunlich's equation, Eq. (5.4). **(B)** Slope of the sorption isotherm/isobar *versus* carotene concentration in supercritical CO_2; open circles represent experimental data points from perturbation analysis (Fig. 5-9); whereas the line represented model predictions using Freundlich's equation with best-fit parameters from (A).

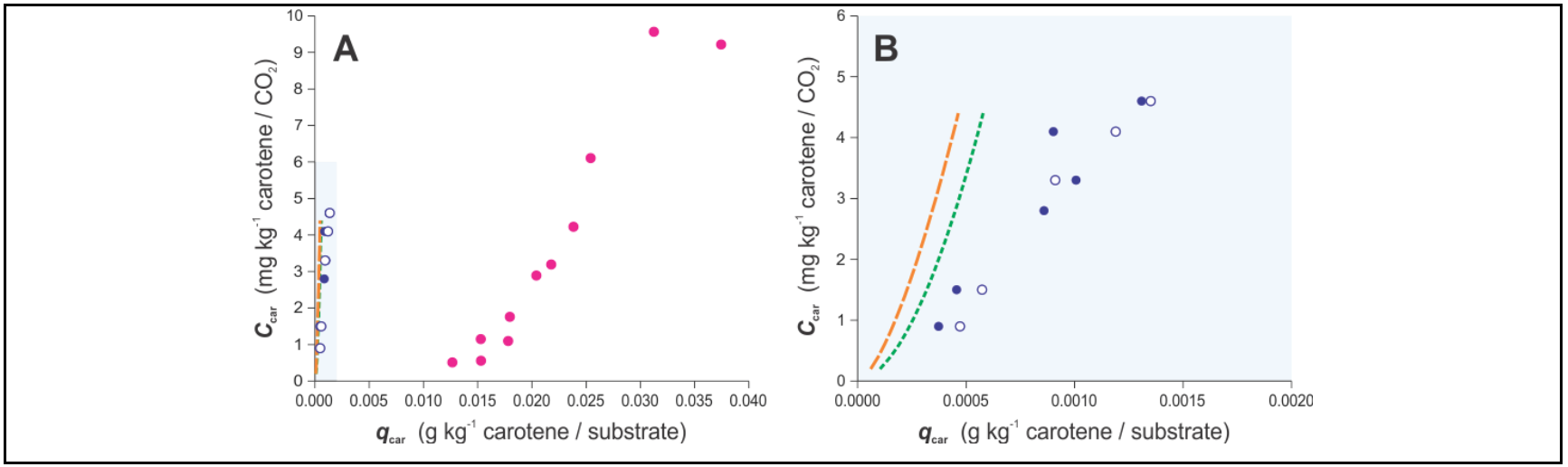

Figure 5-12. Sorption isotherm/isobars for tomato carotene partition between supercritical CO_2 and dried, pelletized, milled, and size-classified tomato. **(A)** Tomato desorption using the static method; closed circles outside highlighted area represent experimental data points. **(B)** Zoom of highlighted area in (A) showing results obtained applying dynamic methods to fully-extracted tomato. Symbols represent experimental data points using frontal analysis for the sorption (closed circles) and desorption (open symbols) steps. Line represent predicts using best-fitted parameters obtained using inverse analysis (Fig. 5-11).

ed in Fig. (5-12A), where two different trends are observed, the dynamic methodologies involving data fitting (perturbation and inverse methods) show lower affinity of carotenes to the tomato matrix than dynamic methodologies using mass balances. The difference between results of the dynamic methodologies might be related to their precision and uncertainties, and an in-depth analysis of their relative advantages and disadvantages might be required, although when comparing between the static and dynamic results, these last seem to show tendencies, with a broad dispersion.

5.5. Conclusions

The proposed dynamic methodologies allowed the determination of isotherm/isobar curves when injecting different concentration of tomato extract in SC CO_2 in a column packed with fully-extracted tomato powder. Desorption of carotenes from pelletized tomato proved to be an irreversible process, with limited affinity of the fully-extracted substrate to tomato carotenoids. It will be convenient to explore in the future solid matrices with higher affinity to the solute or solute mixture (extract). Based on results obtained in this work different experimental approaches might be tested, *i.e.*, the injection of bands or perturbations with controlled and variable concentration of vegetable extract in SC CO_2 to a column packed with (an) adsorbent(s) to be tested.

6. CONCLUSIONS AND FUTURE PERSPECTIVES

The equilibrium partition of the different vegetable systems measured in this thesis show that this mass transfer phenomena (sorption) is a factor that may affect the yield of SCFE processes, and in addition, the different behavior observed for the different measured systems indicates that it is relevant to include it in SCFE mathematical models. In cases where solute-matrix interactions are evidently limiting the SCFE process (i.e., the extraction of red pepper oleoresin where a SCFE process does not remove the total initial solute content, section 4), the experimental measurement of the sorption isotherm/isobar curve aids the identification of the limiting conditions for the oleoresin extraction.

The sigmoidal isotherm/isobar curves obtained for the rapeseed oil partition between prepressed rapeseed and SC CO_2 (Figs. 3-6,7) indicate, that in the equilibrium process, the partition to the SC CO_2 phase is limited by the solubility of the oil, and by comparing the shape with a theoretical non-interaction curve (Fig. 3-5) it was concluded that at specific operational conditions, and at certain residual oil concentrations in the substrate, the sorption affinity of the oil with the substrate impedes the saturation of the SC CO_2 even when there is still enough oil to do it. The red pepper and tomato oleoresin isotherm/isobar curves showed a different trend without a horizontal asymptote, concluding that a lower initial solute content and a different solute-substrate affinity impeded the saturation of the SC CO_2 since the beginning of the equilibration experiments.

The sorption isotherm/isobar curves were adequately modelled with an equation developed and proposed in this thesis (Eq. 3.9), and correlations were found between the variables of the equation and physical properties such as temperature and the density of the SC CO_2. In the case of the rapeseed oil isotherm/isobar curves, a heat of desorption of 32.2 kJ/mol was calculated, value that is within the range of a physisorption process, however, precision and accuracy of the methodology suggest that this result is highly speculative, and improvements to the methodology should be made to clarify this behavior. Briefly, it is required less uncertainty of the measurements at low concentrations both in the substrate and in the SC CO_2.

The isotherm/isobar curve of red pepper oleoresin partitioned between peletized-

milled-sieved red pepper and oil-modified SC CO_2 suggest that the extract (the mixture of oleoresin and oil) acquire a specific extract-substrate affinity that stands between the individual solute-substrate affinities. However, the partition of carotenoids to the SC CO_2 phase showed two different trends, one for the range where apparently the added oil is first extracted, and other for the range where the oleoresin is extracted (by comparing this range with the isotherm/isobar curve measured with pure SC CO_2), this might imply that the added oil had less solute-matrix affinity with the red pepper and therefore was more easily desorbed (assuming that adsorption had place after adding the oil to the substrate at environmental conditions). Nevertheless, the measured concentration of carotenoids in SC CO_2 suggest that the added oil enhanced the total amount of carotenoid that was extracted during the equilibrium measurement, proving its co-solvent effect.

From all the isotherm/isobar curves measured in this work it is apparent that there is an inverse correlation between the solubility of the compounds at the specific operational conditions, and their affinity with their substrates (represented either by smaller initial slopes or by curves more displaced to the C_f axis), this implies that the conditions that enhance the solubility of a solute in SC CO_2 also enhance its desorption.

The inclusion of an isotherm/isobar model, that was based on experimental data, into a robust SCFE model, proved to represent well the experimental extraction data, reducing the number of best-fit parameters to one, which was a value that was not possible to be read from the integral extraction curves (the total amount of extractable solute). Therefore, the hypothesis that, in the extraction of a vegetable substrate with pure or oil-modified SC CO_2, a vegetable and solid matrix interacts with their solutes through sorption phenomena, and its measurement, modelling, and inclusion in extraction models, improves the simulation of experimental extraction data, was proved.

Both of experimental methodologies applied in this thesis to measure the sorption equilibrium partition showed disadvantages that need to be solved so as to reduce the uncertainty in the measurements. In the case of the dynamic (chromatographic) methodology, it has an important advantage over the static methodology in terms of the time required to measure one isotherm/isobar curve, so I recommend to keep developing and improving it so as to find the combination of operational conditions and solute-solid

systems that will allow a more precise measurement. An approach was made by Andrighetti (2014), by measuring the equilibrium partition of tomato oleoresin between SC CO_2 and selected adsorbents (by evaluating activated carbon, microcrystalline cellulose, silica gel, celite, and chitosan in microspheres), whom found that activated carbon had a such high affinity with tomato oleoresin that had to be discarded, microcrystalline cellulose and celite had not affinity with tomato oleoresin, the silica gel exhibited high affinity with tomato oleoresin but the volume of the equilibration cell and the packed column characteristics made impossible to measure the equilibrium, finally choosing the chitosan in microspheres (that exhibited low, yet noticeable, affinity) to measure the sorption isotherm/isobar curves.

NOMENCLATURE

a_s specific surface area (m^2)

b model parameter in Eq. (3.12c) (K)

d_E diameter of the extraction vessel (m)

df_c degrees of freedom of complete model (–)

df_r degrees of freedom of reduced model (–)

d_p particle diameter (m)

f_p value of Fisher-Snedecor function for ($df_r - df_c$) degrees of freedom in the numerator, df_c degrees of freedom in the numerator, and a significance level p (–)

h length of the extractor vessel (m)

j_f flux from broken cells to SC CO_2 (kg m^{-3} s^{-1})

j_s flux from intact cells to broken cells (kg m^{-3} s^{-1})

k parameter of Freundlich's isotherm/isobar equation (-)

k_f film mass transfer coefficient (m/s)

k_p global mass coefficient using a linear driving force (m/s)

k_s mass transfer coefficient from intact to broken cells (m/s)

m_o solute-free substrate (kg)

n isotherm parameter (-)

p significance level (–)

q average solute concentration adsorbed onto the substrate (kg m^{-3} solute/substrate)

q_{Feed} quilibrium solute concentration adsorbed onto the substrate (kg m^{-3} solute/substrate)

q_{Init} initial solute concentration adsorbed onto the substrate (kg m^{-3} solute/substrate)

r grinding efficiency (-)

t extraction time (s)

t_o dead time of a chromatographic column (s)

t_R retention time of a chromatographic column (s)

t_s switch time frequency (s)

$u(y)$ variance of variable y

t_{res} residence time of SC CO_2 in the extraction vessel (s)

z axial position along the bed (m)

Upper case letters

A isotherm parameter, or cross sectional area of extraction vessel (m^2)

A' isotherm/isobar curve parameter (-)

A^o value of parameter A at reference temperature T^o (313.2 K) in Eq. (3.12c)

Bi Biot number (-)

C_1-C_5 equation parameters of the Adachi and Lu model (-)

C_{car}^{Sat} saturation concentration of carotenoids in CO_2 at operation conditions (mg kg^{-1} carotenoids/CO_2)

C_{ext}^{Sat} saturation concentration of extract in CO_2 at operation conditions (g kg^{-1} extract/CO_2)

C_f concentration of oil in the SC CO_2 (g/kg)

C_f^{Feed} equilibrium solute concentration in interparticle SC CO_2 (kg m^{-3} solute/CO_2)

C_f^{Init} initial solute concentration in CO_2 prior to step change to C_f^{Feed} (kg m^{-3} solute/CO_2)

$C_{f(i)}$ oil concentration in SC CO_2 in equilibration period 'i' (g kg^{-1} oil/CO_2)

C_f^* concentration of oil in a SC CO_2 film that is in equilibrium with oil in the surface of pre-pressed oilseed (g/kg)

C_{fo} concentration of oil in the SC CO_2 phase following the static extraction period (g/kg)

$C_{f|\,z,t}$ concentration of oil in the SC CO_2 phase in position z and time t (g/kg)

C_m monolayer concentration of oil in pre-pressed oilseed (g/kg)

C_p solute concentration in intraparticle CO_2 (substrate pores) (kg m^{-3} solute/CO_2)

C_s average concentration of oil in pre-pressed oilseed or adsorbed onto it (g/kg)

C_{sb} average concentration of solute in broken cells (g/kg)

$(C_s)_i$ initial concentration of oil in pre-pressed oilseed (g/kg)

C_{sat} concentration of oil in a saturated SC CO_2 phase (g/kg)

$C_{s(i)}$ average oil concentration adsorbed onto oilseed after equilibration period 'i' (g kg^{-1} oil/substrate)

C_{so} concentration of oil in pre-pressed oilseed following the static extraction period (g/kg)

$C_{s|z,t}$ concentration of oil in pre-pressed oilseed in position *z* and time *t* (g/kg)

C_t transition concentration of oil in pre-pressed oilseed (isotherm parameter)

D diameter of the extraction vessel (m)

D_{12} binary diffusion coefficient of oil in SC CO_2 (m^2/s)

D_e effective diffusion coefficient of oil in pre-pressed oilseed (m^2/s)

D_L axial dispersion coefficient of oil in packed bed (m^2/s)

F microstructural (correction) factor for D_{12}, to account for the resistances to mass transfer in pre-pressed oilseed (-)

J overall extraction rate ($kg\ m^{-2}\ s^{-1}$)

K equilibrium coefficient (-)

L length of the extraction vessel (m)

M_o oil-free substrate (kg)

MW_2 molecular weight of representative solute in tomato extract (Da)

N number of axial nodes in finite difference scheme to solve differential mass balance equations (-)

Pe Peclet number (-)

P equilibration pressure of system (MPa)

P’ atmospheric pressure (MPa)

Q_c mass flow rate of CO_2 in the extraction vessel (kg/s)

R universal gas constant (0.008314 $kJ\ mol^{-1}K^{-1}$)

Re dimensionless Reynolds number (–)

S solubility in SC CO_2 (g/kg)

$S_{(i)}$ oil removed in period ‘i’ (g)

S_o initial oil content in oilseed sample (g)

Sc dimensionless Schmidt number (–)

Sh dimensionless Sherwood number (–)

SSE_c Sum of squared errors of complete model

SSE_r Sum of squared errors of reduced model

T equilibration temperature of system (K)

T_c absolute critical temperature of CO_2 (304.3 K)

T_r reduced temperature of CO_2 (–)

T' temperature of expanded CO_2 in volumetric gas meter (K)

T^o reference absolute temperature (313.2 K)

Q mass flow rate of CO_2 in the extraction vessel (kg/s)

U superficial SC CO_2 velocity in the extraction vessel (m/s)

V volume of the extraction vessel (m^3)

V_{cell} empty volume of equilibrium cell (m^3)

V_{CO2} volume of expanded CO_2 samples (m^3)

V_{IL} volume of the injection loop (μL)

V_{loop} total volume of equilibration system (m^3)

V_{c2} critical volume of representative solute in tomato extract (cm_3/mol)

Greek letters

α shape factor of particle or isotherm parameter (-)

α^o value of parameter α at reference temperature T^o (313.2 K) in Eq. (3.12b) (kg g^{-1} substrate/oil)

δ thickness of leaf (μm)

ΔH total heat of solvation and sorption of oil (kJ/mol)

ΔH_{solv} heat of solvation of oil (kJ/mol)

ΔH_{sorp} heat of desorption of oil (kJ/mol)

Δt time interval in finite difference scheme to solve differential mass balance equations (s)

Δz height interval in finite difference scheme to solve differential mass balance equations (m)

ε (inter-particle) porosity of the packed bed (-)

ε' (inter-particle) porosity of the packed bed and other elements in equilibration system (–)

ε_p porosity of the solid particle (-)

ε_t total (inter- plus intra-particle) porosity of the packed bed (-)

μ viscosity of SC CO_2 (Pa s)

ρ density of SC CO_2 (kg/m^3)

ρ' density of expanded CO_2 (kg/m^3)

ρ_c critical density of CO_2 (468 kg/m_3)

ρ_r reduced density (-)

ρ_b bulk (apparent) density of pre-pressed oilseed in the extraction vessel (kg/m^3)

ρ_{oil} density of oil (kg/m^3)

ρ_s density of substrate (kg/m^3)

τ tortuosity (-)

Ψ sphericity (-)

REFERENCES

Adachi, Y., & Lu, B. C. Y. (1983). Supercritical fluid extraction with carbon dioxide and ethylene. *Fluid Phase Equilibria, 14*, 147-156.

Ahmad, A. L., Chan, C. Y., Abd Shukor, S. R., & Mashitah, M. D. (2009). Adsorption kinetics and thermodynamics of β-carotene on silica-based adsorbent. *Chemical Engineering Journal, 148*(2-3), 378-384.

Ambrogi, A., Cardarelli, D. A., & Eggers, R. (2002). Fractional extraction of paprika using supercritical carbon dioxide and on-line determination of carotenoids. *Journal of Food Science, 67*(9), 3236-3241.

Andrighetti, S. (2014). *Measurement of the equilibrium partition of tomato oleoresin between supercritical CO_2 and selected adsorbents using dynamic methods.* (MSc.), Pontificia Universidad Católica de Chile, Santiago de Chile.

Araus, K. A., Canales, R. I., de la Fuente, J. C., & del Valle, J. M. (2011). Solubility of β-carotene in ethanol- and triolein-modified CO_2. *Journal of Chemical Thermodynamics, 43*(12), 1991-2001.

Araus, K. A., del Valle, J. M., Robert, P. S., & de la Fuente, J. C. (2012). Effect of triolein addition on the solubility of capsanthin in supercritical carbon dioxide. *The Journal of Chemical Thermodynamics, 51*, 190-194.

Benyahia, F., & O'Neill, K. E. (2005). Enhanced Voidage Correlations for Packed Beds of Various Particle Shapes and Sizes. *Particulate Science and Technology, 23*(2), 169-177.

BIPM, IEC, IFCC, ILAC, ISO, IUPAC, IUPAP, OIML. (2008a). Evaluation of measurement data - Guide to the expression of uncertainty in measurement GUM 1995 with minor corrections (JCGM 100 ed.).

BIPM, IEC, IFCC, ILAC, ISO, IUPAC, IUPAP, OIML. (2008b, 2010). Evaluation of measurement data — Guide to the expression of uncertainty in measurement. from www.bipm.org/utils/common/documents/jcgm/JCGM_100_2008_E.pdf

BIPM, IEC, IFCC, ILAC, ISO, IUPAC, IUPAP, OIML. (2008c). Evaluation of measurement data — Supplement 1 to the "Guide to the expression of uncertainty in measurement" — Propagation of distributions using a Monte Carlo method.

Björklund, E., Jaremo, M., Mathiasson, L., Jonsson, J. A., & Karlsson, L. (1998). Illustration of important mechanisms controlling mass transfer in supercritical fluid extraction. *Analytica Chimica Acta, 368*(1-2), 117-128.

Brennecke, J. F., & Eckert, C. A. (1989). Phase-equilibria for supercritical fluid process design. *Aiche Journal, 35*(9), 1409-1427.

Brown, G. G., Foust, A. S., Katz, D. L. V., Schneidewind, R., White, R. R., Wood, W. P., . . . York, J. L. (1950). *Unit operations*. New York: Wiley.

Brunauer, S., Emmett, P. H., & Teller, E. (1938). Adsorption of gases in multimolecular layers. *Journal of the American Chemical Society, 60*(2), 309-319.

Brunner, G. (1994). *Gas extraction. An introduction to fundamentals of supercritical fluids and the application to separation processes*. Darmstadt/New York: Steinkopff/Springer.

Brunner, G., & Johannsen, M. (2006). New aspects on adsorption from supercritical fluid phases. *Journal of Supercritical Fluids, 38*(2), 181-200.

Budich, M., & Brunner, G. (1999). Vapor-liquid equilibrium data and flooding point measurements of the mixture carbon dioxide plus orange peel oil. *Fluid Phase Equilibria, 160*, 759-773.

Bulley, N., Fattori, M., Meisen, A., & Moyls, L. (1984). Supercritical fluid extraction of vegetable oil seeds. *Journal of the American Oil Chemists' Society, 61*, 1362-1365.

Carman, P. C. (1937). Fluid flow through granular beds. *Transactions of the Institution of Chemical Engineers, 15*, 150-166.

Catchpole, O. J., Grey, J. B., & Smallfield, B. M. (1997). Extraction of sage and coriander seed usign near-critical carbon dioxide. In M. A. Abraham & A. K. Sunol (Eds.), *Supercritical Fluids. Extraction and Pollution Prevention*. Washington, DC: American Chemical Society.

Catchpole, O. J., & King, M. B. (1994). Measurement and Correlation of Binary Diffusion Coefficients in Near Critical Fluids. *Industrial & Engineering Chemistry Research, 33*(7), 1828-1837.

Cocero, M. J., González, S., Pérez, S., & Alonso, E. (2000). Supercritical extraction of unsaturated products. Degradation of β-carotene in supercritical extraction processes. *The Journal of Supercritical Fluids*, *19*(1), 39-44.

Coelho, J. A. P., Mendes, R. L., Provost, M. C., Cabral, J. M. S., Novais, J. M., & Palavra, A. M. F. (1997). Supercritical carbon dioxide extraction of volatile compounds from rosemary. *Supercritical Fluids, 670*, 101-109.

Chrastil, J. (1982). Solubility of solids and liquids in supercritical gases. *The Journal of Physical Chemistry, 86*(15), 3016-3021.

Daghero, J., Ruetsch, L., Zacchi, P., & Mattea, M. (2004). *Supercritical CO_2 extraction of hebaceous matrices. Pilot plant experiments and modeling.* Paper presented at the V Encuentro Brasileño sobre Fluidos Supercriticos (EBFS 2004), Florianápolis, Brasil.

Danckwerts, P. V. (1953). Continuous flow systems: Distribution of residence times. *Chemical Engineering Science, 2*(1), 1-13.

de Azevedo, A. B. A., Kieckbusch, T. G., Tashima, A. K., Mohamed, R. S., Mazzafera, P., & de Melo, S. (2008). Supercritical CO_2 recovery of caffeine from green coffee oil: New experimental solubility data and modeling. *Quimica Nova, 31*(6), 1319-1323.

de la Fuente, J. C., Oyarzun, B., Quezada, N., & del Valle, J. M. (2006). Solubility of carotenoid pigments (lycopene and astaxanthin) in supercritical carbon dioxide. *Fluid Phase Equilibria, 247*(1-2), 90-95.

de la Fuente, J. C., Quezada, N., & del Valle, J. M. (2005). Solubility of boldo leaf antioxidant components (Boldine) in high-pressure carbon dioxide. *Fluid Phase Equilibria, 235*(2), 196-200.

de la Fuente, J. C., Valderrama, J. O., Bottini, S. B., & del Valle, J. M. (2005). Measurement and modeling of solubilities of capsaicin in high-pressure CO_2. *Journal of Supercritical Fluids, 34*(2), 195-201.

del Valle, J. M. (2015). Extraction of natural compounds using supercritical CO2: Going from the laboratory to the industrial application. *The Journal of Supercritical Fluids, 96*, 180-199.

del Valle, J. M., Aguilera, J. M., Hohlberg, A. I., Richardson, J. C., & Stanley, D. W. (1993). MODELING of BEAN HARDENING KINETICS DURING STORAGE. *Journal of Food Processing and Preservation, 17*(2), 119-137.

del Valle, J. M., & de la Fuente, J. C. (2006). Supercritical CO_2 extraction of oilseeds: Review of kinetic and equilibrium models. *Critical Reviews in Food Science and Nutrition, 46*(2), 131-160.

del Valle, J. M., de la Fuente, J. C., & Uquiche, E. L. (2012). A refined equation for predicting the solubility of vegetable oils in high-pressure CO_2. *Journal of Supercritical Fluids, 67*, 60-70.

del Valle, J. M., de la Fuente, J. C., Uquiche, E. L., Zetzl, C., & Brunner, G. (2011). Mass transfer and equilibrium parameters on high-pressure CO_2 extraction of plant essential oils. In J. M. Aguilera, R. Simpson, J. Welti-Chanes, D. Bermudez-Aguirre & G. Barbosa-Canovas (Eds.), *Food Engineering Interfaces*. New York: Springer.

del Valle, J. M., Germain, J. C., Uquiche, E., Zetzl, C., & Brunner, G. (2006). Microstructural effects on internal mass transfer of lipids in prepressed and flaked vegetable substrates. *Journal of Supercritical Fluids, 37*(2), 178-190.

del Valle, J. M., Jimenez, M., & de la Fuente, J. C. (2003). Extraction kinetics of pre-pelletized Jalapeno peppers with supercritical CO_2. *Journal of Supercritical Fluids, 25*(1), 33-44.

del Valle, J. M., Mena, C., & Budinich, M. (2008). Extraction of garlic with supercritical CO_2 and conventional organic solvents. *Brazilian Journal of Chemical Engineering, 25*, 532-542.

del Valle, J. M., Napolitano, P., & Fuentes, N. (2000). Estimation of relevant mass transfer parameters for the extraction of packed substrate beds using supercritical fluids. *Industrial & Engineering Chemistry Research, 39*(12), 4720-4728.

del Valle, J. M., Rivera, O., Mattea, M., Ruetsch, L., Daghero, J., & Flores, A. (2004). Supercritical CO_2 processing of pretreated rosehip seeds: effect of process scale on oil extraction kinetics. *Journal of Supercritical Fluids, 31*(2), 159-174.

del Valle, J. M., Rogalinski, T., Zetzl, C., & Brunner, G. (2005). Extraction of boldo (*Peumus boldus* M.) leaves with supercritical CO_2 and hot pressurized water. *Food Research International, 38*(2), 203-213.

del Valle, J. M., & Uquiche, E. (2003). *Critical comparison of mass transfer models for internally-controlled SCF extraction of solid substrates.* Paper presented at the VI International Symposium on Supercritical Fluids (ISSF 2003), Versailles, France.

del Valle, J. M., & Urrego, F. A. (2012). Free solute content and solute-matrix interactions affect apparent solubility and apparent solute content in supercritical CO_2 extractions. A hypothesis paper. *Journal of Supercritical Fluids*(66), 157-175.

Delgado, J. M. P. Q. (2006). A critical review of dispersion in packed beds. *Heat and Mass Transfer, 42*(4), 279-310.

Eggers, R., Ambrogi, A., & Schnitzler, J. v. (2000). Special features of SCF solid extraction of natural products: deoiling of wheat gluten and extraction of rose hip oil. *Brazilian Journal of Chemical Engineering, 17*, 329-334.

Estrella, A., López-Ortiz, J. F., Cabri, W., Rodríguez-Otero, C., Fraile, N., Erbez, A. J., Espartero, J. L., Carmona-Cuenca, I., Chavez, E., Muñoz-Ruiz, A. (2004). Natural lycopene from Blakeslea trispora: all-trans lycopene thermochemical and structural properties. *Thermochimica Acta, 417*(1), 157-161.

Femenia, A., Garcia-Marin, M., Simal, S., Rossello, C., & Blasco, M. (2001). Effects of supercritical carbon dioxide (SC-CO_2) oil extraction on the cell wall composition of almond fruits. *Journal of Agricultural and Food Chemistry, 49*(12), 5828-5834.

Fernandez-Ronco, M. P., Ortega-Noblejas, C., Gracia, I., De Lucas, A., Garcia, M. T., & Rodriguez, J. F. (2010). Supercritical fluid fractionation of liquid oleoresin capsicum: Statistical analysis and solubility parameters. *Journal of Supercritical Fluids, 54*(1), 22-29.

Freundlich, H. (1906). Über die adsorption in lösungen. *Zeitschrift Für Physikalische Chemie, 57*(A), 385-470.

Funazukuri, T., Kong, C. Y., & Kagei, S. (2008). Predictive correlation of binary diffusion and self-diffusion coefficients under supercritical and liquid conditions. *Journal of Supercritical Fluids, 46*(3), 280-284.

Funazukuri, T., Toriumi, M., Yui, K., Kong, C. Y., & Kagei, S. (2009). *Predictive correlation for binary diffusion coefficients of lipids in supercritical carbon dioxide.* Paper presented at the IX International Symposium on Supercritical Fluids (ISSF 2009), Arcachon, France.

Germain, J. C., del Valle, J. M., & de la Fuente, J. C. (2005). Natural convection retards supercritical CO_2 extraction of essential oils and lipids from vegetable substrates. *Industrial & Engineering Chemistry Research, 44*, 2879–2886.

Gomez-Prieto, M. S., Caja, M. M., & Santa-Maria, G. (2002). Solubility in supercritical carbon dioxide of the predominant carotenes of tomato skin. *Journal of the American Oil Chemists' Society, 79*(9), 897-902.

Goodrun, J. W., Kilgo, M. K., & Santerre, C. R. (1996). Oilseed solubility and extraction modeling. In J. W. King & G. R. List (Eds.), *Supercritical Fluid Technology in Oil and Lipid Chemistry*: American Oil Chemist's Society.

Gopalán, B., Goto, M., Kodama, A., & Hirose, T. (2000). Supercritical carbon dioxide extraction of turmeric (*Curcuma longa*). *Journal of Agricultural and Food Chemistry, 48*(6), 2189-2192.

Goto, M., Roy, B. C., & Hirose, T. (1996). Shrinking-core leaching model for supercritical-fluid extraction. *The Journal of Supercritical Fluids, 9*(2), 128-133.

Goto, M., Roy, B. C., Kodama, A., & Hirose, T. (1998). Modeling supercritical fluid extraction process involving solute-solid interaction. *Journal of Chemical Engineering of Japan, 31*(2), 171-177.

Iwai, Y., Hosotani, N., Morotomi, T., Koga, Y., & Arai, Y. (1994). High-Pressure vapor-liquid-equilibria for carbon-dioxide plus linalool. *Journal of Chemical and Engineering Data, 39*(4), 900-902.

Iwai, Y., Morotomi, T., Sakamoto, K., Koga, Y., & Arai, Y. (1996). High-pressure vapor-liquid equilibria for carbon dioxide plus limonene. *Journal of Chemical and Engineering Data, 41*(5), 951-952.

Johannsen, M., & Brunner, G. (1997). Solubilities of the fat-soluble vitamins A, D, E, and K in supercritical carbon dioxide. *Journal of Chemical and Engineering Data, 42*(1), 106-111.

Kao, L., Chen, C. R., & Chang, C. M. J. (2007). Supercritical CO_2 extraction of turmerones from turmeric and high-pressure phase equilibrium of CO_2+turmerones. *Journal of Supercritical Fluids, 43*(2), 276-282.

King, M. B., Bott, T. R., Barr, M. J., Mahmud, R. S., & Sanders, N. (1987). Equilibrium and rate data for the extraction of lipids using compressed carbon dioxide. *Separation Science and Technology, 22*, 1103-1120.

Kwon, K. T., Uddin, M. S., Jung, G. W., Sim, J. E., Lee, S. M., Woo, H. C., & Chun, B. S. (2011). Solubility of red pepper (*Capsicum annum*) oil in near- and supercritical carbon dioxide and quantification of capsaicin. *Korean Journal of Chemical Engineering, 28*(6), 1433-1438.

Langmuir, I. (1916). The constitution and fundamental properties of solids and liquids. Part I. Solids. *Journal of the American Chemical Society, 38*, 2221-2295.

Lavrich, D. J., Wetterer, S. M., Bernasek, S. L., & Scoles, G. (1998). Physisorption and Chemisorption of Alkanethiols and Alkyl Sulfides on Au(111). *The Journal of Physical Chemistry B, 102*(18), 3456-3465.

Lee, A. K. K., Bulley, N. R., Fattori, M., & Meisen, A. (1980). Modelling of supercritical carbon dioxide extraction of canola oilseed in fixed beds. *Journal of the American Oil Chemists' Society, 63*(7), 921-925.

Lemmon, E. W., Huber, M. L., & McLinden, M. O. (2007). NIST Standard Reference Database 23: Reference Fluid Thermodynamic and Transport Properties-REFPROP (Version 8.0). Gaithersburg.

Ma, Q. X., Xu, X., Gao, Y. X., Wang, Q., & Zhao, J. (2008). Optimisation of supercritical carbon dioxide extraction of lutein esters from marigold (*Tagetes erect* L.) with soybean oil as a co-solvent. *International Journal of Food Science and Technology, 43*(10), 1763-1769.

Ma, Y. H., & Evans, L. B. (1968). Transient diffusion from a well-stirred reservoir to a body of arbitrary shape. *Aiche Journal, 14*(6), 956-961.

Machmudah, S., Sulaswatty, A., Sasaki, M., Goto, M., & Hirose, T. (2006). Supercritical CO_2 extraction of nutmeg oil: Experiments and modeling. *Journal of Supercritical Fluids, 39*(1), 30-39.

Marrone, C., Poletto, M., Reverchon, E., & Stassi, A. (1998). Almond oil extraction by supercritical CO_2: experiments and modelling. *Chemical Engineering Science, 53*(21), 3711-3718.

Martinez, J., Monteiro, A. R., Rosa, P. T. V., Marques, M. O. M., & Meireles, M. A. A. (2003). Multicomponent model to describe extraction of ginger oleoresin with supercritical carbon dioxide. *Industrial & Engineering Chemistry Research, 42*(5), 1057-1063.

Martínez, J., Rosa, P. T. V., & Meireless, M. A. A. (2007). Extraction of clove and vetiver oils with supercritical carbon dioxide: Modeling and simulation. *The Open Chemical Engineering Journal, 1*, 1-7.

Mendez-Santiago, J., & Teja, A. S. (1999). The solubility of solids in supercritical fluids. *Fluid Phase Equilibria, 160*, 501-510.

Michel, M., Epping, A., & Jupke, A. (2005). Modelling and Determination of Model parameters. In H. S.-T. (Ed.) (Ed.), *Preparative Chromatography of Fine Chemicals and Pharmaceutical Agents* (pp. 215-312). Weinheim: WILEY-VCH.

Mira, B., Blasco, M., Subirats, S., & Berna, A. (1996). Supercritical CO_2 extraction of essential oils from orange peel. *Journal of Supercritical Fluids, 9*(4), 238-243.

Morotomi, T., Iwai, Y., Yamaguchi, H., & Arai, Y. (1999). High-pressure vapor-liquid equilibria for carbon dioxide plus limonene plus linalool. *Journal of Chemical and Engineering Data, 44*(6), 1370-1372.

Nollet, H., Roels, M., Lutgen, P., Van der Meeren, P., & Verstraete, W. (2003). Removal of PCBs from wastewater using fly ash. *Chemosphere, 53*(6), 655-665.

Núñez, G. A., Gelmi, C. A., & del Valle, J. M. (2011). Simulation of a supercritical carbon dioxide extraction plant with three extraction vessels. *Computers & Chemical Engineering, 35*(12), 2687-2695.

Peper, S., & Dohrn, R. (2012). Sampling from fluid mixtures under high pressure: Review, case study and evaluation. *The Journal of Supercritical Fluids, 66*, 2-15.

Perrut, M., Clavier, J. Y., Poletto, M., & Reverchon, E. (1997). Mathematical modeling of sunflower seed extraction by supercritical CO_2. *Industrial & Engineering Chemistry Research, 36*(2), 430-435.

Poling, B. E., Prausnitz, J. M., & O'Connell, J. P. (2000). *The Properties of Gases and Liquids* (5th ed.). New York, NY.

Puah, C. W. (2005). Supercritical fluid extraction of palm carotenoids. *American Journal of Environmental Sciences, 4*, 264-269.

Puah, C. W., Choo, Y. M., Ma, A. N., & Chuah, C. H. (2007). Solubility of tocopherol and tocotrienols from palm oil in supercritical carbon dioxide. *Journal of Food Lipids, 14*(4), 377-385.

Puiggené, J., Larrayoz, M. A., & Recasens, F. (1997). Free liquid-to-supercritical fluid mass transfer in packed beds. *Chemical Engineering Science, 52*(2), 195-212.

Reverchon, E., & Marrone, C. (1997). Supercritical extraction of clove bud essential oil: isolation and mathematical modeling. *Chemical Engineering Science, 52*(20), 3421-3428.

Ribeiro, A. M., Neto, P., & Pinho, C. (2010). Mean Porosity and Pressure Drop Measurements in Packed Beds of Monosized Spheres: Side Wall Effects. *International Review of Chemical Engineering (Rapid Communications), 2*(1), 40-46.

Rochova, K., Sovova, H., Sobolik, V., & Allaf, K. (2008). Impact of seed structure modification on the rate of supercritical CO_2 extraction. *Journal of Supercritical Fluids, 44*(2), 211-218.

Rosa, P. T. V., & Meireles, M. A. A. (2005). Rapid estimation of the manufacturing cost of extracts obtained by supercritical fluid extraction. *Journal of Food Engineering, 67*(1-2), 235-240.

Ruetsch, L., Daghero, J., & Mattea, M. (2003). Supercritical extraction of solid matrices. Model formulation and experiments. *Latin American Applied Research, 33*(2), 103-107.

Saldaña, M. D. A., Mohamed, R. S., Baer, M. G., & Mazzafera, P. (1999). Extraction of purine alkaloids from mate (*Ilex paraguariensis*) using supercritical CO_2. *Journal of Agricultural and Food Chemistry, 47*(9), 3804-3808.

Saldaña, M. D. A., Sun, L., Guigard, S. E., & Temelli, F. (2006). Comparison of the solubility of beta-carotene in supercritical CO_2 based on a binary and a multicomponent complex system. *Journal of Supercritical Fluids, 37*(3), 342-349.

Saldaña, M. D. A., Temelli, F., Guigard, S. E., Tomberli, B., & Gray, C. G. (2010). Apparent solubility of lycopene and beta-carotene in supercritical CO_2, CO_2 + ethanol and CO_2 + canola oil using dynamic extraction of tomatoes. *Journal of Food Engineering, 99*(1), 1-8.

Salem, L. (1962). Attractive Forces between Long Saturated Chains at Short Distances. *The Journal of Chemical Physics, 37*(9), 2100-2113.

Salimi, A., Fatemi, S., Nei, H. Z. N., & Safaralie, A. (2008). Mathematical modeling of supercritical extraction of valerenic acid from *Valeriana officinalis* L. *Chemical Engineering & Technology, 31*(10), 1470-1480.

Seidel-Morgenstern, A. (2004). Experimental determination of single solute and competitive adsorption isotherms. *Journal of Chromatography A, 1037*(1–2), 255-272.

Shi, J., Khatri, M., Xue, S. J., Mittal, G. S., Ma, Y., & Li, D. (2009). Solubility of lycopene in supercritical CO_2 fluid as affected by temperature and pressure. *Separation and Purification Technology, 66*(2), 322-328.

Shi, J., Mittal, G. S., Kim, E., & Xue, S. J. (2007). Solubility of Carotenoids in Supercritical CO2. *Food Reviews International, 23*(4), 341-371.

Silva, G. F., Gamarra, F. M. C., Oliveira, A. L., & Cabral, F. A. (2008). Extraction of bixin from annatto seeds using supercritical carbon dioxide. *Brazilian Journal of Chemical Engineering, 25*(2), 419-426.

Sips, R. (1948). On the structure of a catalyst surface. *The Journal of Chemical Physics, 16*(5), 490-495.

Sousa, E. M. B. D., Chiavone, O., Moreno, M. T., Silva, D. N., Marques, M. O. M., & Meireles, M. A. A. (2002). Experimental results for the extraction of essential oil

from *Lippia sidoides* Cham. using pressurized carbon dioxide. *Brazilian Journal of Chemical Engineering, 19*(2), 229-241.

Sousa, E. M. B. D., Martinez, J., Chiavone, O., Rosa, P. T. V., Domingos, T., & Meireles, M. A. A. (2005). Extraction of volatile oil from *Croton zehntneri* Pax et Hoff with pressurized CO(2): solubility, composition and kinetics. *Journal of Food Engineering*, *69*(3), 325-333.

Sovová, H. (1994). Rate of the vegetable oil extraction with supercritical CO_2 .1. Modeling of extraction curves. *Chemical Engineering Science, 49*(3), 409-414.

Sovová, H. (2005). Mathematical model for supercritical fluid extraction of natural products and extraction curve evaluation. *Journal of Supercritical Fluids, 33*(1), 35-52.

Sovová, H. (2012). Steps of supercritical fluid extraction of natural products and their characteristic times. *The Journal of Supercritical Fluids, 66*, 73-79.

Sovová, H., Komers, R., Kucera, J., & Jez, J. (1994). Supercritical carbon-dioxide extraction of caraway essential oil. *Chemical Engineering Science, 49*(15), 2499-2505.

Sovova, H., Stateva, R. P., & Galushko, A. A. (2001). Solubility of beta-carotene in supercritical CO_2 and the effect of entrainers. *Journal of Supercritical Fluids, 21*(3), 195-203.

Spricigo, C. B., Bolzan, A., Machado, R. A. F., Carlson, L. H. C., & Petrus, J. C. C. (2001). Separation of nutmeg essential oil and dense CO_2 with a cellulose acetate reverse osmosis membrane. *Journal of Membrane Science, 188*(2), 173-179.

Stahl, E., Schutz, E., & Mangold, H. K. (1980). Extraction of seed oil with liquid and supercritical carbon dioxide. *Journal of Agricultural and Food Chemistry, 28*, 1153-1157.

Subra, P., Castellani, S., Jestin, P., & Aoufi, A. (1998). Extraction of beta-carotene with supercritical fluids - Experiments and modelling. *Journal of Supercritical Fluids, 12*(3), 261-269.

Sun, M., & Temelli, F. (2006). Supercritical carbon dioxide extraction of carotenoids from carrot using canola oil as a continuous co-solvent. *Journal of Supercritical Fluids, 37*(3), 397-408.

Topal, U., Sasaki, M., Goto, M., & Hayakawa, K. (2006). Extraction of lycopene from tomato skin with supercritical carbon dioxide: Effect of operating conditions and solubility analysis. *Journal of Agricultural and Food Chemistry, 54*(15), 5604-5610.

Uquiche, E., Araus, K. A., & del Valle, J. M. (in preparation). Supercritical CO_2 extraction of carotenoids from extruded red pepper using high-oleic sunflower oil as entrainer. *The Journal of Supercritical Fluids*.

Urrego, F. A., Nuñez, G. A., Donaire, Y. D., & del Valle, J. M. (Submitted). Equilibrium partition of rapeseed oil between supercritical CO_2 and prepressed rapeseed. *The Journal of Supercritical Fluids*.

Vasapollo, G., Longo, L., Rescio, L., & Ciurlia, L. (2004). Innovative supercritical CO_2 extraction of lycopene from tomato in the presence of vegetable oil as co-solvent. *Journal of Supercritical Fluids, 29*(1-2), 87-96.

Wakao, N., & Smith, J. M. (1962). Diffusion in catalyst pellets. *Chemical Engineering Science, 17*(11), 825-834.

Wetterer, S. M., Lavrich, D. J., Cummings, T., Bernasek, S. L., & Scoles, G. (1998). Energetics and Kinetics of the Physisorption of Hydrocarbons on Au(111). *The Journal of Physical Chemistry B, 102*(46), 9266-9275.

Young, T. M., & Weber, W. J. (1997). Equilibrium and rate study of analyte-matrix interactions in supercritical fluid extraction. *Analytical Chemistry, 69*(8), 1612-1619.

Zuknik, M. H., Norulaini, N. A. N., & Omar, A. K. M. (2012). Supercritical carbon dioxide extraction of lycopene: A review. *Journal of Food Engineering, 112*, 253-262.

A P P E N D I X E S

APPENDIX A: DETAILS OF MATHEMATICAL MODELS APPLIED IN SECTION (2).

Fig. (A-1) summarizes mass transfer in the extraction vessel, a packed bed of porous spherical particles, for the more complex situation (Model 3) where mass transfer (to the right of the Fig. A-1) depends of oil partition between a pre-pressed oilseed and SC CO_2 in the intra-particle space, diffusion of oil in SC CO_2 in the intra-particle space, and convection of dissolved oil in the surface of the particle to SC CO_2 in the inter-particle space. Finite differences were used to mathematically solve the mass transfer problem; Fig. A-1 (right) shows a differential volume in space (node *n*, axial position *z*) in the extraction vessel.

Differential mass balances depended on a space-time (*z*,*t*) discretization and the specific assumptions of each one of the three models presented in this manuscript, which defined oil partition between pre-pressed oilseed and SC CO_2 (Model 1 and Model 2) or flux of oil from the seeds to the SC CO_2 (Model 3). These mass balances were solved in Matlab 2008b [Math Works, Natick, MA] to calculate concentrations of oil in pre-pressed oilseeds in each element (position along the extraction vessel, time) of the grid, and oil yield as a function of extraction time. The extraction vessel was divided in finite length ($\Delta z = L / N$) nodes, with the number of nodes (N) being selected so that for such number and more there were no differences between simulated integral extraction curves. Time, in turn, was divided in finite intervals corresponding to the time taken by SC CO_2 (superficial velocity U) to go through a node in space ($\Delta t = \Delta z / U$).

A1. Initial condition

A static extraction period was assumed at the beginning when required system conditions (temperature and pressure) can be stabilized and an equilibrium condition in the whole extraction vessel ($C_s \big|_{z,0} = C_{so}$; $C_f \big|_{z,0} = C_{fo}$) can be reached. In the case of Model 2 and Model 3, the initial condition was determined by solving the oil conservation (Eq. A.1) and equilibrium sorption (Eq. A.2) equations simultaneously for C_{so} and C_{fo}:

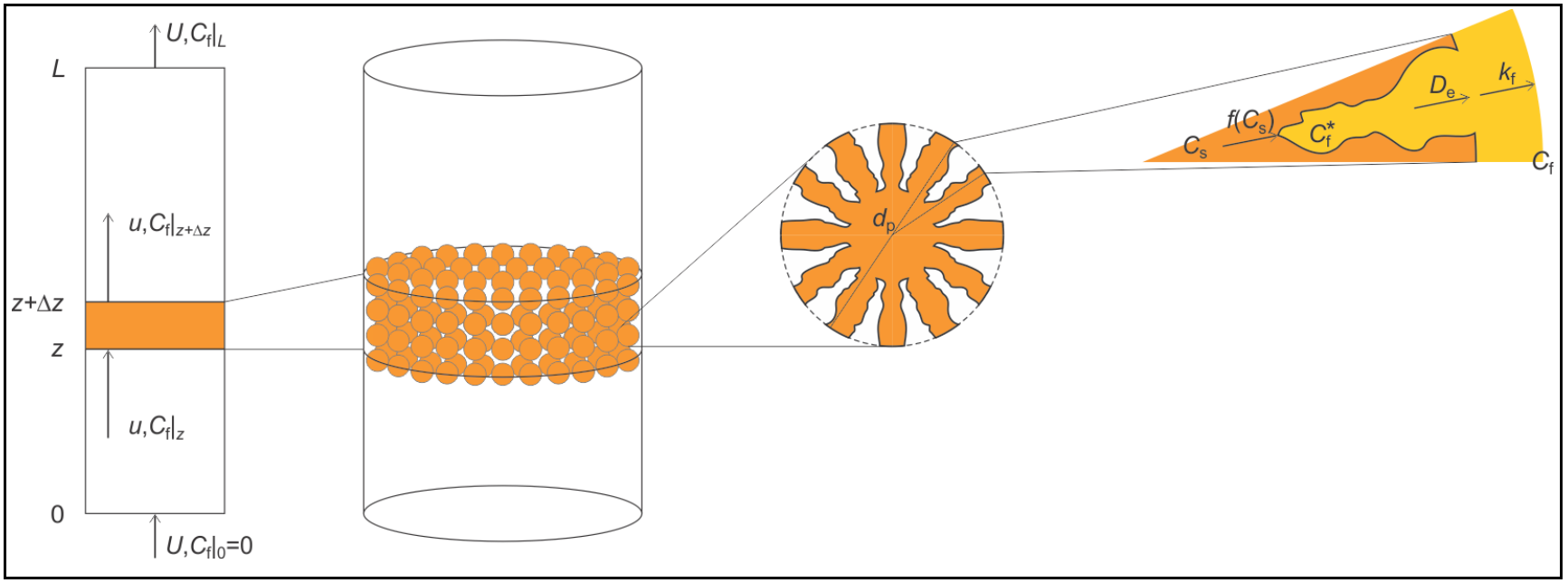

Figure A-1. Identification of elements defining mass transfer in packed bed extraction vessel in which porous spherical particles are extracted by a supercritical CO_2 up-flowing stream.

$$C_{so} + \frac{\varepsilon\ \rho}{\rho_b} C_{fo} = \left(C_s\right)_i \text{, and} \tag{A.1}$$

$$C_{fo} = f\left(C_{so}\right). \tag{A.2}$$

Eqs. (A.1) and (A.2) were solved using minimization routines in Matlab 2008b (fminbnd).

This was slightly modified in the case of Model 1, in which equilibrium is characterized by equal concentrations of oil in SC CO_2 (C_{fo}) in the intra-particle [volume fraction (1-ε) ε_p] and inter-particle (volume fraction ε) spaces. C_{fo} can reach up to C_{sat}, case where excess oil (concentration C_{so}) remains in the solid (Eq. A.3). [Note: In Model 1 the concentration of oil in the oilseed ($C\big|_{z,t}$) corresponds to that of the fraction that in precipitated in the intra-particle space of the pre-pressed seed.] Otherwise, oil is fully dissolved and partitions between the intra- and inter-particle spaces (Eq. A.4).

$$C_{so} = \left(C_s\right)_i - \frac{\left[\varepsilon + \left(1-\varepsilon\right)\ \varepsilon_p\right]\ \rho}{\rho_b} C_{sat} \text{ and}$$

$$C_{fo} = C_{sat} \text{, if } \frac{\rho_b \left(C_s\right)_i}{\varepsilon + \left(1-\varepsilon\right)\ \varepsilon_p} > C_{sat} \tag{A.3}$$

and

$$C_{so} = 0 \text{ and } C_{fo} = \frac{\rho_b \left(C_s\right)_i}{\varepsilon + \left(1-\varepsilon\right)\ \varepsilon_p} \text{, if } > \frac{\rho_b \left(C_s\right)_i}{\varepsilon + \left(1-\varepsilon\right)\ \varepsilon_p} < C_{sat}. \tag{A.4}$$

A2. Boundary condition

There is no oil dissolved in the SC CO_2 fed to the extraction vessel initially (Eq. A.5):

$$C_f\big|_{z,0} = 0 \tag{A.5}$$

A3. Model 1

In this case, the SC CO_2 from the node located immediately downstream (position $z - \Delta z$) enters a given node (position z) while simultaneously the SC CO_2 phase in it moves to the node located immediately downstream (position $z + \Delta z$) (Fig. A-2), and equilibrium instantaneously establishes that can be estimated by solving the oil conservation (Eq. A.6) and equilibrium (Eq. A.7) equations simultaneously:

$$C_s\big|_{z,t+\Delta t} = C_s\big|_{z,t} + \frac{\varepsilon\ \rho}{\rho_b} C_f\big|_{z-\Delta z,t} - \frac{\left[\varepsilon + (1-\varepsilon)\ \varepsilon_p\right]\ \rho}{\rho_b} C_{sat} \text{ and } C_f\big|_{z,t+\Delta t} = C_{sat},$$

$$\text{if } \frac{\rho_b C_s\big|_{z,t} + \varepsilon\ \rho C_f\big|_{z-\Delta z,t}}{\left[\varepsilon + (1-\varepsilon)\ \varepsilon_p\right]\ \rho} > C_{sat}, \text{ or} \quad \text{(A.6)}$$

$$C_s\big|_{z,t+\Delta t} = 0 \text{ and } C_f\big|_{z,t+\Delta t} = \frac{\rho_b C_s\big|_{z,t} + \varepsilon\ \rho C_f\big|_{z-\Delta z,t}}{\left[\varepsilon + (1-\varepsilon)\ \varepsilon_p\right]\ \rho},$$

$$\text{if } \frac{\rho_b C_s\big|_{z,t} + \varepsilon\ \rho C_f\big|_{z-\Delta z,t}}{\left[\varepsilon + (1-\varepsilon)\ \varepsilon_p\right]\ \rho} < C_{sat} \quad \text{(A.7)}$$

A4. Model 2

Conditions in this case equalled those in Model 1, but the oil conservation (Eq. A.8) and equilibrium sorption (Eq. A.9) equations that must be solved simultaneously change, and calculations use the minimization routines in Matlab 2008b (fminbnd):

$$\rho_s C_s\big|_{z,t+\Delta t} + \varepsilon\ \rho C_f\big|_{z,t+\Delta t} = \rho_s C_s\big|_{z,t} + \varepsilon\ \rho C_f\big|_{z-\Delta z,t}, \text{ and} \quad \text{(A.8)}$$

$$C_f\big|_{z,t+\Delta t} = f\left(C_s\big|_{z,t+\Delta t}\right). \quad \text{(A.9)}$$

A5. Model 3

In this case, at difference from those of Model 1 and Model 2, oil transfer from pre-pressed oilseeds to SC CO_2 is partially defined by kinetic factors. The oil that leaves the

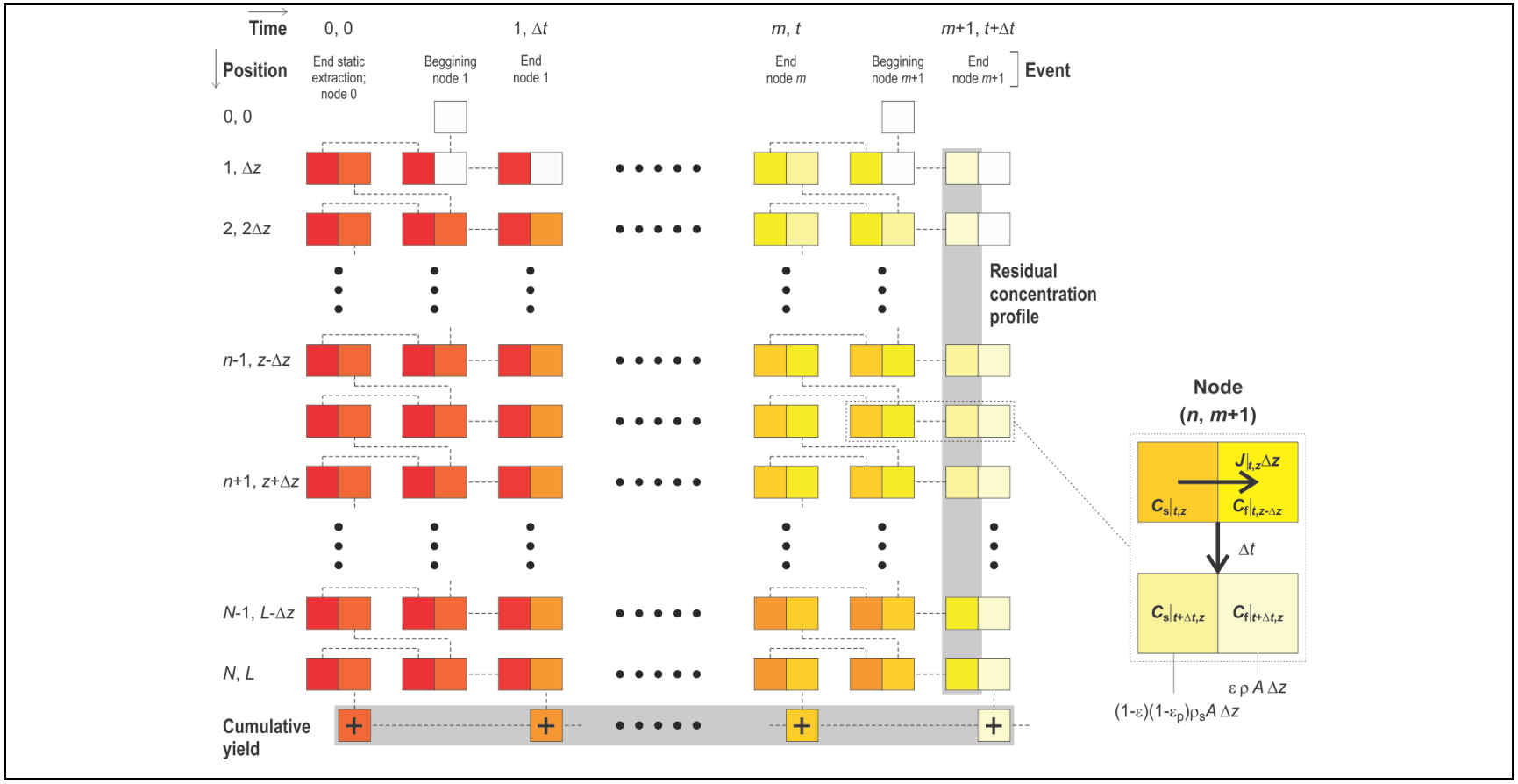

Figure A-2. Schematic representation of the algorithm used to solve differential mass balance equations for the supercritical CO_2 extraction of solid substrate particles in a packed bed extraction vessel, including actualization of concentration values in the solid and fluid phase as a function of axial position in the vessel and time.

oilseed in a node equals the one that enters SC CO_2 in the same node (*J*-term in oil balances equations). Oil conservation requires solving the balances for the oilseed (Eq. A.10) and SC CO_2 (Eq. A.11) in the node simultaneously:

$$C_s\big|_{z,t+\Delta t} = C_s\big|_{z,t} - \frac{J\big|_{z,t+\Delta t/2}\,\Delta t}{\rho_b}, \text{ and} \tag{A.10}$$

$$C_f\big|_{z,t+\Delta t} = C_f\big|_{z-\Delta z,t} + \frac{J\big|_{z,t+\Delta t/2}\,\Delta t}{\varepsilon\,\rho} \tag{A.11}$$

Considering the definition of *J* (Eqs. 2.4-2.6) for the extraction of spherical particles, the final form of Eqs. (A.10) and (A.11) is given by Eqs. (A.12) and (A.13), respectively:

$$C_s\big|_{z,t+\Delta t} = C_s\big|_{z,t} - \left(\frac{30\,k_f}{5+Bi}\right)\left(\frac{1-\varepsilon}{d_p\rho_b}\right)\left[\,f\left(C_s\big|_{z,t}\right) - C_f\big|_{z-\Delta z,t}\right]\Delta t, \text{ and} \tag{A.12}$$

$$C_f\big|_{z,t+\Delta t} = C_f\big|_{z-\Delta z,t} + \left(\frac{30\,k_f}{5+Bi}\right)\left(\frac{1-\varepsilon}{d_p\rho_b}\right)\left[\,f\left(C_s\big|_{z,t}\right) - C_f\big|_{z-\Delta z,t}\right]\Delta t \tag{A.13}$$

A6. Yield

The amount of oil extracted was computed as a function of extraction time (null initial yield, Eq. A.14) taking into account the feed of SC CO_2 to the extraction vessel (*Q*) and the concentration of oil at the exit of the extraction vessel (node *N*, $z = L$) according to Eq. (A.15):

$$Y\big|_o = 0, \text{ and} \tag{A.14}$$

$$Y\big|_t = Y\big|_{t-\Delta t} + Q\;C_f\big|_{L,t}\,\Delta t. \tag{A.15}$$

APPENDIX B: STANDARDIZATION OF THE METHODOLOGY

B1. Implications of the close and open sampling modes

Changes of oil concentration in SC CO_2 due to the pressure change during the sampling step with a closed loop mode were calculated assuming that oil concentration decreases down to the value of oil solubility while pressure drops, and that excess oil precipitates on the substrate. The depressurization was assumed to be isothermal because the equilibrium loop remains heated. By calculation of continuously sampling (reducing) 0.18-g portions of CO_2 from the loop (initially containing ~42 g of CO_2 in ~49 cm^3 of loop) remaining SC CO_2 densities were calculated, then pressure was calculated using the NIST Database (Lemmon et al., 2007) at the temperature and density conditions of CO_2. Oil solubilities were calculated with equation proposed by del Valle et al. (2012) at these conditions, and the apparent oil concentration in SC CO_2 informed in Fig. (2-3) was calculated as the sum of sampled oil (product of oil solubility and sampled CO_2) over sum of sampled CO_2.

Changes of oil concentration in SC CO_2 due to dilution during the sampling step using an open loop mode were calculated for the next two assumptions: (1) continuously sampling 0.18 g of CO_2 from the equilibrated loop and adding 0.18 g of fresh/pure CO_2 to keep pressure constant that mixes perfectly with the SC CO_2 phase remaining in the loop (i.e., oil concentration in the substrate remains unchanged); (2) modelling the equilibrium cell as an extraction vessel applying a predictive kinetic model for the SC CO_2 extraction of oil from oilseeds (del Valle, 2015). In the first case oil concentrations were calculated using mass balances, and apparent concentration of oil in SC CO_2 was calculated as the sum of sampled oil over sum of sampled CO_2, as in the close loop mode.

In the second case the applied kinetic model is an adaptation of "Model 3" proposed by del Valle and Urrego (2012) modified to include the axial dispersion (D_L) of the solute in the SC CO_2 phase flowing through the extraction vessel. Differential mass balances were space- (z) and time- (t) discretized Eqs. (B.1a) and (B.1b), and solved using appropriate initial, Eq. (B.2), and border, Eqs. (B.3a) and (B.3b), conditions.

$$C_{\mathrm{f}}\big|_{z,t+\Delta t} = C_{\mathrm{f}}\big|_{z-\Delta z,t}\left(1-2D_{\mathrm{L}}\frac{\Delta t}{\Delta z^2}\right)+...$$

$$...D_{\mathrm{L}}\left(C_{\mathrm{f}}\big|_{z+\Delta z,t}+C_{\mathrm{f}}\big|_{z-\Delta z,t}\right)\frac{\Delta t}{\Delta z^2}+\frac{J\big|_{z,t}\,\Delta t}{\varepsilon\,\rho}, \quad \text{(B.1a)}$$

$$C_{\mathrm{s}}\big|_{z,t+\Delta t} = C_{\mathrm{s}}\big|_{z,t}-\frac{J\big|_{z,t}\,\Delta t}{\rho_{\mathrm{b}}}, \quad \text{(B.1b)}$$

$$C_{\mathrm{s}}\big|_{i,0}+\frac{\varepsilon\,\rho}{\rho_{\mathrm{b}}}\,f\left(C_{\mathrm{s}}\big|_{i,0}\right)=\left(C_{\mathrm{s}}\right)_{\mathrm{i}} \quad \text{(B.2)}$$

$$C_{\mathrm{f}}\big|_{\Delta z,t}=\left(1+\frac{U\,\Delta z}{D_{\mathrm{L}}}\right)C_{\mathrm{f}}\big|_{0,t} \quad \text{(B.3a)}$$

$$C_{\mathrm{f}}\big|_{L,t}=C_{\mathrm{f}}\big|_{L-\Delta z,t} \quad \text{(B.3b)}$$

$$\text{where } J\big|_{z,t}=k_{\mathrm{p}}a_{\mathrm{s}}\left[\,f\left(C_{\mathrm{s}}\big|_{z,t}\right)-C_{\mathrm{f}}\big|_{z,t}\right], \quad \text{(B.4)}$$

And where, for spherical particles, $a_{\mathrm{p}}=6\left(1-\varepsilon\right)/d_{\mathrm{p}}$.

Mass balances were solved in Matlab 2008b [Math Works, Natick, MA] to calculate concentrations of oil in prepressed oilseeds in each element (position along the tubes and extraction vessel, time) of the grid, and oil yield as a function of extraction time. The tubes and extraction vessel were divided in finite length ($\Delta z = L/N$) nodes, whereas finite time interval was calculated as the one taken by SC CO_2 (superficial velocity U) to go through a node in space ($\Delta t = \Delta z/U$). The number of nodes (N) in space was increased up to the level when there were no differences between simulated integral extraction curves at higher values of N, while at the same time ensuring that Courants‟ condition ($0 < D_{\mathrm{L}}\,\Delta t\,\Delta z^{-2} < 0.5$) was satisfied (del Valle & Urrego, 2012).

Model parameters were estimated using the procedure outlined by del Valle (2015). The density (ρ) and viscosity (μ) of the SC CO_2 phase were estimated using NIST database

(Lemmon et al., 2007) for pure CO_2 at the extraction temperature (T = 50 ºC) and pressure (P = 28 MPa) under the assumption that they are not affected by dissolved oil (a reasonable assumption for this low-solubility solute), whereas the binary diffusivity of the oil in CO_2 (D_{12}) was estimated as a function of the absolute temperature (323.2 K), the density of CO_2, and the molecular weight of a representative component of the oil (885.5 g/mol in the case of triolein) using the equation of Funazukuri et al. (2009). Then, the superficial velocity of SC CO_2 in the packed bed (U) was estimated as a function of its mass flow rate (Q = 0.0177 cm^3/s) and the cross-sectional of the equilibrium cell (A = 2.297 cm^2). Following estimation of the bed height-to-particle diameter (H/d_p) ratio, and dimensionless Reynolds ($Re = \rho\ U\ d_p\ \mu^{-1}$) and Schmidt ($Sc = \mu\ \rho^{-1}\ D_{12}^{-1}$) numbers, the axial dispersion-to-binary diffusivity (D_L/D_{12}) ratio was estimated as a function of *Re*, *Sc*, and H/d_p, using the correlation of del Valle et al. (2011), and the dimensionless Sherwood number ($Sh = k_f\ d_p\ D_{12}^{-1}$) was estimated as a function of *Re* and *Sc* using the correlation of Puiggené et al. (1997). From estimated values of D_L/D_{12} and *Sh* it was possible to estimate the axial dispersion (D_L) and film mass transfer (k_f) coefficients describing oil movement within and towards the SC CO_2 phase in the packed bed, respectively. The effective diffusivity of the oil in the substrate (D_e) was estimated as the ratio of its binary diffusivity in SC CO_2 (D_{12}) and a pretreatment-dependent microstructural factor (F_M) (del Valle et al., 2006) which, in turn, was estimated as a function of the inner porosity of the prepressed seed [ε_p^{-2}, (del Valle et al., 2006; Wakao & Smith, 1962)]. The global mass transfer coefficient in Eq. (B.5) can be estimated as a function of d_p, k_f, and D_e using the following definition for spherical particles (del Valle & Urrego, 2012):

$$k_p = \frac{10\ k_f}{10 + \left(k_f d_p / D_e\right)} \tag{B.5}$$

To solve Eqs. (B.1-B.5) numerically for “square” and “ground” pellets using the mass transfer parameters summarized in Table (B-1), the equilibrium partition in Eqs. (A.2) and (A.4) was represented using Eq. (2.9) with model parameters defined by Eqs. (2.12a-c) for ρ = 857.1 kg/m^3 and T = 323.2 K, i.e.,

$$f\left(C_s\big|_{z,t}\right) = 6.24\left[0.0017\ C_s\big|_{z,t} + \frac{\left(1-0.0017\ C_s\big|_{z,t}\right)\left(C_s\big|_{z,t}\right)^{3.34}}{1.79\times10^{-5}+\left(C_s\big|_{z,t}\right)^{3.34}}\right] \qquad \text{(B.6)}$$

Table B-1. Definition and values of parameters applied while modelling the sampling step with an open loop mode with a kinetic extraction model. Operation conditions of 50 °C and 28 MPa were assumed.

Property	Value	
U (mm/s)	0.077	
ρ (kg/m^3)	857.1	
μ (Pa s)	8.19×10^{-5}	
D_{12} (m^2/s)	3.52×10^{-9}	
Sc (–)	27.1	
	"Ground" pellets	"Square" pellets
d_p (mm)	0.531	5.72
a_p (mm^{-1})	6900	520
L/d_p	344	31.9
D/d_p	32.2	3.00
F	9.87	38.5
D_e (m^2/s)	2.56×10^{-10}	6.56×10^{-11}
Re	0.425	4.59
k_f (m/s)	2.07×10^{-6}	1.29×10^{-6}
Bi	1.54	40.3
k_p (m/s)	1.59×10^{-6}	1.42×10^{-7}
D_L (m^2/s)	1.04×10^{-7}	1.74×10^{-7}

B2. Effect of weight ratio on the gravimetric determination of oil

With the initially designed sampling recipients (50 cm^3 test tubes) measurements of sampled oil were irreproducible. Authors studied the effect of the weight of the different sampler recipients when determining very low amounts of oil (~1 mg). Fig. (B-1) shows

the linear relationship between the uncertainty percentage and sampler/sample ratio. In order to improve the initial weight ratio ($1.4x10^5$ for the worst case scenario, weighing 1 mg in a 50-g test tube into a 90-g test tube holder, 140% uncertainty), vials of approximate 4-17 g ($200\text{-}1.7x10^4$ ratio, 0.2-17% uncertainty) were inserted into test tubes to receive the sampled solute. No 90-g holder was required to weigh vials.

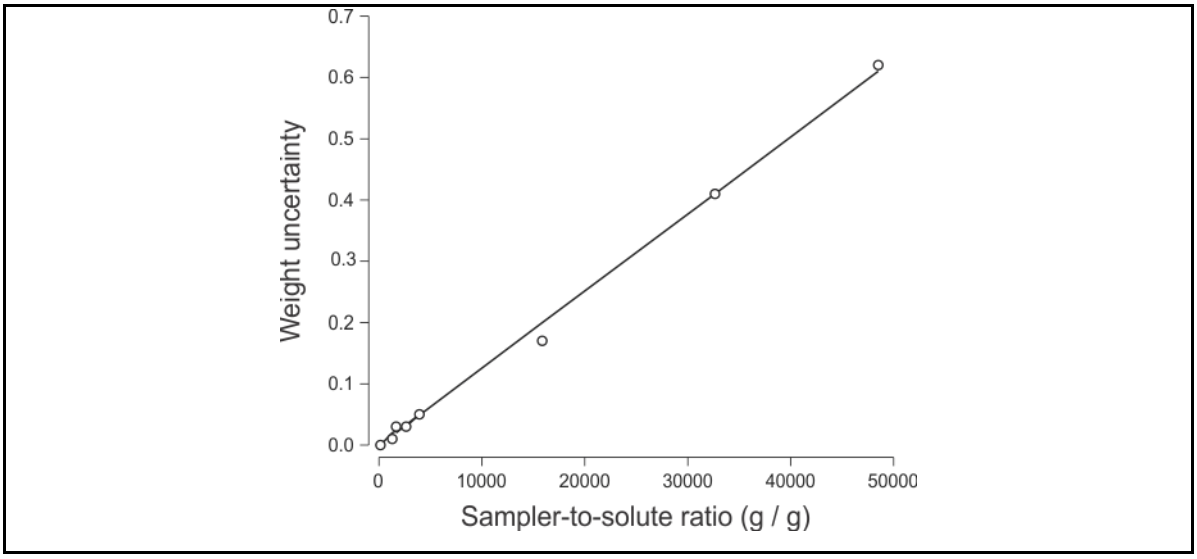

Figure B-1. Uncertainty of oil weight measurements as a function of the ratio between the weight of the sample holder and the oil.

B2. Uncertainty analysis

Based in the Guide to the expression of Uncertainty in Measurement (GUM) (BIPM et al., 2008a, 2008b), authors evaluated the standard uncertainty of isotherm/isobar curves variables (C_f, C_s). Based in the "law of propagation of uncertainties", and output quantities of the methodology, Eqs. (B.7)-(B.8), the standard uncertainty of each point of the isotherm/isobar curve for C_f and C_s are as follows:

$$u^2\left(C_{f(i)}\right)=\left(\frac{\partial C_{f(i)}}{\partial S_{(i)}}\right)^2 u^2\left(S_{(i)}\right)+\left(\frac{\partial C_{f(i)}}{\partial V_{CO_2}}\right)^2 u^2\left(V_{CO_2}\right)+\ldots$$

$$\ldots\left(\frac{\partial C_{\mathrm{f(i)}}}{\partial \rho_{\mathrm{CO_2}}}\right)^2 u^2\left(\rho_{\mathrm{CO_2}}\right) \quad \text{(B.7)}$$

$$u^2\left(C_{\mathrm{s(i)}}\right)=\left(\frac{\partial C_{\mathrm{s(i)}}}{\partial S_{\mathrm{o}}}\right)^2 u^2\left(S_{\mathrm{o}}\right)+\left(\frac{\partial C_{\mathrm{f(i)}}}{\partial \sum_{\mathrm{i=1}}^{\mathrm{n-1}} S_{\mathrm{(i)}}}\right)^2 u^2\left(\sum_{\mathrm{i=1}}^{\mathrm{n-1}} S_{\mathrm{(i)}}\right)+\ldots$$

$$\ldots\left(\frac{\partial C_{\mathrm{s(i)}}}{\partial C_{\mathrm{f(i)}}}\right)^2 u^2\left(C_{\mathrm{f(i)}}\right)+\left(\frac{\partial C_{\mathrm{s(i)}}}{\partial \rho'_{\mathrm{CO_2}}}\right)^2 u^2\left(\rho'_{\mathrm{CO_2}}\right)+\ldots$$

$$\ldots+\left(\frac{\partial C_{\mathrm{f(i)}}}{\partial V_{\mathrm{loop}}}\right)^2 u^2\left(V_{\mathrm{loop}}\right)+\left(\frac{\partial C_{\mathrm{s(i)}}}{\partial M_{\mathrm{o}}}\right)^2 u^2\left(M_{\mathrm{o}}\right) \quad \text{(B.8)}$$

where $u^2\left(\rho_{\mathrm{CO_2}}\right)=\left(\frac{\partial \rho_{\mathrm{CO_2}}}{\partial P}\right)^2 u^2\left(P\right)+\left(\frac{\partial \rho_{\mathrm{CO_2}}}{\partial T}\right)^2 u^2\left(T\right)$, and (B.7a)

$$u^2\left(\rho'_{\mathrm{CO_2}}\right)=\left(\frac{\partial \rho'_{\mathrm{CO_2}}}{\partial P}\right)^2 u^2\left(P\right)+\left(\frac{\partial \rho'_{\mathrm{CO_2}}}{\partial T}\right)^2 u^2\left(T\right) \quad \text{(B.8a)}$$

Values of derivatives in Eqs. (B.7)-(B.8) can be computed as follows:

$$\frac{\partial C_{\mathrm{f(i)}}}{\partial S_{\mathrm{(i)}}}=-\frac{1}{V_{\mathrm{CO_2}}\rho_{\mathrm{CO_2}}} \quad \text{(B.7b)}$$

$$\frac{\partial C_{\mathrm{f(i)}}}{\partial V_{\mathrm{CO_2}}}=-\frac{S_{\mathrm{(i)}}}{V_{\mathrm{CO_2}}^2\rho_{\mathrm{CO_2}}} \quad \text{(B.7c)}$$

$$\frac{\partial C_{\mathrm{f(i)}}}{\partial \rho_{\mathrm{CO_2}}}=-\frac{S_{\mathrm{(i)}}}{V_{\mathrm{CO_2}}\rho_{\mathrm{CO_2}}^2} \quad \text{(B.7d)}$$

$$\frac{\partial C_{s(i)}}{\partial S_o} = \frac{1}{M_o} = 0.04136\ g^{-1} \quad \text{(B.8b)}$$

$$\frac{\partial C_{f(i)}}{\partial \sum_{i=1}^{n-1} S_{(i)}} = \frac{1}{M_o} = -0.04136\ g^{-1} \quad \text{(B.8c)}$$

$$\frac{\partial C_{s(i)}}{\partial C_{f(i)}} = -\frac{V_{loop}\rho}{M_o} = -0.001729 \frac{kg\ CO_2}{g\ substrate} \quad \text{(B.8d)}$$

$$\frac{\partial C_{s(i)}}{\partial \rho_{CO_2}} = -\frac{C_{f(i)} V_{loop}}{M_o} = -2.017 x 10^{-6}\ C_{f(i)} \quad \text{(B.8e)}$$

$$\frac{\partial C_{s(i)}}{\partial V_{loop}} = -\frac{C_{f(i)} \rho_{CO_2}}{M_o} = --35.45\ C_{f(i)}, \text{ and} \quad \text{(B.8f)}$$

$$\frac{\partial C_{s(i)}}{\partial M_o} = \frac{\sum_{j=1}^{i-1} S_{(j)} + \left(C_{f(i)} V_{loop} \rho'_{CO_2}\right) - S_o}{M_o^2} = \frac{\sum_{j=1}^{i-1} S_{(j)} + 0.04181\ C_{f(i)} - 3.530}{584.6} \quad \text{(B.8g)}$$

$$\frac{\partial \rho}{\partial P} = 3.468 \frac{kg}{m^3\ K}, \text{ and} \quad \text{(B.8h)}$$

$$\frac{\partial \rho}{\partial T} = -2.891 \frac{kg}{m^3\ K}. \quad \text{(B.8i)}$$

Values of $\partial\rho'/\partial P'$ y $\partial\rho'/\partial T'$ can be estimated as a function of the temperature of the expanded CO_2 in the volumetric gas meter (T') and atmospheric pressure (P') using NIST database (Lemmon et al., 2007). Table (B-2) informs values of uncertainties u of some variables. The variance of $S_{(i)}$, $u(S_{(i)})$, can be estimated as a percent of the actual weight using the ratio of sample-to sampler informed in Fig. (B-1), and that of the sum $\sum S_{(i)}$ from those of the individual terms using standard formulae. In addition, the

variance of $C_{f(i)}$, $u\left(C_{f(i)}\right)$, estimated using Eq. (B.8), needs to be included in Eq. (2.9) to compute the variance of $C_{s(i)}$, $u\left(C_{s(i)}\right)$.

Table B-2. Variance of selected variables affecting calculations using Eqs. (B.7) and (B.8).

Variable, y	Variance of variable, $u(y)$	Unit	Source
V_{CO2}	0.2	%	Gas meter manual
T'	0.1	ºC	Gas meter thermometer
P'	0.001	MPa	Variation in atmospheric pressure
S_o	0.20	g	Calculated
T	0.5	ºC	Variation within hot air bath
P	0.015	MPa	Syringe pump manual
V_{loop}	1.92	cm^3	Experimental standard deviation
M_o	0.20	g	Calculated

Since probability distributions of the measurands are not obtained with a GUM approach, authors calculated coverage intervals using Monte Carlo simulations. Authors assigned probability distributions to each variable, repeatedly sampled several (a large number of) times, and calculated values of C_f and C_s for each set of samples. This way, the probability distributions of the measurands can be numerically approximated. Sequences of one million random values for each variable were applied. Gaussian (normal) distributions with standard uncertainties obtained from GUM analysis were assigned to all variables, and centered at the measured or calculated value. Measurands were calculated according to Eqs. (B.7) and (B.8). The symmetric 95% coverage intervals were calculated according to sub-clause 7.7.2 of Supplement 1 to GUM (BIPM et al., 2008c). These intervals mean that the probability of the measurands to be above or below the upper and lower limits is believed to be 0.025.